GEOLOGICAL SURVEY
BULLETIN 61

GEOLOGY OF THE RINGAROOMA - BOOBYALLA AREA

TASMANIA DEPARTMENT OF MINES

1982

GEOLOGICAL SURVEY
BULLETIN 61

Geology of the Ringarooma – Boobyalla area

by M.P. McCLENAGHAN, B.Sc.(Hons), Ph.D.,
N.J. TURNER, B.Sc.(Hons), P.W. BAILLIE, B.Sc.(Hons),
A.V. BROWN, B.Sc.(Hons), P.R. WILLIAMS, B.Sc.(Hons), Ph.D.
and W.R. MOORE, B.A., M.Sc.

with contributions by A.V. BROWN, S.M. FORSYTH, D.C. GREEN,
J. McCLENAGHAN, I. McDOUGALL and W.R. MOORE

ISSN 0082-2043
DEPARTMENT OF MINES, GPO BOX 124B, HOBART, TASMANIA 7001 ISBN 0 7246 0509 6

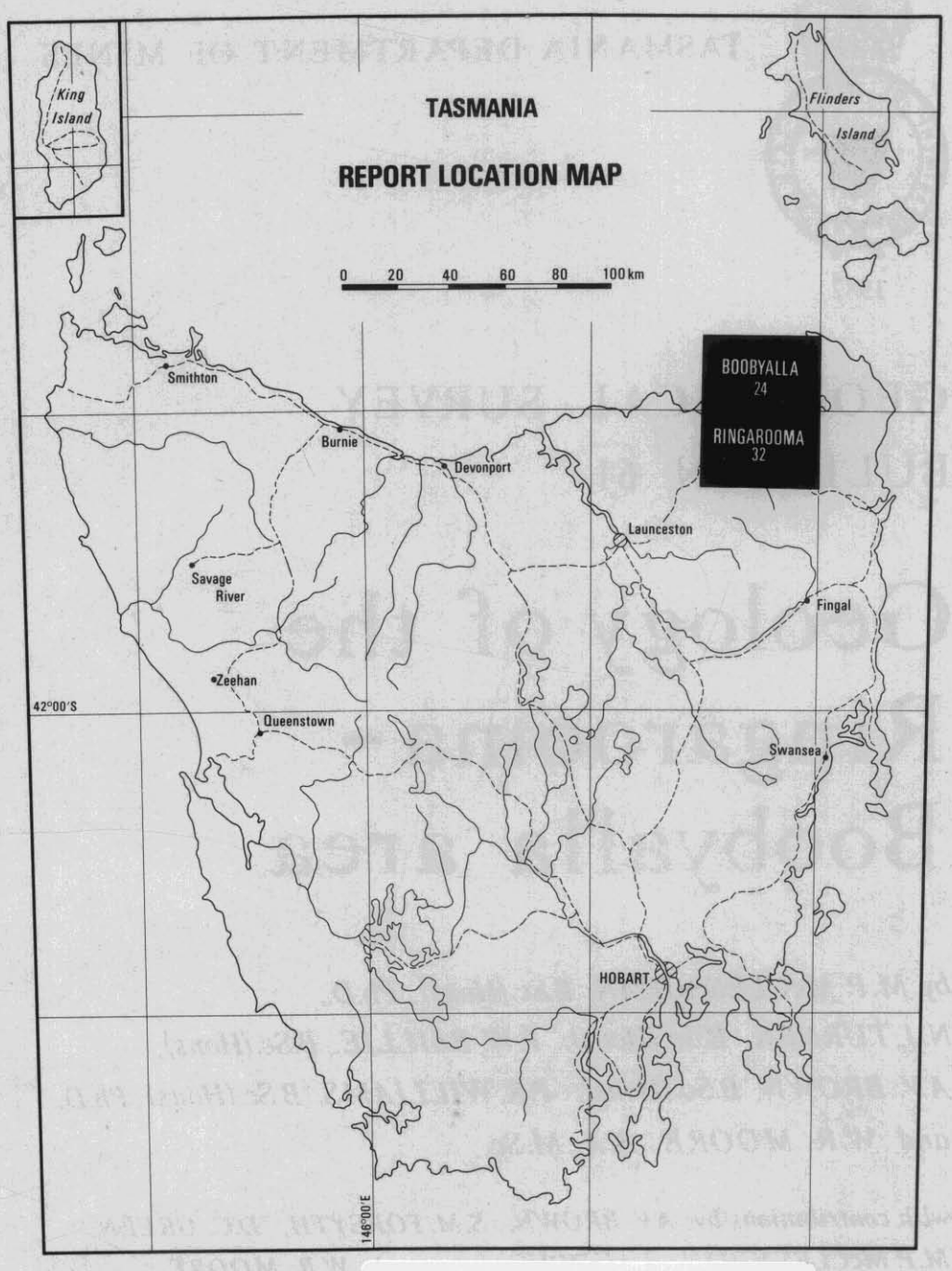

Figure 1.

5 cm

McCLENAGHAN, M.P. *et al.* 1982. Geology of the Ringarooma-Boobyalla area. *Bull.geol.Surv.Tasm.* 61. ISBN 0 7246 0509 6 : ISSN 0082-2043.

CONTENTS

LIST OF FIGURES

LIST OF PLATES

INTRODUCTION

Ringarooma 1:50 000 Map Sheet 8415N (32), which was published in 1977, covers the region between Latitude 41°00' and 41°15'S and Longitude 147°30' and 148°00'E. Boobyalla 1:50 000 Map Sheet 8416S (24), published in 1980, covers the region between Latitude 40°43' and 41°00'S and Longitude 147°30' and 148°00'E. In general, apart from detailed geological reports of mines, previous geological surveys have been reconnaissance in nature, and these investigations have been referred to within this report.

A complete airphoto cover was available for both the Ringarooma and Boobyalla regions, and topographical maps on a scale of 20 chains to the inch, contoured at 25 foot intervals, were used for regional geological mapping. The Ringarooma Sheet is based on mapping mainly during periods from April to November inclusive, 1969 to 1976. The following geologists took part in the Ringarooma survey - A.V. Brown, M.P. McClenaghan, W.R. Moore, N.J. Turner, J. McClenaghan, P.R. Williams, P.W. Baillie, K.D. Corbett, E.B. Corbett, S.F. Cox, D.I. Groves and G.P. Pike. The Boobyalla Sheet is based on geological mapping during the periods April to November inclusive, 1974 to 1978. The following geologists took part in the Boobyalla survey - P.W. Baillie, N.J. Turner, S.F. Cox. The geological surveying was under the supervision of E. Williams.

Many towns were used as centres for the geologists and the numerous roads afforded easy access to all areas of the Ringarooma - Boobyalla region.

A number of geologists have contributed to the following report. The geologists mainly responsible for each section are named with the section-heading. Information attributable to a geologist other than those named with the section-heading is indicated by giving the geologist's initials within parentheses.

SUMMARY OF GEOLOGICAL HISTORY

QUATERNARY	HOLOCENE	Modification of previous landforms with formation of coastal dunes, accumulation of beach sands and re-working of superficial material.
	PLEISTOCENE	Lunette development, accumulation of slope deposits and deposition of sand in sheets and longitudinal dunes. Marine clay and sand, with minor peat and gravel, deposited on gently seaward-sloping plain. *Extensive erosion* partly exhuming pre-Tertiary surface, particularly demonstrated in areas of lower elevation.
	TERTIARY	Ferricrete, associated with weathering and erosion of basalt, formed on Tertiary sediment and older rocks. Silcrete development. Large outpourings of alkali olivine basalt and olivine nephelinite, and accumulations of associated pyroclastic rocks in Early and Middle Miocene times. Local shallow-marine incursion with limestone formation (Late Oligocene-Early Miocene?) Clay, gravel and quartz sand, with occasional carbonaceous horizons, deposited in basins and deep valleys, which may in small part be younger than basaltic rocks. Faulting, gently tilting proved in adjacent areas.
	CRETACEOUS	Andesite lava flows and intrusions of porphyrite and lamprophyre dykes *Extensive erosion*
	JURASSIC	Intrusion of dolerite sheets.
	TRIASSIC	Micaceous quartz sandstone (Upper Parmeener Super-Group).
	PERMIAN	Siltstone and sandstone, often bioturbated, with dropstones (Lower Parmeener Super-Group). *Extensive erosion* (?) Dolerite dyke intrusions
	DEVONIAN	Regional flattening Emplacement (∿370-389 Ma) of granite/adamellite of Blue Tier Batholith, and granodiorite/granite/adamellite of Scottsdale Batholith. Contact metamorphism of surrounding Mathinna Beds. Folding of Mathinna Beds. Mudstone and quartzwacke turbidites, with occasional carbonaceous fragments
	SILURIAN	(Mathinna Beds)

Some of the events listed above are of uncertain age. The proved age-range for the event of 'Faulting, gentle tilting proved in adjacent areas' is later than the Jurassic and precedes the Tertiary deposits of the region. The event of 'Dolerite dyke intrusions' occurred after the emplacement of the Devonian granitic batholiths, but it has not been proved to be pre-Permian in age.

PHYSIOGRAPHY AND LANDSCAPE DEVELOPMENT

PWB, NJT

The region may be divided into the following major physiographic units:

Highland areas rising to a maximum elevation of nearly 900 m, in particular the Blue Tier and Mt Cameron massifs, Cuckoo Hill and Mt Horror.

Coastal areas predominantly of flat plains rising to an elevation of about 40 m, but including higher areas such as Ringarooma Tier and One Tree Hill.

An intervening dissected area.

The distribution of selected heights of the area is shown in Figure 2. An overall gradient away from the south-eastern part of the region is apparent. This gradient is reflected in the rainfall where the higher parts have an annual precipitation in excess of 1 800 mm while some of the coastal areas *e.g.* Tomahawk, receive less than 500 mm. The main population centre of the region, Scottsdale, has an annual rainfall of about 1 000 mm.

This gradient is also shown by the climax vegetation although the pattern is obscured by the extensive clearing and burning that has been carried out in the latter parts of last century and for most of this century. Temperate rain forest, dominated by *Nothofagus* and *Atherosperma*, is the climax vegetation in the higher, wetter parts of the region. Sclerophyll forests formed in the intervening area while coastal heaths dominated the coastal areas. The disappearance of most of the heath lands has been recently documented (Kirkpatrick, 1977).

HIGHLAND AREAS

Although the region lies within the 'fold province' of Davies (1965), with the exceptions of Mt Horror, part of Mt Paris, and Mt Littlechild, granite forms the major highland areas and the folded structure of the Mathinna Beds has had little effect on physiographic development. Within the granite highland areas, tors, often scores of metres in diameter, are common, and probably result from frost modification of two-cycle proto-tors (Davies, 1971).

A local example of lithological control on drainage development is the range of hills extending from Billycock Hill [563386]* through Kamona Ridge and Williams Hill into the coastal area at 480700. The hills are underlain by contact metamorphosed Mathinna Beds sediments and trend parallel to the eastern margin of the Scottsdale Batholith

COASTAL AREAS

The coastal area is one of low elevation and relief compared with the hinterland. The major elevated area within the tract is Ringarooma Tier, which is formed from dolerite, and rises some 100 m above the coastal plain. Dolerite is also the dominant rock type exposed on rocky headlands such as Cape Portland, Tomahawk Point and Croppies Point. Granite crops out at Waterhouse Point.

---

* All grid references lie in 100 km square EQ.

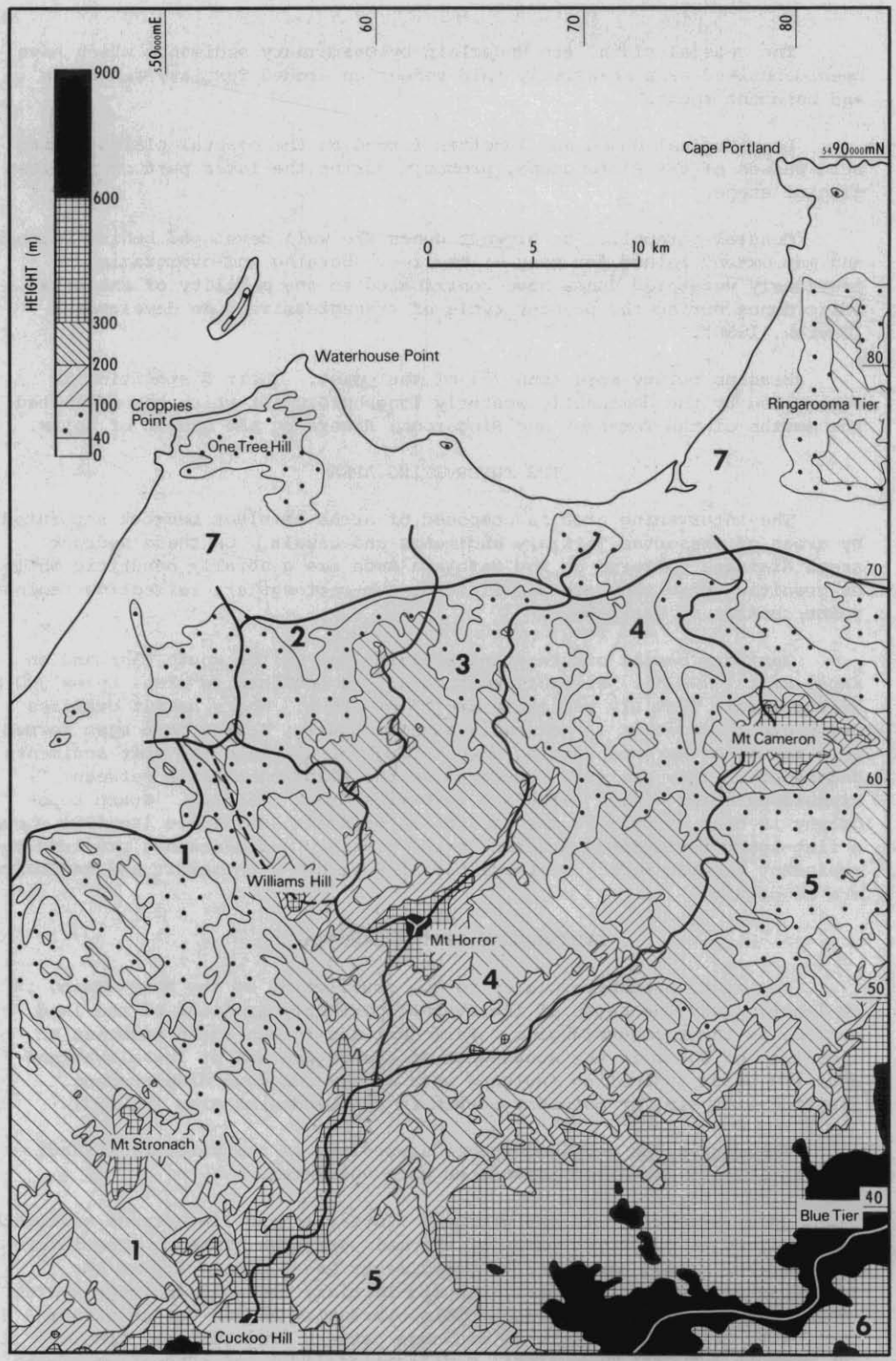

Figure 2. *Selected contour intervals and major drainage systems. 1: Great Forester River; 2: Sheepwash Creek (- - - = inferred old drainage divide); 3: Tomahawk Creek; 4: Boobyalla River; 5: Ringarooma River; 6: George River; 7: Coastal tract.*

The coastal plains are underlain by Quaternary sediments which have been deposited as a relatively thin veneer on eroded Tertiary sediments and basement rocks.

Longitudinal dunes and lunettes formed on the coastal plains during arid phases of the Pleistocene, probably during the later part of the last glacial stage.

Coastal parabolic, or blowout dunes are well developed behind beaches and may extend inland for many kilometres. Burning and overgrazing on previously vegetated dunes have contributed to the mobility of the parabolic dunes during the present cycle of transgressive dune development (Davies, 1965).

Beaches occupy more than 75% of the coast. Their disposition is controlled by the dominantly westerly longshore drift which has deflected the mouths of the Tomahawk and Ringarooma Rivers by the growth of spits.

THE INTERVENING AREA

The intervening area is composed of areas of older bedrock separated by areas of dissected Tertiary sediments and basalt. On these bedrock areas drainage patterns on the Mathinna Beds are generally dendritic while on granitic rocks they are dendritic or sub-rectangular, reflecting regional joint control of drainage.

Tertiary basalt occurs at high elevations in the south east and on Kapai Hill [570425]. However, most basalt is confined to areas below 300 m. Virtually all Tertiary sediments are below 260 m. Where basalt overlies sediments the contact is generally subhorizontal. Scarps have been formed as a result of streams cutting down through basalt into the soft sediments underneath. They are well developed in the Ringarooma River between Ringarooma [610340] and Derby and in Davies Creek [710510]. Scarp topography is also evident in the area north of North Scottsdale [465480] where a flat-lying ferruginous horizon in the Tertiary sediments has provided the resistant capping rock. Drainage patterns within both basalt and sediments are dendritic.

DEVELOPMENT OF THE LANDSCAPE

Faulting, probably related to the downflexing of the Bass Basin, is at least partly the cause of the overall northerly gradient of the land surface in the two quadrangles. Parmeener Supergroup rocks occur at an elevation of 800 m in the south-west of the region and at low elevations near the coast indicating faulting with north-side-down displacement. Faulting with similar movement occurs in the Lyndhurst area [518687].

The region has remained stable since late in the Tertiary without any significant tectonism associated with volcanism.

On a regional scale the Tertiary fluviatile and ?lacustrine sediments are confined to the lower parts of the main drainage systems. The interface between basalt and underlying sediments has a gentle dip to the north indicating that the early- to mid-Tertiary regional drainage system was similar to the existing one. This similarity may be due to either continuity of the same regional drainage pattern from Tertiary time to the present day with very little modification (*NJT*), or exhumation of the Tertiary drainage system by removal of substantial thicknesses of easily eroded sediments and possibly basalt (*PWB*).

Supra-basalt sediments probably occur near the Boobyalla River in the southern part of Boobyalla Quadrangle at 720620 and at Martins Hill [710570] in Ringarooma Quadrangle. No evidence of supra-basalt or sub-basalt sediments of fluvial origin has been found in areas of high elevation.

Modification of the Tertiary drainage pattern is shown by the lateral displacement by basalt of the Ringarooma River which now lies within pre-Tertiary rocks at elevations higher than the lowermost sub-basalt Tertiary deposits known in drill holes. Another example is the capture by Oxberry Creek, a tributary of the Great Forester River, of what in Tertiary time was the upper part [550600] of the Sheepwash Creek drainage system. There is a minimum difference in elevation of about 10 m between the bed of Oxberry Creek and the divide which separates it from the Sheepwash system. The present divide is situated on Tertiary and Quaternary deposits. Oxberry Creek, however, flows westwards to the Great Forester River through a 70 m deep narrow valley eroded through contact metamorphosed Mathinna Beds sediments. Minor tributary streams just above the head of the valley flow into Oxberry Creek such that the acute angle lies at the downstream side at their confluence indicating reversal of drainage.

The Quaternary history is one of eustatic variations in sea level with deposition of marine sediments in the coastal area during incursion(s?) and dune building in the arid climatic conditions generally associated with regression. The sediment-covered exposed marine plains were the source of sand for these dunes. Periglacial processes operated during colder phases of the Pleistocene resulting in the development of tors and the formation of extensive slope deposits.

The effect of man on the landscape has been considerable. Changes in vegetation caused by burning, clearing and overgrazing have resulted in mobilisation of previously stable sand dunes and changes in stream morphology. The best sections where Quaternary sediments were observed during mapping of the coastal area were seen where once small drainage ditches or streams have incised the sediments, sometimes to a depth in excess of 4 m, as a result of the increased run off caused by clearing.

The opposite effect has occurred in the lower parts of the Ringarooma River as a result of tin mining activities where the increased sediment load has resulted in the formation of extensive sand deposits. Shifting sand banks are exposed at low tide at the site of the former deep water port of Boobyalla.

STRATIGRAPHY

MATHINNA BEDS (LOWER ORDOVICIAN-DEVONIAN)

N.J. Turner

There are three tracts of Mathinna Beds in the Ringarooma and Boobyalla Quadrangles. One lies south of Scottsdale, another extends from Ringarooma to Lyndhurst and the third extends from Boobyalla to near Gladstone. These are separated by areas underlain by granitic rocks and a substantial part of each has been thermally metamorphosed. The Mathinna Beds were folded and cleaved and underwent low-grade dynamic metamorphism prior to granite emplacement. Because continuous structural profiles cannot generally be obtained, the total thickness of Mathinna Beds in each tract is unknown. A possible thickness of 350 m is present in the area east of Forester in the Ringarooma - Lyndhurst tract.

In Launceston (Longman, 1966) and Pipers River (Marshall, 1970)

Quadrangles, which are south-west and west of the Ringarooma Quadrangle respectively, the Mathinna Beds have been subdivided into pelitic and psammitic/pelitic sequences. Only the latter division has been recognised in the Ringarooma and Boobyalla Quadrangles where the sequence consists of alternating beds of quartzwacke or poorly-sorted siltstone and mudstone. As is the case elsewhere in north-eastern and eastern Tasmania (*e.g.* Williams, 1959), textures and structures in the quartzwacke indicate deposition from turbidity currents. The best sections showing sedimentary features are in the Ringarooma - Lyndhurst tract along roads west of Warrentinna and roads east of Forester and Kapai, also along the railway WSW of Telita.

Quartzwacke beds range in thickness from a few centimetres to exceptionally thick beds of about two metres. The common range is 0.4 - 0.8 m. Thin beds are usually finer-grained than thick beds. Silt-grade beds of several centimetres thickness interbedded with mudstone beds of similar thickness can form zones up to several metres thick. Generally the mudstone between quartzwacke beds is thin. However, thicknesses of up to several metres are not uncommon.

Graded bedding is ubiquitous in quartzwacke. There is a lower division of individual beds which grade from coarse- or medium-grained sandstone to medium- or fine-grained sandstone. Angular mudstone clasts occur in some lower divisions and carbonaceous fragments and mud pellets are present near the top of some. Above the lower division there is a 5 - 10 cm thick upper division which contains bedding lamination and grades from fine-grained sandstone to siltstone. Planar lamination is generally present in the lower part of the upper division and cross-lamination in the upper part. In some beds the lamination is disrupted and in others it is convoluted. Where coarser-grained, thicker quartzwacke units are in contact, the laminated zone may be absent. The lower division of beds and the two parts of the upper division correspond to the A, B and C divisions of turbidite units as defined by Bouma (1962).

The soles of most quartzwacke beds lack sole-marks although casts of flutes and longitudinal ridge and furrow structure are present on some. Flame structures and pseudonodules occur in some beds.

Fresh quartzwacke is dark grey, dark bluish-grey or greenish-grey. Commonly it is weathered and is fawn, orange or brown. The compositional variation in a typical quartzwacke bed 0.7 m thick is as follows. In the basal part there is about 80% (volume estimate) of very angular, low sphericity, very-poorly-sorted grains of quartz up to 0.8 mm across with less than 2% grains of plagioclase (probably albite or andesine) and relatively-coarse grains of detrital muscovite. Accessory tourmaline and opaque minerals are present also a few fragments of chert and fine-grained, felsic (?igneous) rock. The matrix consists of dimensionally-aligned muscovite of dynamo-metamorphic origin and subordinate, fine-grained quartz. Most quartzwacke contains substantial mica in the matrix. However, some exceptionally siliceous units containing only 5 - 10% mica were found (*e.g.* on loop road at Williams Hill near 557543).

Material from near the top of the lower division, shows composition and grain characteristics similar to the basal part except that grain size is finer, ranging up to 0.3 mm. In the top 100 mm bedding lamination is developed with planar lamination passing upwards into cross-lamination. Fine-grained, dimensionally aligned, green-tinted muscovite is the principal mineral constituent. Angular silt-grade quartz comprises less than 15% of the rock and there is about 5% of an apple-green, micaceous mineral (probably

chlorite) and a few per cent of very fine-grained, carbonaceous material. A few centimetres thickness of mudstone occurs between the laminated zone and the base of the overlying quartzwacke bed.

Where fresh the pelitic materials interbedded with quartzwacke are dark grey or dark green in colour, but, commonly they are weathered and are brown, orange, red or purple. The pelite may be poorly cleaved, slaty, or phyllitic. Thinner units are generally uniform compositionally and do not show bedding lamination. However, thicker units consist of thin (few centimetres) beds of lighter-coloured siltstone or very fine-grained sandstone and darker coloured mudstone. Cross-lamination may be present in the siltstone/sandstone beds. Fine-grained, green-tinted, dimensionally-aligned muscovite is the principal constituent of each rock type. Up to several per cent of carbonaceous material may be present. Subordinate, angular quartz is present in the silty and sandy beds.

Carbonaceous fragments and thin, interweaving, tubular structures defined by colour and textural variations in the upper parts of some turbidite units were the only features of probably biogenic origin observed. Cookson (1937) described carbonaceous plant fragments collected from thin beds of fine-grained sandstone about 190 m south of the now defunct Mara Siding [615453] on the Launceston - Herrick railway. She compared them with *Hostimella* sp., a primitive plant from rocks of similar lithology in Victoria. The Victorian rocks are regarded as Early Devonian (VandenBerg, *et al*, 1976). The age of the Mathinna Beds at Back Creek in Pipers River Quadrangle is Early Ordovician (Banks and Smith, 1968) and at Wrinklers Creek near Scamander it is Early Devonian (Banks, *in* Groves, 1977). Both ages are based on graptolites from pelitic rocks.

PARMEENER SUPER-GROUP

P.W. Baillie

Rocks of the Parmeener Super-Group (Banks, 1973) crop out in isolated locations near areas of dolerite in the region. Stratigraphic relationships have not been observed.

Waterhouse Island [535826]

On the south-eastern coast of Waterhouse Island indurated pebbly siltstone and sandstone crop out on the shore platform and at a small cliff section. The siltstone is generally finely laminated but may show small-scale festoon cross-bedding. Beds are generally less than 50 mm in thickness though some coarser sandstone beds may reach a thickness of up to 200 mm. Some of the sandier beds show grading. Bioturbation is often present. All rock types contain abundant, often angular, pebbles of quartzite, vein-quartz, granite, siltstone, metamorphosed quartz-wacke and laminated quartzite.

These rocks are lithostratigraphically correlated with the Lower Parmeener Super-Group (Pu on the map).

Tomahawk Point and Tomahawk Island [638767]

Well-sorted, medium-grained, micaceous quartz sandstone is exposed on the shore platform on the eastern side of both Tomahawk Point and Tomahawk Island. The beds are well laminated and show development of large-scale cross-bedding, with individual troughs up to three metres across and 0.2 m deep. These rocks are lithologically correlated with the Upper Parmeener Super-Group.

Mayfield Flat area [835716]

East of Mayfield Flat are a variety of lithological units which include pebbly siltstone, pebbly sandstone, medium to coarse sandstone, quartz grits and lithic sandstone. All rocks are unfossiliferous. One and a half kilometres east of these rocks on the Eddystone sheet M.J. Clarke has recovered *Eurydesma* from rocks of similar lithology. This probably indicates that the rocks of this area belong to the lower parts of the Lower Parmeener Super-Group.

Red Hills

Intruded by dolerite at 832772 is a small outcrop of coarse, well-sorted quartz sandstone with some isolated clasts of quartz, slate and granite. Because of the coarse nature of the rock it was not clear whether the isolated clasts were dropstones or not. For this reason the rock is assigned to the Parmeener Super-Group, undifferentiated.

Cape Portland

Excavations of waterholes west of the homestead at Cape Portland [825855] has exposed cross-bedded quartz sandstone that has been referred to as Tertiary in age (Jennings and Sutherland, 1969). The sandstone is well lithified and often micaceous. Rare clay pellets occur. Bedding is sometimes defined by concentrations of heavy minerals. The well developed cross-bedding gives the rock a flaggy appearance. On lithological grounds these rocks are correlated with the Upper Parmeener Super-Group of other parts of Tasmania.

Mt Littlechild *(MPM)*

A poorly-sorted conglomerate with sub-rounded quartz pebbles (60 mm) set in a quartz-rich matrix occurs on the east side of Mt Littlechild [818313] associated with a coarse quartz-rich sandstone. It seems probably that these rocks belong to the Parmeener Super-Group.

TERTIARY

A.V. Brown
W.R. Moore
P.W. Baillie

Non-marine deposits *(PWB)*

The Tertiary sediments are difficult to map as they are generally poorly exposed throughout the region. Often the existence of these moderately to weakly consolidated deposits is recognised largely by the distribution of rounded quartz gravel float. Careful extension of mapping of Tertiary deposits away from areas of relatively good exposure generally reduces difficulties. Problems are caused by the lack of dateable material and lithological marker beds. These problems increase where the sediments appear to be thin and are overlain by, or are close to, Quaternary sediments. For example the quartz gravels of coastal and nearby areas of low relief which are similar in lithology are Quaternary in age as they can be shown to have been deposited over marine terraces (*e.g.* Qrg on the Pipers River Sheet). Elsewhere inland, similar gravels have been encountered in drill holes that have penetrated Tertiary sediments. In areas marginal to those of such undoubted Tertiary deposits their age is uncertain as they may be lag deposits, reworked Tertiary or primary Tertiary sediments.

Tertiary sediments cover about one half of the area west of the Billycock-Kamona-Williams Hill ridge (*WRM*). Most of these sediments are found in an extensive area north of Scottsdale with isolated areas to the south in the upper Great Forester River and its headwater tributaries. East of the ridge, a narrow arcuate area of Tertiary sediments extends from south of the Ringarooma township to south of Mount Cameron and this is associated with small isolated areas in the upper reaches of the Wyniford River. Other isolated areas occur to the east of the Tomahawk River, around Martins Hill and in the upper reaches of the Boobyalla River.

The western area is underlain by a large basin in which two major leads have been found (Moore, *in prep.*). This basin, the Scottsdale Basin extends north beneath the marine terrace of the coastal plain. On the coastal plain the Tertiary sediments are not exposed as they are overlain by a cover of Quaternary sediments, but they have been recognised by their distinct lithology in a series of water bores drilled along the coastal plain, west of the Great Forester River to the granodiorite-Mathinna Beds contact on the Bulger Hills-Toddy Plain ridge (*WRM*).

Beneath the Quaternary sedimentary cover two deep leads within the Scottsdale Basin (Leaman and Jordan, 1971; Moore, *in prep.*) join 2km south-east of the granodiorite hill [445610] on the Bridport and Waterhouse Road. The eastern margin of this outlet approximates to the western margin of the Ringarooma-Boobyalla Sheet and is 2 km wide; having an average depth along the Waterhouse-Bridport road of 60 m of dominantly Tertiary sediments; and runs in north-westerly direction for 3-4 km from the junction of the two leads towards the coast.

In contrast, to the east, the Ringarooma-Mt Cameron area (*AVB*) is underlain by a confined valley system with a small terminating basin (see Economic Geology). The smaller isolated areas around the Tomahawk and Boobyalla Rivers are valley systems which drained to the north.

Over the entire region the Tertiary sediments are remarkably similar in lithology. They consist of a sequence of angular quartz granule gravel (grits), quartz sand, and buff-white clay with some local basal conglomerate, river gravel or mudstone.

In the Mt Cameron Basin-Lead system (*AVB*) basal units are of dominantly conglomerate or coarse gravel (up to 20 m thick) composed of rounded cobbles and pebbles derived from granitic rock, vein quartz and metamorphosed Mathinna Beds, in a matrix of angular granule gravel, coarse quartz sand and clay. Overlying the basal units are irregular, interbedded and interdigitating beds and lenses of angular granule gravel, very coarse sand, sand and clay. The most common occurrences are units of glassy quartz, granule gravel with a matrix of sandy clay, interbedded with very coarse sand lenses, sand and clay lenses, and clay lenses.

In the Pioneer and Hasties open-cuts (*AVB*) there are excellent exposures of these Tertiary sedimentary units, which include lenses of cross-sectional dimensions ranging from 100 m x 30 m of thick buff coloured clay to 150 mm x 25 mm of coarse sand and granule gravel.

In lower parts of the sequence occasional carbonaceous horizons occur, and in some areas these horizons are partially altered to coal whereas in other places they are replaced by marcasite. Such carbonaceous horizons are exposed in many of the tin mining sluicings and open-cuts throughout the region (for example Pioneer, Hasties and Mt Stronach mines).

The thickest sequence of Tertiary sediment encountered in a drill-hole in the Ringarooma-Mt Cameron system is 123 m on the Herrick-Boobyalla road [742543]. (Appendix 1 Drill hole 7).

Sediments within the Ringarooma-Mt Cameron system contain microflora that have been correlated with those of marine Longfordian Age, Early Miocene (Harris, 1968). Harris collected samples from six different localities - Branxholm, Wood's Property, Endurance, Anchor Hill, New Edina Pit and from the Great Forester River in the Mount Stronach area (assumed to be the Mt Stronach mine).

The Tertiary sediments found between the Boobyalla and Little Booby-alla Rivers (*NJT*) are lithologically similar to the sediments found in the Ringarooma-Mt Cameron lead and basin system. The greatest proven thickness in this area is 60 m (drill hole 6 (Jennings, 1968)).

In the upper reaches of the Boobyalla River (*NJT*) thin deposits of Tertiary sediment are exposed. These consist mainly of coarse-grained angular sand and granules with minor pebble horizons. The pebbles are of vein quartz and Mathinna Beds sediments. Large-scale cross-bedding is present in some sand units which outcrop with 1-2 m horizons of silty and sandy clay with sand and gravel lenses.

Thin residual deposits of Tertiary sediments occur east of the Toma-hawk River. These sediments consist dominantly of pebbly sands, sandy gravels, and gravels of vein quartz and Mathinna Beds sediments.

There are very few exposures of the Tertiary sediments in the Scotts-dale Basin (*WRM*) and these are confined mainly to the southern margin of the basin. The two best exposures in the area are the Mt Stronach and Hayes open-cut mines near the Great Forester River. The sediments exposed are similar to those of the Ringarooma-Mt Cameron system (*i.e.* exposed in the Pioneer, Endurance and Hasties open-cuts).

In spite of the intensive drilling undertaken, no detailed litho-logical correlation of individual lithostratigraphic units has been possible within the Scottsdale Basin. In a few specific areas recognisable basal lithological units of conglomerate, coarse river gravel, coarse sand or micaceous mudstone overlie the granite basement. Beds of quartz gravel, fine quartz sand, and white clay with rare carbonaceous bands have been found higher in the Tertiary sequence. For much of the area the Tertiary sediments merge into the underlying deeply chemically weathered granite where no precise boundary can be recognised from drill cuttings. There is a transitional zone, often up to 30 m thick, in some of the drill holes, particularly in the eastern part of the Scottsdale Basin.

Overall there is a general increase in the clay content of the Tertiary sediments, both as separate lenses and mixed with the quartz granule gravel and coarse sand, towards the southern margin of the Scottsdale Basin. There is a higher percentage of clay within the Tertiary sediments of the basins in the upper Great Forester River. On the western margin of the basin at Springfield drilling encountered a 64 m sequence of soft micaceous mudstone lithologically similar to the mudstone found at the base of the Tertiary sequence in two localities in the Scottsdale Basin (Moore, in prep.).

The total proved thickness of the Tertiary sediments in the Scottsdale Basin is 225 m and in the two smaller isolated basins at Tonganah and

Springfield in the upper Great Forester River area it is 58 and 76 m, respectively.

Ferricrete horizons occur at the Tertiary sediment-basalt interface at Bulgers Hill, near the eastern margin of the Scottsdale Basin, North Scottsdale (*WRM*) and around Winnaleah (*AVB*). Ferricrete and derived lag forms a surface cap above the Tertiary sediments resulting in flat-topped hills, through the Scottsdale Basin and in the area of the Ringarooma-Boobyalla Rivers. The formation of the ferricrete horizon is considered to be due to iron enrichment and cementation of Tertiary sediments during weathering and removal of the overlying basaltic rock (*AVB,WRM*), which is thought to have covered most of the Scottsdale Basin and the basin to the south of Mt Cameron.

Small outcrops of silcrete (greybilly) occur sporadically throughout the quadrangles, often forming small isolated ellipsoidal hills (*e.g.* Sugar Rock HIll (*WRM*), 489478) or low ridges (*e.g.* west of the Pioneer-Mt Cameron road (*AVB*)). In other areas silcrete forms flat pavement outcrops (Tuckers Creek, Red Quarry and Walpole Creek areas (*WRM*). In some areas the silcrete is in close association with granitic rocks whereas in other areas they form surface horizons above the Tertiary sedimentary sequence.

An elongate tracer of Tertiary gravels and sands occur in the White Rock area [680640] (*PWB, NJT*) extending northwards in a NNE direction. Good exposures are seen in the old mine workings at White Rock where there are up to 10 m of well sorted quartz gravel, coarse quartz sand and some clay horizons. A Quaternary microflora has been identified from this locality (Harris, 1968) although no further information is given as to the exact site from which the sample was obtained. The sample could have come from a horizon at or near the surface. On lithological grounds these deposits are considered to be Tertiary.

Diamond and rotary drill holes [770701] have penetrated over 400 m of Cretaceous and Cainozoic sediments. The Cretaceous sediments (Appendix 7) consist of poorly sorted boulder conglomerates which contain dolerite boulders boulders several metres in diameter, pebble conglomerate and poorly sorted medium- to coarse-grained ferruginous sandstone. Clast lithologies include dolerite, Mathinna Beds slate, quartzite, sandstone and a purplish siltstone. The sequence is interpreted as having been rapidly deposited on an active fault scarp (*PWB, WRM*).

The sequence drilled is dominantly a coarse conglomerate, with boulder, cobbles and pebbles of dolerite and cleaved mudstone and dirty sandstone pebbles of Mathinna Beds. Pebbles of Precambrian quartzite, siltstone and silty sandstone of Permian sediments as well as sandstone of Triassic age are not uncommon. Massive soft fine white sandstone and soft grey and black organic mudstone, sometimes with wood fragments, are lithologically different to the Tertiary sediments encountered and described elsewhere from the region; their age is unknown.

From shallow water bore and tin exploration drilling it is now known that these conglomeratic sediments extend beneath a cover of Quaternary sediments under the Boobyalla Plains to the mouth of the Boobyalla-Ringarooma Rivers and extend east to the Great Northern Plains where dolerite crops out (Moore and Leaman, 1974; Braithwaite, 1977). They are deposited in a narrow WNW-ENE trench which has the dolerite of the Ringarooma Tier as its northern boundary and a ridge of Permian sediments

as its eastern boundary. Isolated dolerite and the granite and Mathinna Beds north of Mt Cameron form the southern boundary (*PWB*). The western boundary is in Ringarooma Bay. Contacts, where drilled, are very steep (Moore and Leaman, 1974).

On the northern flanks of Mt Cameron several Tertiary leads occur (*SFC*). These deposits overlie deeply weathered granitic rocks and are composed of sub-rounded boulders or pebbles of quartz in a clay and sand matrix. These basal deposits are overlain by crudely stratified conglomerate composed of rounded quartz pebbles, and sand and clay horizons. Isolated outcrops on the tops of knolls south of the Ringarooma River attest to the former presence of an extensive mantle of Tertiary sediments.

A further Tertiary Valley, infilled with sediments and basalt occurs in the Cape Portland area (*PWB, WRM*). Two water bores were drilled, one of which [834853] drilled 44 m of basalt and bottomed in Mathinna Beds sediment. The other hole [840850] drilled through 1.5 m of fine sand; 14 m of sandy clay, thought to be Quaternary sediments; into basalt-derived clay, deeply weathered basalt and Tertiary clay to a depth of 55 m. These basalts are part of a complex series of basalt Tertiary sediment filled valleys or basins that extend south as far as Rushy Lagoon-Targetts Flat in the neighbouring Eddystone sheet beneath Quaternary sediment cover.

Marine limestone *(PWB)*

Scattered float of marine limestone occurs over a small area in a paddock north of the homestead at Cape Portland [829879]. It is light grey in colour, thinly bedded and contains very abundant ostracads and rare foraminifera. A lagoonal or shallow water origin is suggested. Its age is Late Oligocene/Early Miocene (Quilty, 1972) which corresponds to the major marine transgression following terrestial sedimentation in Bass Basin (Robinson, 1974; Brown, 1976).

QUATERNARY

P.W. Baillie

Quaternary deposits of the region include fluviatile, aeolian, slope and marine deposits. Table 1 is a provisional stratigraphic framework of the Quaternary of the region.

Quaternary deposits of the Boobyalla and Ringarooma Quadrangles fall conveniently into three broad groups - coastal, slope, and fluvial deposits.

Coastal deposits

Mapping near the coast has involved the investigation of large areas covered by superficial deposits. The geomorphology, stratigraphy and pedogenesis of these sediments have been studied with a view to understanding the Quaternary history of the area.

The deposits have been subdivided into four units:

Younger aeolian dune sand, beach sand and gravel	Qhb (Boobyalla)	Qpu (Boobyalla)
Talus	Qpt (Boobyalla)	
	Qt (Ringarooma)	
Older aeolian sand	Qpo (Boobyalla)	
	Qw (Ringarooma	
Clay, sand, minor peat and gravel, sometimes with	Qpc (Boobyalla)	
marine shells and transported fragments	Qm (Ringarooma)	

Table 1. QUATERNARY DEPOSITS

Series	Holocene	Pleistocene	
		Last Glacial	Last Interglacial
Soils	Minor leaching, peat formation	Strong podsol, groundwater podsol development	?Palaeosol at Sheepwash Creek
Marine and related deposits	Beach sands, gravels		Sand, clay, minor peat and gravel
Aeolian	Dune sand	Lunette formation Dune sand: sheets and longitudinal dunes	
Talus and slope deposits		Talus, slope deposits	
Fluviatile/ Alluvial	Alluvium and related deposits		

Clay, sand, minor peat and gravel

The upper surface of this unit forms a gently seaward-sloping plain with a maximum height of about 40 m above present sea level. The unit consists of flat-bedded sand of variable lithology overlying Tertiary and older rocks in coastal areas.

Thickness varies from 14 m to less than one metre. The lithology ranges from well sorted coarse quartz sand, through finer sand and poorly-sorted sandy clay to occasional beds of clay. The sand show variable sorting from good to poor and exhibit rapid vertical and horizontal variation. The best sections are observed in overdeepened drainage ditches at Barooga [490680], Carisbrooke [660706] and West Wyambi [690672] properties.

Drilling of this unit at Leedway [594714] showed the presence of rounded, thick, fragmental mollusc shells in a very coarse quartz sand (*PWB*). Fragmented thick shelled marine molluscs at various horizons were found in several drill holes on the Koreen, Deepwater, Marengo and Jetemby properties (*WRM*).

Within this unit, but having unknown stratigraphic relationships, is a small body of freshwater marl. It occurs at Waterhouse Point [464774] at a height of about 32 m above sea level. The thickness is less than 2 m and the rock consists of small-shelled gastropods and bivalves in a clayey calcareous matrix. Foraminifera are absent. Very fine detrital quartz makes up less than 2% of the rock.

Older aeolian sand

This unit overlies the above unit, Tertiary sediments, and basement rocks and consists of well-sorted, fine- to medium-grained sand (often calcareous when fresh) that sometimes shows high angle cross-bedding. The most common soil type developed on the sand is a mature podsol, which con-

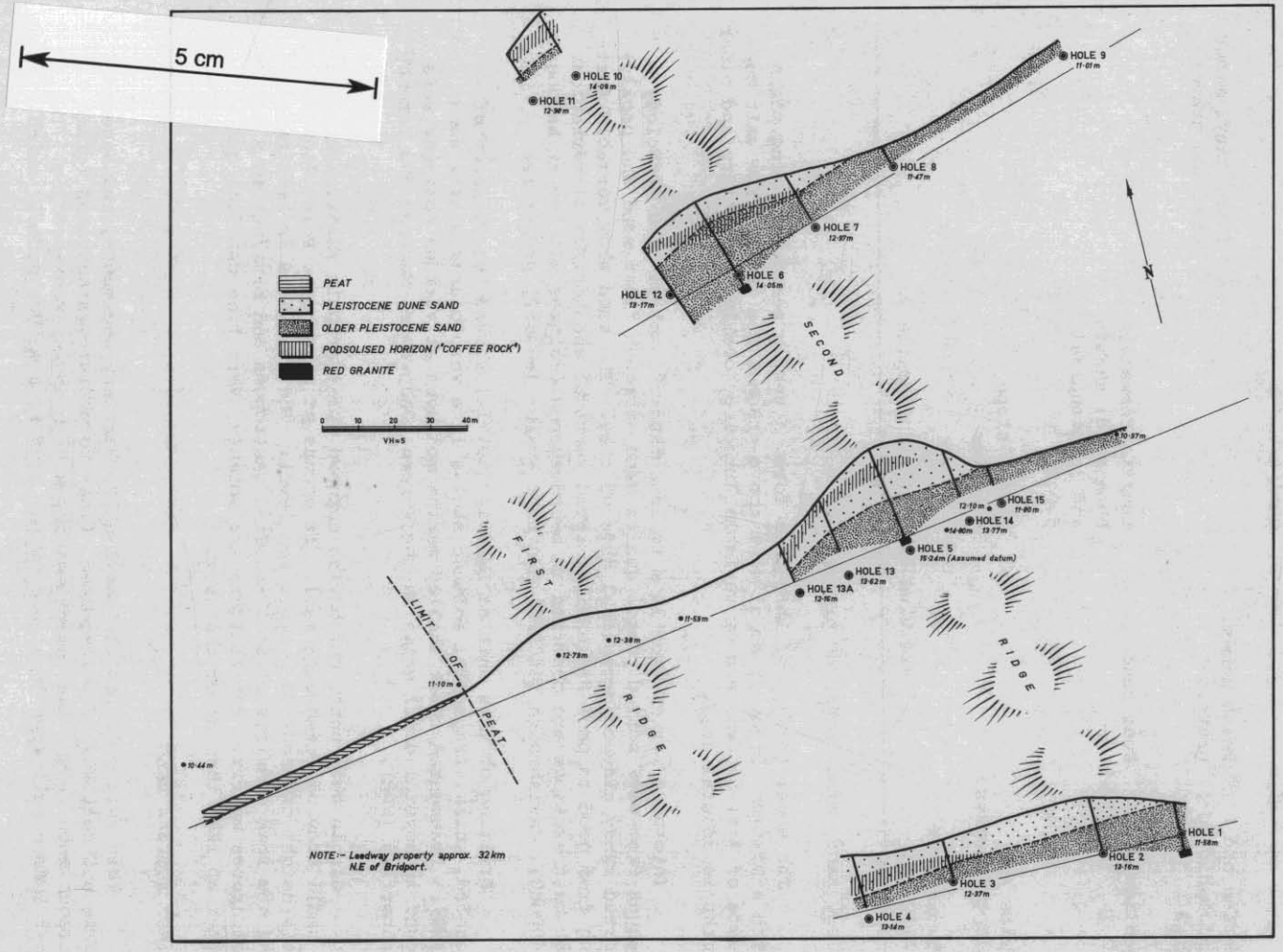

Figure 3. *Sections across a double lunette on the Leedway property, approximately 32 km north-east of Bridport.*

sists of a dark, humic rich A1 horizon, a bleached A2 and an orange-yellow coloured iron-enriched B2 horizon. The profile may be up to two metres thick.

In areas where internal drainage is poor a groundwater podsol may develop. This has a thicker A1 than the normal podsol, a thinner A2 and a very thick B2, usually dark brown in colour due to enrichment by humates and iron oxides. The B2 horizon ('coffee rock') may exceed three metres in thickness.

In the lower parts of Sheepwash Creek [524711] older aeolian sand (Qpo) with high angle cross-bedding overlies clayey sand and coarse sand (Qpc). Cross-bedding relationships within the dune sand indicates that some erosion of the dunes has occurred. The contact is not absolutely clear but it appears that the dune sand overlies rather than is interbedded with the coarser sand. Within this contact zone is a problematical lenticular organic horizon. Further investigation should resolve whether it is a palaeosol developed on the older sand before deposition of the dune sand or a peat accumulation within the dune sand.

The older aeolian sand occurs as three main morphological types. The dominant form is a series of WNW-ESE trending parabolic blowout or longitudinal fixed dunes. Some of these dunes are shown on the Boobyalla map. Sheets and subdued dunes of older aeolian sand extend for several kilometres draped over higher bedrock areas and may attain elevations of 200 m (*PWB, NJT*).

Younger than the dunes and also showing strong soil development are a series of lunettes. They are developed on both dune and underlying coarser sand. No clay lunettes have been found. A double lunette was drilled at Leedway [594714] and the results (fig. 3) show that it was formed on a pre-existing irregular surface on the older, coarser sand.

Because both the dune sand (Qpo) and the older sand and clays (Qpc) are usually only seen on the ground as grey clayey sand they are normally shown on the Boobyalla map as undifferentiated Qpu.

Younger aeolian dune sand, beach sand and gravel

These sands are the youngest of the coastal deposits and consist of dune and beach sand.

The dune sand consists of very well-sorted, fine- to medium-grained calcareous sand. At the western end of Little Waterhouse Lake they stratigraphically overlie older aeolian sand. The dunes consist of mainly parabolic and transverse forms. They show little, if any, soil development. The maximum development observed is leaching of carbonate from the upper 300 mm. Carbonate rhizomorphs are common in recently deflated areas.

Aboriginal artifacts have been found at several localities associated with deflation hollows in the dunes.

Beach sand associated with the present beaches ranges in grain size from fine sand to cobbles.

Shingle ridges formed by storm action reach heights in excess of 5 m above the high water mark in the Cape Portland area.

Slope deposits

Slope deposits are common in areas underlain by Mathinna Beds (*NJT*). Stratified deposits consisting of alternating layers of coarse and fine angular fragments are exposed in some artificial cuttings. Dip is generally sub-parallel to the general slope. A fine-grained matrix is present in some horizons. In natural settings the character of slope deposits is obscured by a soil profile.

In the Ringarooma Quadrangle slope deposits have been mapped north of Kamona [570460] and at Trig Hill [590565] (*NJT*). In these areas detritus derived from Mathinna Beds sediments has moved downslope from areas underlain by the parent rock type over areas underlain by granitic rocks and Tertiary sediments. North of Kamona the downslope movement is up to about one kilometre. Drilling at several localities indicated the presence of up to 10.5 m of slope deposits. A small component of quartz granules of granitic origin is present in the slope deposits on the eastern side of Trig Hill.

Apparently interbedded with the older aeolian sand at Little Waterhouse Lake [512751] is a deposit consisting of angular, oriented, slabs of dolerite, ranging in size from 20 mm to 500 mm, in a sand/clay matrix. These have been called Pleistocene gelifluction deposits (Bowden, in Colhoun, 1975). While this may be possible it must be borne in mind that all dolerite outcrops in the area are very closely jointed and would yield small slab-like fragments which would orient themselves on moving downhill regardless of the process involved. Although the deposit may not be a gelifluctate it must have formed at a time when the vegetation was much sparser than at present.

Similar dolerite talus occurs at Cape Portland [846843] and on the eastern side of Waterhouse Island [533824].

Fluvial deposits (Ga, Qha)

Areas of river alluvium, swamp and marsh deposits have been mapped mainly on the basis of morphology. They are relatively level areas, generally adjacent to water-courses. Boundaries shown on the maps correspond generally with breaks of slope on the edge of such areas.

The alluvium usually consists of an organic rich soil underlain by clay and clayey sand or gravel. Very few vertical sections were observed.

At Banca [675582] 4 m of sediment consists of angular to sub-rounded quartz particles up to 20 m in a yellow clayey matrix. Occasional well-sorted bands of coarse sand are present.

The Boobyalla River east of Banca is a misfit, as are many other streams throughout the region, and it appears likely that deposition of sediments took place under a wetter climate than the present.

Large areas of alluvium occur near the mouth of the Ringarooma River. Within this area swamp and flood plain deposits are common.

Discussion

Grain size parameters for the various sediment types are shown in Figure 4 . The various dune sands are very similar whereas the oldest unit (Qpc) is a mixture of various lithologies.

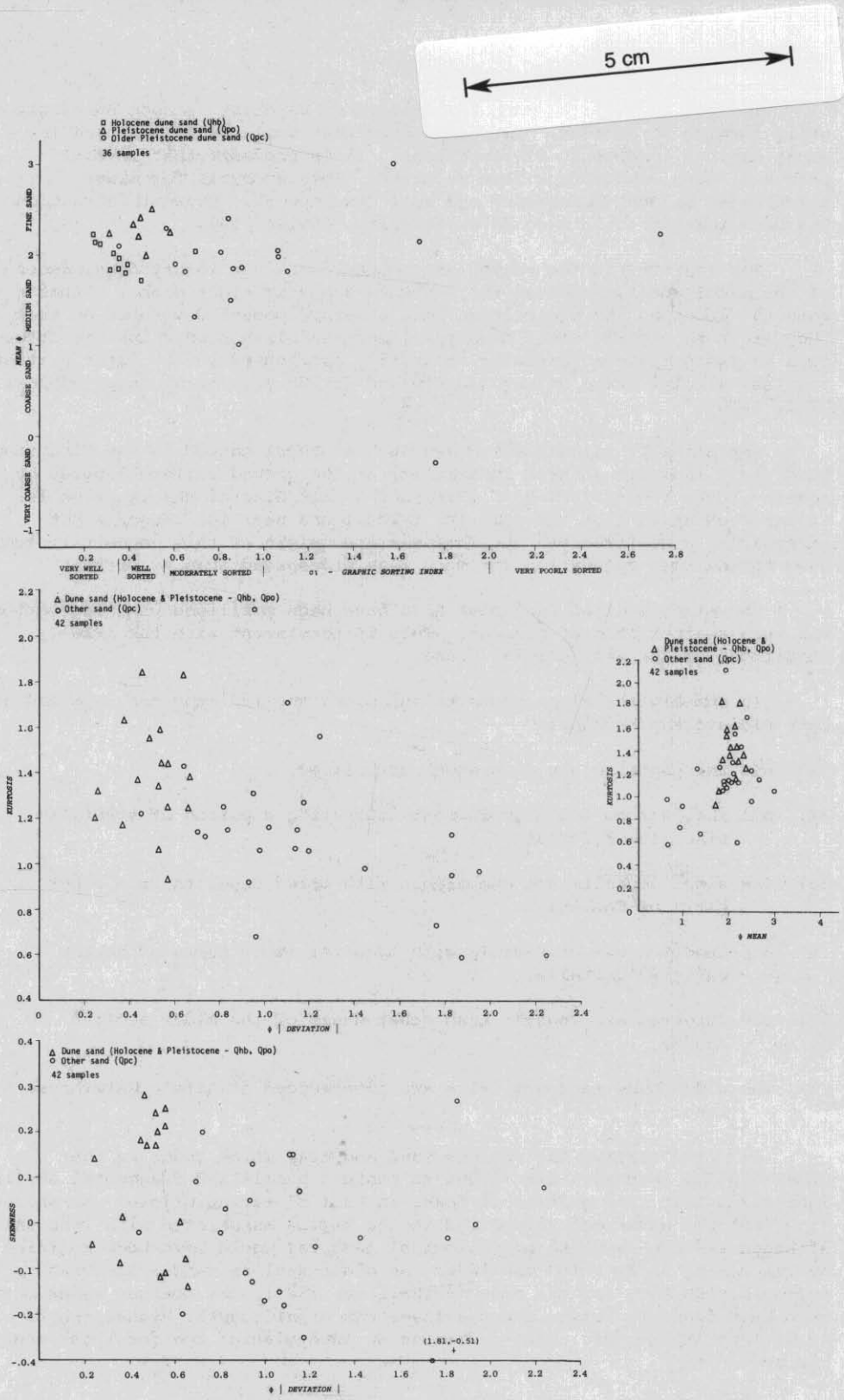

Figure 4. *Grain size analysis of Quaternary sands.*

The younger aeolian sand is regarded as Holocene because dunes are still forming at present. The sand shows weak soil development and the dunes exhibit immaturity of topography. It is probable that several phases of dune development have occurred. This accounts for minor differences in dune topography and soil development. Blowout initiation has been related to burning or overgrazing (Davies, 1965).

The lunettes in the region are younger than the longitudinal dunes of the older aeolian sand as the lunettes transect older dunes. Since both the lunettes and older dunes have a mature podsol developed on them they are both clearly older than the younger aeolian sand. Lunette formation in south-eastern Australia is usually attributed to the later part of the last glacial stage between 10 000 and 26 000 years b.p. (*e.g.* Bowler, 1971, 1976).

Rhythmically stratified screes such as those mapped in the Ringarooma Quadrangle indicate general instability of the ground surface induced by severe winter frosts (Colhoun, 1978) and a Last Glacial age is probable. It has been shown that the dolerite talus found near the coast is not necessarily a gelifluctate but whatever the origin of this deposit it must have formed when vegetation was much less widespread than at present.

The older aeolian sand must also have been mobilised when vegetation was much sparser than at present. This is consistent with the arid conditions of the Last Glacial stage.

In summary the slope deposits and older aeolian sand are regarded as Late Pleistocene because:

(1) All the deposits are at present stabilised,

(2) All show strong soil development indicating a period of stability since their formation,

(3) The slope deposits are comparable with dated deposits from other parts of Tasmania,

(4) The lunettes are comparable with those of other parts of south-eastern Australia,

(5) The lunettes are younger than other dunes of the older aeolian sands,

(6) The older dune sand and talus are interbedded at Little Waterhouse Lake.

As noted earlier the coarser sand and clay which underlie the older aeolian sand have been found to contain shells and fragmental shells, indicating that this unit is at least in part of marine origin. No shoreline features have been recognised in the region associated with this unit, although any pre-existing morphological features would have been modified by the strong winds which mobilised the older aeolian sand. Assuming tectonic stability for the area (Sutherland, 1973), the coarser sands must have been deposited while the sea level was significantly higher (up to 40 m) than at present. This indicates an Interglacial age for these sediments.

IGNEOUS ROCKS

DEVONIAN GRANITIC ROCKS

PETROGRAPHY AND FIELD CHARACTERISTICS

Introduction and classification

The Nockolds (1954) classification has been used in this report. The correspondence between the divisions and names used in this classification and that proposed by Streckeisen (1967) is given in Table 2 . Mineral proportions were almost entirely estimated visually and felspar compositions determined by the Michel-Lévy method. A small number of model analyses from the region are listed in Groves (1977) and Baillie (1973). Due to the uncertainty inherent in these methods all non granodiorite bodies have been referred to in the map legends as granite/adamellites and subdivision has been based on grain size, mica type and quantity and phenocryst type, these being features that could be recognised in the field. Rocks in which muscovite could generally be recognised in hand specimen were described as muscovite rocks and as minor muscovite if it could only be recognised in thin section. In Table 3 the keys for the granitic rocks from the Ringarooma and Boobyalla Sheets are reproduced. Attention is drawn to several symbols defined in the Boobyalla Key not appearing in the Ringarooma Key.

Table 2. COMPARISON OF THE CLASSIFICATIONS OF NOCKOLDS AND STRECKEISEN FOR GRANITIC ROCKS

% alkali feldspar in total modal feldspar	Nockolds (1954) classification used in this report	Streckeisen (1976) classification
90	Alkali granite	Alkali granite
	Calc-alkali granite	Syenogranite
60		
	Adamellite	Monzogranite
40		
	Granodiorite	Granodiorite
10		
	Tonalite	Tonalite

Chemical analyses have also been used to discriminate between different granite types. It was found that a Ti/10-Rb-Sr triangular diagram (fig. 5) allowed a division of granitic rocks from the Blue Tier Batholith

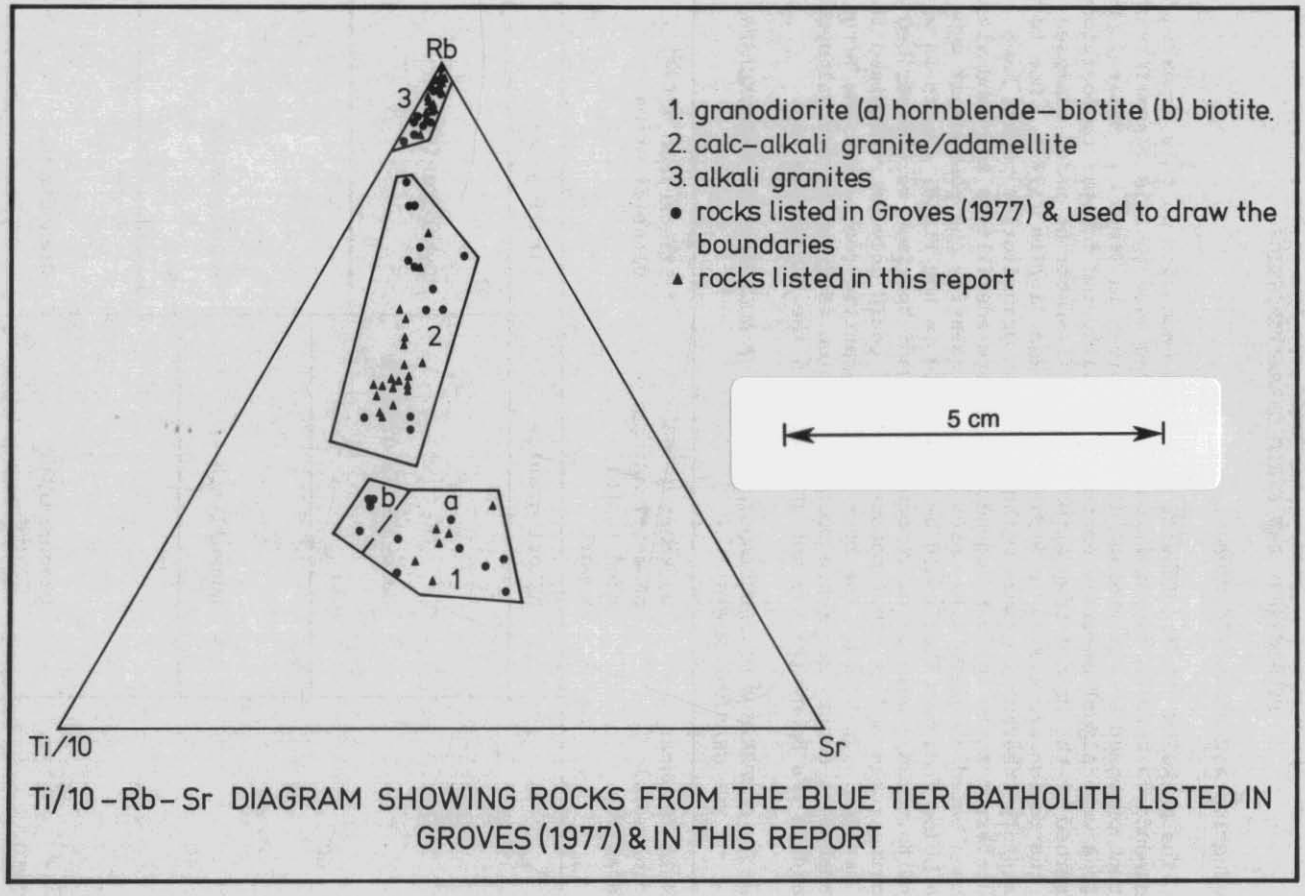
Rb
3
2
b
a
1
Ti/10
Sr
1. granodiorite (a) hornblende–biotite (b) biotite.
2. calc–alkali granite/adamellite
3. alkali granites
• rocks listed in Groves (1977) & used to draw the boundaries
▲ rocks listed in this report
5 cm
Ti/10 – Rb – Sr DIAGRAM SHOWING ROCKS FROM THE BLUE TIER BATHOLITH LISTED IN GROVES (1977) & IN THIS REPORT

Figure 5.

Table 3. DEVONIAN GRANITIC ROCK SYMBOLS USED FOR THE BOOBYALLA AND RINGAROOMA SHEETS

BOOBYALLA SHEET

MINOR GRANITE INTRUSIONS

Dm	Quartz-feldspar porphyry (Dmpb), aplite (Dma), quartz-muscovite rocks (Dmq), fine-grained granite/adamellite (Dmg), coarse-grained granite (Dmd), garnetiferous quartz-feldspar porphyry with minor medium-grained dolerite of unknown age (Dmpg), quartz-orthoclase-tourmaline pegmatite (Dmc).

MAJOR GRANITE INTRUSIONS

SCOTTSDALE BATHOLITH

Dsg	Biotite-hornblende granodiorite.

BLUE TIER BATHOLITH

Dbag	Porphyritic, fine- to coarse-grained garnet-bearing biotite-muscovite granite/adamellite (Dbag).
Dbau: Dbaem	Dominantly fine- to medium-grained granite/adamellite (Dbau); equigranular, dominantly medium-grained, biotite-variable muscovite granite/adamellite (Dbaem); porphyritic fine- to medium grained biotite-muscovite (Dbapq, Dbapf) and biotite-minor muscovite (Dbapq´, Dbapsf´) granite/adamellite (1) with phenocrysts of feldspar and rounded quartz (Dbapq, Dbapq´) (2) with phenocrysts of feldspar (Dbapf), sparse phenocrysts (Dbapsf´).
Dbau: Dbapq/Dbapq´	
Dbau: Dbapf/Dbapsf´	
Dbapc/Dbaps	Porphyritic, coarse-grained biotite and biotite-minor muscovite granite/adamellite (Dbapc), sparsely porphyritic to equigranular (Dbaps).
Dbg/Dbb	Biotite-hornblende granodiorite (Dbg-near EQ690735), biotite granodiorite (Dbb). Areas of float and small outcrops of granodiorite and hornfelsed Mathinna Beds indicated by decoration on Dbb, Dbg.

RINGAROOMA SHEET

MINOR GRANITIC INTRUSIONS

Dm	Quartz-feldspar porphyry (Dmp); aplite (Dma); fine-grained granite/adamellite, equigranular (Dmga), porphyritic (Dmgp); garnetiferous quartz-feldspar porphyry (Dmpg); quartz-orthoclase pegmatite (Dmc).

MAJOR GRANITIC INTRUSIONS

SCOTTSDALE BATHOLITH

Dsau: Dsac	Biotite adamellite (Dsau). Coarse-grained, pink, biotite adamellite (Dsac).
Dsau: Dsam	Medium-grained, pink, biotite adamellite (Dsam).
Dsau: Dsah	Coarse-grained, pink, hornblende-biotite adamellite (Dsah).
Dsau: Dsaw	Medium- to coarse-grained, sparsely porphyritic, white biotite adamellite (Dsaw).
Dsg	Biotite-hornblende granodiorite (Dsg).

BLUE TIER BATHOLITH

Dbau: Dbae	Equigranular, fine- to coarse-grained, biotite-muscovite granite/adamellite (Dbae).
Dbau: Dbap: Dbapq	Porphyritic, fine- to medium-grained, biotite-muscovite granite/adamellite (Dbap). (1) with phenocrysts of feldspar and rounded quartz (Dbapq); (2) with phenocrysts of feldspar (Dbapf) - locally coarse-grained porphyritic (Dbapp).
Dbau: Dbap: Dbapf	
Dbau: Dbap: Dbapp	
Dbapc: Dbapcc	Porphyritic, coarse-grained biotite and biotite-minor muscovite granite/adamellite (Dbapc); coarse- to very coarse-grained variety (Dbapcc); variety with >2% muscovite (Dbapcm).
Dbapc: Dbapcm	
Dbg	Biotite-hornblende granodiorite (Dbg).

Table 4. MAJOR GRANITIC BODIES OF THE BLUE TIER BATHOLITH (GROVES, 1977) AND GRANITE TYPE SYMBOLS USED IN THIS REPORT

Groves (1977)		Symbols of granite types used in this report falling within the body												
Rock body name	Rock type	Dbg	Dbapc	Dbapcc	Dbapcm	Dbau	Dbaps	Dbapq	Dbapq'	Dbaf	Dbasf'	Dbapp	Dbae	Dbaem	Dbag
Pyengana Pluton	Hornblende-bearing granodiorite	x													
Poimena Pluton	Porphyritic biotite granite/adamellite with fine- to medium-grained groundmass		x	x	x					x					
Boobyalla Pluton	Garnet-bearing medium- to coarse-grained biotite-muscovite granite/adamellite														x
Sheoak Hill Pluton	Foliated fine- to medium-grained biotite-muscovite granite/adamellite													x	
Little Mt Horror Sheet	Medium-grained biotite-muscovite granite, medium-grained biotite adamellite, aplite quartz porphyry and microgranite					x									
Mt Cameron Sheets	Medium- to coarse-grained biotite granite/adamellite, minor porphyritic biotite granite/adamellite, biotite muscovite granite/adamellite greisenised granite greisen veins						x	x	x	x	x		x		

Table 4. (continued)

Groves (1977)		Symbols of granite types used in this report falling within the body												
Rock body name	Rock type	Dbg	Dbapc	Dbapcc	Dbapcm	Dbau	Dbaps	Dbapq	Dbapq'	Dbaf	Dbasf'	Dbapp	Dbae	Dbaem	Dbag
Mt Paris Mass	Medium-grained biotite granite/adamellite, biotite-muscovite granite/adamellite, greisenised granite and greisen veins, biotite-muscovite granite porphyry					x		x					x		
Lottah Sheets	Medium-grained biotite granite/adamellite, biotite-muscovite granite/adamellite, greisenised granite and greisen veins, biotite-muscovite granite porphyry							x		x		x	x		

into three main groups, granodiorite, calc-alkali granite/adamellite and alkali granite. The diagram boundaries are drawn on the basis of the classification of analysed rocks listed in Groves (1977). These three groups may correspond with three phases of intrusive activity with the granodiorites having been intruded first and the alkali granites last (see Gee and Groves, 1971).

The rocks of the Blue Tier Batholith have been divided into a number of petrological types forming various major bodies considered to be discrete structural entities by Gee and Groves (1971) and Groves (1977). This division suggests that each body was emplaced as a single mass. The divisions used in this report are without genetic implication and based only on petrological and chemical character of the granites. Table 4 lists the major bodies in the Ringarooma/Boobyalla region named by Gee and Groves (1971) and Groves (1977) together with the granite type symbols used in this report falling within the body.

K-Ar and Rb-Sr age determinations on the granitic rocks of the Scottsdale and Blue Tier Batholiths sampled at a number of localities within and outside the region indicate that they have a very similar age of emplacement (McDougall and Leggo, 1965). The K-Ar results for the Scottsdale Batholith were obtained from biotite and hornblende and yielded ages ranging between 363 and 377 Ma. The Rb-Sr dates of 373 Ma and 387 Ma obtained from two of the samples were considered to be in good agreement with the K-Ar values. The K-Ar results for the Blue Tier Batholith were obtained from biotite and range from 363 to 375 Ma. The Rb-Sr date of 389 Ma appears to be significantly older than the K-Ar ages and may indicate that some argon loss has occurred (McDougall and Leggo, 1965).

Biotite-hornblende granodiorite (Dsg). This rock type is a grey medium-grained seriate to sparsely porphyritic granodiorite that occurs widely throughout the Scottsdale Batholith (*NJT, SFC*). The phenocrysts of untwinned and partly altered potash feldspar appear to be of late origin. They are anhedral grains containing medium-grained inclusions of hornblende, biotite, plagioclase and quartz. Rounded margins on subhedral plagioclase inclusions, and lobate projections of potash feldspar into plagioclase indicate late replacement of plagioclase by potash feldspar. The presence of myrmekite at contacts between plagioclase and surrounding potash feldspar also indicates late replacement.

The groundmass consist of quartz, plagioclase, potash feldspar, biotite and hornblende (*NJT, SFC*). Biotite (<3 mm) is pleochroic from pale brown to very dark brown. It occurs as single flakes or in aggregates (5-10 mm). The biotite contains sparse zircon inclusions with metamict haloes and minor alteration to chlorite is present. Hornblende (<4 mm), which is pleochroic from pale green (α) through bright green (β) to brownish green (λ), occurs as anhedral to euhedral grains either singly or grouped with biotite grains. Biotite inclusions in hornblende are common. The plagioclase (<5 mm) often displays oscillatory zoning as well as simple and polysynthetic twinning. Many grains are at least partly saussuritised. The plagioclase determined by the Michel-Lévy method, is andesine. Biotite, hornblende, sphene and minor quartz occur as inclusions in plagioclase. Potash feldspar is a minor constituent of the groundmass and is intergranular to biotite, hornblende and plagioclase and contains inclusions of these minerals. Quartz (<5 mm) contains inclusions of plagioclase, hornblende and biotite. The sequence of crystallisation indicated by the textural relationship is biotite, hornblende, plagioclase, quartz and potash feldspar (*NJT*).

The granodiorite has a variably developed planar fabric defined by the elongation of quartz aggregates and alignment of mafic minerals (*NJT, SFC*).

Many quartz grains display undulose extinction, and less commonly deformation bands. Other evidence of post crystallisation ductile deformation is the presence of gently bent biotite plates and plagioclase twin lamellae (*NJT*).

Sparse angular, metamorphosed sandstone xenoliths (*SFC*) occur in the granodiorite chiefly in the Kamona-Tulendeena area [550420] but rounded to sub-rounded, or rarely, angular, melanocratic quartz diorite inclusions are more common with a wide range in size (20-300 mm in diameter). When rounded these xenoliths have oblate to flattened ellipsoidal forms with their shortest axis approximately perpendicular to the foliation in the host granodiorite. The longest axis of oblate ellipsoidal xenoliths shows a random distribution in the plane of the foliation. In places where the foliation in the granodiorite is not readily visible, rounded ellipsoidal xenoliths have no preferred orientation.

Medium to coarse-grained, sparsely-porphyritic, white biotite adamellite (Dsaw). This rock type is a white to light grey medium- to coarse-

---

* based on notes of N.J. Turner and S.F. Cox.

grained seriate to sparsely porphyritic biotite adamellite (*SFC, NJT*). The sparse phenocrysts are potash feldspar with minor perthitic intergrowths.

The groundmass consists of quartz, plagioclase, potash feldspar and biotite. Biotite (<2 mm), pleochroic from pale to dark brown contains inclusions of zircon and shows alteration to chlorite. It occurs as flakes, some of which are overgrown by fine-grained biotite. Subhedral zoned plagioclase (<10 mm) is partly saussuritised and has biotite inclusions. Some quartz grains (<6 mm) appear to be partly resorbed, penetrated, and enclosed in perthitic potash feldspar indicating that the latter has had a late growth. Crescentic and elongate rounded inclusions of quartz in potash feldspar may be exsolution or replacement features. Potash feldspar is present in equal or slightly greater proportion to plagioclase.

The textural relationships indicate the crystallisation sequence as biotite, plagioclase, quartz and potash feldspar (*NJT*).

A variably developed planar fabric is defined by the elongation of quartz aggregates and the biotite (*NJT*).

Coarse-grained, pink biotite adamellite (Dsac). This rock type is a distinctive pink equigranular, coarse-grained, biotite adamellite consisting of quartz, plagioclase, potash feldspar and biotite (*SFC*). The plagioclase (3-4 mm) is hypidiomorphic to anhedral, and often extensively altered with normal and oscillatory zoning. Quartz tends to show subhedral to rounded convex grain boundaries against potash feldspar, and the latter often occurs as thin selvages separating rational quartz grain boundaries. Potash feldspar (4-8 mm) is anhedral, with simply twinning and perthitic structures. Biotite (<2 mm) occurs as equidimensional subhedral to anhedral plates scattered through the rock.

Coarse-grained, pink hornblende-biotite adamellite (Dsah). This rock type is similar to the pink ?biotite equigranular, coarse-grained biotite adamellite (Dsac) except that it contains up to 7% prismatic hornblende (3 x 5 mm) (*SFC*).

The occurrence of this rock type south of Tulendeeena [555315] where it is in contact with granodiorite suggests that it has assimilated some biotite hornblende granodiorite and crystallised hornblende as a primary phase.

Medium-grained, pink, biotite adamellite (Dsam). This rock type differs from the pink coarse-grained biotite adamellite (Dsac) in hand specimen only by having a fine- to medium-grain size (*SFC*). However, a single chemical analysis of it (plot 74, table 5) shows a considerable difference from three analyses of the Dsac rock type (plots 72, 73, 75 table 5) and indicates that its composition is that of an alkali granite and not an adamellite (*MPM*). If this analysis is typical this body should be described as a biotite granite, not an adamellite.

Blue Tier Batholith

M.P. McCleneghan

Biotite-hornblende granodiorite (Dbg). This rock type occurs between 735405 and 755335 to the east of the Mt Paris area were it forms part of the Pyengana Pluton (Gee and Groves, 1971). Two other smaller areas are at 670550, south of Banca, and on the coast near 684736.

To the east of the Mt Paris area the rock is a grey, medium-grained

Table 5. CHEMICAL ANALYSES OF GRANITIC ROCKS

Plot No.	1	2	3	4	5	6	7	8	9	10	11	12
Analysis No.	735120	735121	735126	735127	735128	735129	735130	735131	735132	735133	735134	735135
SiO_2	64.5	65.7	73.5	75.0	74.7	75.8	74.3	75.2	74.6	74.9	75.3	75.1
TiO_2	0.67	0.53	0.37	0.07	0.06	0.09	0.08	0.09	0.08	0.08	0.08	0.07
Al_2O_3	14.3	14.4	13.1	13.5	13.5	13.7	13.2	14.1	13.2	12.9	13.1	13.1
Fe_2O_3	1.1	1.5	0.66	0.60	0.59	0.60	0.69	0.77	0.47	0.59	0.48	0.44
FeO	4.1	3.2	2.2	1.2	0.98	0.91	1.1	1.0	1.2	1.2	0.91	1.3
MnO	0.1	0.08	0.05	0.03	0.02	0.03	0.03	0.03	0.03	0.03	0.03	0.03
MgO	2.9	2.6	0.53	0.04	0.02	0.06	0.07	0.06	0.02	0.03	0.04	0.03
CaO	4.6	4.2	1.5	0.46	0.25	0.36	0.48	0.27	0.39	0.39	0.45	0.45
Na_2O	2.3	2.5	3.0	3.4	3.3	3.3	3.6	3.0	3.4	3.3	3.2	3.4
K_2O	3.1	3.3	4.1	4.3	4.6	4.2	4.0	4.3	4.2	4.4	4.3	4.5
P_2O_5	0.24	0.2	0.12	0.12	0.9	0.13	0.13	0.11	0.16	0.12	0.15	0.13
H_2O^+												
H_2O^-												
CO_2												
SO_3	<0.01	<0.01	<0.01	<0.01	<0.01	<0.01	<0.01	<0.01	<0.01	<0.01	<0.01	<0.01
Cl												
L.O.I.	2.1	2.3	1.0	1.3	1.2	1.5	1.6	1.6	2.2	1.4	1.4	1.4
Total	100.01	100.51	100.13	100.02	100.12	100.68	99.28	100.53	99.95	99.34	99.44	99.95
Trace elements (ppm)												
Li	40	60	65	160	160	240	160	245	290	235	260	205
Sn	<5	7	5	10	19	36	19	32	40	29	29	23
Rb	250	275	335	950	940	1040	920	1100	1150	1020	1080	1080
Sr	340	340	110	12	7	24	20	26	10	27	12	15
Y	34	35	70	50	50	55	50	50	50	55	55	50
Zr	175	100	200	55	55	60	60	55	60	60	60	55

Table 5. (continued)

Plot No.	13	14	15	16	17	18	19	20	21	22	23	24
Analysis No.	735136	735137	735138	735139	735140	735141	735142	735143	735144	735145	735146	735147
SiO_2	80.9	75.4	76.6	74.9	74.9	75.0	74.4	74.8	64.7	72.5	66.6	73.7
TiO_2	0.07	0.08	0.08	0.08	0.08	0.08	0.06	0.06	0.57	0.34	0.52	0.06
Al_2O_3	11.7	13.1	12.7	13.3	13.5	13.2	13.4	13.5	14.1	12.4	14.3	13.4
Fe_2O_3	0.68	0.36	0.87	0.50	0.63	0.44	1.3	0.51	0.50	0.29	0.98	0.42
FeO	0.98	1.3	0.91	0.91	1.1	1.2	0.52	1.3	4.1	2.5	3.6	1.4
MnO	0.02	0.03	0.04	0.02	0.04	0.04	0.01	0.03	0.09	0.05	0.08	0.04
MgO	0.12	0.05	0.03	0.03	0.03	0.03	0.03	0.03	2.4	1.3	2.1	0.02
CaO	0.24	0.44	0.42	0.18	0.15	0.38	0.34	0.44	4.4	2.9	3.9	0.51
Na_2O	0.05	3.2	3.1	3.1	3.0	3.2	4.2	3.6	2.4	2.1	2.4	3.0
K_2O	1.8	4.6	4.4	4.5	4.4	4.5	4.7	4.4	3.2	3.6	3.7	4.5
P_2O_5	0.14	0.13	0.12	0.14	0.10	0.17	0.13	0.14	0.21	0.13	0.19	0.14
H_2O^+												
H_2O^-												
CO_2												
SO_3	<0.01	<0.01	<0.01	<0.01	<0.01	<0.01	<0.01	<0.01	<0.01	<0.01	<0.01	<0.01
Cl												
L.O.I.	2.4	1.5	1.5	1.5	2.0	1.5	1.2	1.4	2.1	1.5	2.1	1.6
Total	99.1	100.19	100.77	99.16	99.93	99.74	100.29	100.21	98.77	99.61	100.47	98.79
Trace elements (ppm)												
Li	200	135	190	200	315	300	45	140	50	35	45	180
Sn	1100	26	28	24	160	39	18	35	18	10	6	55
Rb	760	930	930	1115	1500	1500	820	890	265	260	265	1060
Sr	13	16	16	18	14	15	6	8	340	310	305	15
Y	40	50	50	55	55	17	40	40	35	20	35	45
Zr	50	60	70	65	60	55	58	55	170	130	165	55
Nb												

Table 5. (continued)

Plot No.	25	26	27	28	29	30	31	32	33	34	35	36
Analysis No.	735148	735149	735701	735702	735703	735704	735705	735706	735707	735708	735709	735710
SiO_2	74.5	74.9	72.2	73.1	73.2	72.0	72.4	73.3	72.5	71.3	72.1	71.4
TiO_2	0.11	0.08	0.29	0.31	0.28	0.29	0.29	0.26	0.29	0.35	0.39	0.41
Al_2O_3	12.9	12.9	13.2	13.0	13.8	13.7	13.2	12.8	13.3	13.5	13.0	13.1
Fe_2O_3	1.1	0.82	1.1	1.1	0.6	0.69	0.78	0.73	0.68	0.31	1.0	0.98
FeO	1.0	1.1	1.6	1.7	1.8	1.7	1.7	1.6	1.8	2.4	2.0	2.1
MnO	0.04	0.03	0.05	0.04	0.05	0.05	0.05	0.05	0.05	0.06	0.06	0.06
MgO	0.03	0.03	0.50	0.58	0.66	0.58	0.50	0.50	0.50	0.75	0.75	0.83
CaO	0.57	0.42	1.5	1.7	1.5	1.7	1.5	1.4	1.5	1.9	1.9	2.0
Na_2O	3.3	3.4	3.0	3.0	3.0	3.0	2.9	2.6	2.8	2.8	2.2	3.1
K_2O	4.3	4.3	4.4	4.1	4.6	4.6	4.5	4.4	4.3	4.1	3.9	3.7
P_2O_5	0.13	0.11	0.10	0.10	0.12	0.10	0.10	0.09	0.10	0.10	0.12	0.12
H_2O^+			1.2	1.2	1.1	1.2	1.1	1.2	1.2	1.2	1.3	1.2
H_2O^-			0	0	0	0	0	0	0	0	0	0
CO_2												
SO_3	<0.01	<0.01	<0.01	<0.01	<0.01	<0.01	<0.01	<0.01	<0.01	<0.01	<0.01	<0.01
Cl												
L.O.I.	1.7	1.1										
Total	99.68	99.19	99.14	99.83	100.71	99.61	99.02	98.93	99.02	98.77	98.72	99.00
Trace elements (ppm)												
Li	180	220	80	70	70	78	75	65	83	78	95	80
Sn	37	36	15	20	8	26	20	21	25	20	26	23
Rb	1030	1020	390	340	370	350	410	400	410	355	370	340
Sr	18	10	110	130	136	115	110	95	110	125	120	135
Y	55	53	45	45	45	60	45	45	40	50	45	55
Zr	65	70	160	155	160	155	130	135	135	170	175	185
Nb												

Table 5. (continued)

Plot No.	37	38	39	40	41	42	43	44	45	46	47	48
Analysis No.	735711	735712	741645	741646	742515	742516	742517	742518	742519	742520	742521	742522
SiO_2	70.4	72.0	64.4	59.4	74.0	76.1	75.6	75.8	75.5	75.8	75.6	76.7
TiO_2	0.42	0.29	0.5	0.66	0.25	0.01	0.01	<0.01	<0.01	0.05	<0.01	0.06
Al_2O_3	13.8	13.9	16.3	15.7	14.2	13.9	14.1	14.0	14.0	13.2	13.4	13.1
Fe_2O_3	0.83	0.57	1.2	1.5	0.42	0.05	0	0.45	0.40	0.42	0.16	0.51
FeO	2.4	1.7	3.5	4.6	1.4	1.2	1.2	0.81	0.98	0.75	1.1	1.2
MnO	0.06	0.04	0.09	0.14	0.05	0.05	0.05	0.07	0.05	0.04	0.05	0.06
MgO	0.75	0.50	2.8	5.2	0.55	0.02	0.02	0.03	0.03	0.07	0.04	0.07
CaO	2.1	1.2	4.4	6.8	1.6	0.37	0.21	0.49	0.36	0.40	0.40	0.46
Na_2O	3.0	2.7	2.8	3.0	3.1	3.6	3.4	3.5	3.6	3.1	3.5	3.2
K_2O	3.9	5.1	3.4	1.8	4.6	4.5	4.4	4.2	4.3	4.8	4.3	4.6
P_2O_5	0.15	0.15	0.21	0.12	0.10	0.09	0.10	0.13	0.09	0.06	0.09	0.08
H_2O^+	1.4	1.3	1.1	1.3	0.80	0.74	0.93	0.70	0.59	0.57	0.71	0.56
H_2O^-	0	0	0.25	0.28	0	0	0	0	0	0	0	0
CO_2					0.12	0.13	0.06	0.09	0.10	0.04	0.17	0.12
SO_3	<0.01	<0.01	<0.03	<0.03	<0.02	<0.02	<0.02	<0.02	<0.02	<0.02	<0.02	<0.02
Cl					<0.01	<0.01	<0.01	<0.01	<0.01	<0.01	<0.01	<0.01
F					0.10	0.49	0.53	0.50	0.42	0.28	0.44	0.30
Total	99.21	99.45	100.95	100.50	101.37	101.25	100.61	100.77	100.42	99.58	99.97	101.02
Trace elements (ppm)												
Li	90	65	70	95	84	260	268	256	260	148	236	200
Sn	24	25	12	11	15	29	29	23	32	27	30	24
Rb	350	460	169	127	287	848	862	857	838	635	873	653
Sr	135	95	287	267	105	6	8	10	8	14	10	12
Y	50	40	28	24	38	46	44	45	44	43	47	71
Zr	185	155	110	82	117	33	36	29	38	65	28	75
Nb					17	22	25	17	24	17	24	17

Table 5. (continued)

Plot No.	49	50	51	52	53	54	55	56	57	58	59	60
Analysis No.	742523	742524	742525	742526	742527	742528	742529	742530	742536	742596	742597	742598
SiO_2	76.0	77.3	76.8	75.2	72.9	76.0	75.0	75.0	72.9	76.2	75.2	75.9
TiO_2	0.07	0.06	0.06	0.15	0.27	0.02	0.01	0.02	0.29	0.05	0.05	0.04
Al_2O_3	12.5	13.1	12.8	13.7	14.4	13.5	14.3	13.7	13.8	13.3	13.3	13.8
Fe_2O_3	0.49	0.36	0.62	0.42	0.33	0.29	0.05	0.64	0.73	0.40	0.68	0.32
FeO	0.88	1.2	0.91	1.1	1.8	1.4	1.3	0.91	1.7	1.1	1.1	0.26
MnO	0.03	0.04	0.04	0.05	0.04	0.04	0.05	0.06	0.05	0.04	0.05	0.02
MgO	0.06	0.05	0.05	0.29	0.60	0.03	0.01	0.04	0.58	0.06	0.05	0.03
CaO	0.39	0.49	0.30	0.71	1.4	0.45	0.26	0.47	1.6	0.46	0.39	0.35
Na_2O	2.7	2.9	3.1	3.2	3.2	3.3	3.8	3.3	3.0	3.3	3.4	4.1
K_2O	5.2	5.1	4.7	4.8	4.6	4.7	4.3	4.3	4.4	4.4	4.5	4.9
P_2O_5	0.06	0.06	0.05	0.10	0.15	0.08	0.09	0.11	0.11	0.15	0.14	0.11
H_2O^+	0.70	0.61	0.79	0.85	0.86	0.65	0.84	1.2	0.83	0.51	0.42	0.42
H_2O^-	0	0	0	0	0	0	0	0	0	0.08	0.05	0.07
CO_2	0.13	0.10	0.04	0.06	0.13	0.34	0.11	0.14	0.05	0.24	0.20	0.10
SO_3	<0.02	<0.02	<0.02	<0.02	<0.02	<0.02	<0.02	<0.02	<0.02	<0.02	<0.02	<0.02
Cl	<0.01	<0.01	<0.01	<0.01	<0.01	<0.01	<0.01	<0.01	<0.01	<0.01	<0.01	<0.01
F	0.25	0.29	0.19	0.12	0.13	0.42	0.41	0.49	0.11	0.33	0.42	0.13
Total	99.46	101.66	100.45	100.75	100.81	100.82	100.53	100.38	100.15	100.62	99.95	100.55
Trace elements (ppm)												
Li	84	122	122	44	68	130	248	360	60	210	220	30
Sn	19	37	22	22	16	25	33	37	23	37	32	18
Rb	465	572	541	349	291	599	849	895	313	750	804	584
Sr	14	15	11	63	102	8	11	14	124	15	18	7
Y	77	69	63	33	37	40	36	41	37	30	38	25
Zr	81	63	62	72	92	36	28	27	120	34	37	29
Nb	17	24	20	11	18	16	27	23	14	24	23	14

Table 5. (continued)

Plot No.	61	62	63	64	65	66	67	68	69	70
Analysis No.	742599	742600	742601	742602	742603	742604	742605	742606	742607	742608
SiO_2	75.6	75.4	76.1	76.1	76.1	76.1	75.8	75.5	75.4	73.5
TiO_2	0.04	0.05	0.06	0.06	0.06	0.06	0.08	0.03	0.10	0.03
Al_2O_3	14.2	13.5	13.4	13.1	12.9	13.1	12.9	13.9	13.7	15.1
Fe_2O_3	0.31	0.80	0.38	0.19	0.39	0.81	0.45	0.64	0.53	0.37
FeO	0.62	0.81	0.78	1.1	1.2	0.88	1.3	0.75	0.52	0.52
MnO	0.03	0.06	0.04	0.05	0.04	0.04	0.05	0.03	0.04	0.04
MgO	0.02	0.05	0.05	0.05	0.06	0.05	0.06	0.04	0.16	0.01
CaO	0.21	0.43	0.17	0.41	0.41	0.42	0.45	0.21	0.53	0.43
Na_2O	3.4	3.4	3.2	3.3	3.3	3.2	2.5	3.7	3.3	4.2
K_2O	4.6	4.4	4.3	4.3	4.6	4.5	4.8	3.8	4.8	3.9
P_2O_5	0.13	0.14	0.10	0.13	0.13	0.11	0.08	0.12	0.12	0.36
H_2O^+	0.73	0.65	0.71	0.36	0.39	0.40	0.58	0.72	0.42	0.35
H_2O^-	0.19	0.03	0.10	0.08	0.08	0.11	0	0.06	0.14	0
CO_2	0.03	0.03	0.08	0.20	0.16	0.10	0.11	0.25	0.08	0.07
SO_3	<0.02	<0.02	<0.02	<0.02	<0.02	<0.02	<0.02	<0.02	<0.02	<0.02
Cl	<0.01	<0.01	<0.01	<0.01	<0.01	<0.01	<0.01	<0.01	<0.01	<0.01
F	0.27	0.38	0.27	0.35	0.28	0.32	0.31	0.29	0.05	0.39
Total	100.38	99.63	99.04	99.78	100.10	100.20	99.47	100.04	99.89	99.27
Trace elements (ppm)										
Li	175	200	230	185	145	150	145	120	15	465
Sn	25	31	40	37	32	28	32	27	22	42
Rb	708	781	779	671	652	610	586	698	311	1650
Sr	10	15	13	10	10	11	12	14	45	15
Y	40	36	43	36	42	41	61	31	32	6
Zr	26	43	43	41	45	51	55	26	49	19
Nb	25	23	22	19	19	18	24	30	11	76

Table 5. (continued)

Plot No.	71	72	73	74	75	76	77
Analysis No.	741222	741223	741224	741225	741226	741227	741235
SiO_2	76.9	74.5	74.6	76.4	73.4	67.4	72.2
TiO_2	<0.02	0.10	0.11	0.02	0.13	0.43	0.25
Al_2O_3	12.9	13.6	13.2	12.9	13.3	14.6	13.7
Fe_2O_3	0.63	0.58	0.43	0.61	0.38	0.62	0.58
FeO	0.58	1.5	1.6	0.81	2.6	3.9	2.2
MnO	0.03	0.04	0.03	0.05	0.05	0.07	0.05
MgO	0.03	0.37	0.38	0.04	0.38	1.8	0.77
CaO	0.47	1.1	1.2	0.49	1.3	3.2	1.8
Na_2O	4.3	3.6	3.5	4.1	3.6	3.6	3.5
K_2O	4.0	4.4	4.3	4.3	4.1	2.8	3.6
P_2O_5	<0.04	0.05	<0.04	<0.04	0.06	0.18	0.12
SO_3	<0.03	<0.03	<0.03	<0.03	<0.03	<0.03	<0.03
Loss on ignition	0.39	0.64	0.67	0.35	0.32	0.72	0.77
Total	100.23	100.48	100.02	100.07	99.61	99.32	99.54
Trace elements (ppm)							
Li	25	70	45	55	45	55	50
Sn	14	9	5	10	6	4	15
Rb	451	251	206	394	209	144	187
Sr	<6	84	90	<6	85	267	128
Y	137	52	32	58	39	53	48
Zr	102	119	156	76	150	144	148

equigranular biotite-hornblende granodiorite consisting of quartz, plagioclase, potash feldspar, biotite and hornblende. Brown biotite (<3 mm) is present as isolated grains or in aggregates frequently associated with the hornblende. Green hornblende (0.5-3 mm) occurs in single, larger euhedral and occasionally zoned crystals, or as clusters of small crystals. Zircon and apatite are common inclusions in both hornblende and biotite. Plagioclase (<3 mm) often shows oscillatory zoning and sericitic alteration. The plagioclase ranges from andesine to oligoclase as determined by the Michel-Lévy method. Microprobe determination of the composition of plagioclase, potash feldspar, biotite, and hornblende is presented in Table 6. Accessory sphene and opaque ore minerals are present in some specimens. Textural features suggest the sequence of crystallisation is biotite, hornblende, plagioclase, quartz and potash feldspar. Three modal analyses from the continuation of this rock body south of the Ringarooma Sheet are given by Groves (1977).

Melanocratic quartz diorite xenoliths are common and range from 20-500 mm in diameter.

Contacts of the small body of rock south of Banca were not found in outcrop. In this body (*NJT*) there is a range in composition from hornblende-biotite granodiorite to biotite adamellite. The rocks are equigranular or very sparsely feldspathyric with the groundmass composed of quartz, plagioclase, potash feldspar, biotite, and hornblende (in the granodiorite but not the adamellite). Hornblende is present as relatively large grains, has biotite inclusions and is frequently associated with biotite clusters. Textural evidence indicates the same crystallisation sequence as for the rocks in the first area.

There is a marked foliation defined by the elongation of quartz aggregates and alignment of mafic minerals (*NJT*).

In the coastal area (fig.69) hornblende granodiorite occurs on either side of an equigranular, biotite-muscovite adamellite (Dbaem) (*NJT*). The contacts with this rock type are shear zones. Other contacts are with Mathinna Beds and are intrusive. East of the equigranular, biotite-muscovite adamellite (Dbaem) the granodiorite is sparsely feldsparphyric and to the west it is equigranular. Plagioclase has a compositional range similar to other granodiorites. Its crystallisation partly coincided with hornblende crystallisation. Rocks in each zone are strongly foliated and contain mylonitic shears. Grains of all mineral species show deformation in thin section and biotite, hornblende and quartz are variably recrystallised. Biotite may be partially altered to green chlorite and plagioclase can be extensively sericitised. Xenoliths of hornfelsed Mathinna Beds are present in both zones. Medium-grained, melanocratic xenoliths also occur.

Biotite Granodiorite (Dbb). Between the Boobyalla River [721706] and the Little Boobyalla River [743638] there is small NNW-trending mass of porphyritic biotite granodiorite which has intruded and hornfelsed Mathinna Beds (*SFC*). Adjacent smaller areas of granodiorite also intrude the Mathinna Beds, some of which are dyke-like and others of which may be small lenses or domes. At 748637 there is a small area of strongly metamorphosed Mathinna Beds sandstone extensively quartz-veined and intruded by lenses and sheets of granodiorite, leucogranite, and minor pegmatite.

The granodiorite is a pale-grey, medium- to coarse-grained rock generally containing a few per cent of potash feldspar phenocrysts (<40 mm) (*SFC*). The bulk of the rock is composed of roughly equal proportions of plagioclase and quartz, with less abundant potash feldspar, brown biotite,

and accessory apatite. Quartz occurs as elongate grain aggregates up to 15 mm long, consisting of elongate interlocking grains with sutured grain boundaries. Feldspar grains are often bent and fractured. Subhedral and tabular plagioclase is often over a centimetre in length and may

contain small biotite inclusions. Determinations of plagioclase composition by the method of Michel-Lévy indicate a most calcic phase of An58 (labradorite) and a most sodic phase of An30 (oligoclase-andesine). The latter values were obtained from the rims of zoned grains. The potash feldspar shows sporadic cross-hatched twinning. Biotite (0.5-3 mm) occurs as small isolated plates or elongate clusters of several grains and is frequently bent or kinked.

The sequence of mineral crystallisation appears to have been biotite (first), plagioclase, quartz, potash feldspar.

Most outcrops of the biotite granodiorite (Dbb), whether in the main mass or in satellite bodies, contain a strong foliation (*SFC*) defined by alignment of biotite flakes, a weak alignment of potash feldspar phenocrysts, and marked elongation of quartz aggregates and strings of biotite. Grains of all constituent mineral species may show deformation in thin section and biotite and quartz may be partially recrystallised. Biotite may be partially altered to green chlorite and plagioclase can be extensively altered sericitised, particularly in the cores of zoned grains.

Rounded ellipsoidal melanocratic xenoliths (<200 mm) (*SFC*), are common throughout the exposed area of granodiorite, but rarely form more than a few per cent of the rock. In many cases the xenoliths show an alignment sub-parallel to the foliation defined by other elements. Potash feldspar phenocrysts are frequently present within the xenoliths which are a fine-grained (1.5-0.5 mm) granoblastic aggregate of plagioclase, quartz, and reddish brown biotite, together with minor orthoclase and hornblende.

Small enclaves of biotite granodiorite occur within the medium-grained biotite-muscovite adamellite (Dbaem) (*NJT*) at 703683 along the boundary of that rock type with the Mathinna Beds.

Porphyritic, coarse-grained biotite and biotite-minor muscovite granite/adamellite (Dbapc). This rock type shows considerable uniformity in composition and texture and occurs widely throughout the eastern part of the region and forms the Poimena Pluton (Gee and Groves, 1971). Contacts with the Mathinna Beds are sharp and intrusive. Porphyritic, coarse-grained biotite and biotite-minor muscovite granite/adamellite (Dbapc) is intruded by major granitic types described under Dbau (dominantly fine- to medium-grained granite/adamellite) and by all types of minor granitic intrusions. A small Dbapc intrusion is present in quartz-feldspar porphyry (DmP) at 681737 (*NJT*). Intrusive relationships with respect to granodiorite have not been directly observed. It is inferred from structural evidence in the Boobyalla region that the granodiorite is older (*NJT*).

The rock is a pale grey coarse-grained porphyritic biotite granite or adamellite. The phenocrysts are euhedral to subhedral tabular potash feldspar showing string and patch perthite and Carlsbad twinning. They may be surrounded by thin zones (a few millimetres) in which there is biotite enrichment relative to the bulk of the groundmass. The outer parts of the phenocrysts are intergrown with the surrounding minerals suggesting that they grew at least partly in situ (*NJT*). The proportion of phenocrysts ranges from a few per cent to about 50% throughout the region and phenocrysts may be concentrated in small pods or veins having

a pegmatitic appearance. The length of the phenocrysts is generally 30-50 mm but may range up to 75 mm. Frequent inclusions of biotite, quartz and plagioclase are a feature of the phenocrysts. The plagioclase inclusions may be arranged in trains parallel to the crystal boundary.

The coarse- to medium-grained groundmass contains quartz, plagioclase, potash feldspar and biotite with only very minor muscovite. Quartz displays straight to sutured quartz - quartz grain boundaries. Grains may contain subgrains and strain lamellae and usually have undulose extinction. Recrystallisation of quartz is variable. Other mineral species generally have undulose extinction but do not show recrystallisation. The plagioclase is polysynthetically twinned, of subhedral tabular habit, and often has oscillatory zoning. The composition as determined by the Michel-Lévy method ranges from andesine to oligoclase. The potash feldspar is partly sericitised, anhedral and contains patch and string microperthite. Biotite (1-2 mm) occurs as isolated flakes or more commonly as decussate textured clusters. The muscovite when present occurs as small anhedral plates. Accessory zircon and apatite are usually present as inclusions in biotite.

Textural and inclusion evidence indicates that the sequence of crystallisation of groundmass minerals was biotite (first), plagioclase, quartz and muscovite (?together), potash feldspar (*NJT*).

Modal analyses of this rock type have been carried out by Groves (1977) from Pioneer [790517] and Baillie (1973) from the Little Mt Horror area. Groves (1977) also provides simplified compositions (% mass) based on rock analyses, analysed biotite composition, X-ray determination of potash feldspar composition and modal analysis. The variable proportion of large potash-feldspar phenocrysts makes modal analysis difficult but the rock type appears to range in composition from adamellite to granite.

Sparsely distributed xenoliths are present in most areas (*NJT*). They range up to 0.5 m across and can have irregular, discoidal or ellipsoidal shapes. Most consist of a few per cent (by volume) of relatively large (10-20 mm) crystals of potash and plagioclase feldspar and quartz in a medium-grained granoblastic groundmass of quartz and untwinned feldspar. Both quartz and untwinned feldspar in the groundmass are riddled with inclusions of plagioclase and brown biotite. The biotite content of the groundmass is variable and may exceed 50% by volume. Minor chlorite, epidote and green, uniaxial, pleochroic mica may be present. Medium-grained, quartz-feldspar-muscovite xenoliths are also present but are rare. Xenoliths of hornfelsed Mathinna Beds may be present near contacts. Rare biotite-rich schlieren were found in the Mt Cameron area (*SFC*).

Compositional layering. Compositional layering occurs in Dbapc (porphyritic, coarse-grained biotite-minor muscovite granite/adamellite) in a number of localities south of Pioneer (*e.g.* 788482) (*PRW*). Layering is either rare or absent in other areas.

Layering in the occurrences south of Pioneer can usually be divided into three zones.

(1) An upper equigranular zone of fine-grained, dark, biotite-quartz-feldspar rock with biotite in abundance.

(2) A middle equigranular zone of feldspar-rich rock, the feldspar having graphic quartz intergrowths.

(3) A lower equigranular zone of feldspar-quartz-biotite-minor muscovite granite which passes gradationally downwards into normal porphyritic biotite granite.

Above the biotite-rich zone the granite has an unusually high proportion of phenocrysts but it passes gradationally upwards into normal porphyritic granite. Feldspar aggregates often occur above the layered zone. An example of more complex layering which is generally similar to this model is shown in Figure 6.

In the two small intrusions near 682735 the layering is due to variation in the relative proportions of biotite and felsic minerals and to variation in the abundance of alkali-feldspar phenocrysts. The latter variation produces bands that are equigranular or sparsely porphyritic and bands that are porphyritic to highly porphyritic. Contacts between the two types of bands may be extremely sharp (plate 1) or gradational. Biotite rich layers are best developed within the equigranular to sparsely porphyritic bands although thin, wispy layers may be present in porphyritic bands. There is progressive increase in biotite content downwards in some layers. Trough shaped structures suggestive of erosion of magma currents occur in one band (Groves and Jennings, 1973, pl.9).

In sparsely porphyritic rocks the phenocrysts show marked alignment parallel to the compositional layering. Where phenocrysts are abundant they show a parallel statistical alignment. Small xenoliths which are abundant in places in the eastern intrusion may also show marked alignment parallel to the compositional layering. Xenoliths are mostly comprised of Mathinna Beds hornfels. Rounded, coarse- and medium-grained, biotite-rich granitic xenoliths are also present and form small accumulations of cobble-sized individuals in places. A few medium-grained quartz-feldspar-muscovite granitic xenoliths are also present.

Orientation of the compositional layering is similar in each intrusion and is fairly uniform throughout. Dip is shallow to moderate south-west. This is discordant with respect to structures in the Mathinna Beds which are host to the eastern intrusion. The layering is generally subparallel to gently dipping upper contacts of the eastern intrusion but can be highly oblique to steeply dipping contacts (plate 2). All contacts with the country rocks of both intrusions are sharp. High obliquity of layering with respect to some contacts indicates that assimilation is not a major process in generating the layering. Thin felsic and biotite-rich layers occur adjacent to some gently dipping contacts and mimic their form. Such minor layering may result from wall-rock reaction.

Porphyritic very coarse-grained biotite and minor muscovite granite/adamellite (Dbapcc). This rock type is a very coarse-grained (20-30 mm) variant of the porphyritic, coarse-grained biotite and biotite-minor muscovite granite/adamellite (Dbapc) from which it differs only in grain size. It occurs in association, and apparently having a gradational relationship, with Dbapc on the southern slope of Mt Cameron in the area around 760605 (*AVB*).

Porphyritic coarse-grained biotite and muscovite granite/adamellite with muscovite >2% (Dbapcm). This rock type also has an apparent gradational relationship with the porphyritic, coarse-grained biotite and biotite-minor muscovite granite/adamellite (Dbapc) (*AVB*) and differs from it in having slightly smaller phenocrysts and finer grained groundmass together with up to 10% muscovite, which can be seen in hand specimen and which has allowed it to be distinguished in the field from the normal Dbapc type.

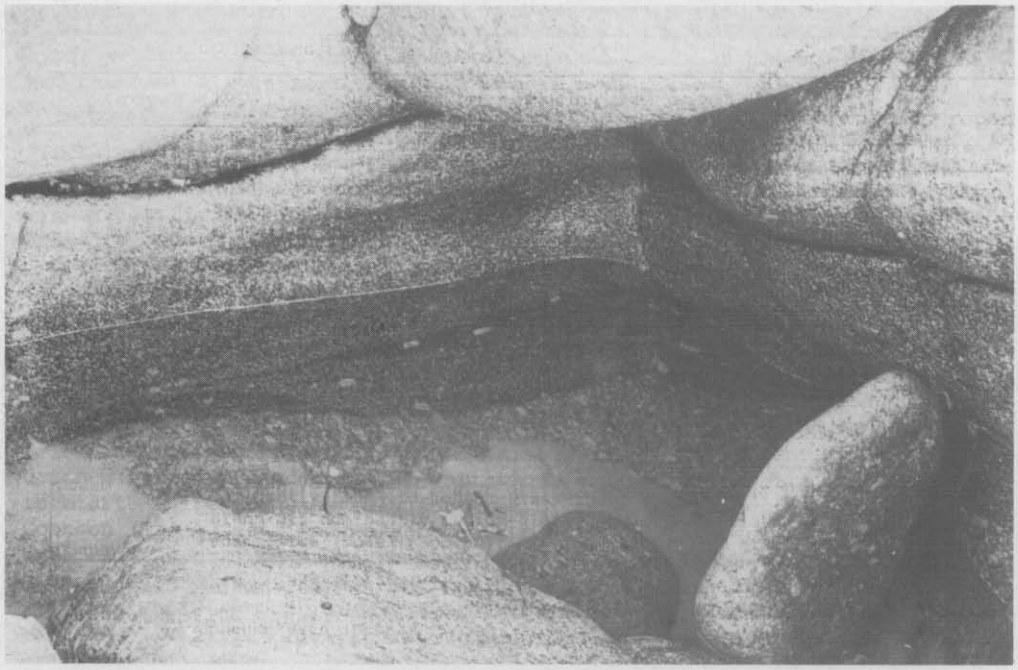

Plate 1. *Compositional layering in porphyritic, coarse-grained biotite-minor muscovite granite/adamellite (Dbapc) showing sharp contacts between two types of bands. (NJT).*

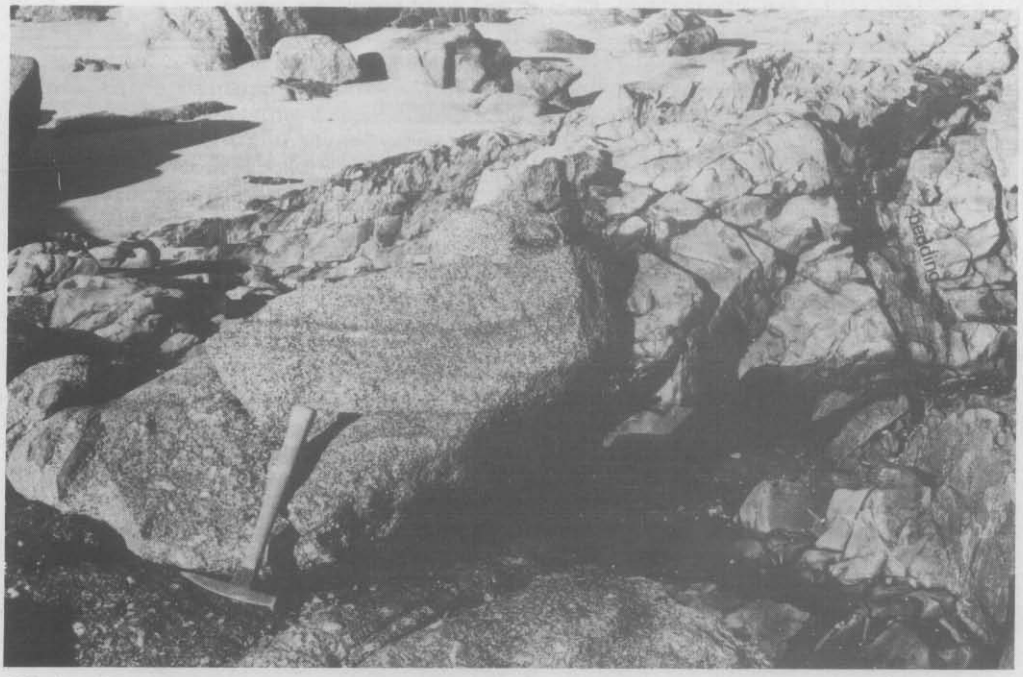

Plate 2. *Compositional layering in porphyritic, coarse-grained biotite-minor muscovite granite/adamellite (Dbapc), oblique to steeply dipping contact. (NJT).*

5 cm

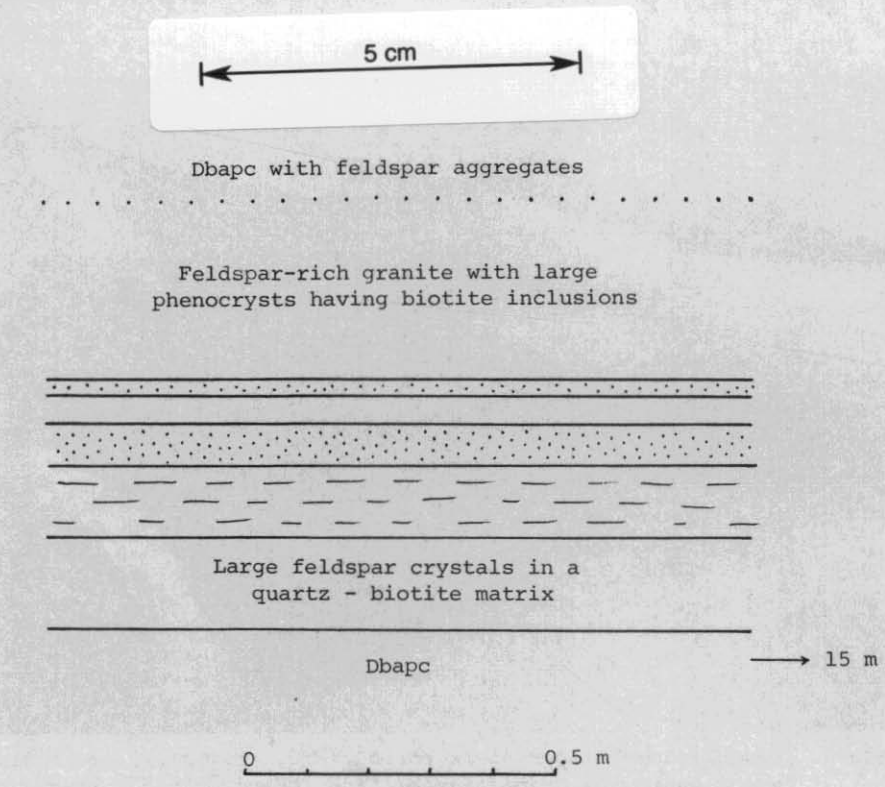

Figure 6. *Layering in porphyritic, coarse-grained biotite-minor muscovite granite/adamellite* [*788482*]

This rock type is similar to rocks mapped as porphyritic fine- to medium-grained, biotite-muscovite granite/adamellite with feldspar phenocrysts, elsewhere. It crops out in an irregular elongate NE-SW shaped zone from 715561 to 730540. The central part of the zone contains the highest proportion of muscovite.

Sparsely porphyritic to equigranular, coarse-grained biotite and minor muscovite granite/adamellite (Dbaps). On the northern side of the Mt Cameron area [776646 to 841645] this rock type has an east-west trending intrusive contact with the Mathinna Beds (*SFC*). The contact with the porphyritic, coarse-grained biotite and biotite-minor muscovite granite/adamellite (Dbapc) rock type on the north and north-eastern flanks of Mt Cameron appears to be transitional over several tens of metres, though exposure is not continuous (*SFC*). On the south-eastern flank [840618 to 780620] the change in rock types at the contact with Dbapc takes place over a distance of less than two metres, however again the contact was not observed in continuous exposure (*SFC*).

The rock type is coarse-grained equigranular to sparsely porphyritic with up to 5% tabular potash feldspar phenocrysts (30-40 mm) (*SFC*). The coarse-grained groundmass contains quartz, plagioclase, potash feldspar and biotite with accessory muscovite and zircon. The subhedral plagioclase (5-8 mm) has albite and pericline twinning and is partly sericitised. Both

normal and oscillatory zoning is present. The potash feldspar is perthitic and may have Carlsbad twinning and contain small inclusions of tabular plagioclase, lobate quartz and biotite. Quartz (2-8 mm) frequently has straight or gently curved quartz-quartz grain boundaries and may have undulose extinction. Biotite flakes (1-2 mm) may be bent and are usually arranged along the boundaries of larger grains of quartz and feldspar. Muscovite (<0.5 mm) occurs as minor flakes sometimes in distinct fracture zones.

Porphyritic, fine- to coarse-grained garnet-bearing biotite-muscovite granite/adamellite (Dbag). This texturally variable rock type, which has intruded the Mathinna Beds, crops out over a roughly semi-circular area straddling the Gladstone-Waterhouse road at 750697 and on the banks of the Ringarooma River at 795687 (*SFC*) and forms the Boobyalla Pluton (Groves, 1977).

Extending south-west of the porphyritic, fine- to coarse-grained garnet-bearing biotite-muscovite granite/adamellite (Dbag) from a point [742689] in close proximity to its contact with the Mathinna Beds is a dyke of garnetiferous quartz-feldspar porphyry (Dmpg) which has a similar petrographic character to rocks within Dbag close to the contact. The dyke intrudes porphyritic, coarse-grained biotite and biotite-minor muscovite granite/adamellite (Dbapc), dominantly fine- to medium-grained granite/adamellite (Dbau), biotite granodiorite (Dbb) and Mathinna Beds. In view of the likely genetic relationship between this dyke and Dbag, it appears that Dbag is the youngest of the major granitic bodies in this area (*NJT*).

The marginal parts of the mass are composed of fine- to medium-grained potash feldspar and quartz-porphyritic biotite-garnet granite having distinctive anhedral to globular quartz phenocrysts (<10 mm), and blocky potash feldspar phenocrysts (<50 mm) in a hypidiomorphic to allotriomorphic granular groundmass of quartz, potash feldspar, plagioclase, green-brown biotite, and muscovite (*SFC*). There are also some vermicular intergrowths of quartz and alkali feldspar. Red-brown garnets are a minor but characteristic component occurring as aggregates of small grains (<1 mm) intergrown with fine biotite clusters (5-20 mm in diameter). Less commonly, garnet is present as isolated subhedral grains (<3 mm). Where the rock is weathered, the garnet-biotite clusters and zoned plagioclase weather out to form distinctive semi-spherical pits.

At a distance of over half a kilometre from the contact the granite is dominantly coarse-grained with variable potash feldspar phenocryst content (*SFC*). Potash feldspar phenocrysts with patch and stringlet perthite and minor cross-hatched twinning forms up to 20% of the rock. Inclusions of cuspate to lobate quartz, some of which envelop biotite flakes (<1 mm) also occur. Quartz constitutes about 30% of the rock and forms anhedral grains (<10 mm), having sutured to straight or gently curved grain boundaries, undulose extinction, and a little subgrain development. Plagioclase (20%) is anhedral to tabular (<20 mm) with normal and oscillatory zoning. Groundmass potash feldspar is of a similar grain size. Biotite is present as reddish brown flakes (<3 mm) and is more abundant than muscovite which occurs as discrete plates (<1 mm). Garnet occurs as individual grains and in clusters with biotite.

Generally, phenocryst content and groundmass grain size are very variable. In the fine- to medium-grained varieties, globular quartz constitutes up to 15% of the rock, and potash feldspar phenocrysts range between 5 and 20%. The phenocrysts frequently show no preferred orientation.

Equigranular, dominantly medium-grained, biotite-variable muscovite granite/adamellite (Dbaem). This rock type forms an elongate body cropping out in the Sheoak Hill area from 700670 to 687736 on the foreshore (*NJT*) and is an equigranular medium-grained biotite-muscovite adamellite and forms the Sheoak Hill Pluton (Groves, 1977). Contacts between it and other rock types are either shear zones or are poorly exposed. Thin dykes which are petrographically and structurally comparable with Dbaem occur within biotite-hornblende granodiorite (Dbg) on the foreshore, therefore, Dbaem may be younger than Dbg.

Xenoliths are rare in the equigranular, dominantly medium-grained, biotite-variable muscovite granite/adamellite (Dbaem). Rounded melanocratic types are present near the eastern contact on the foreshore.

The rock sonsits of quartz, plagioclase, potash feldspar, biotite and muscovite (*NJT*). The biotite, pleochroic from pale brown to dark red-brown, occurs as relatively large isolated flakes which commonly contain zircon inclusions. Muscovite is also present as large flakes replacing plagioclase, cross-cutting biotite or intergrown with quartz. Topaz may be present as small, optically continuous, relicts within large muscovite grains. Subhedral to anhedral plagioclase which is sometimes zoned, with rare reverse zoning, has andesine as its most calcic composition (determined by the Michel-Lévy method). Potash feldspar is intergranular to quartz and frequently contains inclusions of quartz, muscovite and plagioclase. Accessory apatite and green-brown tourmaline are often present.

On the coast [688736] these rocks are considerably altered, the biotite is largely altered to chlorite; the plagioclase more extensively altered to sericite; and recrystallisation or granulation of quartz and feldspar to a very fine grain size occurs along fractures and in patches. In hand specimen the most altered material is very fine-grained and consists of irregular elongate lenticules of dark green colour (≈15 mm long) in a fawn or cream groundmass. The lenticules define a crude foliation.

A single modal analysis is presented by Groves (1977, p.37).

Equigranular, fine- to coarse-grained, biotite-muscovite granite/adamellite (Dbae). Rocks of this type have been distinguished, in the Mt Paris [660400], Mt Cameron (*e.g.* 755595) (*AVB*) and Masher Hill [810420] (*JM*) areas and form part of the bodies referred to by Groves (1977) as the Mt Paris Mass, the Mt Cameron Sheets and the Lottah Sheets. A small area of granite north of Mt Horror [610540] shown as Dbae is comparable to rocks at Mt Cameron described as Dbaps (sparsely porphyritic to equigranular, coarse-grained biotite and minor muscovite, granite/adamellite) (*NJT*).

In the north-west of the Mt Paris area this rock type intrudes the Mathinna Beds and has a sharp or gradational contact over 50-60 m with the quartz and feldspar porphyritic granite (Dbapq). In the Masher Hill area it has sharp contacts with the (porphyritic) coarse-grained biotite and biotite-minor muscovite granite/adamellite (Dbapc) and is thought to intrude it. The development of pegmatitic patches is common near contacts (*e.g.* at 816409). The intrusive relationships of the two granites can be seen on a tributary of Cotton Creek at 833433 and at 832433 (*JM*). Here the porphyritic granite is above the equigranular granite with an irregular and undulating contact generally dipping westward. The underlying equigranular granite occurs as windows in the porphyritic granite. On the stream at 831428 a dyke of equigranular microgranite intrudes the porphyritic granite and stems from the large mass of equigranular granite of this locality (*JM*).

Table 6. ELECTRON MICROPROBE ANALYSES OF PLAGIOCLASE FROM EQUIGRANULAR, FINE TO COARSE-GRAINED, BIOTITE MUSCOVITE GRANITE/ADAMELLITE (Dbae).

	Specimen A (plot 14, table 5)				Specimen B (plot 9, table 5)			
	Average albite	Average area analysis potash-feldspar	Average Na rich potash-feldspar phase	Average K rich potash-feldspar phase	Average albite	Average area analysis potash-feldspar	Average Na rich potash-feldspar phase	Average K rich potash-feldspar phase
SiO_2	67.67	65.33	65.85	64.61	66.74	65.43	66.17	65.25
Al_2O_3	20.67	18.95	19.17	19.34	20.57	19.26	19.28	18.76
CaO	0.40	1.39	0.97	1.20	0.55	1.06	0.68	1.13
Na_2O	10.60	2.79	5.04	0.19	11.30	4.45	7.11	2.16
K_2O	0.64	11.52	8.94	14.64	0.82	9.78	6.74	12.70
No. of analyses	5	3	3	4	3	2	2	1
Structural formulae								
Si	11.831	11.896	11.888	11.865	11.738	11.854	11.871	11.926
Al	4.261	4.669	4.080	4.188	4.266	4.114	4.078	4.042
Σ	16.092	15.965	15.968	16.053	16.004	15.968	15.949	15.968
Ca	0.075	0.272	0.189	0.237	0.105	0.207	0.132	0.221
Na	3.595	0.986	1.766	0.070	3.855	1.565	2.475	0.765
K	0.144	2.676	2.061	3.431	0.184	2.261	1.543	2.961
Σ	3.814	3.934	4.016	3.738	4.144	4.033	4.150	3.947
Total	19.906	19.899	19.984	19.791	20.148	20.001	20.099	19.915
Or	4	68	51	92	4	56	37	75
Mol Ab	94	25	44	2	93	39	60	19
% An	2	7	5	6	3	5	3	6

Table 7. COMPOSITION OF SHEET SILICATES FROM BIOTITE-MUSCOVITE GRANITE ADAMELLITES (SPECIMENS OF PLOTS 9 AND 14 TABLE 5)

	Average biotite	Muscovite	Alteration material from biotites				
SiO_2	38.30	48.54	48.77	46.87	52.47	53.20	54.68
TiO_2	0.24	0	0	0	0	1.15	0
Al_2O_3	23.56	32.24	38.51	36.51	41.78	44.50	45.33
FeO	27.39	7.98	9.02	11.23	3.42	0.71	0
MnO	0.53	0	0	0	0	0	0
MgO	0.22	0	0	0	0	0	0
CaO	0.77	0.84	0.32	0.59	0.34	0	0
K_2O	8.96	10.42	3.37	4.82	2.00	0.46	0
Pre-normalised total	96.8	94.9	84.6	69.9	81.6	92.0	83.4
No. of analyses	7	1	1	1	1	1	1
Structural formula							
Tet Si	5.569	6.345					
Al	2.341	1.655					
Σ	8	8					
Oct Al	1.765	3.312		X Ca	0.122	0.117	
Ti	0.027	0		K	1.689	1.737	
Fe	3.386	0.872		Σ	1.811	1.854	
Mn	0.066	0		Total	15.104	14.041	
Mg	0.044	0					
Σ	5.293	4.184					

Table 8. MODAL ANALYSES OF BIOTITE-MUSCOVITE GRANITE/ADAMELLITES

	Dbapq J74/16	Dbae J74/8	Dbae 73/694
Quartz	31.8	34.6	32.2
Potash feldspar	38.1	33.2	31.6
Plagioclase	23.9	29.7	30.0
Biotite	4.0	1.1	3.8
Muscovite	0.6	1.3	0.8
Chlorite	1.4	-	-
Ore	0.2	0.1	-
Topaz	-	-	1.6

The equigranular granite consists of quartz, plagioclase, potash feldspar, biotite and muscovite with an average grain size between 3-5 mm. Electron microprobe analyses of the plagioclase from two specimens confirm the Michel-Lévy determinations and give an albite composition with $An_{0.02-0.03}$ (table 6). The plagioclase shows minor zoning and sericitic alteration. In some specimens the biotite is pleochroic from light to dark brown but frequently the pleochroism is from almost colourless to light brown with a slight green tint. Biotite commonly shows alteration along cleavage traces (see table 7 for biotite and alteration material analyses). Muscovite is present as isolated flakes (see table 7 for analyses) or closely associated with biotite, having apparently been altered from it, and is also present as an alteration product of potash feldspar and in association with accessory topaz. In some specimens which contain the very pale biotite there is also mica which is pleochroic from colourless to pale violet, possibly zinnwaldite. High lithium is a feature of the analyses of this rock type. Topaz, fluorite, tourmaline and cassiterite are common accessory minerals and small inclusions of zircon are sparsely present in the biotite. Small blebs of cassiterite are occasionally present along the cleavage traces of altered biotite. The potash feldspar is perthitic and electron microprobe analyses of the two phases and an average composition obtained by analysing large parts of perthitic crystals are presented in Table 6. In one specimen (72-429) minor garnet is overgrown by biotite, muscovite and chlorite (*JM*). Another garnet crystal encloses a euhedral quartz grain that shows the dihexahedral shape typical of high temperature β quartz. Two modal analyses of this lithology are presented in Table 8 (*JM*).

Porphyritic, fine- to medium-grained, biotite-muscovite granite/adamellite with phenocrysts of feldspar and rounded quartz (Dbapq). Rocks of this type have been separately distinguished in the same areas and form part of the same granite bodies referred to by Groves (1977) as for the equigranular, fine- to coarse-grained, biotite-muscovite granite/adamellite (Dbae). Small bodies also occur at 645690 (*PWB*).

In the north-west Mt Paris area this rock type intrudes the Mathinna Beds and is also thought to intrude the porphyritic coarse-grained biotite and biotite-minor muscovite granite/adamellite (Dbapc). A sharp contact between it and the Dbapc rock type is exposed at 835433 on a tributary of Cotton Creek (*JM*). This rock type is very similar to the quartz and feldspar porphyry dykes (Dmp) cutting the Dbapc rock type, suggesting that it is also later (*JM*).

The groundmass of this granite type is very similar to Dbae (the equigranular, fine- to coarse-grained, biotite-muscovite granite/adamellite) with which it has gradational relationships (*JM*). Quartz phenocrysts may range up to 9 mm and corrosion of the outline is common. Potash feldspar phenocrysts (<40 mm) have Carlsbad twinning and braid perthitic structures. A single modal analysis is presented in Table 8 (*JM*).

Porphyritic, fine- to medium-grained biotite-minor muscovite granite/adamellite (Dbapq´). Several small bodies of this rock type have been distinguished in the Mt Cameron area (*e.g.* at 752616 and 757630). It shows transitions into the porphyritic, coarse-grained biotite and biotite-minor muscovite granite/adamellite (Dbapc) (*SFC*) and is continuous with the porphyritic, fine to medium-grained, biotite-muscovite granite/adamellite with phenocrysts of feldspar and rounded quartz (Dbapq) on the Ringarooma Sheet.

The rock is fine- to medium-grained with phenocrysts of perthitic potash feldspar (<40 mm) and globular quartz. The feldspar phenocrysts

have rounded to cuspate inclusions of quartz. The quartz phenocrysts are up to 7 mm in diameter (rarely 10 mm) and show sub-grain development and straight, gently curved, or sutured grain boundaries. The groundmass is seriate textured, ranging in grain size from 1-4 mm, and is composed of oscillatory zoned plagioclase, perthitic potash feldspar, quartz, biotite and very minor muscovite.

Porphyritic, fine- to medium-grained, biotite-muscovite, granite/adamellite with phenocrysts of feldspar (Dbapf). Rocks of this type have been distinguished in the Mt Cameron [770600] and Masher Hill [810420] areas and form part of the bodies referred to by Groves (1977) as the Mt Cameron Sheets and the Lottah Sheets. Other bodies occur at 645690 and south of Pioneer [683514]. The rock type contains sparse large orthoclase phenocrysts and abundant small plagioclase phenocrysts. In addition quartz phenocrysts are present.

In several areas [765412, 790426, 808423 and 812411] this rock type can be seen to grade into the equigranular, fine- to coarse-grained, biotite-muscovite granite/adamellite (Dbae) (*JM*). In other areas [800450, 800402, 774584, 767497 and 830345] granite occurs with the same hand specimen characteristics except that it is more melanocratic. South of the Groom River, between 822359 and 839351, this more melanocratic variety of Dbapf (porphyritic, fine- to medium-grained, biotite-muscovite, granite/adamellite with phenocrysts of feldspar) has a sharp boundary with the Dbae granite type and appears to grade into the porphyritic, coarse-grained biotite and biotite-minor muscovite granite/adamellite (Dbapc) along Lehners Ridge [820342]. The field relations of the more melanocratic variety of the Dbapf granite type in the other areas is not clear, however, chemical analyses from Cross Creek [800450] and the area at 774485 show clearly their much greater chemical similarity (see fig. 7) to the Dbapc granite type than to the Dbae granite type or to the porphyritic, fine- to medium-grained, biotite-muscovite granite/adamellite with phenocrysts of feldspar and rounded quartz (Dbapq) so it is likely that in those areas it is also gradational to it. Thus the symbol Dbapf on the map includes rocks which are similar in hand specimen character but probably belong to different intrusive phases and differ chemically.

Thin section examination of the more melanocratic variety of Dbapf (porphyritic, fine- to medium-grained, biotite-muscovite, granite/adamellite with phenocrysts of feldspar) shows textural similarity to the porphyritic, coarse-grained biotite and biotite-minor muscovite granite/adamellite (Dbapc) but is more quartz rich and contains a greater proportion of plagioclase and muscovite. The more leucocratic variety has accessory minerals topaz and fluorite which are common in both the Dbae (equigranular, fine- to coarse-grained, biotite-muscovite granite/adamellite) and the Dbapq (porphyritic, fine- to medium-grained, biotite-muscovite granite/adamellite with phenocrysts of feldspar and rounded quartz) granite types but not in the Dbapc type.

Field relationships of the porphyritic, fine- to medium-grained, biotite-muscovite, granite/adamellite with phenocrysts of feldspar (Dbapf) in the Mt Cameron area are unclear.

A minor north-east trending dyke-like body of the porphyritic, fine- to medium-grained, biotite-muscovite, granite/adamellite with phenocrysts of feldspar (Dbapf) crops out south of Banca at 685575 (*PWB*).

A coarse-grained variety of Dbapf (porphyritic, fine- to medium-

grained, biotite-muscovite, granite/adamellite with phenocrysts of feldspar) mapped under the symbol Dbapp crops out at 714415 where it has gradational relationships with the Dbapf rock type (*JM*).

Fine- to medium-grained biotite and minor muscovite granite/adamellite with sparse phenocrysts of feldspar (Dbapsf). Rocks of this type have been distinguished in the Mt Cameron area (*SFC*) and differ from Dbapf (porphyritic, fine- to medium-grained, biotite-muscovite, granite/adamellite with phenocrysts of feldspar) by the lesser proportion of muscovite and feldspar phenocrysts. It forms flat lenses or sheets within the porphyritic, coarse-grained biotite and biotite-minor muscovite granite/adamellite (Dbapc) on the northern flanks of Mt Cameron.

Dominantly fine- to medium-grained granite/adamellite (Dbau). The symbol Dbau has been used in those areas containing the equigranular, fine- to coarse-grained, biotite-muscovite granite/adamellite (Dbae), the porphyritic, fine- to medium-grained, biotite-muscovite granite/adamellite with phenocrysts of feldspar and rounded quartz (Dbapq) and the porphyritic, fine- to medium-grained, biotite-muscovite granite/adamellite with phenocrysts of feldspar (Dbapf) where they cannot be specifically distinguished.

The southern part of the Mt Paris area contains a complex intermingling of the equigranular, fine- to coarse-grained, biotite-muscovite granite/adamellite (Dbae) and the porphyritic, fine- to medium-grained, biotite-muscovite granite/adamellite with phenocrysts of feldspar and rounded quartz (Dbapq) which have gradational relationships. The rocks of this area form part of the body referred to by Gee and Groves (1971) as the Mt Paris Mass. Over a large part of the south-west of this area the rocks 20 to 30 m from the contact with the Mathinna Beds, have undergone greisenisation so that at the contact the rock is mainly quartz-muscovite or some cases almost pure quartz. Greisen veins occur in the area close to the contact with the Mathinna Beds between Bells Hill [696352] and Rattler Hill [730348]. An analysis of one of the veins is presented in Table 5 plot 13. The greisens are medium-grained rocks composed almost entirely of quartz and muscovite with accessory topaz, fluorite, cassiterite, wolframite and sulphide minerals (chalcopyrite, arsenopyrite, pyrrhotite, pyrite, sphalerite).

An irregular area of granitic rock has been mapped under the symbol Dbau in the area from Little Mt Horror [681598 (*PWB*) to 610678] (*NJT*). The southern part of this body has been referred to by Groves (1977) as the Little Mt Horror Sheet. Within the whole of this area there is a complex distribution of aplite, biotite-muscovite granite and biotite-muscovite adamellite. The grain size of these rock types ranges from fine to medium (0.5-2 mm) (*PWB*).

Small areas of coarse-grained porphyritic biotite granite/adamellite with potash feldspar phenocrysts, similar in character to Dbapc (porphyritic, coarse-grained biotite and biotite-minor muscovite granite/adamellite), occur within the area mapped as Dbau. These may be either rafts or segments between intrusive bodies (*PWB, NJT*).

Textures of the fine- to medium-grained rocks may be equigranular or porphyritic. Mica content varies from trace amounts to about 10% by volume and either muscovite or biotite may be dominant. Porphyritic rocks include types similar to Dbapc (porphyritic, coarse-grained biotite and biotite-minor muscovite granite/adamellite) but of medium rather than coarse grain size. The common type of porphyritic rock is comparable with the porphyritic, fine- to medium-grained, biotite-muscovite granite/adamellite with

phenocrysts of feldspar and rounded quartz (Dbapq). It contains sparse to abundant phenocrysts of quartz and potash feldspar. Quartz phenocrysts (<10 mm) may either be rounded, due to absorption, or euhedral. Potash feldspar phenocrysts generally range up to about 30 mm in length with exceptional grains to 50 mm. In places the phenocrysts show alignment. Patches of biotite and, unusually, muscovite up to 10 mm across may be present. Biotite commonly contains numerous inclusions with metamict haloes. Equigranular rocks are comparable with the equigranular, dominantly medium-grained, biotite-variable muscovite granite/adamellite (Dbaem). Neither evidence of grain deformation, apart from undulose extinction, nor evidence of substantial recrystallisation was found in any of the rock types.

Two analyses are listed in Groves (1977) from this rock mass. One (702697) plots in field 2 of Figure 5 and is described as an adamellite and is probably from a small area of Dbapc (porphyritic, coarse-grained biotite and biotite-minor muscovite granite/adamellite) while the other (702698) plots in field 3 and is a granite. This latter rock probably belongs to the biotite-muscovite body which is intrusive into the Dbapc granite type.

To the south-west of Mt Cameron an area of numerous small outcrops of various granite types included within Dbau (dominantly fine- to medium-grained granite/adamellite) occur.

The rocks described above under the symbols Dbau, Dbae, Dbapq and Dbapf (leucocratic type) may probably all be more accurately described as alkali granites and all analyses from them in this report, plot in the alkali granite field 3 of Figure 5.

Minor Granitic Intrusions *M.P. McClenaghan*

Quartz-feldspar porphyry (Dmp). In the south-east of the Ringarooma sheet dykes of pale-grey quartz-feldspar porphyry intrude the porphyritic, coarse-grained biotite and biotite-minor muscovite granite/adamellite (Dbapc) but have not been seen to intrude the equigranular, fine- to coarse-grained biotite-muscovite granite/adamellite (Dbae) (*JM*). They show a strong similarity to the porphyritic, fine- to medium-grained, biotite-muscovite granite/adamellite with phenocrysts of feldspar and rounded quartz (Dbapq) (*JM*) associated with the Dbae granite type. The dykes generally range from 3 to 13 m in width.

From 838397 to 832392 a dyke trending at 55° can be traced for some distance flanked by two dolerite dykes (Dcdl).

Euhedral to slightly rounded and resorbed quartz (<5 mm) is the dominant phenocryst type in this area. The quartz frequently shows the dihexahedral form typical of quartz that originally crystallised as β-quartz. Subordinate feldspar phenocrysts (<9 mm) consist mostly of plagioclase with minor perthitic potash feldspar. The feldspar shows considerable sericitic alteration and the plagioclase is oligoclase as determined by the Michel-Lévy method. The groundmass is fine-grained (<0.1 mm) and consists of quartz, potash feldspar, biotite and muscovite with accessory, topaz, zircon, iron ore and apatite.

In the Sheoak Hill area [683703] a quartz-feldspar porphyry dyke of similar character intrudes granitic rock types Dbapc (porphyritic, coarse-grained biotite and biotite-minor muscovite granite/adamellite), Dbaem (equigranular, dominantly medium-grained, biotite variable muscovite granite/adamellite) and the Mathinna Beds (*NJT*). The phenocrysts constitute up to 60% of the rock with plagioclase (<10 mm) dominant over quartz (<5 mm).

On the coast at 681737 a quartz-feldspar porphyry is separated from the main mass of Dbapc (porphyritic, coarse-grained biotite and biotite-minor muscovite granite/adamellite) by a thin sliver of Mathinna Beds on the western side and has an intrusive contact with Mathinna Beds on the eastern side (*NJT*). It is intruded by compositionally banded granitic rocks comparable with Dbapc. The porphyry contains less than 20% phenocrysts of plagioclase, quartz and biotite in a fine- to medium-grained groundmass of biotite, plagioclase, quartz, muscovite, potash feldspar and minor chlorite.

Garnetiferous quartz-feldspar porphyry (Dmpg). A garnetiferous quartz-feldspar porphyry dyke is discontinuously exposed from 609554 to 742689, a distance of about 19 km (*NJT*). The maximum width of the dyke is about 30 m. The dyke intrudes granite types Dbapc (porphyritic, coarse-grained biotite and biotite-minor muscovite granite/adamellite), Dbau (dominantly fine- to medium-grained granite/adamellite), Dbb (biotite granodiorite) and Mathinna Beds and is similar to the biotite garnet granite occurring in the area around 750695. Very small exposures of dolerite containing clinopyroxene occur at numerous places along the length of the dyke.

The porphyry contains up to 30% phenocrysts of feldspar (<60 mm) quartz (<15 mm) and subordinate garnet. The plagioclase phenocrysts have considerable sericitic alteration and alteration to epidote. Determination by the Michel-Lévy method indicates that they are andesine. The quartz phenocrysts are rounded due to resorption. The euhedral garnet phenocrysts form less than one per cent of the rock, are deep red in colour and partially altered to chlorite. The groundmass consists of medium-grained potash feldspar, plagioclase, green mica and minor quartz (<5%). The quartz in the groundmass also has embayments and appears to be partly resorbed.

Granite/adamellite (Dmg, Dmgp, Dmge). Small dyke-like bodies of fine- to medium-grained granite/adamellite occur throughout the region. The thickness of individual bodies is generally less than 50 m although several larger bodies near 620605 range up to 150 m. These rocks have a similar character to larger bodies of granite-adamellite in the Little Mt Horror area [680600] mapped under the symbol Dbau (*PWB, NJT*). Some of these small dyke-like bodies have sharp boundaries with the country rock whilst for others the nature of the contact is unclear (*PWB*). On the Ringarooma Sheet distinction has been made between equigranular (Dmge) and porphyritic (Dmgp) granite/adamellite bodies whereas on the Boobyalla Sheet they have not been distinguished since both types may occur in a single body.

Quartz-orthoclase pegmatite (Dmc). At 625578 there is a small reddish coloured very coarse-grained (<40 mm) dyke-like body of quartz-orthoclase pegmatite which consists of a mixture of potash feldspar, quartz and plagioclase (*PWB*).

At Tobacco Hill 557732 abundant float consists of pegmatite (Dmc) containing orthoclase and quartz with large nodules of tourmaline (<100 mm) (*PWB*).

Granite (Dmd). A small body of granite crops out at 632728 on the Tomahawk River, consisting dominantly of reddish potash feldspar with quartz, plagioclase and chlorite (*PWB*).

Aplite (Dma). Late stage acid dykes are widespread throughout the region. They are leucocratic, medium- to fine-grained, generally with a saccharoidal texture and are composed of quartz and feldspar, occasionally with minor amounts of biotite and muscovite; they occur as dykes and veins.

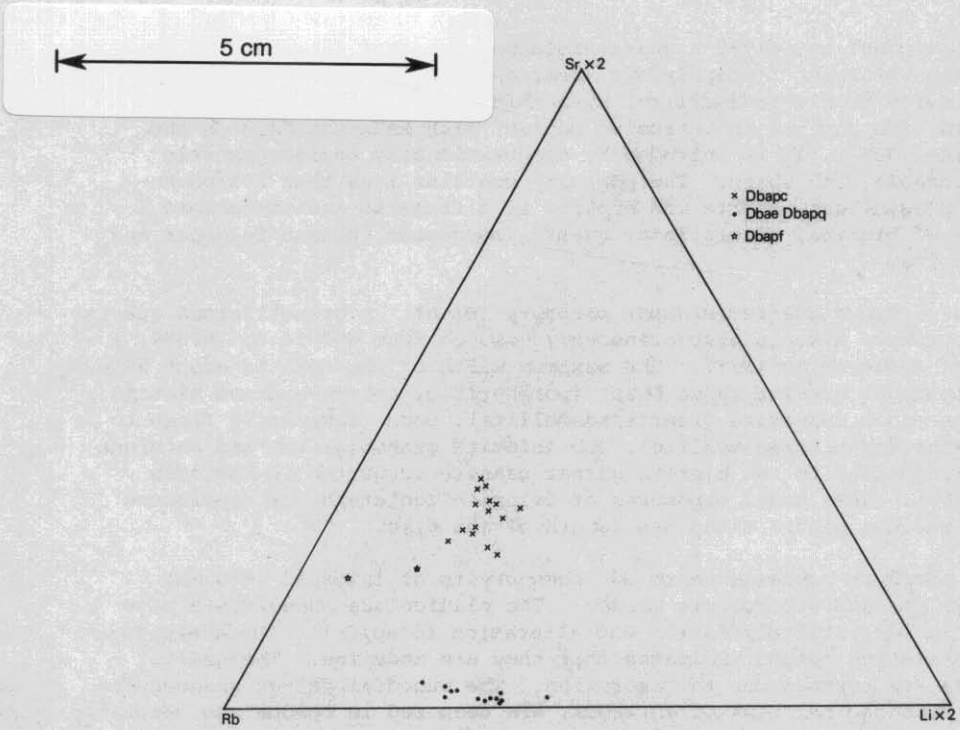

Figure 7. *Rb-Sr x 2-Li x 2 diagram showing the greater similarity of rock type Dbapf to Dbapc than to Dbae and Dbapq.*

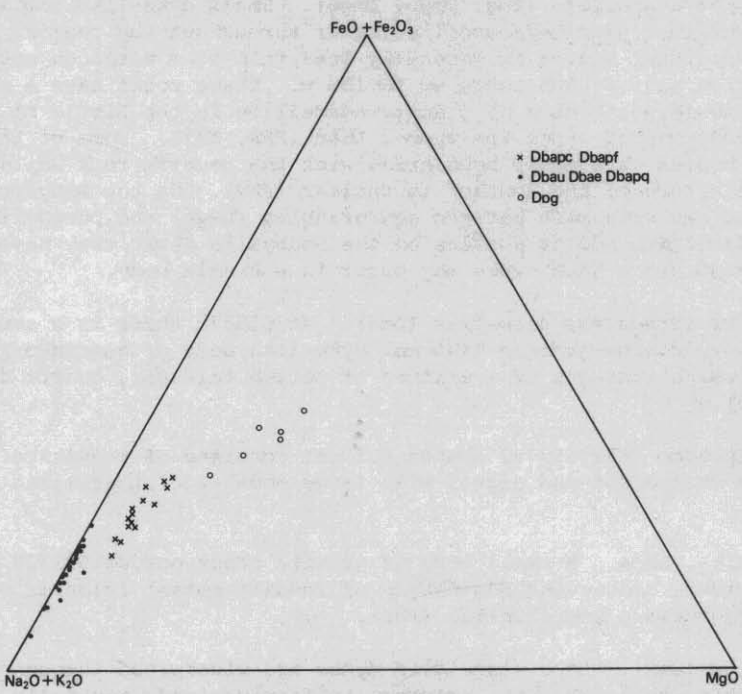

Figure 8. *AFM diagram showing plot of granitic rocks from the Blue Tier Batholith listed in this Bulletin.*

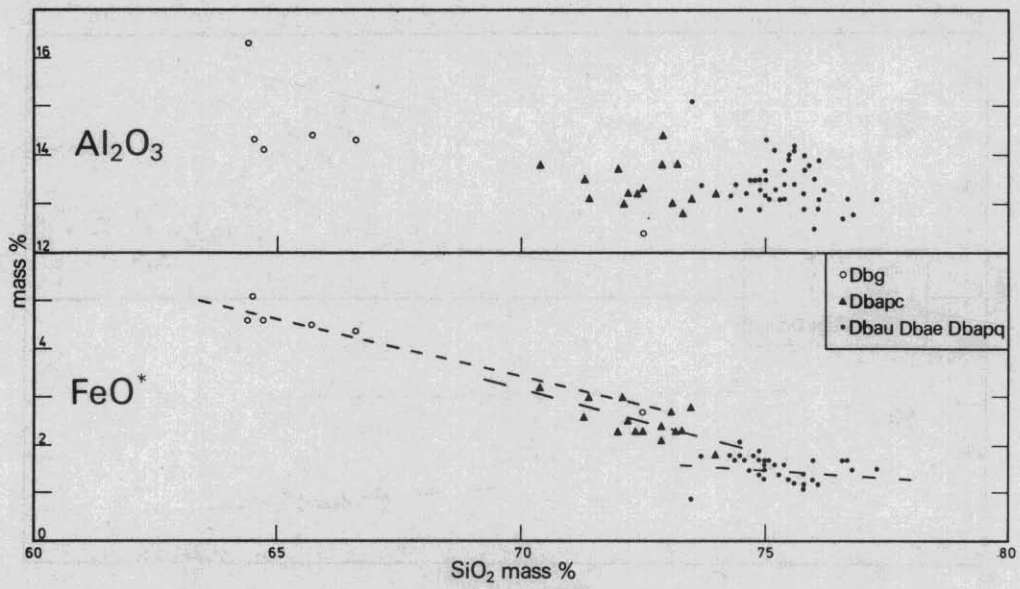

Figure 9. *Harker variation diagrams for granitic rocks, Al_2O_3 and FeO against SiO_2.*

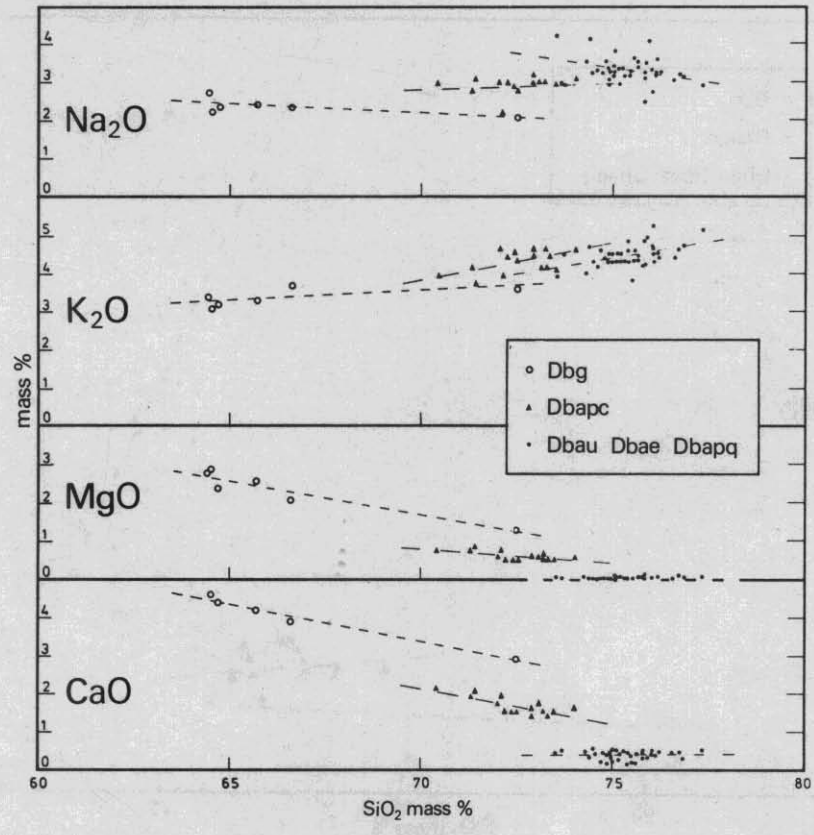

Figure 10. *Harker variation diagrams for granitic rocks, Na_2O, K_2O, MgO and CaO against SiO_2.*

5 cm

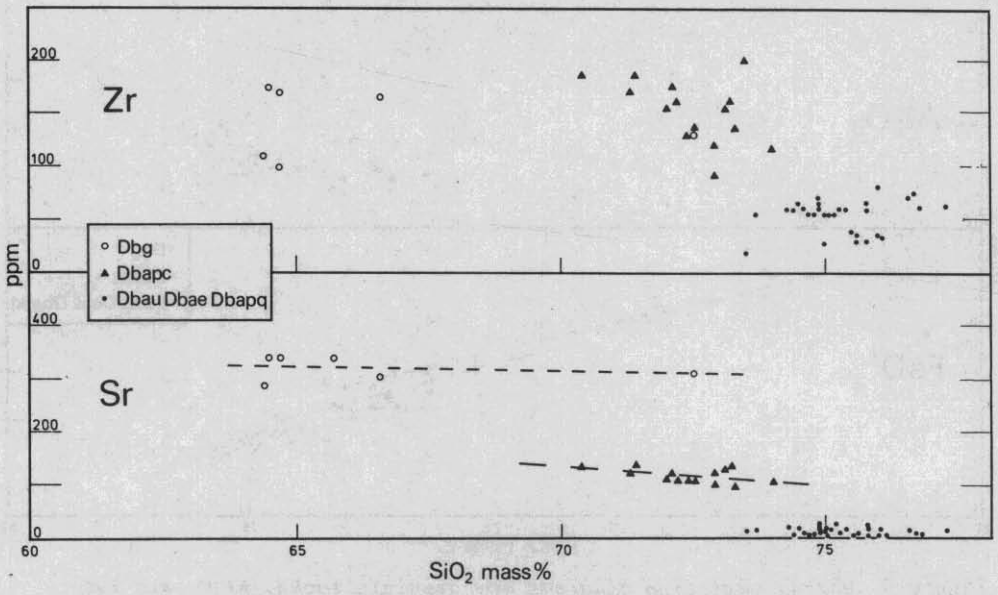

Figure 11. *Harker variation diagrams for granitic rocks, Zr and Sr against SiO_2.*

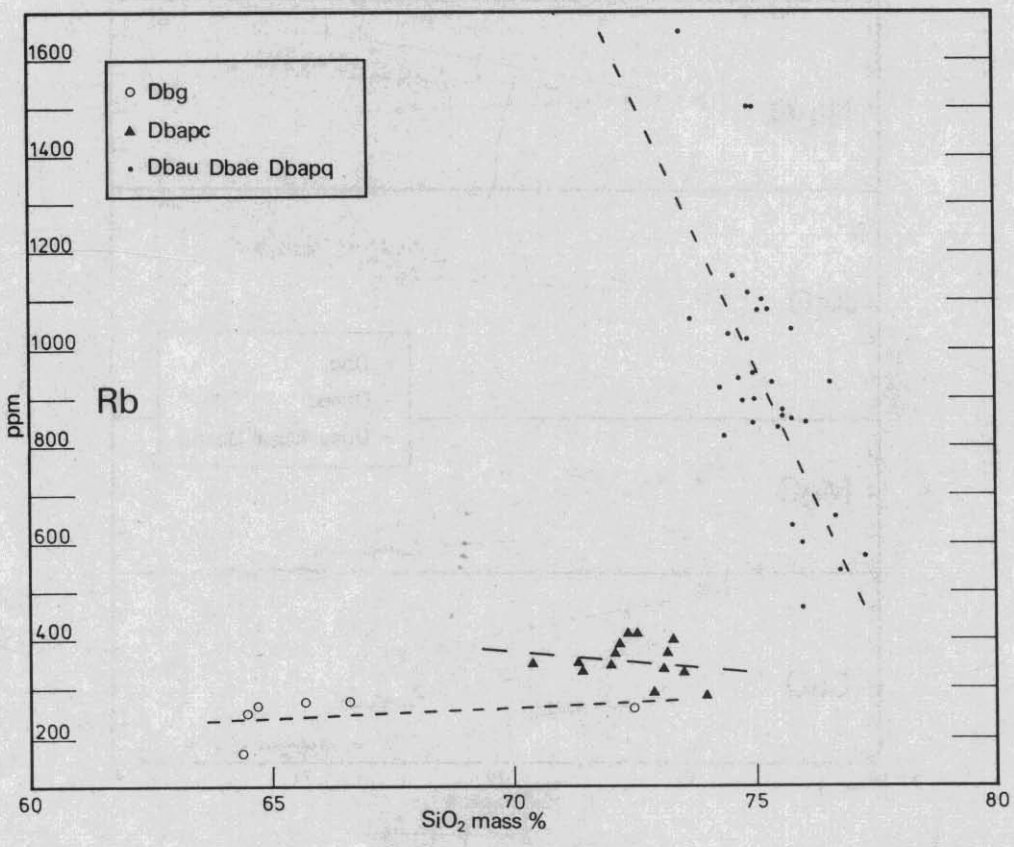

Figure 12. *Harker variation diagrams for granitic rocks, Rb against SiO_2.*

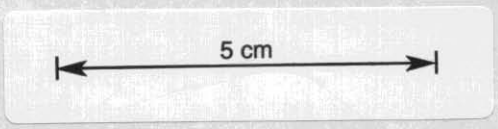

Table 9. CIPW NORMS OF GRANITIC ROCKS

Plot No.	1	2	3	4	5	6	7	8	9	10	11
Analysis No.	735120	735121	735126	735127	735128	735129	735130	735131	735132	735133	735134
Q	23.53	24.70	35.34	37.31	37.02	39.54	36.66	41.43	37.54	37.57	39.08
Or	18.32	19.50	24.23	25.41	27.19	24.82	23.64	25.41	24.82	26.00	25.41
Ab	19.46	21.16	25.39	28.77	27.92	27.92	30.46	28.39	28.77	27.92	27.08
An	19.54	18.33	6.66	1.50	0.65	0.94	1.53	0.62	0.89	1.15	1.25
Co	0	0	1.29	2.70	2.85	3.38	2.39	4.28	2.74	2.29	2.72
Di	1.41	0.98	0	0	0	0	0	0	0	0	0
Hy	12.23	9.91	4.30	1.75	1.30	1.23	1.55	1.26	1.79	1.72	1.30
Mt	1.60	2.18	0.96	0.87	0.86	0.87	1.00	1.12	0.68	0.86	0.70
Il	1.27	1.01	0.70	0.13	0.11	0.17	0.15	0.17	0.15	0.15	0.15
Ap	0.57	0.47	0.28	0.28	0.21	0.31	0.31	0.26	0.38	0.28	0.36
Hm	0	0	0	0	0	0	0	0	0	0	0
Fl	0	0	0	0	0	0	0	0	0	0	0
Ca											

Plot No.	12	13	14	15	16	17	18	19	20	21	22
Analysis No.	735135	735136	735137	735138	735139	735140	735141	735142	735143	735144	735144
Q	36.56	72.89	37.61	40.71	39.07	39.87	37.97	31.57	35.55	23.67	36.95
Or	26.59	10.64	27.19	26.00	26.59	26.00	26.59	27.78	26.00	18.91	21.28
Ab	28.77	0.42	27.08	26.23	26.23	25.39	27.08	35.54	30.46	20.31	17.77
An	1.38	0.28	1.33	1.30	0	0.09	0.78	0.84	1.27	18.25	13.54
Co	2.13	9.57	2.37	2.36	3.33	3.77	2.78	1.10	2.35	0	0.09
Di	0	0	0	0	0	0	0	0	0	0	0
Hy	2.04	1.46	2.16	0.97	1.24	1.52	1.86	0.08	2.00	11.41	7.12
Mt	0.64	0.99	0.52	1.26	0.73	0.91	0.64	1.54	0.74	0.73	0.42
Il	0.13	0.13	0.13	0.15	0.15	0.15	0.15	0.11	0.11	1.03	0.65
Ap	0.31	0.33	0.31	0.28	0.33	0.24	0.40	0.31	0.33	0.50	0.31
Hm	0	0	0	0	0	0	0	0.34	0	0	0
Fl	0	0	0	0	0	0	0	0	0	0	0
Ca											

Table 9. (continued).

Plot No.	23	24	25	26	27	28	29	30	31	32	33
Analysis No.	735146	735147	735148	735149	735701	735702	735703	735704	735705	735706	735707
Q	25.38	37.30	37.57	37.45	33.48	34.92	33.17	31.73	33.68	36.98	35.00
Or	21.87	26.59	25.41	25.41	26.00	24.23	27.18	17.18	26.59	26.00	25.41
Ab	20.31	25.39	27.92	28.77	25.39	25.39	25.39	25.39	24.54	22.00	23.69
An	17.32	1.62	1.98	1.37	6.79	7.78	6.66	7.78	6.79	6.36	6.79
Co	0	3.00	2.09	2.15	1.01	0.78	1.45	0.93	1.07	1.43	1.55
Di	0.65	0	0	0	0	0	0	0	0	0	0
Hy	10.00	2.25	0.90	1.34	2.89	3.22	4.08	3.61	3.34	3.24	3.60
Mt	1.42	0.61	1.60	1.19	1.59	1.59	0.87	1.00	1.13	1.06	0.98
Il	0.99	0.11	0.21	0.15	0.55	0.59	0.53	0.55	0.55	0.49	0.55
Ap	0.45	0.33	0.31	0.26	0.24	0.24	0.28	0.24	0.24	0.21	0.24
Hm	0	0	0	0	0	0	0	0	0	0	0
Fl	0	0	0	0	0	0	0	0	0	0	0
Ca											

Plot No.	34	35	36	37	38	39	40	41	42	43	44
Analysis No.	735708	735709	735710	735711	735712	741645	741646	742515	742516	742517	742518
Q	32.74	38.74	32.89	31.40	32.86	19.91	12.09	34.40	36.89	37.91	38.75
Or	24.23	23.48	21.87	23.05	30.14	20.09	10.64	27.19	26.59	26.00	24.82
Ab	23.69	18.62	26.23	25.39	22.85	23.69	25.39	26.23	30.46	28.77	29.62
An	8.77	8.64	9.14	9.44	4.97	20.46	24.06	5.27	3.11	0	0
Co	1.24	1.99	0.65	1.19	2.12	0.52	0	2.19	0	3.75	3.70
Di	0	0	0	0	0	0	7.20	0		0	0
Hy	5.55	4.18	4.55	5.00	3.49	11.75	15.84	3.27	2.29	2.33	1.32
Mt	0.45	1.45	1.42	1.20	0.83	1.74	2.18	0.61	0.07	0	0.65
Il	0.67	0.74	0.78	0.80	0.55	0.95	1.25	0.48	0.02	0.02	0
Ap	0.24	0.28	0.28	0.35	0.35	0.50	0.28	0.24	0.21	0.24	0.31
Hm	0	0	0	0	0	0	0	0	0	0	0
Fl	0	0	0	0	0	0	0	0.35	0.99	1.07	1.00
Ca											

Table 9. (continued).

Plot No.	45	46	47	48	49	50	51	52	53	54	55
Analysis No.	742519	742520	742521	742522	742523	742524	742525	742526	742527	742528	742529
Q	37.35	38.83	37.82	39.56	39.78	39.98	40.19	36.37	32.72	37.69	35.32
Or	25.41	28.38	25.41	27.19	30.73	30.14	27.78	28.37	27.19	27.78	25.41
Ab	30.46	26.23	29.62	27.08	22.85	24.54	26.23	27.08	27.08	27.92	32.16
An	0	0	0	0	0	0	0	1.68	4.29	0	0
Co	3.42	2.91	2.99	2.86	2.43	2.81	2.61	2.63	2.59	2.98	3.40
Di	0	0	0	0	0	0	0	0	0	0	0
Hy	1.64	1.20	2.08	1.97	1.30	2.01	1.26	2.24	4.16	2.45	2.48
Mt	0.58	0.61	0.23	0.74	0.71	0.52	0.90	0.61	0.48	0.42	0.07
Il	0	0.10	0	0.11	0.13	0.11	0.11	0.29	0.51	0.04	0.02
Ap	0.21	0.14	0.21	0.19	0.14	0.14	0.12	0.34	0.36	0.19	0.21
Hm	0	0	0	0	0	0	0	0	0	0	0
Fl	0.85	0.56	0.89	0.60	0.50	0.58	0.38	0.23	0.24	0.85	0.83
Ca	0.23	0.09	0.39	0.27	0.39	0.23	0.09	0.14	0.30	0.77	0.25

Plot No.	56	57	58	59	60	61	62	63	64	65	66
Analysis No.	742530	742536	742596	742597	742598	742599	742600	742601	742602	742603	742604
Q	38.73	34.11	39.31	37.46	33.11	37.79	37.82	39.76	39.53	38.36	39.77
Or	25.41	26.00	26.00	26.59	28.96	27.19	26.00	25.41	25.41	27.19	26.59
Ab	27.92	25.39	27.92	28.77	34.69	28.77	28.77	27.08	27.92	27.92	27.08
An	0	6.17	0	0	0.14	0	0	0	0	0	0
Co	3.62	1.84	3.11	2.84	1.70	3.63	3.15	3.48	3.02	2.49	2.97
Di	0	0	0	0	0	0	0	0	0	0	0
Hy	1.32	3.58	1.83	1.59	0.26	0.92	0.98	1.22	1.98	2.01	1.05
Mt	0.93	1.06	0.58	0.99	0.46	0.45	0.13	0.55	0.28	0.57	1.17
Il	0.04	0.55	0.10	0.10	0.08	0.08	1.16	0.11	0.11	0.11	0.11
Ap	0.26	0.26	0.36	0.33	0.26	0.31	0.10	0.24	0.31	0.31	0.26
Hm	0	0	0	0	0	0	0	0	0	0	0
Fl	0.99	0.21	0.65	0.84	0.25	0.53	0.33	0.54	0.70	0.55	0.64
Ca	0.32	0.11	0	0	0	0	0	0	0	0	0

Table 9. (continued).

Plot No.	67	68	69	70	71	72	73	74	75	76	77
Analysis No.	742605	742606	742607	742608	741222	741223	741224	741225	741226	741227	741235
Q	41.90	38.99	36.95	33.82	35.34	32.96	33.61	34.59	31.62	23.95	31.92
Or	28.37	22.46	28.37	23.05	23.64	26.00	25.41	25.41	24.23	16.55	21.27
Ab	21.16	31.31	27.92	35.54	36.39	30.46	29.62	34.69	30.46	30.46	29.62
An	0	0	0	0	2.14	5.13	5.76	2.23	6.06	14.70	8.15
Co	3.59	3.70	2.69	3.97	0.71	1.03	0.68	0.68	0.72	0.26	1.06
Di	0	0	0	0	0	0	0	0	0	0	0
Hy	2.13	0.95	0.83	0.70	0.66	3.11	3.40	1.14	5.27	10.55	5.16
Mt	0.65	0.93	0.77	0.54	0.91	0.84	0.62	0.88	0.55	0.90	0.84
Il	0.15	0.06	0.19	0.06	0.02	0.19	0.21	0.04	0.25	0.82	0.47
Ap	0.19	0.28	0.28	0.85	0.07	0.12	0.07	0.07	0.14	0.43	0.28
Hm	0	0	0	0	0	0	0	0	0	0	0
Fl	0.62	0.57	0.08	0.74	0	0	0	0	0	0	0
Ca	0	0	0.18	0.16	0	0	0	0	0	0	0

Table 10. INDEX TO ANALYSES OF GRANITIC ROCKS LISTED IN TABLES 5, 9 AND APPENDIX 5, TABLE 1

Analysis No.	Department and thin section No.	Grid reference (EQ)	Plot No.	Map Symbol
735120	73/516	741357	1	Dbg
735121	73/517	745361	2	Dbg
735126	73/522	729466	3	Dbapc
735127	73/444	730366	4	Dbau
735128	73/523	736356	5	Dbau
735129	73/445	728360	6	Dbau
735130	73/446	732354	7	Dbau
735131	73/524	688369	8	Dbau
735132	73/447	695364	9	Dbau
735133	73/525	702362	10	Dbau
735134	73/526	703354	11	Dbau
735135	73/527	705349	12	Dbau
735136	73/528	718336	13	
735137	73/448	728345	14	Dbau
735138	73/449	727350	15	Dbau
735139	73/529	719355	16	Dbau
735140	73/530	714361	17	Dbau
735141		720365	18	Dbau
735142	73/450	732375	19	Dbau
735143	73/451	730377	20	Dbau
735144	73/452	728839	21	Dbg
735145	73/456	736388	22	Dbg
735146	73/453	736372	23	Dbg
735147	73/457	294346	24	Dbau
735148	73/454	703345	25	Dbau
735149	73/455	707380	26	Dbau
735701		82684936	27	Dbapc
735702		81015068	28	Dbapc
735703		83695173	29	Dbapc
735704		82255127	30	Dbapc
735705		80734885	31	Dbapc
735706		80624784	32	Dbapc
735707		81104736	33	Dbapc
735708		79925171	34	Dbapc
735709		80885290	35	Dbapc
735710		79825036	36	Dbapc
735711		79784942	37	Dbapc
735712		77384850	38	Dbapf
741645	74/435	746379	39	Dbg
741646	74/460	655377	40	
742515	74/516	826433	41	Dbapc
742516	74/527	794410	42	Dbae
742517		795410	43	Dbae
742518	74/528	802411	44	Dbae
742519	74/529	800411	45	Dbae
742520	74/530	799411	46	Dbae
742521		790434	47	Dbae
742522	74/532	792433	48	Dbapq
742523		780428	49	Dbapq
742524	74/533	793429	50	Dbapq
742525		791434	51	Dbapq

Table 10. (continued).

Analysis No.	Department and thin section No.	Grid reference (EQ)	Plot No.	Map Symbol
742526	74/534	792448	52	Dbapf
742527	74/535	784443	53	Dbapc
742528	74/536	786426	54	Dbae
742530		802411	56	Dbae
742536	74/526	790453	57	Dbapc
742596	75/41	726377	58	Dbau
742597	75/47	724383	59	Dbau
742598	75/48	729382	60	Dbau
742599	75/49	733379	61	Dbau
742600	75/50	710352	62	Dbau
742601	75/51	704369	63	Dbau
742602	75/52	701384	64	Dbau
742603	75/53	688392	65	Dbau
742604	75/54	692403	66	Dbau
742605	75/55	688418	67	Dbau
742606	75/56	727409	68	Dbau
742607	75/57	815356	69	Dbapf
742608	75/58	831364	70	Dbae
741222	74/303	56573793	71	
741223		56573793	72	Dsac
741224	74/304	56833765	73	Dsac
741225	74/309	54164045	74	Dsam
741226	74/310	53824027	75	Dsac
741227		55054010	76	Dsg
741235	74/405	52293796	77	Dsaw

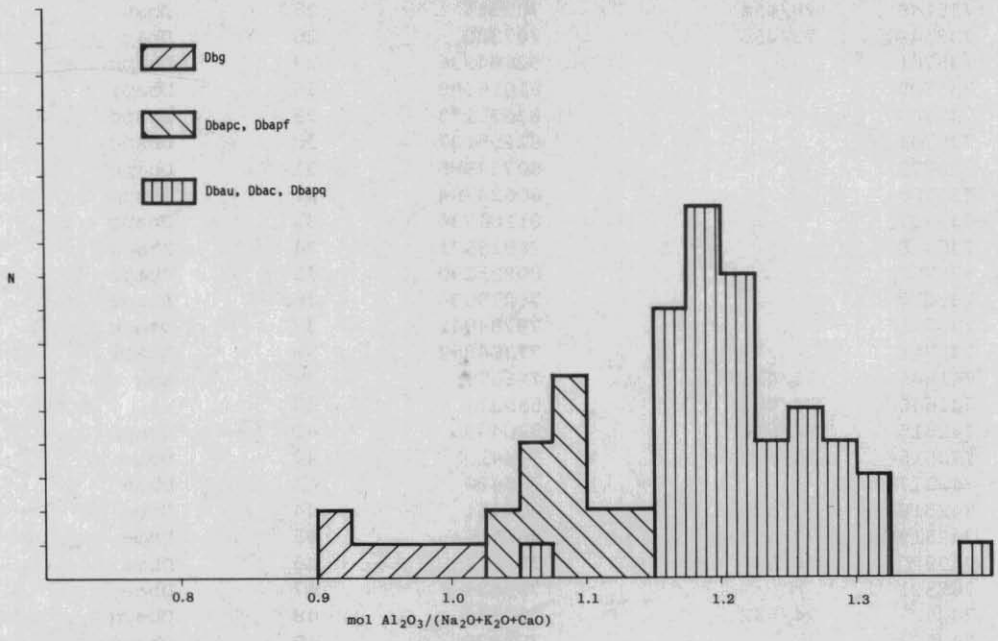

Figure 13. *Histogram of mol. $Al_2O_3/(Na_2O+K_2O+CaO)$ values for granitic rocks of the Blue Tier Batholith.*

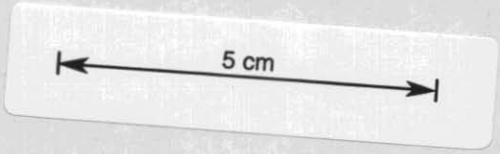

A 10 m wide dyke occurs on the Frome River at 788418 and larger bodies occur on the southern slopes of Mt Cameron between 764600 and 804607. In many places (*e.g.* 788418) they can be seen to be structurally controlled, often with irregular margins following pre-existing joints (*JM*).

GEOCHEMISTRY

Major and trace element chemistry and CIPW norms of granitic rocks from the Ringarooma map sheet are presented in Tables 5 and 9. Geochemical variations shown by the rocks from the Blue Tier Batholith are illustrated by an AFM diagram (fig. 8) and by Harker variation diagrams (figs. 9-12). The AFM diagram shows a typical calc-alkali trend but it is noticeable that there is a small gap between the three groups of rocks distinguished on the diagram which are essentially granodiorite (Dbg), adamellite (Dbapc, Dbapf) and alkali granite (Dbau, Dbae, Dbapq). This threefold division is brought out more clearly in the Harker diagrams where the same rocks can be seen to belong to three chemical suites. For each suite there is an approximately linear relationship between SiO_2 and the other elements forming trends characteristic of that suite. These suites will be referred to as the granodiorite, adamellite, and alkali granite suites. The difference between the suites is most marked among the major elements for CaO, MgO and FeO (total Fe) with the granodiorite suite being richer in these oxides than the adamellite suite and it in turn richer than the alkali granite suite, for similar SiO_2 values. For the trace elements the difference between the suites is brought out clearly by Sr and the difference between the alkali granite suite and the others is very marked for Rb and Li.

Analyses from the Scottsdale Batholith rocks are similar to those from the Blue Tier Batholith except that the adamellites are more sodic and slightly less potassic.

The approximately linear relationships between SiO_2 and the other elements for the three suites suggests that it may be useful to consider the origin of these granitic rocks in terms of the restite model of granitoid genesis (White and Chappell, 1977). This model postulates that some granitoid suites consist of melt and residium (= restite) and that the variation between different rock bodies making up the suite is produced by different degrees of separation of restite and melt thus giving straight lines on Harker variation diagrams. Since the granitoids are a mixture of crystallised melt and restite, their bulk composition is a reflection of their source rock. This allows a distinction to be made between those granites derived by the melting of sedimentary rocks from those granites derived by the melting of igneous rocks due to the different geochemical characteristics of these rock types. Sedimentary rocks have gone through the weathering process and have had Na and Ca removed to be concentrated in sea water, evaporites and limestones while K is absorbed by clays during sedimentation and diagenesis. Thus pelitic sedimentary rocks are strongly peraluminous, i.e. $(Al/Na + K + (Ca/2)) > 1.1$ and have low Na/K ratios. Because pelitic rocks are enriched in Rb relative to Sr, with time, they become enriched in radiogenic strontium thus giving high initial Sr^{87}/Sr^{86} ratios. Conversely igneous rocks which have not been through a sedimentary cycle have high total Na, K and Ca relative to Al and high Na/K ratios.

Using these and other criteria it is possible to decide the sedimentary (S-type) or igneous (I-type) nature of the source rocks for the three suites. In Figure 13 a histogram of $Al/Na + K + (Ca/2)$ values shows that the granodiorite suite rocks have values less than the 1.1 suggested by Chappell and White (1974) as marking a boundary between the I- and S-type

Table 11. ANALYSES OF MATHINNA BEDS ROCKS

	South of Ansons Bay	Scottsdale Sidling		
	Pelite	Shale	Siltstone	Fine-grained sandstone
Analysis No.	762466	38035	38036	38073
SiO_2	56.8	61.45	78.15	81.11
TiO_2	0.71	0.85	0.56	0.53
Al_2O_3	21.2	19.94	10.70	10.66
Fe_2O_3	1.5	5.14	3.18	2.72
FeO	4.9	-	-	-
MnO	0.04	-	-	-
MgO	3.0	2.19	1.75	1.40
CaO	0.43	0.03	0.09	0.11
Na_2O	0.48	0.50	0.37	0.13
K_2O	5.6	5.36	2.29	1.55
P_2O_5	0.12	0.11	0.06	0.12
H_2O	4.1	3.95	2.32	0.48
H_2O	0.60	-	-	-
CO_2	0.05	-	-	-
F	0.06	-	-	-
Total	99.59	99.52	99.47	98.82
Trace elements				
Rb	228	124	94	204
Sr	50	-	-	20
Ab/An	7.5	∞	112.5	∞

Analyses 38035 - 38037 from Skrzecynski 1971.

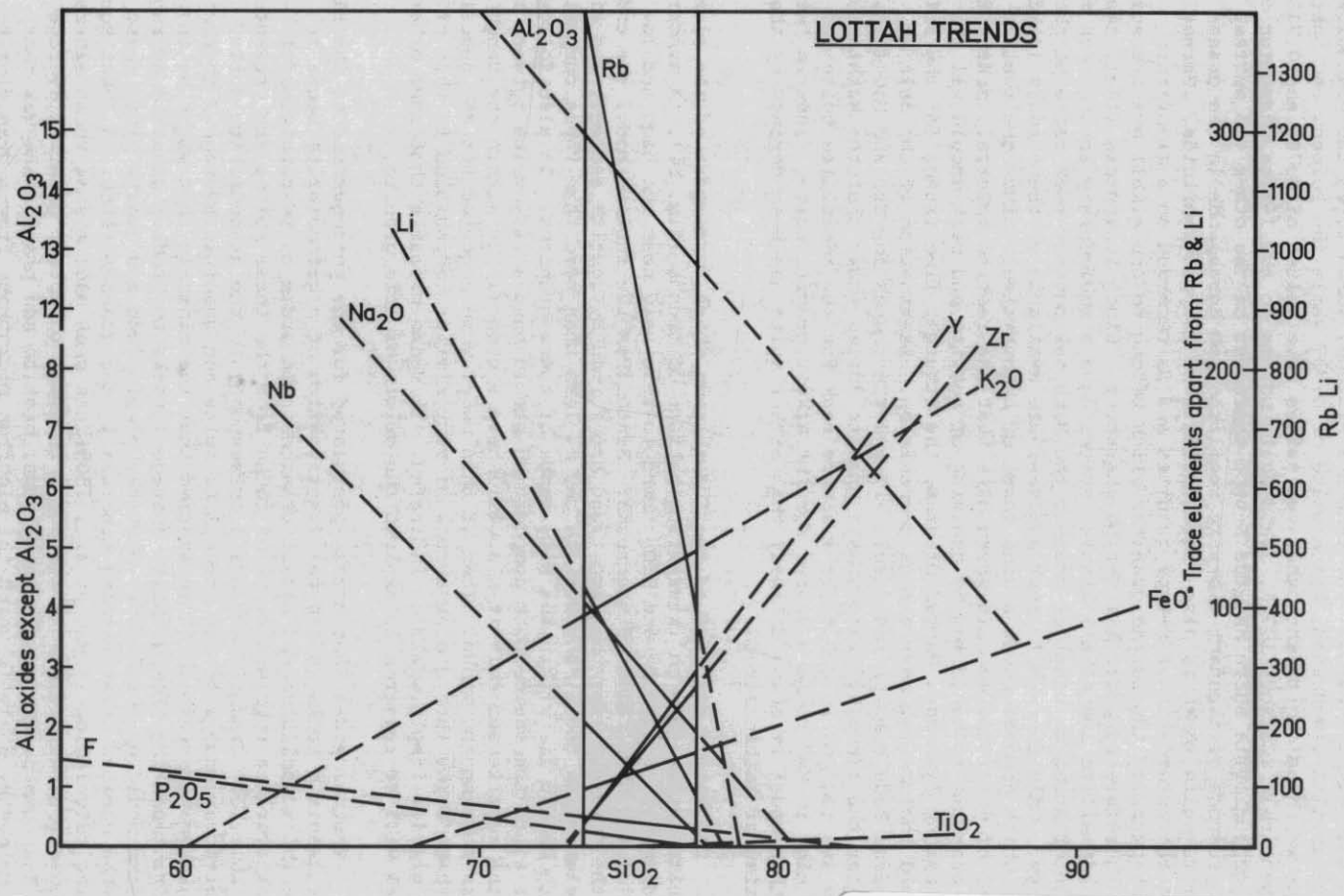

Figure 14. *Trends for alkali granites of the Lottah Mass.*

granites and therefore have I-type characteristics. The other two suites mostly have S-type values. Another criteria is the initial Sr^{87}/Sr^{86} ratio with S-type granites generally having values greater than 0.708 and I-type values of 0.704 - 0.706. The Pyengana Plutons, which forms the granodiorite suite in this discussion, has a value of 0.707 while the Poimena and Lottah rocks which belong to the other two suites have values of 0.709 and 0.710 respectively (Cocker, 1977). This again points to the I-type character of the granodiorite suite and the S-type character of the other two suites. The presence of abundant dioritic xenoliths and hornblende in the granodiorite suite rocks is also characteristic of I-type granitoids. Garnet is a characteristic of S-type granites and is recorded as a minor rare constituent of the Lottah granites which belong to the alkali granite suite and therefore supports its S-type character. Since it appears likely that the adamellite and alkali granite suites have a sedimentary source rock it is interesting to consider whether the Mathinna country rock could be that source. Only four whole rock analyses are available of these rocks (Table 11), which however cover a wide range of composition. Since the restite model of granitoid genesis postulates that the restite material, source rock and granitic rocks formed by unmixing of restite and melt should all lie on a straight line on a Harker diagram, the straight line trends for the suites should include the source rock composition. Examination of the data on Mathinna Beds composition (Table 11) and the trends for CaO and MgO (fig. 10) for the adamellite and alkali granite suites shows that the Mathinna Beds are too low in CaO to be a source rock for the adamellite suite and too high in MgO to be a source for the alkali granite suite. Thus in terms of this model it seems unlikely that either suite has been derived by the melting of Mathinna Beds.

The alkali granites of the Lottah mass which forms part of the alkali granite suite, show an interesting pattern of trends (fig. 14). A number of elements, *e.g.* P_2O_5 and TiO_2 trend to zero very near the high and low end of the SiO_2 range of the rocks. Since from the restite model the ends of the straight line unmixing trend are formed by restite and melt and since no element in these compositions can be less than zero then these compositions should lie within the SiO_2 range of these granites. It also follows that since the source rock composition should have a SiO_2 value between that of the restite and melt it also will have a composition within the range of rocks forming the trend. Thus if this model were accepted for the genesis of these rocks then a source rock of very similar composition to that of the granite itself would be indicated. It seems probable that some other model will be required to explain the origin of this granite.

Another model that may be postulated for the petrogenesis of the Blue Tier granitic rocks is crystal fractionation of a granodiorite magma to give the adamellites and alkali granites. In order to test this model three averages representative of rocks from the three suites are presented in Table 12. Granitic average 1 corresponds to the granodiorite suite, granitic average 2 to the adamellite suite and granitic average 3 to the alkali granite suite. It is assumed that the minerals that might be involved in fractionating from granitic average 1 rocks to produce granitic average 2 rocks would be hornblende, biotite, plagioclase and quartz since these are the earlier crystallising minerals in the granodiorites. A least squares mixing calculation (Bryan *et al.*, 1969) has been made mixing these mineral compositions with granitic average 2 in order to obtain granitic average 1. The composition of the hornblende, biotite and plagioclase was that determined by analysis using the electron microprobe from a granodiorite specimen (table 13). H_2O was not considered in the calculation and all compositions involved were recalculated to 100% on an anhydrous basis (table 14). This is justified on the grounds that the H_2O content of the analysed

Table 12. AVERAGE COMPOSITIONS AND CIPW NORMS OF THREE GRANITIC ROCK TYPES FROM THE RINGAROOMA MAP SHEET

	1 Average Dbg	2 Average Dbapc	3 Average Dbau, Dbae & Dbapq		1	2	3
SiO_2	66.27	72.43	75.35	Q	25.60	34.07	38.20
TiO_2	0.52	0.32	0.06	Or	19.97	25.18	26.30
Al_2O_3	14.30	13.39	13.42	Ab	20.48	24.45	28.26
Fe_2O_3	1.32	0.77	0.56	An	18.17	7.57	0
FeO	3.50	1.86	1.02	Co	0	1.25	3.11
MnO	0.08	0.05	0.04	Di	0.58	0	0
MgO	2.35	0.61	0.04	Hy	10.19	3.86	1.48
CaO	4.07	1.67	0.38	Mt	1.91	1.12	0.81
Na_2O	2.42	2.89	3.34	Il	0.99	0.61	0.11
K_2O	3.38	4.26	4.45	Ap	0.47	0.26	0.33
P_2O_5	0.20	0.11	0.14	Fl	-	-	0.69
H_2O^+	1.40	1.11	0.79	Ca	-	-	0.27
H_2O^-	0.37	0.02	0.15				
CO_2	-	-	0.12*				
F	-	-	0.35*				
Trace elements (ppm)							
Li	50	76	201				
Sn	10	19	32				
Rb	247	354	883				
Sr	320	117	13				
Y	31	47	45				
Zr	142	152	49				
Nb	-	-	24*				
Mg/Li	283	48	1				
K/Rb	114	100	42				
Number of analyses	6	15	44 (* 25 for CO_2, F, Nb)				

Table 13. MINERAL COMPOSITION AND STRUCTURAL FORMULAE OF MINERALS FROM GRANODIORITE EAST OF MT PARIS (plot number 39, table 5).

	Plagioclase		Potash feldspar				Biotite				Hornblende
SiO_2	56.30	56.22	64.67	64.84			36.58	36.95			45.26
TiO_2	0	0	0	0.12			3.06	3.16			0.66
Al_2O_3	27.72	27.76	18.71	18.69			14.86	14.86			7.44
Cr_2O_3	0.16	0.13	0	0			0.17	0			0.22
Fe_2O_3	-	-	-	-			-	-			3.13
FeO	0	0	0	0			19.45	18.86			15.79
MnO	0	0	0	0			0	0			0.21
MgO	0	0	0	0			11.86	12.04			10.32
CaO	8.97	9.08	0.87	0.78			0.54	0.48			12.87
Na_2O	6.59	6.54	0.46	0.63			0	0			1.17
K_2O	0.24	0.27	15.19	14.93			9.87	9.68			0.92
H_2O	0	0	0	0			3.93	3.96			1.99
Total	99.98	100.02	100.02	99.99			99.98	99.99			99.98
Si	10.12	10.11	11.92	11.93	Tet	Si	5.57	5.59	Tet	Si	6.81
Al	5.87	5.88	4.06	4.05		Al	2.43	2.41		Al	1.19
Fe^{+3}	-	-	-	-		Σ	8.00	8.00		Σ	8.00
Cr	0.02	0.02	0	0	Oct	Al	0.18	0.25	Oct	Al	0.13
Ti	0	0	0.02	0.02		Fe^{+3}	-	-		Ti	0.07
Mg	0	0	0	0		Cr	0	0		Fe^{+3}	0.35
Fe^{+2}	0	0	0	0		Ti	0.35	0.36		Fe^{+2}	1.99
Na	2.30	2.28	0.16	0.23		Mg	2.69	2.72	M1-3	Cr	0.03
Ca	1.73	1.75	0.17	0.15		Fe^{+2}	2.48	2.39		Mg	2.31
K	0.06	0.06	3.57	3.50		Mg	0	0		Mn	0.03
Total	20.10	20.10	19.90	19.88		Σ	5.70	5.72		Σ	4.91
Or	1.35	1.49	91.42	90.20		Ca	0.09	0.08	X M1-3		0
Ab	56.31	55.73	4.19	5.82		Na	0	0		Ca	2.08
An	42.34	42.78	4.38	3.98		K	1.92	1.87	M4	Na	0
						Σ	2.01	1.95		Σ	2.08
					Total		15.71	15.67	A	Na	0.34
										K	0.18
										Σ	0.52
									Total		15.51

Hornblende formula calculated by the method developed by Papike *et al.* (1974) for maximum Fe^{+3}. Ideal H_2O content assumed and analyses normalised to 100.

Table 14. COMPOSITION OF MINERALS USED IN THE FIRST MIXING CALCULATION INVOLVING GRANITIC AVERAGES 1 AND 2

	Hornblende	Biotite	Plagioclase	Quartz
SiO_2	46.430	38.310	56.347	100.00
TiO_2	0.681	3.242	0	0
Al_2O_3	7.629	15.312	27.783	0
FeO*	19.099	19.960	0	0
MnO	0.220	0	0	0
MgO	10.587	12.454	0	0
CaO	13.204	0.530	9.039	0
Na_2O	1.203	0	6.575	0
K_2O	0.942	10.188	0.255	0

Compositions of hornblende, biotite and plagioclase determined by electron microprobe from a granodiorite specimen (plot number 39, table 5).

* all iron as FeO

Table 15. COMPARISON OF CALCULATED COMPOSITION OF GRANITIC AVERAGE 1 WITH ACTUAL COMPOSITION, MIXING HORNBLENDE, BIOTITE, QUARTZ AND PLAGIOCLASE WITH GRANITIC AVERAGE 2

	Granitic average 1	Granitic average 1 calculated	Residual	Square of residual
SiO_2	67.568	67.5679	-0.0001	0.0000
TiO_2	0.531	0.5098	-0.02115	0.0004
Al_2O_3	14.581	14.5343	-0.04662	0.0021
FeO*	4.781	4.9069	0.1259	0.0158
MnO	0.082	0.0487	-0.03324	0.0011
MgO	2.396	2.4036	0.00760	0.0000
CaO	4.145	3.9551	-0.18988	0.0360
Na_2O	2.463	2.9275	0.46459	0.2158
K_2O	3.449	3.2797	-0.16929	0.0286
				Σ 0.3001

% of material required to be added to granitic average 2 to obtain least squares fit to granitic average 1: 47.34.

% of different minerals in this material.

Hornblende	20.46	Plagioclase	40.36
Biotite	17.71	Quartz	21.47

Table 16. COMPOSITIONS OF MINERALS USED IN THE SECOND MIXING CALCULATION INVOLVING GRANITIC AVERAGES 2 AND 3

	Biotite	Plagioclase	Potash feldspar	Quartz
SiO_2	36.705	51.555	65.683	100.000
TiO_2	2.987	0	0	0
Al_2O_3	19.632	23.740	18.570	0
FeO*	25.693	0	0	0
MnO	0.042	0	0	0
MgO	5.655	0	0	0
CaO	0.426	5.040	0	0
Na_2O	0.213	8.865	2.719	0
K_2O	8.642	0	13.028	0

* all iron as FeO

Table 17. MINERAL/MELT DISTRIBUTION COEFFICIENTS USED IN CALCULATIONS

Mineral	Rb	Sr
Plagioclase	0.041	4.4
Potash feldspar	0.659	3.87
Biotite	3.26	0.12
Hornblende	0.014	0.22
Hypersthene	0.0027	0.0085
Apatite) Ilmenite) Magnetite) Sphene) Quartz)	0	0

Data from Hanson (1978).

Table 18. DEFINITIONS OF SYMBOLS USED IN TRACE ELEMENT MODELLING (AFTER HANSON, 1978, TABLE 1)

X^i	=	Mass fraction of phase i in the solid.
Kd^i	=	Mineral/melt mass distribution co-efficient of a trace element for phase i.
D	=	Bulk distribution co-efficient of a given trace element for the residual mineral phases at a time of separation of melt and residue; $D = \Sigma_i^n X^i Kd^i$.
Do	=	Bulk distribution co-efficient of a given trace element at the onset of melting.
p^i	=	Fractional contribution of phase i to the liquid or mass normative fraction of mineral i in the melt.
P	=	$\Sigma_i^n p^i Kd^i$.
Co	=	Mass concentration of a trace element in parent.
C_L	=	Mass concentration of a trace element in a derived melt.
C_S	=	Mass concentration of a trace element in the residual mineral phases.
D	=	C_S/C_L.
F	=	Mass fraction of melt relative to original parent.

rocks may not be that of the magma from which they crystallised due to loss of volatiles during the last stages of cooling. The results of the calculation are presented in Table 15. The difference between the calculated and actual composition of four of the oxides are greater than the limits of accuracy of the analyses making up the averages. The result, therefore does not support the fractionation model, however data on the possible fractionating phases are very limited and slightly different fractionating mineral compositions might yield a different result.

For the derivation of granitic average 3 rocks from granitic average 2 rocks biotite, plagioclase, potash feldspar and quartz were considered as the possible fractionating minerals and a mixing calculation made. Compositions representing the fractionating minerals (table 16) have been mixed with granitic average 3 to obtain granitic average 2. The biotite composition is taken from Groves (1977, table 22) and comes from a rock of the same type as those avaraged to form the granitic average 2. The potash feldspar is taken as Or 77 and the plagioclase as An 25 which are average values quoted in Groves (1977 p. 32) for the same rock type. The calculation yields a negative value for the proportion of granitic average 3 to be mixed with the postulated fractionating minerals. This indicates that this model is invalid for the mineral composition used in the calculation, however more data on the composition of possible fractionating minerals is required to more rigorously test it.

The fractionation model tested by the first mixing calculation involving separation of hornblende, biotite, plagioclase and quartz from granitic average 1 to give granitic average 2 can also be tested by their Rb and Sr concentrations. For this purpose the Rayleigh fractionation law as applied by Newman *et al.*, (1954) can be used to describe the trace element concentration of the differentiated melt, Cl, relative to the parent melt Co:

$$Cl/Co = F^{(D-1)}$$

where F is the fraction of the melt left and D is the bulk distribution coefficient of the trace element in crystals settling out of the melt (these and other symbols used later are listed in Table 18). The assumption of this fractionation law is that there is essentially instantaneous equilibrium precipitation of an infinitesimally small amount of crystals which immediately settle out of the melt and are immediately covered by another layer of crystals which prevent the earlier formed crystals from equilibrating with the evolving melt (Hanson, 1978).

The bulk distribution coefficient (D) has been calculated from the proportions of minerals indicated by the mixing calculation together with the mineral/melt distribution coefficient listed in Table 17. The fraction of residual melt (F) is the fraction of granitic average 2 required to be mixed with the fractionating minerals. Using these values the Rb and Sr values for granitic average 2 are calculated as 320 ppm and 186 ppm compared with the actual values of 354 ppm and 117 ppm. This result does not support the fractionation model but again more data on the composition of the fractionating minerals might change the result.

Another model for the petrogenesis of the granitic rocks of the Blue Tier Batholith is fractional crystallisation coupled with accumulation (McCarthy and Groves, 1979). This model postulates the intrusion of a magma of adamellite composition at a relatively high structural level as a sheet like mass. At the time of intrusion, the only liquidus minerals were plagioclase, hornblende, biotite and quartz. These minerals crystallised along the roof, walls and floor of the body, because of the cooling effect of the adjacent metasedimentary rocks. As a result of the homogenizing effect of

diffusion and especially convection this mineral assemblage continued to crystallise for a considerable time. Crystallisation in this manner caused the melt to become more potassic, and potash feldspar become a liquidus mineral. Continued inward crystallisation gave rise to adamellites and finally in the terminal stages, to granites (McCarthy and Groves, 1979).

In this model all granitic rocks in the batholith are accumulates and do not represent magmas. A possible problem with the model is the Zr values in the granodiorites and adamellites. Experimental work on the solubility of Zr in felsic liquids (Watson, 1979) has shown that it is strongly dependent on molar $(Na_2O + K_2O)/Al_2O_3$ with little sensitivity to temperature, SiO_2, Na_2O/K_2O or other compositional factors. Zirconium solubility appears to be controlled by the formation of alkali-zirconium silicate complexes of simple (2:1) alkali oxide:ZrO_2 stoichiometry. For silicate melts where molar $(Na_2O + K_2O/Al_2O_3)$ is less than 1, less than 100 ppm of Zr can dissolve before zircon crystals are formed. Since the three granitic averages representative of the range of granitic composition in the batholith have molar $Na_2O + K_2O$ less than molar Al_2O_3 it seems reasonable to assume that this was the case with the postulated source magma. Thus the original magma would not be expected to have more than 100 ppm of Zr dissolved in it. Any Zr greater than that value would be in the form of zircon crystals as residual minerals from the melting event that produced the magma. That the original magma was saturated with Zr can be concluded from the Zr values of 142 and 152 from granitic averages 1 and 2. One would expect that the first accumulate formed would therefore accumulate all the zircon crystals not dissolved in the melt. Thus the granodiorites would be expected to be very much richer in Zr than the adamellites however as the above figures show, this is not the case.

It would be expected with this model that the chemical variation within the batholith would be continuous or where there were gaps due to insufficient sampling or non exposure of some intermediate rock type that a reasonable extrapolation could be made to join the data in a single trend. The earlier discussion postulating three suites of rocks each with its own characteristic trend is an argument against this fractionation accumulation model.

Groves (1977) suggests there may be vertical zonation in the chemistry of muscovite-biotite granites. This can be tested to a certain extent for the granite in the Mt Paris area since the analyses come from a wide range of levels. No systematic variation could be detected for major elements, however a plot of Rb and Li against height (figs. 15 , 16) shows that rocks from the higher levels near the roof zone have a tendency to have high Rb and Li values with the effect being much more marked for Rb.

The results of microprobe analyses of plagioclase and potash feldspar from two granite specimens (plots 9 and 14, table 5) in the Mt Paris area are shown in Table 6 . All points are plotted in Figures 17 and 18 on a Ca-Na-K diagram. The average potash feldspar composition (table 6) was obtained by defocussing the electron beam so that a large part of the perthitic crystal was analysed. Stormer (1975) and Whitney and Stormer (1977) derived two expressions from which the composition of co-existing plagioclase and potash feldspar can be used to calculate their temperature of crystallisation. One of these expressions is for feldspar in the sanidine - high albite structural state and the other is for feldspar in the microcline - low albite state. XRD determination of the structural state of the potash feldspar in the two granite specimens from the Mt Paris area indicates a triclinicity value of approximately 0.70 and thus the microcline - low alibite expression is more appropriate and has been used in calculation. In Figure 19 the calculated temperatures are plotted on a

P-T diagram together with the granite solidus curve (Carmichael *et al.*, 1974, p. 265). The first specimen (plot 9) intersects the curve at 0.5 - 1.0 Kb suggesting that this is the pressure at which the granite crystallised if the feldspar crystallised from a melt. The other specimen (plot 14) yielded a lower temperature which suggests that it crystallised under sub-solidus conditions. This specimen comes from the roof zone of the granite and the first from about 250 m lower in the granite body. It seems possible that volatiles may have collected in the roof zone and allowed recrystallisation under lower temperature conditions. The composition of the two perthitic phases in the potash feldspar also allow the temperature of unmixing to be calculated which is approximately 60° lower than that for the average potash feldspar-plagioclase temperature.

If the pressure of crystallisation was 0.5 - 1.0 Kb muscovite could not have crystallised from the melt since the muscovite and quartz stability curve (Carmichael *et al.*, 1974, p. 265) intersects the granite solidus curve at about 3.5 Kb. The alteration of biotite to muscovite in granites of the Mt Paris area therefore probably took place under sub-solidus conditions.

The preceding discussion may be summarised by the following main points:

(1) The granitic rocks of the Blue Tier Batholith may be divided into the granodiorite, adamellite and alkali granite suites based on their petrology and chemistry;

(2) The granodiorite suite may have been derived from igneous source rocks and the adamellite and alkali granite suites from sedimentary source rocks;

(3) The petrogenesis of the rocks from the Lottah mass cannot be explained by the restite model unless they have been derived from melting a granitic rock of very similar composition;

(4) The Mathinna Beds are unlikely to have been a source rock for any of the granitic rocks;

(5) Derivation of the granitic rocks in the batholith from an original magma of granodioritic composition is unlikely;

(6) A fractionation accumulation model does not explain the Zr concentrations in the granodiorites and adamellites. It also does not explain the division of the batholith into distinct suites;

(7) The granite of the Mt Paris area probably crystallised from a melt at 0.5 - 1.0 Kb and 700 - 750°C and also underwent sub-solidus recrystallisation at about 600°C in the roof region of the intrusion.

FORM OF INTRUSIONS

M.P. McClenaghan

A sheet like form has been ascribed to most of the younger muscovite-biotite granite bodies in the Blue Tier Batholith (Gee and Groves, 1971; Groves and Taylor, 1973). Gee and Groves (1971) describe the granites referred to in this report by the symbols Dbae (equigranular, fine- to coarse-grained, biotite-muscovite granite/adamellite), Dbapq (porphyritic, fine- to medium-grained, biotite-muscovite granite/adamellite with pheno-

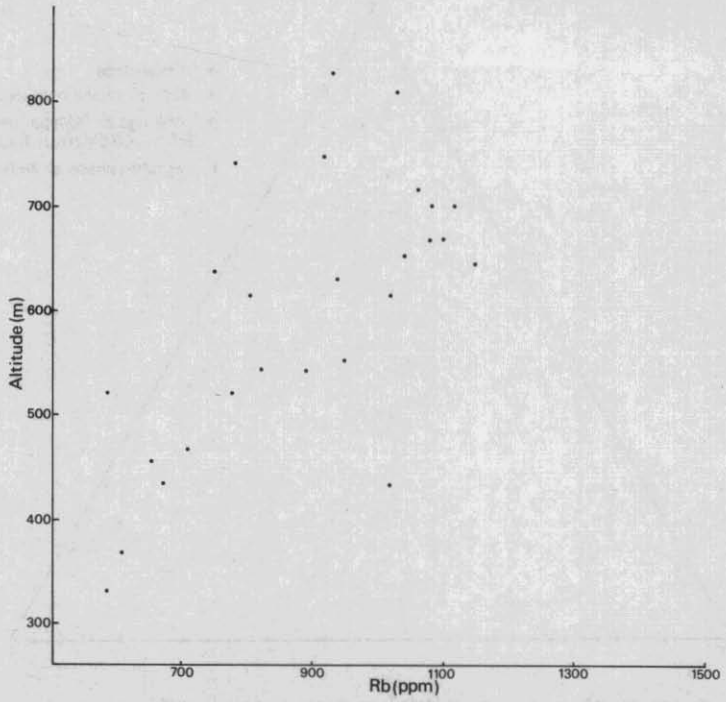

Figure 15. *Relationship between height and Rb content of granite mapped as Dbau in the Mt Paris area.*

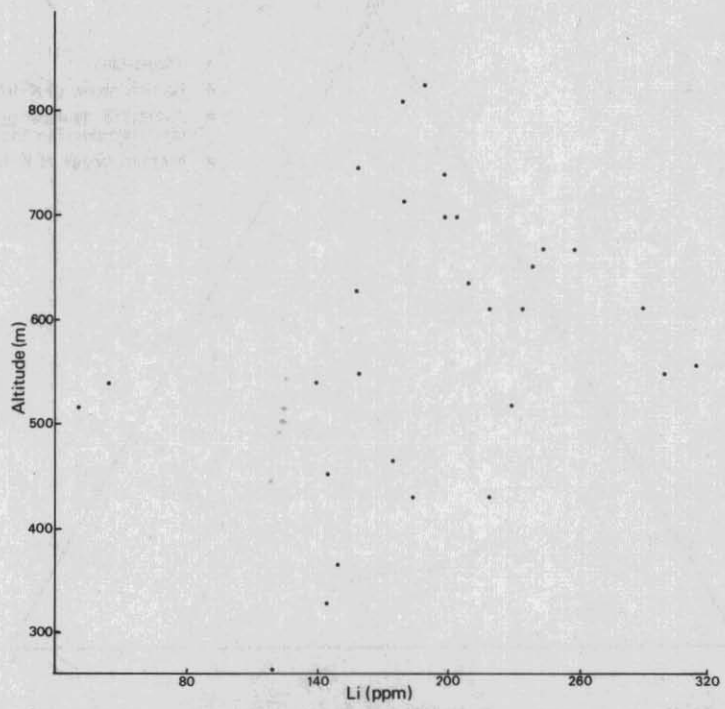

Figure 16. *Relationship between height and Li content of granite mapped as Dbau in the Mt Paris area.*

5 cm

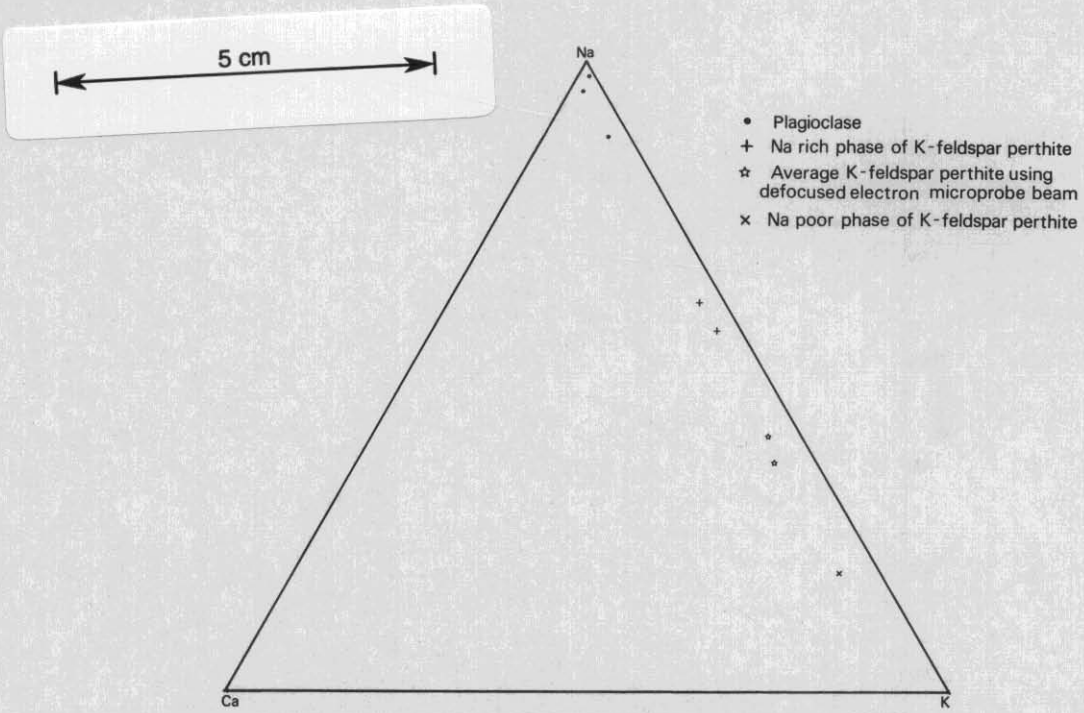

Figure 17. *Ca-Na-K diagram of feldspar compositions from specimen plot 9, table 5, as determined by electron microprobe.*

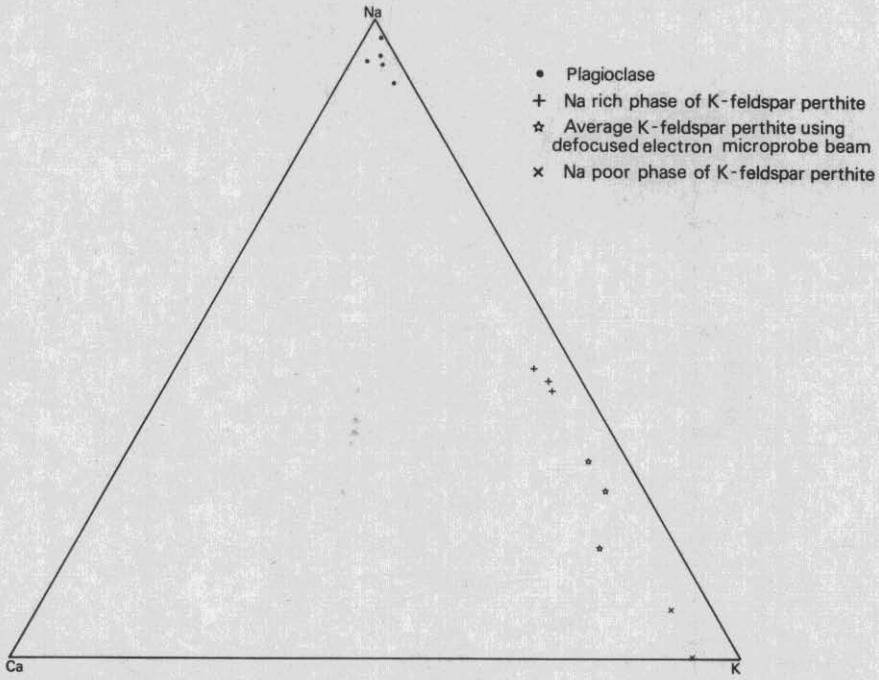

Figure 18. *Ca-Na-K diagram of feldspar compositions from specimen plot 14, table 5, as determined by electron microprobe.*

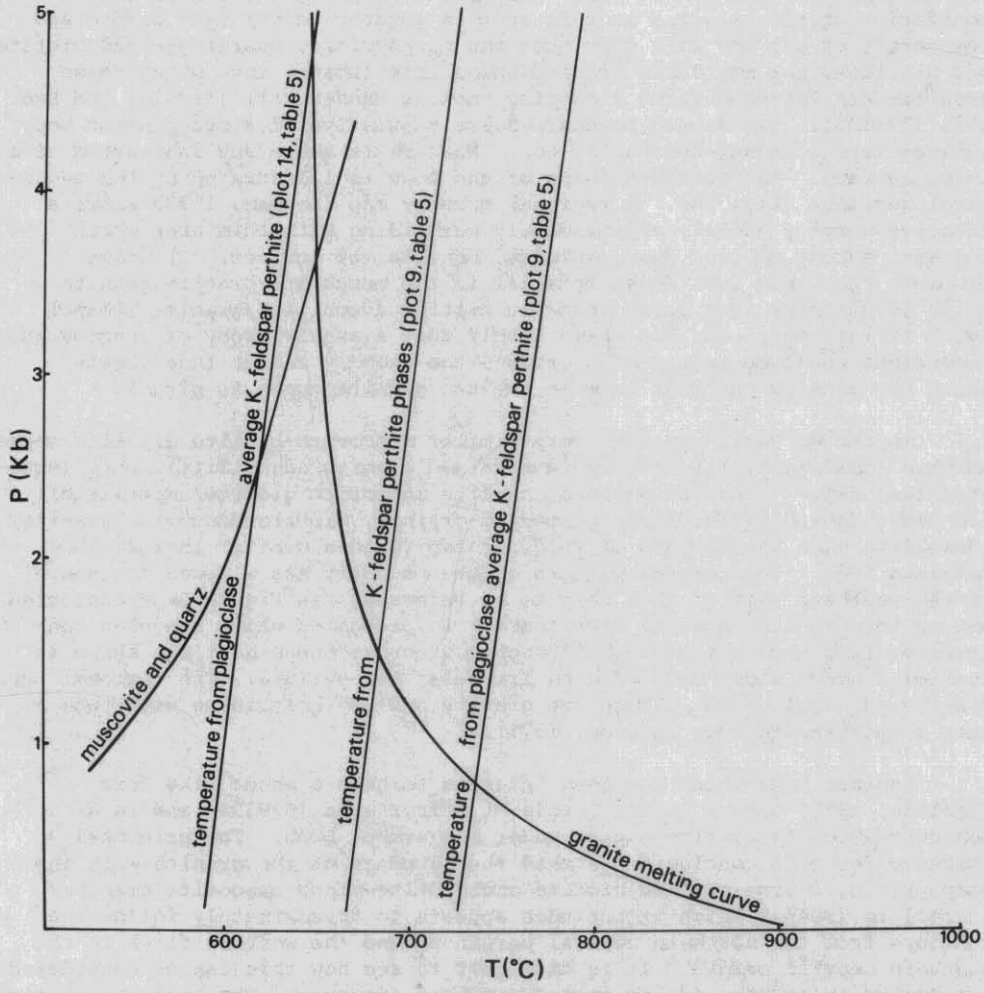

Figure 19. *Pressure-temperature diagram showing temperatures derived from feldspar compositions from granites from the Mt Paris area.*

5 cm

crysts of feldspar and rounded quartz) and Dbapf (in part) (porphyritic, fine- to medium-grained, biotite-muscovite, granite/adamellite with phenocrysts of feldspar) occurring on the high ground east of Weldborough, as 'essentially sheet-like bodies' and name them the Lottah Sheets. In Groves and Taylor (1973) where the results of drilling is presented, it is made clear that the sheet form is based on analogy with the supposed form of similar granites elsewhere in the Blue Tier Batholith and that no drill holes penetrated the base of the presumed sheet; thus the drilling does not substantiate the sheet form. The present mapping has established the boundaries of the granites in this area in greater detail than before and inspection of the map will show that the porphyritic, coarse-grained biotite and biotite-minor muscovite granite/adamellite (Dbapc) into which these granites are intruded forms a capping rock at Masher Hill [813418] and Emu Hill [798525]. The mapped boundaries are suggestive of a steep sided body with an irregular sub-horizontal top. Nowhere is there any indication of a lower surface. The inferred shape of the body is illustrated by two geological sections (fig. 20). A regional gravity map (Leaman, 1973) shows a negative gravity anomaly approximately coinciding with this area which suggests a body of less dense material beneath the surface. It seems probable that this less dense material is the muscovite-biotite granite which is slightly less dense than the biotite adamellite/granite (Dbapc) which it intrudes. It also seems likely that a massive body of considerable dimensions would be required to produce the anomaly rather than sheets since the density contrast between the two granite types is slight.

In the Mt Paris area the very similar muscovite-biotite granites mapped as Dbau (dominantly fine- to medium-grained granite/adamellite), Dbae (equigranular, fine- to coarse-grained, biotite-muscovite granite/adamellite) and Dbapq (porphyritic, fine- to medium-grained, biotite-muscovite granite/adamellite with phenocrysts of feldspar and rounded quartz) intrude the Mathinna Beds. The complex pattern of the boundary has allowed the shape of the southern part of this body to be inferred. In Figure 21 a contoured map of the granite/Mathinna Beds contact is presented which has been constructed from numerous geological sections across the area. The shape is that of a steep sided body with an irregular top surface. The regional gravity map again shows a negative gravity anomaly coinciding with this late stage granite body (Leaman, 1973).

Another body which has been inferred to have a sheet like form (Baillie, 1973) occurs in the Little Mt Horror area [678594] and is a muscovite-biotite granite mapped under the symbol Dbau. The principal evidence for this conclusion is that the boundary of the granite with the porphyritic, coarse-grained biotite and biotite-minor muscovite granite/adamellite (Dbapc) which it intrudes appears to approximately follow the contours from the northern central margin around the western flank to the southern central margin. It is difficult to see how this can be considered conclusive in an area of low relief and poor exposure. The southern margin is thought to be vertical. A small mass of Dbapc rock type mapped at the top of Little Mt Horror (Baillie, 1973) suggested as the top of the intrusion and thus allowing an estimate of the thickness, is now considered to belong to the Dbau (dominantly fine- to medium-grained granite/adamellite) rock type. The trace of contacts of the Dbau bodies further north and northwest which form part of a belt including Little Mt Horror indicate dips ranging from steep to shallow. The intrusions appear to have an irregular form. These bodies also lie on a zone of negative gravity anomaly (Leaman, 1973), which however extends beyond their limits. No firm conclusion about the subsurface extent of the Dbau granite body can be drawn from these data.

The muscovite-biotite granites of the Mt Cameron area [790610] have

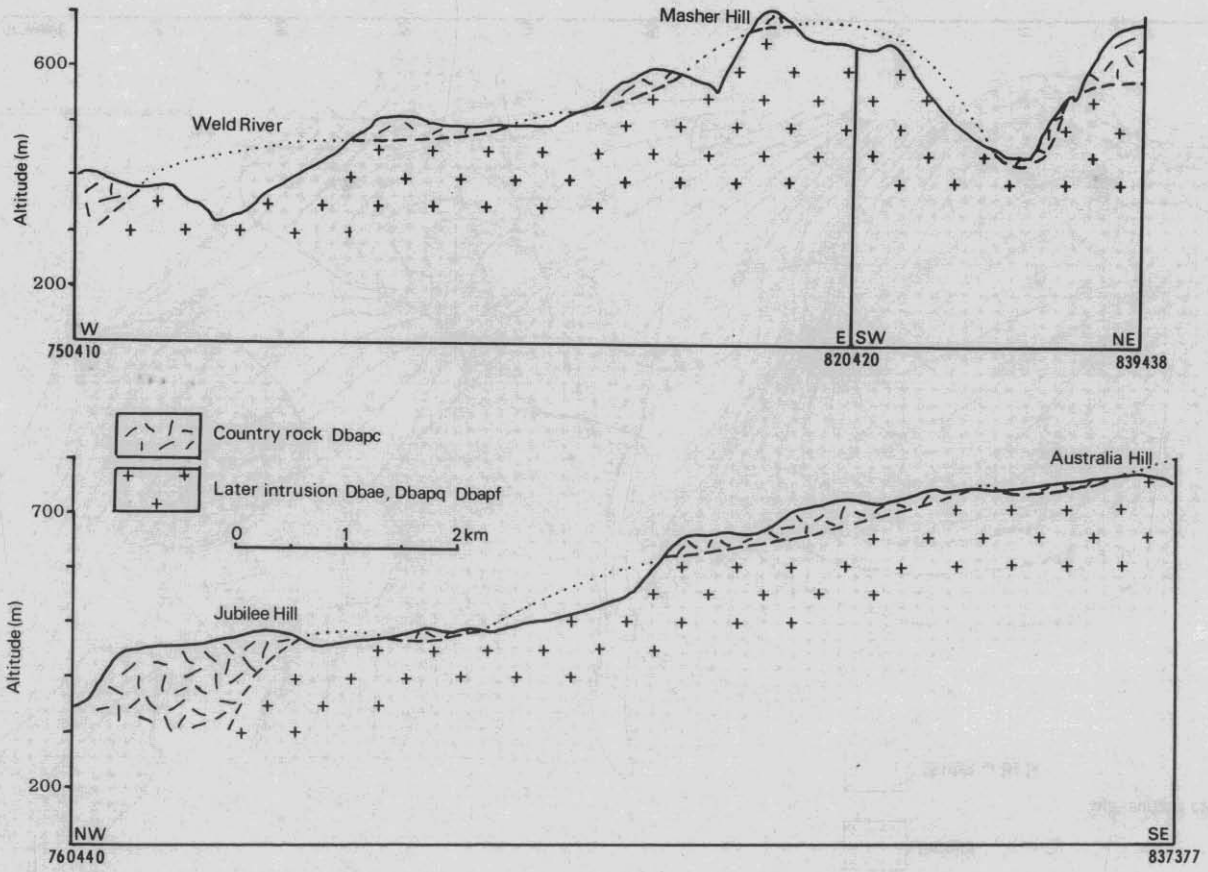

Figure 20. *Geological sections from the south-western part of the Ringarooma Quadrangle.*

5 cm

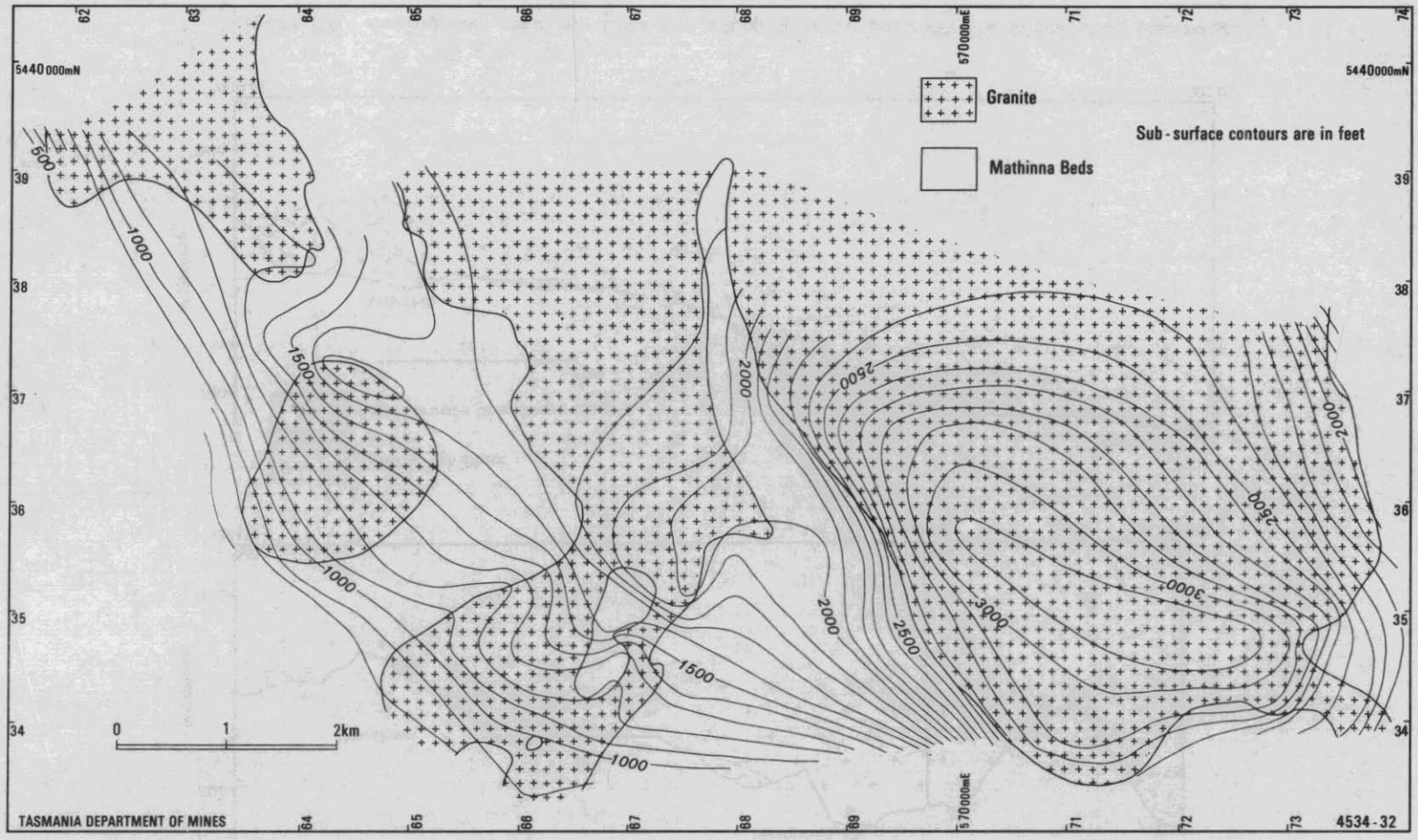

Figure 21. *Contour map of the granite/Mathinna Beds contact in the south-western part of the Ringarooma Quadrangle.*

also been described as having a sheet like form (Groves, 1977). The south-western area of Mt Cameron consists of a number of granite types, with boundaries between the types ranging from sharp to gradational. The boundaries probably outline irregular layers dipping gently to the south-west (*AVB*).

The nature of the contact relationships of the Blue Tier and Scottsdale Batholiths and the Ringarooma-Lyndhurst tract of Mathinna Beds are discussed in the section on thermal metamorphism (*NJT*). Variation in width of the aureole of the Blue Tier Batholith provides a qualitative guide to the dip of the contact. The dip is relatively shallow around Mt Horror where the aureole is wide and is relatively steep between Trig Hill and Lyndhurst where the aureole is narrower. These qualitative estimates are consistent with quantitative estimates based on gravity data (Leaman, 1977). The gravity data further indicate that the total vertical extent of the Mathinna Beds is at least 8 km. Variations in aureole width of the Scottsdale Batholith near Kamona do not relate solely to the dip of the contact. The gravity data indicate that granodiorite in the area is thin (fig. 33) and overlies the main granite/Mathinna Beds contact which is several kilometres west of the surface contact.

LATE DEVONIAN(?) - CRETACEOUS(?) DOLERITE DYKES

M.P. McClenaghan

Medium-grained basic dykes ranging from 1-30 m in thickness (DCdl) occur sparsely throughout the south-east of the Ringarooma sheet. The dykes are vertical and trend 030°-055° with one dyke at 833493 having a sharp change in direction along its length.

The dykes generally have a uniform texture and mineralogy and consist of a framework of plagioclase laths (<3 mm) with intergranular and sub-ophitic green hornblende and iron oxide. In some specimens small amounts of clinopyroxene are present altering to hornblende. Minor alteration of the hornblende to biotite is common particularly in the neighbourhood of the larger iron oxide grains. Iron oxide occurs as larger euhedral to subhedral grains (0.5 mm) and also as much smaller grains along cleavage planes in the hornblende, where it has exsolved. Sparse phenocrysts of plagioclase (<8 mm) are present in some specimens. Composition of the plagioclase ranges from bytownite to labradorite. Mineral compositions determined by electron microprobe from one specimen are listed in Table 20 with analyses totals normalised to one hundred and ideal water content assumed for the amphibole and biotite. The most anorthite-rich plagioclase composition was taken from a phenocryst and the least from a small plagioclase grain in the groundmass.

The dyke at 833493 shows a different mineralogical character from those described above (*PRW*). The material intergranular to a framework of plagioclase laths consists of clinopyroxene, chlorite, epidote, iron oxide, and clacite with euhedral quartz grains. Another specimen taken from the same dyke at another point is less altered and contains orthopyroxene intergranular to the plagioclase laths. This specimen also contains calcite.

Five specimens of the first mineralogical character described above, were analysed and the results are presented in Table 19 together with the CIPW norms. A plot of these specimens on an alkali-silica diagram (fig. 22) shows they mostly fall just within the tholeiitic field. Tertiary alkali basalt from the Weldborough Pass area (table 21), Jurassic dolerites from the Mt Wellington sill (Edwards, 1942) and Cretaceous igneous rocks from the Cape Portland area (Jennings and Sutherland, 1969) have also been plotted

Table 19. ANALYSES AND CIPW NORMS OF SAMPLES FROM DOLERITE DYKES

Plot No.	1	2	3	4	5
Analysis No.	735113	741647	741650	742537	742538
SiO_2	48.5	47.1	48.4	49.8	48.8
TiO_2	2.8	1.5	1.2	1.4	3.1
Al_2O_3	14.4	18.2	16.9	16.1	14.1
Fe_2O_3	3.1	1.5	2.0	1.8	1.9
FeO	11.8	8.4	7.3	8.2	12.1
MnO	0.23	0.19	0.16	0.20	0.24
MgO	5.1	8.1	8.1	7.6	5.4
CaO	8.5	9.9	10.7	10.1	9.0
Na_2O	2.4	2.5	2.5	2.6	2.7
K_2O	1.2	0.53	0.29	0.28	0.65
P_2O_3	0.39	0.32	0.15	0.22	0.65
H_2O^+	2.0	1.6	2.0	1.8	1.5
H_2O^-	0.47	0.40	0.27	0	0
CO_2	-	-	-	0.03	0.01
SO_3	<0.01	<0.03	0.04	0.19	0.23
Cl	-	-	-	0.02	0.02
F	-	-	-	0.12	0.12
Total	100.89	101.14	100.81	100.46	100.52
Trace elements (ppm)					
Li	40	20	30	25	40
Sn	8	12	36	31	15
Rb	155	27	27	27	40
Sr	265	167	160	249	286
Y	60	30	59	32	55
Zr	215	66	26	90	264
Nb	-	-	-	6	15
Ni	58	97	48	44	53
Cu	33	24	12	69	13
Co	-	-	-	39	41
Zn	235	129	104	165	214
Rb/Sr	0.58	0.16	0.17	0.11	0.14
CIPW Norms					
Q	1.60	0	0	0.23	1.75
Or	7.09	3.13	1.71	1.65	3.84
Al	20.31	21.15	21.15	21.70	22.55
An	24.98	36.87	34.04	31.59	24.59
Di	12.18	8.26	14.62	13.14	12.81
Hy	21.54	9.29	14.09	23.77	22.57
Ol	0	13.77	6.51	0	0
Mt	4.49	3.48	4.08	2.61	2.75
Il	5.32	2.85	2.28	2.66	5.89
Ap	0.92	0.76	0.36	0.52	1.49
Py	0	0	0.07	0.35	0.43
Ca	-	-	-	0.07	0.02

Table 20. MINERAL COMPOSITION AND STRUCTURAL FORMULAE OF MINERALS FROM ANALYSED DOLERITE DYKE (PLOT NUMBER 2, TABLE 19).

	Hornblende			Biotite			Plagioclase		
SiO_2	48.13	47.88		37.07		49.96	51.12	53.76
TiO_2	0.56	0.78		1.65		0.10	0.07	0.12
Al_2O_3	7.88	7.98		17.07		31.94	31.45	29.17
Cr_2O_3	0.20	0.22		0.10		0.18	0.21	0.17
Fe_2O_3	8.86	8.32		-		-	-	-
FeO	7.06	7.95		17.33		0.42	0.16	0.76
MnO	0	0		0		0	0	0
MgO	14.15	14.01		14.76		0.12	0	0
CaO	9.82	9.34		0.46		14.67	13.88	11.51
Na_2O	1.10	1.07		0		2.56	3.08	4.37
K_2O	0.14	0.23		7.50		0	0	0.10
H_2O	2.08	2.08		4.05		0	0	0
Total	99.98	99.99		99.99		99.95	99.97	99.96
Tet Si	6.92	6.90	Tet Si	5.48	Si	9.11	9.28	9.73
Al	1.08	1.10	Al	2.52	Al	6.86	6.73	6.23
Σ	8.00	8.00	Σ	8.00	Fe^{+3}	-	-	-
Oct Al	0.25	0.26	Oct Al	0.46	Cr	0.03	0.03	0.02
M1-3Ti	0.06	0.08	Fe^{+3}	-	Ti	0.01	0.01	0.02
Fe^{+3}	0.96	0.90	Cr	0.01	Mg	0.03	0	0
Fe^{+2}	0.67	0.70	Ti	0.18	Fe^{+2}	0.06	0.02	0.12
Cr	0.02	0.02	Mg	3.26	Na	0.91	1.09	1.54
Mg	3.03	3.01	Fe^{+2}	2.14	Ca	2.87	2.70	2.23
Mn	0	0.02	Mn	0	K	0	0	0.02
Σ	4.99	4.99	Σ	6.05	Total	19.88	19.86	19.91
XM1-3	0.18	0.26	Ca	0.07	Or	0	0	0.00
M4 Ca	1.51	1.44	Na	0	Al	0.24	0.21	0.41
Na	0.31	0.30	K	1.42	An	0.76	0.71	0.59
Σ	2.00	2.00	Σ	1.49				
A Na	0	0	Total	15.54				
K	0.03	0.04						
Σ	0.03	0.04						
Total	15.02	15.03						

Hornblende formula calculated by the method developed by Papike *et al.* (1974) for maximum Fe^{+3}. Ideal H_2O content assumed and analyses normalised to 100.

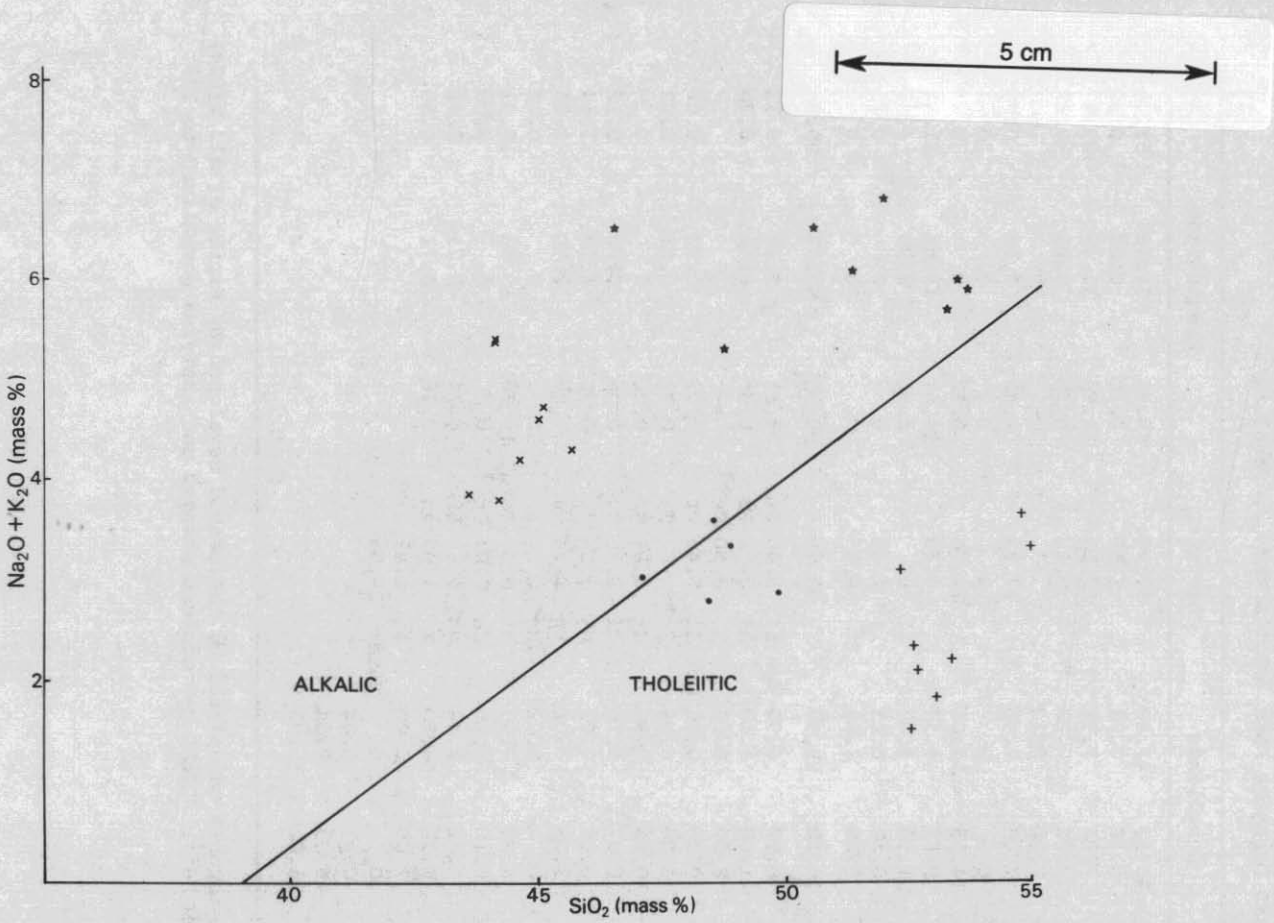

Figure 22. *Alkali-silica diagram for dolerite dykes (DCdl) from the Ringarooma sheet and various other Tasmanian igneous rocks. DCdl (•) numbered as in table 19, Jurassic dolerites (+) - Edwards, 1942, p.467, Tertiary alkali basalts from the Weldborough Pass area (table 21)(×), Cretaceous igneous rocks from the Cape Portland area - Jennings and Sutherland, 1969 (★). Alkali and tholeiitic fields from Macdonald and Katsura (1964).*

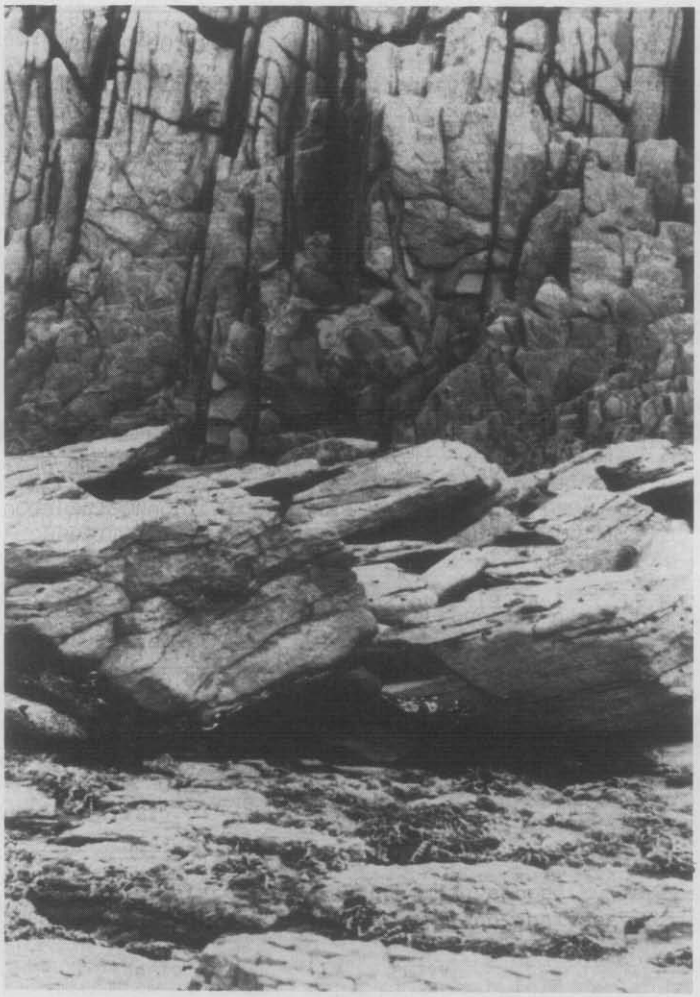

Plate 3. *Dolerite/Lower Parmeener Super-Group contact, Waterhouse Island. (PWB)*

Figure 4. *Xenolith of Upper Parmeener Super-Group within dolerite at Tomahawk Point. (PWB)*

Figure 5. *Andesite overlying dolerite at Petal Point. (PWB)*

for comparison. It is clear that the dolerites have little resemblance to any of these groups.

The dolerites are later than the granites, since they intrude all granite types, which indicates a post Upper Devonian age. Field evidence cannot define the age more closely, however, their chemical dissimilarity to the Tertiary basalts suggests they are not Tertiary and must therefore be older.

JURASSIC DOLERITE

P.W. Baillie

Dolerite occurs on the Boobyalla map sheet near the coast in three main areas:

(*a*) Croppies Point [500775] - Waterhouse Island [530830]

(*b*) Tomahawk Point [637766]

(*c*) a north - south belt of country extending from Aberfoyle Hill [787702] northwards to Foster Islands [822914] north-east of Cape Portland.

In all areas the dolerite is remarkably uniform and is medium- to coarse-grained with closely spaced joints that give the rock a characteristic 'slabby' appearance in outcrop. The joints show no preferred orientation either in the vertical or horizontal planes. In places the rock exhibits 'pseudo-crossbedding' as a result of these joints.

Age relationships

(1) On Waterhouse Island [528820] dolerite intrudes rocks of the Lower Parmeener Super-Group (Plate 3). Contacts are both concordant and transgressive.

(2) South of Waterhouse Point [545793] dolerite is faulted against adamellite.

(3) At Tomahawk Point and on Tomahawk Island dolerite is intrusive into quartz sandstone of the Upper Parmeener Super-Group. Occasional xenoliths of country rock occur within the dolerite. (Plate 4).

(4) At Petal Point [797850] andesite of Cretaceous age overlies dolerite (Plate 5).

(5) At Red Hills [832772] dolerite intrudes Parmeener Super-Group rocks of unknown assignment.

The concordant contacts observed on Waterhouse Island and Tomahawk Point occur on the eastern margins of those outcrops and dip in a westerly direction at about 10° indicating that the dolerite is the basal part of a sill. This is supported by gravity evidence (Leaman and Symonds, 1975). The fact that the more easterly of these contacts is with rocks of a higher stratigraphic horizon suggests the presence of a large fault between Waterhouse Island and Tomahawk Point.

Rocks from the Cape Portland area are typical of upper levels of differentiated bodies in Tasmania (Jennings and Sutherland, 1969).

CRETACEOUS APPINITES

P.W. Baillie

Cape Portland

Appinitic rocks occur in the Cape Portland area and a full petrological summary is presented in Jennings and Sutherland (1969). Three main groups are recognised.

Porphyrite complex. The main exposures are on the eastern slopes of Vinegar Hill [826876] and the small knoll to the south-east. As noted by Jennings and Sutherland (1969) actual bedrock exposure is sparse and precise delineation of rock boundaries is impossible. The rocks contain phenocrysts of hornblende, augite and biotite in a groundmass of plagioclase, potash feldspar, and quartz. For a full summary refer to Jennings and Sutherland (1969). Plagioclase is the only mineral common to all varieties of this rock type.

The relationship between the complex and older dolerite is unclear. No field relationships have been observed but it is noteworthy that in the proved lava flow of similar composition (see below) hexagonal jointing is a conspicuous feature as well as minor vesicules. This feature is absent in the Vinegar Hill mass.

C. Brooks (*in litt.*, 14.6.1971) gives a Rb/Sr age of 103±23 Ma and a K/Ar age of 91±1 Ma for rocks from the complex.

Lamprophyre dykes. The dykes are generally narrow with well defined margins against the dolerite they intrude. Most can be proved to have dilational origin controlled by pre-existing joints in the dolerite. Figure 23, showing the location, orientation and form of the dykes is taken from Jennings and Sutherland (1969, p. 51).

The dykes are biotite and/or hornblende porphyry and ar dominantly spessartite with minor kersantite and vogesite (Jennings and Sutherland, 1969).

C. Brooks (*in litt.*, 14.6.1971) gives Rb/Sr radiometric ages for two of the dykes as 94±20 and 98±23 Ma.

Andesite flows. Two andesite flows are exposed on the dolerite foreshore at Petal Point [797850] (Plate 5). The interface between the lower flow and underlying dolerite is a gently undulating surface. Both flows show prominent hexagonal cooling joints, individual hexagons being up to 0.4 m in diameter and greater than one metre in height. Some vesicules are present. A conspicuous feature of both flows is the presence of rounded hornblende/minor pyroxene xenoliths up to 100 mm in diameter. The xenoliths are larger and more abundant in the lower flow. Phenocrysts of hornblende within the rock are larger and more abundant than any others observed in the Cape Portland area, some being over 10 mm in length. The phenocrysts show a fairly well developed sub-horizontal flow alignment. Rounded granite xenoliths less than 10 mm in diameter are fairly common in the andesite flows.

Other areas

Two small lamprophye dykes are intrusive into dolerite near its contact with Permian rocks on Waterhouse Island [529820].

On the Tomahawk River [639640] a dyke of similar composition to the

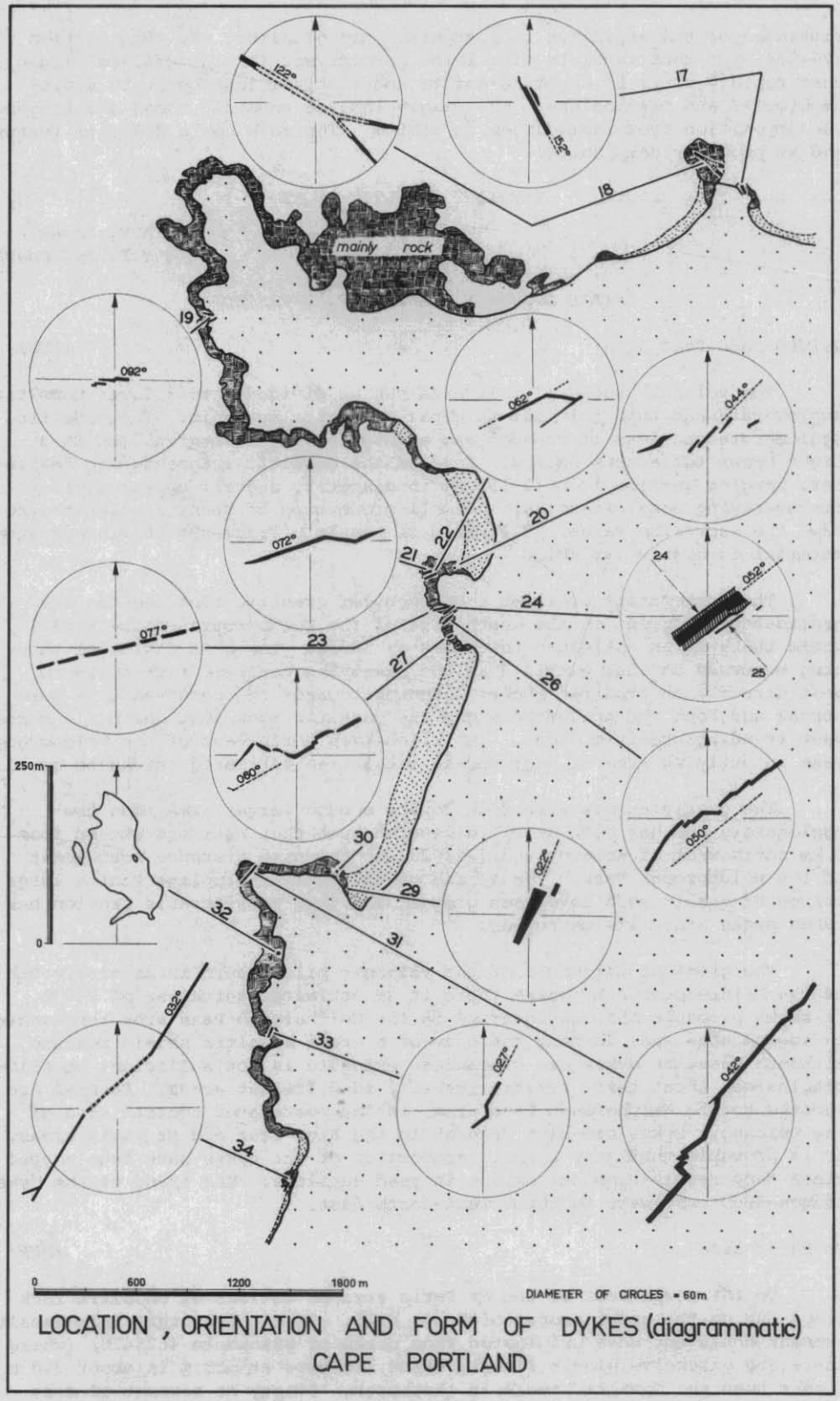

Figure 23.

5 cm

remainder of the appinites is intrusive into granites. In thin section (77-551) the rock consists of olivine phenocrysts (at the chilled margin) that rapidly alter to aegerine-augite and biotite; together with sodic amphibole? and plagioclase. The plagioclase is commonly zoned and ranges in composition from labradorite to albite. The rock has a dolerite texture and is probably camptonite.

TERTIARY BASALTIC ROCKS

A.V. Brown
M.P. McClenaghan

FIELD OCCURRENCE AND CHARACTERISTICS

Weldborough Pass area *(MPM)*

The volcanic rocks of this area can be divided into a lower basaltic agglomerate and tuff unit and an upper basaltic lava unit. The basaltic agglomerate consists of rounded and angular basaltic material set in a light brown tuffaceous matrix. Some of the basaltic fragments are vesicular, ranging in size from 10-150 mm in diameter, and all appear similar to the overlying basaltic rocks. A small proportion of granitic clasts also have the same size range. The ratio of basaltic fragments to fine-grained material is highly variable.

The agglomerate overlies a basement of granitic rock and has its greatest development on the south side of the Weldborough Pass [795340] where there is an estimated thickness of 150 m. There is a gradual thinning westward so that within 3 km the overlying basaltic rock comes to rest directly on granitic rock. Thinning towards the north-east is more abrupt and both the agglomerate and the basaltic rock abut against a north-west trending granitic slope. Two kilometres north-west of the Weldborough Pass an outlying area of agglomerate attains an estimated thickness of 90 m.

The overlying basaltic rock covers a much larger area than the agglomerate and has been deeply dissected such that outliers extend from 3 km north-west of Weldborough [744420] to the same distance south-east of the Weldborough Pass. The spread of the outliers implies that a large volume of basalt must have been present and that considerable erosion has taken place since its extrusion.

The greatest thickness of the volcanic pile occurs in an area south of the Weldborough Pass where there is an estimated thickness of 230 m. It seems probable that agglomerate in the Weldborough Pass area represents an agglomerate cone forming the core of a small basaltic shield volcano. Although basaltic dykes are widespread exposure is not sufficient to allow conclusions about their relative density in different areas. Several are exposed to the Weldborough Pass area, in the postulated central area of the volcano. Dykes are also present in the Blue Tier and Mt Paris areas. It is probable that only a small proportion of the dykes have been mapped since they rarely crop out except in road cuttings. The trend of the dykes ranges from east-west to south west-north east.

Mt Paris area *(MPM)*

To the north-west of the Mt Paris area an outlier of basaltic rock crops out on the upper slopes of Grays Hill. It is clear that this basaltic remnant could not have originated from north of Branxholm [625420] (where there are extensive basalt flows), since its base at 520 m is about 300 m higher than the basaltic rocks in that area. It may be remnant of more

extensive basaltic flows covering the Mt Paris area, although its appearance suggests a plug.

In the Cascade River area [677435] and at Mutual Hill [705445] several small areas of basaltic rock occur. Based on their matching petrological character and similar level these are clearly outliers of the extensive basaltic flows north of Derby.

Ringarooma-Winnaleah area *(AVB)*

Flat-lying basaltic flows overlie Tertiary and Mathinna Beds sediments in the Ringarooma area west of Mt Paris. In the immediate Ringarooma area [598345] there are at least two flows (*MPM*). The basaltic rock at the topographically higher level is an alkali olivine basalt while that at lower level is an olivine nephelinite. In the Legerwood area [576362] a lobe of basanite extends west resting on granitic rocks of the Scottsdale Batholith and constitutes a third distinct flow (*MPM*). The source for the first two of these flows is probably to the south-west since there is a gentle rise in the base surface in that direction.

From Legerwood, a north-easterly trending area of basaltic rock flows overlap Tertiary sediment as far north as Wagners Hill [721524]. Remnants of the northward continuation of these flows extend to the northern boundary of the Ringarooma Quadrangle and then into the Boobyalla Quadrangle.

As in other areas in Tasmania (Sutherland, 1969), the flows of the Ringarooma-Winnaleah area are valley fill, having extruded through numerous small necks and fissures, rather than flood plain or central volcano types. In the Legerwood-Wagners Hill area the flows dominantly overlie Tertiary sediment, but have overflowed the partially infilled valley margins and rest on older country rock to the north-west and south-east. The thickest remaining pile of flows (120 m at 684478) occurs between Derby and Winnaleah. Suspected source necks through granitic rocks occur at 720482, 727529 and 737505 whilst numerous elongate fissures cut Mathinna Beds sediments [631467, 648481, 667492]. One suspected conduit [694480] has cut through approximately 70 m of basaltic rock flows. Next to this conduit is 3 - 4 m of tuffaceous agglomerate which is capped by higher flows.

The main valley-fill flows of the Ringarooma-Winnaleah area are olivine nephelinite with minor limburgite. Occasionally alkali olivine basalt crops out beneath the olivine nephelinite [693491] but the main occurrence of alkali olivine basalt is as remnant outcrops to the north [720567, 697559] and west [631467,649511] of the olivine nephelinite flows. Within these remnants of alkali olivine basalt flows there are areas of pyroxene glomeroporphyritic alkali olivine basalt [657510, 620493].

Spinel lherzolite and websterite xenoliths, as well as megacrysts of olivine, clinopyroxene and spinel occur in some olivine nephelinite flows [727529, 731823, 645456].

Scottsdale area *(WRM)*

This area consists dominantly of thick red soil with basalt boulders, cobbles and pebbles between widely separated poor basalt outcrops. Flows are thin and are very frequently completely weathered to red soil for their entire thickness. Drilling has established that the thick flows of hard unweathered basalt present in the eastern areas of the Ringarooma sheet are not found in the Scottsdale region.

The largest continuous area of basalt and derived soil is 18 square kilometres centered around the town of Scottsdale [431430]. Here an undulating plateau extends south-west for 3 km towards Springfield [364258] and 9 km to the north-west of Jetsonville [352363] onto the Pipers River sheet (Marshall *et al.*, 1965). Two kilometres north-east of Scottsdale four remnant areas of the Scottsdale basalt are found capping hills at North Scottsdale. This flow is known to be 40 m thick in the Scottsdale area and 47 m thick in North Scottsdale area.

In the North Scottsdale area a lower basalt flow is also present, and crops out along the Waterhouse-Scottsdale Road [471472], in Surveyors Creek [478480], and in the two headwater tributaries [457491 and 465493] of Devils Creek. It occurs 20 - 30 m below the base of the upper basalt, and is thin in contrast. This flow may extend as far west as Tuckers Creek, where a discontinuous layer of basalt boulders and cobbles occur [448453 - 458469]. There is no evidence from either mapping or drilling that this lower basalt extends into the Scottsdale area.

A drill hole sited on the upper basalt [461491] recorded a remnant thickness of 11 m for this flow, then Tertiary sediment from 11 - 16 m, then more basalt to 47 m. This hole did not finish in granodiorite, as shown in error on the Ringarooma map. A second bore, sited on the lower flow [465493] recorded only 10 m of weathered basalt and derived soil overlying Tertiary sediment. This bore bottomed in granodiorite at a depth of 82.3 m.

Detailed knowledge of the lower basalt - Tertiary sediment interface is minimal, but a series of auger holes in one area [476480 - 464482] outlines a steep, irregular contact with considerable local relief.

The lower of the two flows distinguished around North Scottsdale extruded through the granodiorite and flowed north-eastward into the southern portion of the Surveyors Creek lead of the Scottsdale Tertiary Basin (Moore, *in prep.*). The upper flow was far more extensive and extruded through the granodiorite near Scottsdale to flow to the north-westward to fill the Jetsonville lead of the Scottsdale Tertiary Basin. It also flowed north and north-eastwards over a thin Tertiary cover over the granodiorite divide that separated the Jetsonville lead from the eastern part of the basin to flow into North Scottsdale area and to fill the Surveyors Creek Lead (Moore, *in prep.*). This upper flow also continued to the west on the granodiorite to West Scottsdale, on the Piper River Sheet (Marshall, *et al.*, 1965), and also isolated the Tertiary sediments of the Springfield basin, to the south, from those of the main Tertiary Scottsdale basin and capped granodiorite and Mathinna Beds sediments to the south-east at Walduck Hill [435403].

Two isolated basalt and red soil capped hills occur north-east of North Scottsdale. At 500610 the basalt and derived soil overlies Tertiary sediment, whilst at 492605 the underlying rock type is not known.

The Scottsdale basalts have proved too weathered for radiometric dating but are considered to be equivalent to those on the eastern part of the sheet.

Cape Portland area *(PWB)*

Two lava types are present in the Cape Portland area, tholeiitic basalt and alkali basalt (Jennings and Sutherland, 1969).

The basalt occupies a north-south depression extending from 826849 northwards to the coast. Drill hole evidence (Hole 2) at Cape Portland indicates that alkali olivine basalt (specimen 73-432) occurring at a depth of 6 m overlies strongly altered tholeiitic basalt (specimen 77-431), occurring at a depth of 40 m which is very similar to tholeiites described by Jennings and Sutherland (1969, p.61). This suggests that the tholeiites are older than the alkali olivine basalt in this area.

PETROGRAPHY

Introduction *(AVB, MPM)*

The petrography of the basaltic rocks from the Scottsdale area has not been studied due to the difficulty in obtaining unaltered rock. Petrographic notes are given by Marshall (1970, appendix 5) for the adjoining area of Springfield-West Scottsdale in the Pipers River Quadrangle which include descriptions of alkali olivine basalt and olivine nephelinite.

The petrography and geochemistry of the basaltic rocks in the Cape Portland area are described by Jennings and Sutherland (1969).

The basaltic rocks of the Ringarooma-Winnaleah and Weldborough Pass-Mt Paris areas fall naturally into two types, alkali olivine basalt, and olivine nephelinite, on the basis of their petrographic and chemical characteristics. K-Ar age determination (*AVB*) (arranged with AMDEL by L. Black of the B.M.R. on behalf of Geological Survey of Tasmania) on whole rock specimens from the Winnaleah area (appendix) gave ages of Middle-Early Miocene for samples of olivine nephelinite (72-316, 15.9 ± 0.6 m.y.), porphyritic alkali olivine basalt (W1 - 4, 16 ± 0.3 m.y. and alkali olivine basalt (W3 - 1, 15.6 ± 0.3 m.y.).

Petrography *(MPM)*

Alkali olivine basalt. The alkali olivine basalts of the Weldborough Pass area are very uniform in character: all are porphyritic, with phenocrysts (1 - 3 mm) constituting 20 - 50% of the rock, 25% being the most common value. Olivine is the dominant phenocryst, with minor amounts of plagioclase and augite in some specimens. The olivine phenocrysts show an almost continuous size range with the matrix olivines (0.1 - 0.75 mm). The groundmass is much finer grained (0.05 - 0.75 mm) and contains labradorite/andesine, olivine, augite and iron-titanium oxide minerals. The plagioclase laths frequently show flow alignment. Augite shows the purplish-brown colouration typical of titanium rich augite.

The character of the Grays Hill alkali olivine basalt is very similar to those of the Weldborough Pass. At Grays Hill small masses of dolerite consist of labradorite and light brown augite as sub-ophitic patches, together with iron-titanium oxide minerals and intersertal patches of brown glass and cryptocrystalline material. This mineralogy represents a slightly different composition from the basaltic rocks as no olivine is present and hence the rock must be less undersaturated. It is probably xenolith material brought up by the basalt.

The basaltic dykes in the Mt Paris area have a very similar character to the basaltic rock from Grays Hill and the Weldborough Pass are.

The alkali olivine basalts of the Ringarooma-Winnaleah area fall into three main petrographic types. The first of these contains abundant olivine phenocrysts (0.2 - 1.5 mm) forming 20 - 25% of the rock, set in a

very fine-grained matrix (0.05 - 0.1 mm) consisting of labradorite, pale purplish-brown titanaugite and iron-titanium oxide minerals. Sparse small augite phenocrysts (0.2 - 1 mm) also occur in some specimens. The second type is coarser grained with olivine phenocrysts (0.6 - 1.5 mm) only slightly larger than the matrix (0.5 - 1 mm) which also contains olivine together with pale purplish-brown titanaugite, iron-titanium oxide minerals and larger laths of labradorite (0.5 - 1 mm) enclosing the other minerals. The labradorite shows zoning and pale brown glassy patches are often present. The third variety is distinguished by very abundant purplish-brown titanaugite, (1 - 3 mm) forming 30 - 50% of the rock, in glomeroporphyritic patches (2 - 3.5 mm). A small proportion of olivine phenocrysts (1 - 2mm) occur sometimes enclosed in the pyroxene glomeroporphs. The matrix (0.2 - 1 mm) is comparatively coarse with olivine, titanaugite, labradorite and iron-titanium oxide minerals. Small glassy patches are present in some specimens.

In addition to the alkali olivine basalt described above, a flow of basanite occurs near Legerwood which consists of sparse olivine phenocrysts (1.5 - 2 mm) within a matrix of olivine (0.1 - 3 mm), titanaugite, labradorite (1 - 3mm), iron-titanium oxide minerals and intergranular patches of nepheline. The groundmass labradorite encloses the other matrix minerals.

Olivine nephelinite. (AVB) In thin section the olivine nephelinite consists of olivine phenocrysts in a groundmass of olivine, titaniferous augite, nepheline and iron-titanium oxide minerals. The olivine phenocrysts are irregular to equant subhedral grains ranging in size from 0.2 mm to 0.5 mm and are randomly distributed throughout the rock. Phenocrysts usually occupy between 10 and 20%, by volume, of a sample. The groundmass is dominated by euhedral to subhedral, elongate, purplish-brown titaniferous augite crystals. These crystal grains are usually less than 0.15 mm long but some are up to 0.3 mm in length. Together with the groundmass olivine (equant up to 0.15 mm) and augite, subhedral grains of opaque minerals (titaniferous magnetite?) are embedded in a mosaic of randomly orientated granular nepheline.

Megacrysts of olivine, clinopyroxene and spinel have been observed in some olivine nephelinite samples. The samples all came from the area of maximum spinel lherzotite and websterite xenolith occurrence (Wagners Hill,) [721523]. The olivine crystals are subhedral, (approximately 3 mm x 2 mm) and show deformation lamellae (72-427), whilst the clinopyroxene grain (10 mm x 5 mm, 72-383) has orthopyroxene exsolution lamellae and a 2 mm reaction corona with the enclosing magma. One spinel megacryst (77-329, 6 mm x 3 mm) was identified by electron probe analyses as alumina rich, titaniferous magnetite [Fe $(Fe_{1.38}\ Ti_{0.32}\ Al_{0.28}\ Cr_{0.02})_2\ O_4$]. This megacryst contained three (0.2 mm) apatite grains as inclusions.

Thin sections of limburgite samples exhibit olivine phenocrysts (0.3 mm) and smaller (0.1 mm) subhedral to anhedral grains of titaniferous (?) magnetite in an irregular mat of bonded purplish-brown titaniferous augite grains and brown glass. In the more vitric samples the glass is bright reddish brown and is studded with skeletal arrays of black rod-shaped opaque minerals and accretions of powdery opaque grains. Subhedral to anhedral black opaque grains (titaniferous magnetite(?) 0.1 mm) occur around the boundaries of olivine phenocrysts. In more crystalline specimens the glass ranges from pale brown to almost colourless and contains dominantly granular opaque minerals with minor skeletal assemblages of rod shaped grains. The bonded nature of the augite is also less distinct.

Table 21. ANAALYSES AND CIPW AND RITTMANN NORMS OF BASALTIC ROCKS

Plot No.	1	2	3	4	5	6	7	8
Analysis No.	735112	735114	735115	735116	735117	735118	735119	735122
SiO_2	44.1	45.1	44.6	45.0	44.1	43.4	43.6	45.7
TiO_2	2.4	2.2	2.2	2.1	2.8	2.2	2.8	2.4
Al_2O_3	13.6	15.4	15.1	14.6	15.2	14.1	15.0	15.3
Fe_2O_3	4.6	5.5	5.9	5.2	5.7	5.3	5.6	5.4
FeO	8.0	6.8	6.4	5.8	7.6	6.2	7.9	6.8
MnO	0.18	0.20	0.19	0.16	0.22	0.19	0.19	0.17
MgO	9.4	7.6	8.1	8.4	6.8	10.0	8.2	6.6
CaO	10.1	9.5	9.4	10.3	8.1	10.1	9.6	9.8
Na_2O	2.3	3.6	3.0	2.1	4.3	2.0	3.0	3.0
K_2O	1.2	1.1	1.2	1.3	1.1	0.84	0.85	1.3
P_2O_5	0.62	0.74	0.71	0.57	1.0	0.64	0.76	0.56
H_2O^+	2.2	2.4	2.4	3.0	2.0	4.3	2.1	2.0
H_2O^-	1.1	0.75	0.86	1.2	0.65	0.85	0.47	1.1
CO_2	-	-	-	-	-	-	-	-
Total	99.8	100.89	100.06	99.73	99.57	100.12	100.07	100.13
Trace elements (ppm)								
Ba	-	-	-	-	-	-	-	-
Cu	44	85	54	51	39	58	61	66
Cr	-	-	-	-	-	-	-	-
Li	5	15	15	15	15	5	5	15
Ni	250	137	128	178	55	171	103	87
Rb	50	38	48	45	33	39	23	38
Sc	-	-	-	-	-	-	-	-
Sr	755	800	830	700	1060	760	950	780
Y	29	34	35	27	36	32	31	28
Zr	210	260	280	255	350	245	185	215
CIPW Norms								
Or	7.09	6.50	7.09	7.68	6.50	4.96	5.02	7.68
Ab	19.46	24.23	24.41	17.77	27.11	16.92	23.25	25.39
An	23.24	22.61	24.19	26.57	18.93	27.02	24.95	21.44
Lc	-	-	-	-	-	-	-	-
Ne	-	3.38	0.53	-	5.03		1.16	-
Di	18.29	15.71	14.13	16.48	11.81	14.97	14.17	16.41
Ol	16.10	11.96	12.58	5.42	12.26	9.53	14.36	9.27
Mt	5.37	6.96	7.54	6.53	6.96	6.67	6.82	6.67
Il	4.56	4.18	4.18	3.99	5.32	4.18	5.32	4.56
Ap	1.47	1.75	1.68	1.35	2.37	1.52	1.80	1.33
Rittmann Norms								
Sanidine	6.5	4.2	5.5	7.4	4.1	2.3	1.5	6.3
Plagioclase	47.9	51.7	53.3	51.8	52.0	53.9	55.0	55.2
Nepheline	1.0	5.8	3.0	-	8.1	-	3.4	1.8
Leucite	-	-	-	-	-	-	-	-
Clinopyroxene	21.8	18.2	23.6	13.9	21.7	16.7	19.2	20.3
Olivine	17.5	14.4	16.0	12.4	14.6	16.9	16.9	12.1
Magnetite	1.7	1.9	1.8	1.4	2.2	1.4	1.8	1.7
Ilmenite	2.3	2.1	2.2	2.1	2.8	2.3	2.9	2.3
Apatite	1.4	1.7	1.6	1.3	2.3	1.5	1.7	1.3
Colour Index	43.2	36.5	36.6	39.5	33.5	42.3	38.3	35.4

Table 21. (continued).

Plot No.	9	10	11	12	13	14	15	16
Analysis No.	735123	735124	735125	741643	741644	741649	742063	742064
SiO_2	45	44.1	44.2	40.6	44.3	39.7	38.1	39.5
TiO_2	2.3	2.7	2.1	3.1	2.4	3.5	3.2	2.7
Al_2O_3	14.6	14.0	13.7	10.6	12.0	11.6	9.8	10.2
Fe_2O_3	4.4	5.6	4.9	3.7	3.0	6.2	5.4	5.4
FeO	8.1	7.5	7.4	9.9	8.9	8.6	11.0	8.6
MnO	0.18	0.20	0.18	0.19	0.17	0.20	0.25	0.20
MgO	9.0	8.3	10.0	12.3	11.7	11.3	12.4	14.1
CaO	9.6	8.9	9.9	11.0	9.5	10.0	10.9	11.6
Na_2O	3.1	4.4	2.8	4.0	2.4	3.8	1.6	3.8
K_2O	1.5	0.97	1.0	1.3	1.3	1.2	0.5	1.3
P_2O_5	0.63	0.95	0.62	1.0	0.65	1.1	1.0	1.1
H_2O^+	1.5	2.0	2.2	2.1	1.8	2.3	3.9	1.5
H_2O^-	0.56	0.78	0.71	0.80	1.2	0.33	2.4	0.79
CO_2	-	-	-	-	-	-	0.76	0.24
Total	100.47	100.4	99.71	100.59	99.32	99.83	101.21	101.03
Trace elements (ppm)								
Ba	-	-	-	-	-	-	612	435
Cu	68	52	75	46	38	44	91	48
Cr	-	-	-	-	-	-	400	600
Li	5	15	15	10	5	5	10	10
Ni	181	132	235	239	227	205	251	351
Rb	43	33	36	16	12	10	<4	12
Sc	-	-	-	-	-	-	15	18
Sr	855	1260	700	753	503	701	1818	1155
Y	31	34	30	25	19	20	25	27
Zr	220	265	215	205	117	215	287	238
CIPW Norms								
Or	8.86	5.73	5.91	7.68	7.68	7.09	2.96	0.39
Ab	18.20	23.07	19.91	0.03	16.94	6.95	12.13	-
An	21.49	15.59	21.86	7.13	18.13	11.05	18.08	6.94
Lc	-	-	-	-	-	-	-	5.72
Ne	4.30	7.67	2.05	18.32	1.81	13.66	0.76	17.42
Di	17.70	17.85	18.53	32.80	19.86	24.87	19.79	33.27
Ol	16.16	12.86	16.58	18.17	21.46	15.41	23.24	18.96
Mt	5.08	6.82	5.95	5.37	4.35	8.99	7.83	7.83
Il	4.37	5.13	3.99	5.89	4.56	6.65	6.08	5.13
Ap	1.49	2.25	1.47	2.37	1.54	2.60	2.37	2.61
Rittmann Norms								
Sanidine	9.0	3.7	4.2	8.5	9.0	7.8	0.9	0.5
Plagioclase	43.2	42.8	46.8	5.4	38.5	15.5	34.6	3.4
Nepheline	5.7	10.8	3.6	18.8	2.0	16.7	2.0	18.7
Leucite	-	-	-	-	-	-	-	5.5
Clinopyroxene	20.3	21.2	21.9	42.9	23.7	32.8	25.6	43.9
Olivine	16.4	15.3	18.4	19.6	21.5	20.7	27.4	22.3
Magnetite	1.9	2.2	1.7	2.5	1.8	2.5	1.9	2.3
Ilmenite	2.1	2.2	1.9	-	2.0	1.4	2.9	-
Apatite	1.4	2.2	1.4	2.3	1.5	2.6	2.5	2.6
Colour Index	40.7	40.9	44.0	65.0	49.0	57.4	57.8	68.6

Table 21. (continued).

Plot No.	17	18	19	20	21	22	23	24
Analysis No.	742065	742066	742067	742068	742069	742070	742071	742072
SiO_2	39.8	38.5	37.8	38.2	42.2	43.6	45.4	40.9
TiO_2	2.7	3.0	3.1	3.0	2.5	2.7	2.5	2.7
Al_2O_3	10.3	10.2	10.4	9.8	11.2	13.1	12.6	10.8
Fe_2O_3	4.2	3.8	4.1	3.5	3.5	3.0	2.3	3.9
FeO	9.0	10.4	9.7	10.1	10.4	8.7	10.0	9.7
MnO	0.18	0.19	0.19	0.20	0.21	0.19	0.18	0.20
MgO	14.6	12.6	12.7	12.7	12.4	10.5	10.0	12.6
CaO	11.3	11.5	11.5	11.8	10.2	10.1	10.1	10.8
Na_2O	3.6	2.3	1.7	1.1	3.6	2.5	3.3	4.2
K_2O	1.3	1.1	0.9	1.3	1.4	1.4	1.4	1.4
P_2O_5	1.1	1.1	0.99	1.0	0.89	0.69	0.71	1.2
H_2O^+	1.6	3.9	4.9	5.3	1.7	2.4	1.6	1.5
H_2O^-	0.60	1.6	2.1	2.1	0.21	0.32	0.20	0.34
CO_2	0.20	0.24	0.16	0.13	0.43	1.30	0.13	0.32
Total	100.48	100.43	100.24	100.23	100.84	100.50	100.42	100.56
Trace elements (ppm)								
Ba	439	452	413	457	400	530	389	378
Cu	46	45	46	54	56	62	48	57
Cr	500	400	400	300	400	500	200	400
Li	5	5	10	10	5	10	10	5
Ni	385	228	227	259	328	291	195	329
Rb	20	17	8	21	15	22	16	8
Sc	18	15	17	25	17	21	12	22
Sr	1093	1021	1190	1231	885	799	820	1054
Y	26	29	26	33	30	27	25	32
Zr	239	276	271	310	231	187	173	218
CIPW Norms								
Or	1.34	6.50	5.32	7.68	8.27	8.27	8.27	8.27
Ab	-	1.42	3.02	1.27	6.64	19.90	15.66	1.65
An	8.11	14.26	18.09	17.96	10.27	20.39	15.43	6.48
Lc	4.97	-	-	-	-	-	-	-
Ne	16.50	9.77	6.16	4.35	12.90	0.68	6.65	18.36
Di	31.46	27.37	25.18	26.65	25.60	13.64	23.67	29.84
Ol	21.68	21.31	20.99	21.52	22.38	22.87	18.92	19.83
Mt	6.09	5.51	5.95	5.08	5.08	4.35	3.34	5.66
Il	5.13	5.70	5.89	5.70	4.75	5.13	4.75	5.13
Ap	2.61	2.61	2.35	2.37	2.11	1.63	1.68	2.84
Rittmann Norms								
Sanidine	5.4	6.9	5.0	-	10.4	9.1	9.7	10.1
Plagioclase	4.8	17.2	23.7	26.0	17.2	45.1	34.9	6.5
Nepheline	18.2	10.3	7.1	1.8	13.0	0.8	6.2	18.7
Leucite	1.4	-	-	7.4	-	-	-	-
Clinopyroxene	41.5	35.2	32.8	32.9	31.4	16.0	27.6	38.5
Olivine	23.5	23.4	24.4	24.3	21.6	19.8	16.2	20.2
Magnetite	2.1	1.9	1.7	1.6	2.3	1.5	1.9	2.4
Ilmenite	-	1.7	2.4	3.2	0.8	2.6	1.7	-
Apatite	2.6	2.7	2.5	2.5	2.0	1.5	1.6	2.8
Colour Index	67.1	62.3	61.3	61.9	56.1	39.9	47.3	61.0

Table 21. (continued).

Plot No.	25	26	27	28	29	30	31	32
Analysis No.	742073	742074	742075	742076	742077	742078	742079	742080
SiO_2	41.6	41.6	42.4	42.2	39.0	41.6	44.4	41.4
TiO_2	2.5	2.6	2.6	2.6	2.8	2.5	2.5	2.7
Al_2O_3	11.0	11.6	11.5	11.2	10.3	10.7	12.0	11.2
Fe_2O_3	2.8	3.7	2.9	3.7	5.3	3.9	2.8	4.9
FeO	10.0	9.8	9.8	9.5	9.2	9.2	10.1	8.7
MnO	0.20	0.19	0.19	0.20	0.20	0.20	0.19	0.20
MgO	11.9	11.9	12.3	12.4	13.0	12.8	10.7	12.4
CaO	9.8	10.0	10.3	10.3	10.8	10.4	10.0	10.4
Na_2O	4.0	3.7	4.1	3.6	3.8	4.5	3.0	4.4
K_2O	1.6	1.3	1.5	1.2	1.4	1.0	1.3	1.5
P_2O_5	0.95	0.85	0.86	0.94	1.2	1.1	0.67	1.0
H_2O^+	1.5	1.3	0.80	2.3	2.5	1.7	2.3	1.7
H_2O^-	0.18	0.31	0.19	0.19	0.26	0.34	0.00	0.00
CO_2	1.3	0.13	0.24	0.16	0.24	0.86	0.13	0.08
Total	99.33	98.98	99.68	100.49	100.00	100.80	100.09	100.58
Trace elements (ppm)								
Ba	395	401	497	440	414	404	380	426
Cu	59	59	60	49	23	57	50	62
Cr	200	200	200	300	400	400	300	400
Li	15	10	10	10	10	20	10	10
Ni	326	294	315	292	353	379	251	339
Rb	17	16	18	12	8	10	17	15
Sc	20	21	21	14	18	19	17	21
Sr	991	844	976	940	1498	1049	742	1151
Y	28	28	27	26	33	32	25	31
Zr	256	241	254	249	366	281	208	265
CIPW Norms								
Or	9.46	7.68	8.87	7.09	6.57	5.91	7.68	8.87
Ab	9.13	6.24	3.76	7.84	-	8.67	14.71	2.13
An	7.34	11.21	8.55	10.86	6.91	6.05	15.44	6.38
Lc	-	-	-	-	1.34	-	-	-
Ne	13.39	13.60	16.76	12.26	17.42	15.93	5.78	19.01
Di	21.64	25.73	28.47	26.53	29.73	26.35	23.42	30.42
Ol	22.74	20.36	20.61	20.59	18.95	20.95	20.11	17.34
Mt	4.06	5.37	4.21	5.37	7.69	5.66	4.06	7.11
Il	4.75	4.94	4.94	4.94	5.32	4.75	4.75	5.13
Ap	2.25	2.01	2.04	2.23	2.84	2.61	1.59	2.37
Rittmann Norms								
Sanidine	13.7	9.3	11.6	8.6	7.9	7.7	9.1	10.6
Plagioclase	16.1	18.2	11.8	19.3	4.4	13.7	33.7	5.8
Nepheline	13.7	14.3	16.5	12.7	19.6	16.7	5.6	19.9
Leucite	-	-	-	-	-	-	-	-
Clinopyroxene	27.2	32.0	35.9	32.9	40.0	33.6	27.8	39.4
Olivine	21.0	20.6	19.4	21.0	22.2	21.2	18.3	19.4
Magnetite	2.2	2.2	2.2	2.1	2.5	2.3	1.9	2.4
Ilmenite	0.4	1.0	-	0.9	-	-	1.7	-
Apatite	2.2	2.0	2.0	2.2	2.9	2.5	1.5	2.3
Colour Index	50.8	55.9	57.5	56.8	64.6	57.0	49.7	61.2

Table 21. (continued).

Plot No.	33	34	35	36	37	38	39	40
Analysis No.	742081	742082	742083	742084	742085	742086	742087	742088
SiO_2	41.5	41.9	41.9	42.2	41.3	40.6	41.8	44.8
TiO_2	2.7	2.6	2.6	2.8	2.5	2.7	2.6	2.4
Al_2O_3	11.1	11.2	11.1	13.6	11.2	10.7	11.2	12.0
Fe_2O_3	3.9	3.6	3.9	3.8	2.8	4.3	3.1	2.8
FeO	9.8	9.7	9.7	9.0	10.1	9.4	10.0	9.8
MnO	0.20	0.20	0.20	0.18	0.19	0.21	0.21	0.19
MgO	12.7	12.0	12.8	8.6	11.3	13.1	12.4	11.5
CaO	10.6	10.6	9.9	10.1	10.9	10.9	11.0	9.7
Na_2O	4.4	3.7	4.2	4.5	2.7	3.7	3.2	2.3
K_2O	1.2	1.2	1.4	1.5	1.2	1.1	1.0	1.3
P_2O_5	1.0	1.2	1.2	1.1	0.78	1.2	0.88	0.63
H_2O^+	1.9	2.8	1.1	2.2	3.6	2.0	2.8	2.5
H_2O^-	0.07	0.34	0.24	0.42	0.34	0.28	0.55	0.83
CO_2	0.08	0.20	0.24	0.13	0.24	0.20	0.20	0.16
Total	101.15	101.24	100.48	100.13	99.15	100.39	100.94	100.91
Trace elements (ppm)								
Ba	418	441	453	497	416	432	410	385
Cu	58	49	59	67	50	56	49	50
Cr	500	400	400	200	200	400	400	400
Li	10	10	5	5	10	10	5	10
Ni	323	303	373	194	249	332	286	249
Rb	13	7	13	19	17	11	15	13
Sc	19	13	15	12	17	17	17	16
Sr	1063	1129	1068	1498	926	1126	1183	724
Y	27	30	26	33	28	32	29	25
Zr	276	267	277	265	208	271	218	160
CIPW Norms								
Or	7.09	7.09	8.27	8.87	7.09	6.50	5.91	7.68
Ab	2.11	7.62	6.03	9.31	7.05	3.67	6.50	17.70
An	6.99	10.41	7.30	12.48	14.90	9.34	13.24	18.58
Lc	-	-	-	-	-	-	-	-
Ne	19.03	12.83	15.99	15.58	8.56	14.97	11.15	0.96
Di	30.91	26.56	26.01	23.88	26.28	28.50	27.59	19.68
Ol	19.77	20.19	21.62	13.72	20.18	20.55	21.27	22.55
Mt	5.66	5.22	5.66	5.51	4.06	6.24	4.50	4.06
Il	5.13	4.94	4.94	5.32	4.75	5.13	4.94	4.56
Ap	2.37	2.84	2.84	2.61	1.85	2.84	2.08	1.49
Rittmann Norms								
Sanidine	8.6	8.7	11.2	10.2	7.9	7.5	6.2	9.1
Plagioclase	7.7	18.6	11.7	23.3	25.5	12.1	22.2	40.9
Nepheline	19.2	13.2	16.6	17.0	8.6	15.8	11.1	0.4
Leucite	-	-	-	-	-	-	-	-
Clinopyroxene	39.6	32.9	33.3	28.9	32.4	36.8	33.7	23.3
Olivine	20.0	20.3	21.5	14.1	19.7	22.0	21.0	20.8
Magnetite	2.4	2.2	2.4	2.3	1.9	2.2	2.0	1.7
Ilmenite	-	0.8	-	1.5	1.5	0.3	1.2	2.0
Apatite	2.3	2.8	2.7	2.5	1.9	2.8	2.1	1.4
Colour Index	62.0	56.2	57.2	46.7	55.6	61.3	57.9	47.8

Table 21. (continued)

Plot No.	41	42	43	44	45	46	47	48
Analysis No.	742089	742090	742091	742092	742093	742094	742095	742096
SiO_2	42.1	45.3	45.3	40.0	45.6	43.6	44.1	42.3
TiO_2	2.6	2.5	2.4	2.7	2.5	2.5	2.5	2.7
Al_2O_3	11.4	12.5	10.9	10.3	12.4	12.0	13.6	13.1
Fe_2O_3	3.0	3.5	3.1	4.2	2.6	2.9	3.3	3.8
FeO	10.3	8.6	7.8	9.2	9.5	10.7	8.2	8.1
MnO	0.21	0.17	0.15	0.20	0.18	0.23	0.19	0.19
MgO	12.2	9.6	11.2	14.6	9.6	10.6	11.0	11.0
CaO	10.6	10.5	14.0	11.1	10.4	9.8	9.6	10.8
Na_2O	3.8	2.8	2.0	3.7	2.9	3.1	2.5	2.6
K_2O	1.2	1.5	1.2	1.4	1.4	1.4	1.2	1.5
P_2O_5	0.86	0.66	0.49	1.0	0.70	0.69	0.53	0.85
H_2O^+	1.6	2.3	2.0	1.9	2.0	1.1	2.2	2.6
H_2O^-	0.30	0.15	0.15	0.07	0.24	0.44	0.41	0.46
CO_2	0.11	0.08	0.13	0.05	0.16	0.98	0.22	0.11
Total	100.28	100.16	100.82	100.42	100.18	100.04	99.55	100.11
Trace elements (ppm)								
Ba	429	403	333	444	403	406	427	579
Cu	53	46	25	42	53	56	62	58
Cr	200	400	700	500	400	300	300	200
Li	10	10	10	10	5	5	10	10
Ni	267	185	189	384	180	236	261	242
Rb	11	19	19	17	13	12	17	36
Sc	17	18	31	20	16	18	26	22
Sr	836	720	538	1139	725	798	789	930
Y	31	24	25	33	27	28	28	34
Zr	231	158	143	245	168	188	199	230
CIPW Norms								
Or	7.09	8.87	7.09	0.17	8.27	8.27	7.09	8.87
Ab	4.51	16.90	7.83	-	17.76	16.09	17.99	9.01
An	10.51	17.11	17.22	7.36	16.68	14.70	22.35	19.65
Lc	-	-	-	6.36	-	-	-	-
Ne	14.97	3.68	4.93	16.96	3.67	5.49	1.72	7.04
Di	28.81	24.25	38.52	32.06	23.72	18.82	16.35	22.10
Ol	20.96	15.38	12.60	21.77	17.33	22.35	20.19	17.54
Mt	4.35	5.08	4.50	6.09	3.77	4.21	4.79	5.51
Il	4.94	4.75	4.56	5.13	4.75	4.75	4.75	5.13
Ap	2.04	1.56	1.16	2.37	1.66	1.63	1.26	2.01
Rittmann Norms								
Sanidine	8.5	10.8	8.0	3.9	10.0	9.9	6.3	8.9
Plagioclase	16.0	36.2	25.1	4.0	38.0	34.4	46.5	31.8
Nepheline	14.8	4.0	4.4	18.5	3.3	5.5	2.1	8.0
Leucite	-	-	-	3.1	-	-	-	-
Clinopyroxene	35.8	28.7	46.3	42.1	27.9	22.1	19.3	26.4
Olivine	20.0	15.1	12.5	23.3	15.2	20.0	20.1	18.8
Magnetite	2.2	1.7	1.3	2.2	1.7	2.1	1.5	1.6
Ilmenite	0.6	1.8	1.0	-	1.8	1.9	2.4	2.2
Apatite	2.0	1.5	1.1	2.3	1.6	1.6	1.2	2.0
Colour Index	58.5	47.3	61.0	67.7	46.6	46.0	43.3	49.1

Table 21. (continued).

Plot No.	49	50	51	52	53	54	55
Analysis No.	742097	742098	742099	761163	761164	761165	761166
SiO_2	39.3	46.3	45.1	40.0	39.9	39.5	40.6
TiO_2	3.3	2.3	2.4	2.5	2.6	2.6	2.5
Al_2O_3	10.3	12.4	12.0	9.6	9.8	9.7	10.6
Fe_2O_3	4.4	1.2	3.0	4.7	4.8	4.8	2.5
FeO	10.1	9.9	9.6	8.6	8.5	8.8	10.5
MnO	0.21	0.17	0.17	0.23	0.21	0.22	0.22
MgO	13.0	11.0	11.2	14.5	14.5	15.5	11.5
CaO	11.8	9.6	9.7	11.3	11.4	11.4	10.1
Na_2O	1.8	2.6	2.9	3.6	3.6	3.6	4.0
K_2O	1.2	1.2	1.3	1.4	1.4	1.4	1.5
P_2O_5	1.1	0.55	0.63	1.1	1.1	0.99	0.98
H_2O^+	3.3	2.0	1.9	1.4	1.5	1.7	2.8
H_2O^-	0.85	0.45	0.50	0.34	0.26	0.14	0.27
CO_2	0.13	0.21	0.16	0.1	0.1	0.11	1.9
Total	100.79	99.88	100.56	99.57	99.67	100.46	99.97
Trace elements (ppm)							
Ba	486	358	382	200	220	210	210
Cu	48	43	46	74	69	38	94
Cr	400	300	300	630	680	590	540
Li	10	10	10	-	-	-	-
Ni	261	229	231	390	380	380	280
Rb	8	17	20	9	5	5	8
Sc	18	18	16	15	15	16	15
Sr	1892	710	691	920	910	920	980
Y	29	25	23	26	24	23	27
Zr	262	147	164	260	250	260	280
CIPW Norms							
Or	7.09	7.09	7.68	2.35	1.36	-	8.87
Ab	2.48	20.23	16.72	-	-	-	9.79
An	16.48	18.62	15.89	5.90	6.45	6.17	6.54
Lc	-	-	-	4.65	5.42	6.49	-
Ne	6.91	0.96	4.24	16.50	16.50	16.50	13.03
Di	27.23	19.54	21.88	33.67	33.59	30.05	20.33
Ol	20.96	23.67	21.57	20.23	19.92	23.30	23.38
Mt	6.38	1.74	4.35	6.82	6.96	6.96	3.63
Il	6.27	4.37	4.56	4.75	4.94	4.94	4.75
Ap	2.61	1.30	1.49	2.61	2.61	2.35	2.32
Rittmann Norms							
Sanidine	7.4	7.3	9.1	4.1	3.0	-	13.3
Plagioclase	19.8	45.2	36.1	2.7	3.1	-	16.3
Nepheline	7.4	-	3.9	17.7	17.8	17.8	13.4
Leucite	-	-	-	3.1	4.0	2.7	-
Clinopyroxene	34.6	24.2	25.7	44.3	44.3	46.7	26.0
Olivine	23.8	17.9	19.7	23.0	22.8	25.1	21.1
Magnetite	1.8	1.6	1.9	2.2	2.2	2.3	2.3
Ilmenite	2.2	1.9	1.7	-	-	-	0.2
Apatite	2.7	1.2	1.4	2.6	2.6	2.4	2.3
Colour Index	62.3	45.7	49.0	69.5	69.3	74.1	49.5

Table 22. INDEX TO ANALYSES OF BASALTIC ROCKS LISTED IN TABLE 21

Analysis No.	Department and thin section No.	Grid reference (EQ)	Plot No.
735112	72/211	647397	1
735114	72/396	802355	2
735115	72/397	801352	3
735116	72/398	799347	4
735117	72/400	741335	5
735118	72/404	799352	6
735119	72/405	793350	7
735122	73/519	805376	8
735123	73/520	786379	9
735124	73/518	804370	10
735125	73/521	812356	11
741643	74/428	603336	12
741644	74/429	598345	13
741649	74/441	637340	14
742063	72/425	746500	15
742064	72/426	737505	16
742065	72/427	740503	17
742066	72/428	645449	18
742067	72/429	645442	19
742068	72/430	636444	20
742069	72/431	640455	21
742070	72/432	631467	22
742071	72/433	727525	23
742072	72/434	654459	24
742073	72/435	646456	25
742074	72/438	645446	26
742075	72/440	708491	27
742076	72/441	694480	28
742077	72/442	694478	29
742078	72/443	698477	30
742079	72/444	682477	31
742080	72/445	683489	32
742081	72/446	680468	33
742082	72/448	672454	34
742083	72/449	666460	35
742084	72/450	665462	36
742085	72/451	668467	37
742086	72/452	688463	38
742087	72/453	689465	39
742088	72/454	697559	40
742089	72/455	657511	41
742090	72/456	658512	42
742091	72/162	615501	43
742092	73/537	739505	44
742093	73/638	658511	45
742094	73/639	661538	46
742095	73/640	667492	47
742096	73/641	666492	48
742097	75/361	609434	49
742098	75/362	589391	50
742099	76/363	567354	51
761163	72/381	727529	52
761164	72/384	727529	53
761165	72/386	727511	54
761166	74/648	645456	55

Table 23. AVERAGE COMPOSITION OF BASALTIC ROCK TYPES

	Olivine nephelinite	Alkali basalt	Silica undersaturated basalt (Manson, 1967)
SiO_2	40.75	44.42	43.44
TiO_2	2.66	2.46	2.54
Al_2O_3	10.78	13.18	12.84
Fe_2O_3	4.26	3.92	4.17
FeO	9.16	8.51	8.57
MnO	0.20	0.19	0.19
MgO	13.15	9.87	10.22
CaO	10.77	10.02	10.22
Na_2O	3.89	2.99	3.48
K_2O	1.38	1.23	1.26
P_2O_5	1.08	0.70	0.85
H_2O^+	1.71	2.11	1.96
H_2O^-	0.26	0.56	0.43
CO_2	0.17	0.15 (12)	0.10
Ba	356	406 (12)	342 (14)
Cu	54	53	54
Cr	431	342 (12)	343 (14)
Li	8 (10)	10	10
Ni	342	195	217
Rb	12	26	23
Sc	17	19 (12)	18 (14)
Sr	1099	814	945
Y	29	29	30
Zr	263	205	232
No. of analyses except were indicated	13	22	22

Table 24. SUGGESTED 'PRIMITIVE' BASALTIC ROCKS

Plot No.	16	17	44	52	53	54		13	47
Analysis No.	742064	742065	742092	761163	761164	761165	Average	741644	742095
SiO_2	40.24	40.67	40.74	41.12	40.91	40.21	40.65	45.57	45.67
TiO_2	2.75	2.76	2.75	2.57	2.67	2.65	2.69	2.47	2.59
Al_2O_3	10.39	10.52	10.49	9.87	10.05	9.87	10.20	12.34	14.08
Fe_2O_3	2.29	2.17	2.20	2.20	2.19	2.23	2.21	2.16	1.93
FeO	11.65	11.09	11.23	11.21	11.17	11.35	11.30	11.00	9.83
MnO	0.20	0.18	0.20	0.24	0.21	0.22	0.21	0.17	0.20
MgO	14.36	14.92	14.87	14.91	14.87	15.78	14.95	12.03	11.39
CaO	11.81	11.55	11.30	11.62	11.69	11.60	11.59	9.77	9.94
Na_2O	3.87	3.68	3.77	3.70	3.69	3.66	3.73	2.47	2.59
K_2O	1.32	1.32	1.43	1.44	1.44	1.42	1.40	1.34	1.24
P_2O_5	1.12	1.12	1.02	1.13	1.13	1.01	1.09	0.67	0.55
$\frac{100Mg}{Mg+Fe^{2+}}$ for $\frac{Fe^{3+}}{Fe}$ as analysed	74.5	74.3	73.9	75.0	75.3	75.9	74.8	70.08	70.50
$\frac{100Mg}{Mg+Fe^{2+}}$ for $\frac{Fe^{3+}}{Fe} = 0.15$	68.7	70.6	70.2	70.3	70.3	71.2	70.2	66.08	67.38
Ni (ppm)	351	385	384	390	380	380	378	227	261
% melting K_2O	9.8	9.8	9.1	9.0	9.0	9.1	9.3	9.72	10.47
% melting P_2O_5	5.4	5.3	5.9	5.3	5.3	6.0	5.5	8.98	10.95

Major elements. Major and trace element analyses, together with CIPW and Rittmann norms of fifty-five randomly collected samples from the above areas are presented in Table 21. Fifteen of these analyses have been rejected from further consideration due to excess H_2O, CO_2 and Fe_2O_3 content. The values used for rejection are those of Manson (1967). The unifying factor of the majority of the rejected samples appears to be a high zeolite content, which is correlated with the occurrence of the specimens from the basal part of flows on the basalt-sediment interface. As the specimens were otherwise fresh, contamination by volatile rich sediments at the time of extrusion is suggested. The total of the mass per cent for one other sample was excessively high (plot 12, (101.79)) and the sample is also rejected. The total of the mass per cent of five other analyses also falls outside the range of 99 - 101 stipulated by Manson, but as they vary only by minus 0.02 to plus 0.24 they have been included in the general plots but excluded when the average composition for the various 'basalt' types were calculated.

An alkali-silica plot of the remaining thirty nine analyses (fig. 24) show the alkalic nature of the rocks from these areas. The division between alkali olivine basalt and olivine nephelinite is also clear. Both these groups fall at the base of the respective lineages, A = alkali olivine basalt and E = olivine nephelinite, as defined by Coombs and Wilkinson (1969) for undersaturated basaltic rocks.

When plotted on a standard AFM diagram (fig. 25) the fields of the olivine nephelinites and alkali olivine basalt overlap. The alkali olivine basalt field shows a small degree of differentiation which is comparable to the basal part of the generalised alkali basalt trends obtained from the Hebridean and Hawaiian provinces.

In comparison to the AFM plot, a Streckeisen PFA diagram using Rittman norms (fig. 26) shows a spread of the alkali olivine basalt and olivine nephelinite. The alkali olivine basalt lies between the plagioclase apex and line AA´ and the olivine nephelinite samples lie along a curved zone from line BB´ to the feldspathoidal apex. Between AA´ and BB´ is a small zone of overlap between the two rock types and into which the two limburgitic samples plot.

Average composition of alkali-basalt and olivine nephelinite are presented in Table 23 to facilitate a chemical comparison between these two petrologically distinct rock types from the areas under discussion with other areas of similar basaltic rocks. Also shown in this table is an average 'silica undersaturated (nephelinite normative) basalt' for the area, based strictly on an average of those analyses, whether of alkali olivine basalt or olivine nephelinite, selected by Manson's (1967) basalt screen. Figure 27 shows the position of these averages in relation to their respective fields on a Streckeisen PFA plot.

Trace elements. On the basis of trace element content the basaltic rocks of the Weldborough Pass-Mt Paris area, and the Ringarooma-Winnaleah area can be distinguished irrespective of their similarity in major element and petrographic character.

The relationship of nickel to zirconium content provides a test for an olivine fractionation model since nickel is a highly compatible element in the olivine lattice and will be removed from the melt by olivine fractionation whilst zirconium is an incompatible element and will accumulate

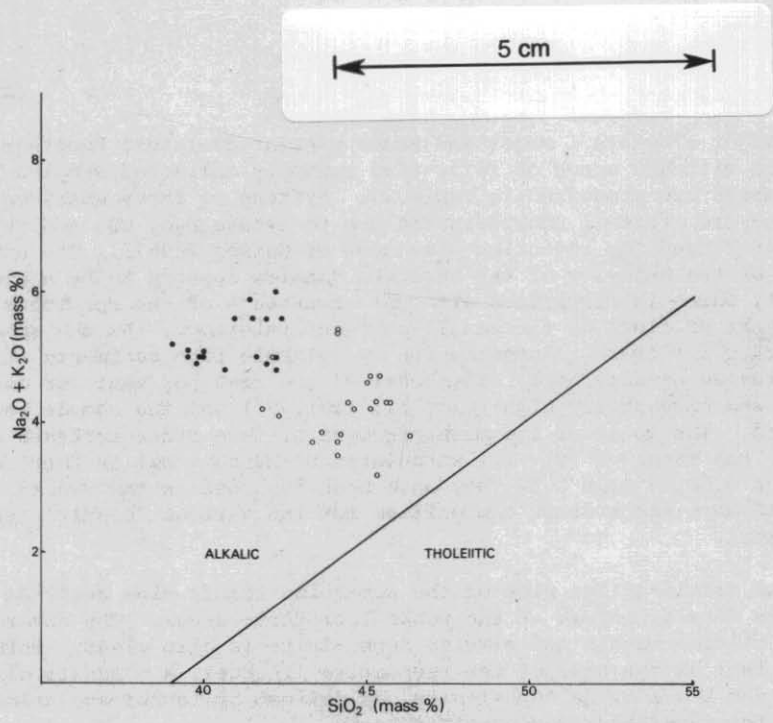

Figure 24. *Alkali-silica diagram of basaltic rocks from the Ringarooma-Winnaleah-Weldborough Pass areas. Alkali and tholeiitic fields from Macdonald and Katsura (1964).*

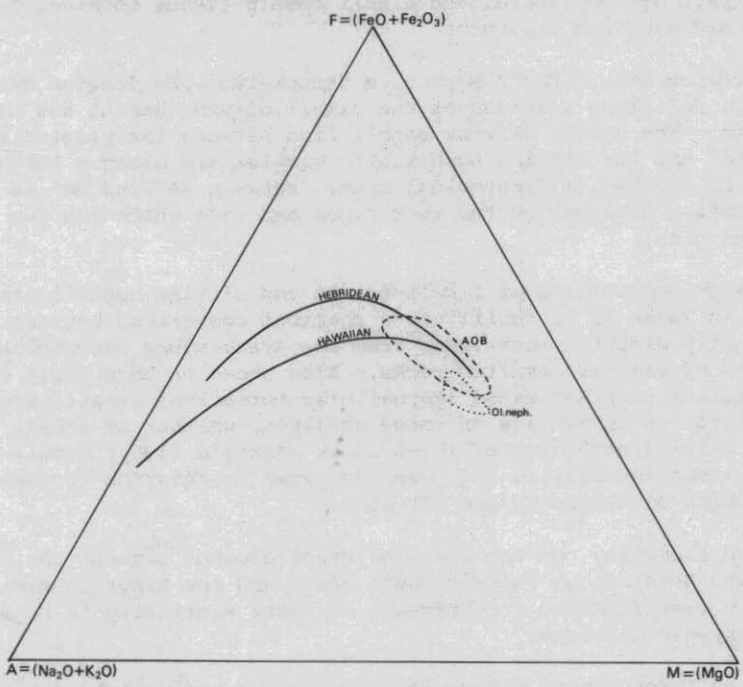

Figure 25. *AFM diagram (mass%) showing fields of alkali olivine basalt (AOB) and olivine nephelinite (Ol.neph.) for analyses listed in table 21. Generalised Hebridean and Hawaiian alkalic trends shown for comparison.*

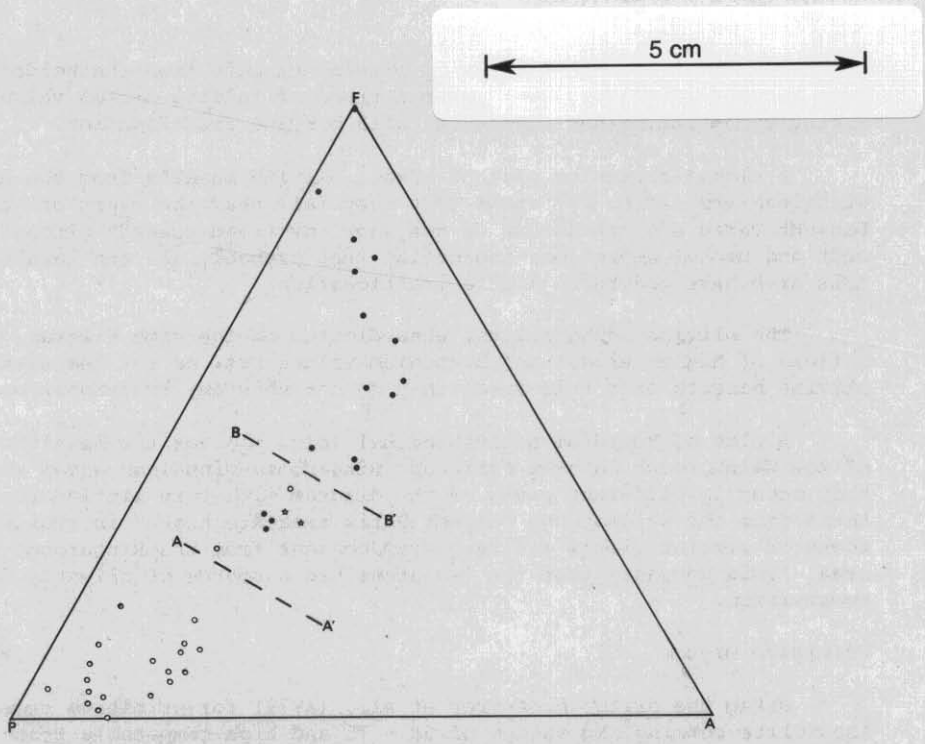

alkali olivine basalt (o), olivine nephelinite (•), limburgite (☆)

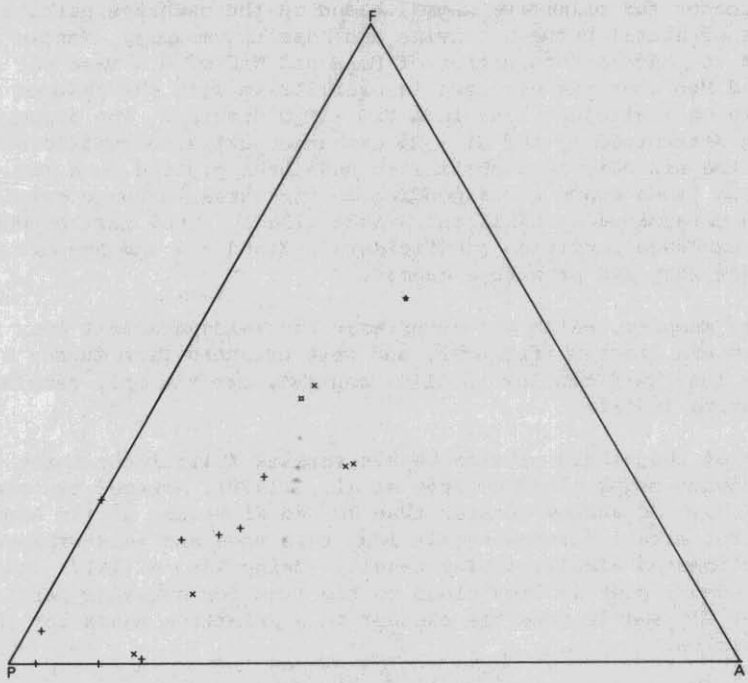

Analyses rejected because of excess H_2O (+), excess CO_2 (×), excess Fe_2O_3 (¤), excessively high total (★)

Figure 26. *Rittmann normative minerals plotted on PFA diagrams. P = plagioclase, F = nepheline + leucite + sodalite, A = sanidine + anorthoclase or orthoclase.*

in the melt. A plot of the alkali olivine basalts from the Weldborough Pass-Mt Paris area (fig. 28) shows a trend of falling nickel values with rising zirconium values consistent with olivine fractionation.

A nickel-zirconium plot of alkali olivine basalts from the Ringarooma-Winnaleah area (fig. 29) shows that they fall near the start of Weldborough Pass-Mt Paris area trend but do not show any trend towards zirconium enrichment and nickel depletion, indicating that probably all the basalts from this area have undergone little fractionation.

The olivine nephelinites, when plotted on the same diagram, fall in a field of higher nickel and zirconium values but, as for the alkali olivine basalts from this area, they do not show any fractionation trend.

A plot of rubidium against nickel (fig. 30) for the basaltic rocks of the Weldborough Pass-Mt Paris and Ringarooma-Winnaleah areas show that they occur in different parts of the diagram with very little overlap. Rocks from the Weldborough Pass-Mt Paris area are higher in rubidium than rocks of similar nickel and zirconium content from the Ringarooma-Winnaleah area. This suggests that the two areas had a source of slightly different composition.

Primitive magmas *(MPM, AVB)*

Using the criteria of Frey *et al.*, (1978) for primitive magmas (spinel lherzolite bearing, Mg values of 68 - 75 and high compatable trace element content (Ni, Co, Sc)), six olivine nephelinite samples (table 24) appear to be primitive. Nickel content has also been suggested by Sato (1977) as an indicator for primitive magma, based on the exchange partition coefficients of nickel between olivine and basaltic magmas. Mantle olivine is assumed to have a composition of Fo_{90} and NiO of 0.4 mass per cent. The NiO and MgO contents of magma in equilibrium with the assumed mantle olivine lie on a straight line in a NiO - MgO diagram. The slope of the line being determined by the Ni - Mg exchange partition coefficient. In Figure 31 the six olivine nephelinites have been plotted on a NiO - MgO diagram with lines drawn corresponding to the three exchange partition coefficients determined by Häkli and Wright (1967). They fall between the lines for exchange partition coefficients 2.3 and 2.6 and support the conclusion that they are primitive magmas.

These samples, which all occur near the feldspathoidal apex in the Streckeisen PFA diagram (fig. 26), and were excluded from Manson's 'basalt' average as they were too low in Al_2O_3 content, are the only samples to have CIPW normative leucite.

None of the alkali olivine basalt samples fulfill the three criteria for a primitive magma cited by Frey *et al.*, (1978), however two samples (table 24) have Mg values greater than 70 and Ni values at the high end of the range for alkali olivine basalt from this area and thus represent the least fractionated alkali olivine basalt. Using Sato's (1977) criteria (fig. 31) sample plot 47 lies close to the line for exchange partition coefficient 2.6 and is thus the closest to a primitive magma for the alkali olivine basalts.

Following Frey *et al.*, (1978) on the basis of K_2O and P_2O_5 content of the suspected primitive basalts, and using the composition of pyrolite given by them from Ringwood (1966), the percentage of partial melting required to produce the average primary olivine nephelinite and the least fractionated alkali olivine basalt have been calculated (table 24).

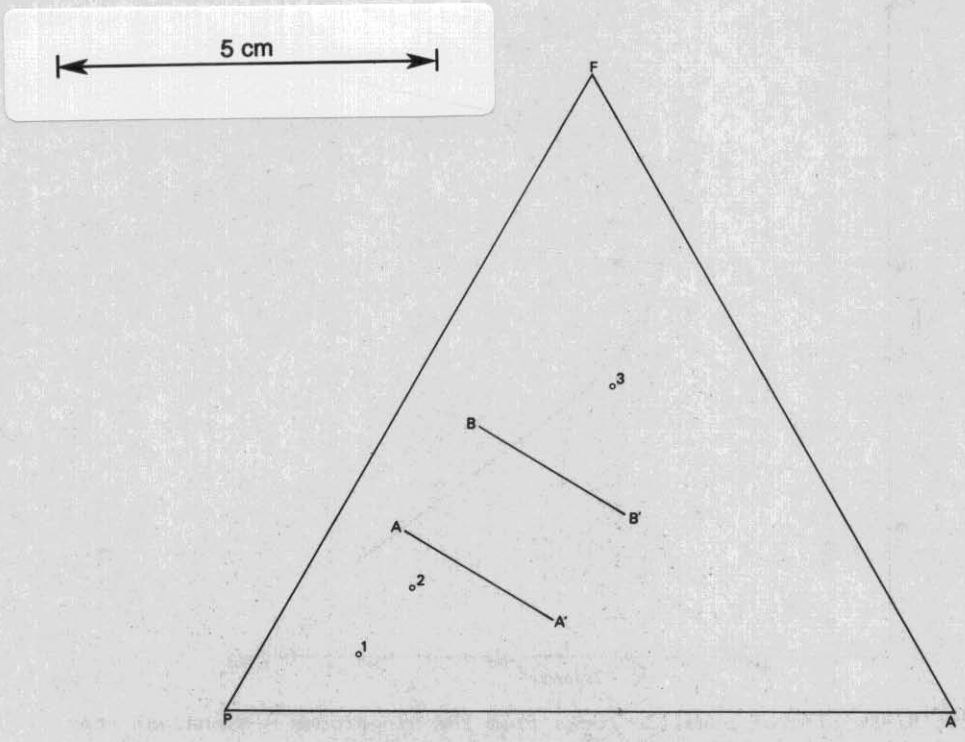

Figure 27. *Rittmann normative minerals plotted on a PFA digram. P = plagioclase, F = nepheline + leucite + sodalite, A = sanidine + anorthoclase + orthoclase, for the averages presented in table 23. 1 = average alkali basalt, 2 = average silica undersaturated basalt, 3 = average olivine nephelinite.*

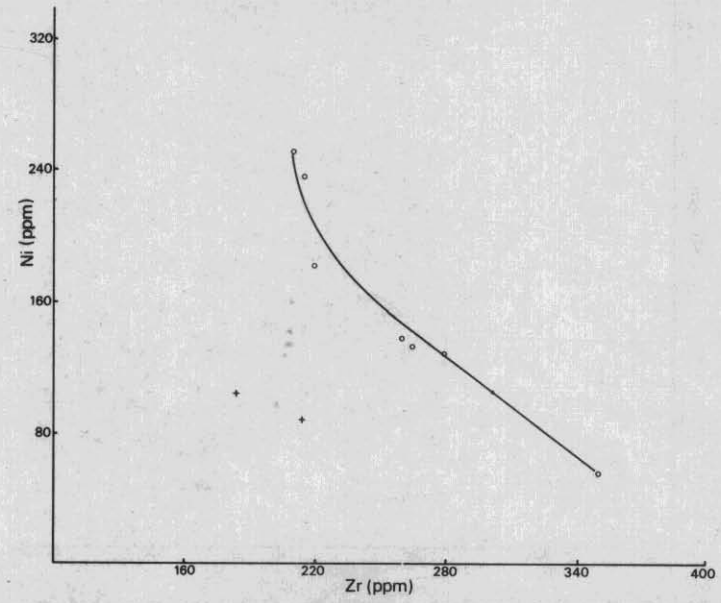

Figure 28. *Ni-Zr plot of the basaltic rocks of the Weldborough Pass - Mt Paris area. ∘ = alkali olivine basalts with olivine and minor amounts of pyroxene phenocrysts; + = as for ∘ but with additional plagioclase phenocrysts.*

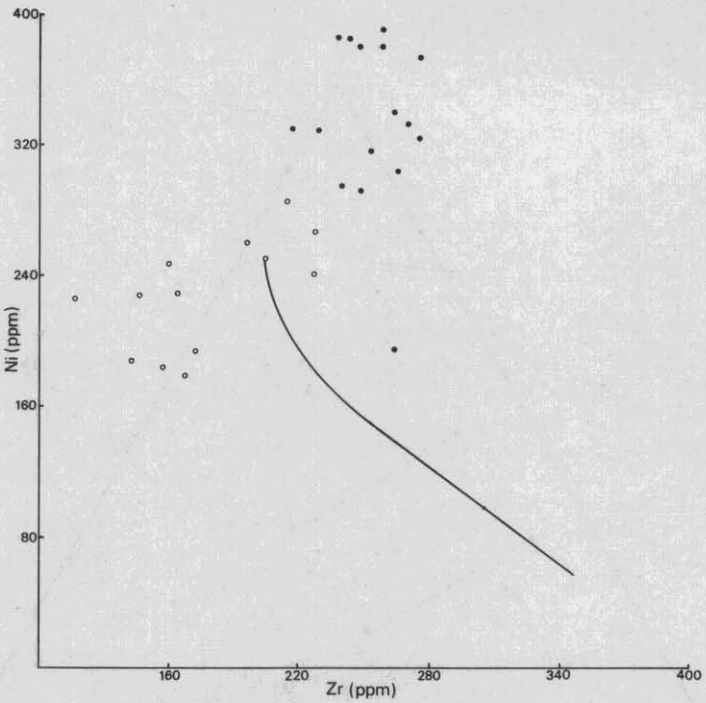

Figure 29. *Ni-Zr plot of basaltic rocks from the Ringarooma - Winnaleah area showing the Weldborough Pass - Mt Paris trend.*
• = olivine nephelinites, ∘ = alkali olivine basalts.

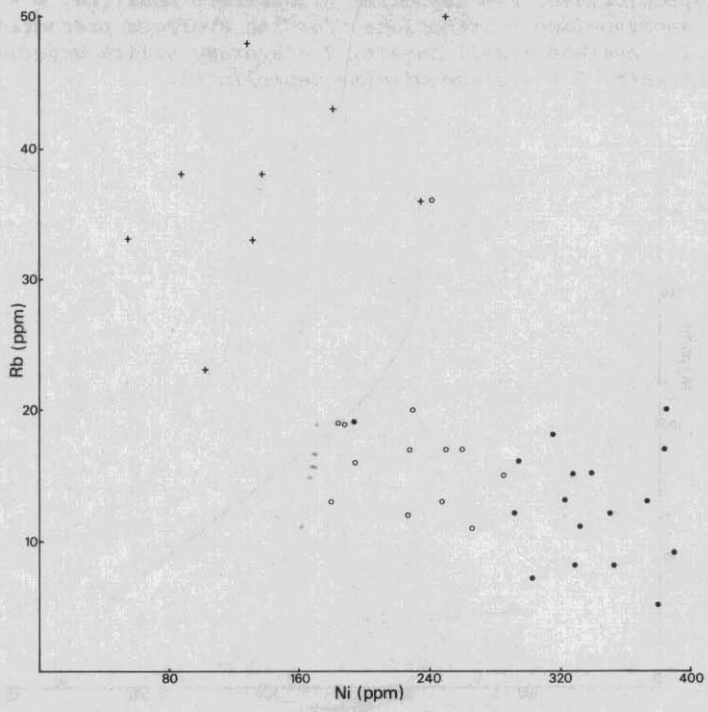

Figure 30. *Rb-Ni plot of basaltic rocks from the Weldborough Pass - Mt Paris and the Ringarooma-Winnaleah areas. ∘ = olivine nephelinites. Alkali olivine basalts from the Ringarooma - Winnaleah area (∘) and the Weldborough Pass - Mt Paris area (+).*

5 cm

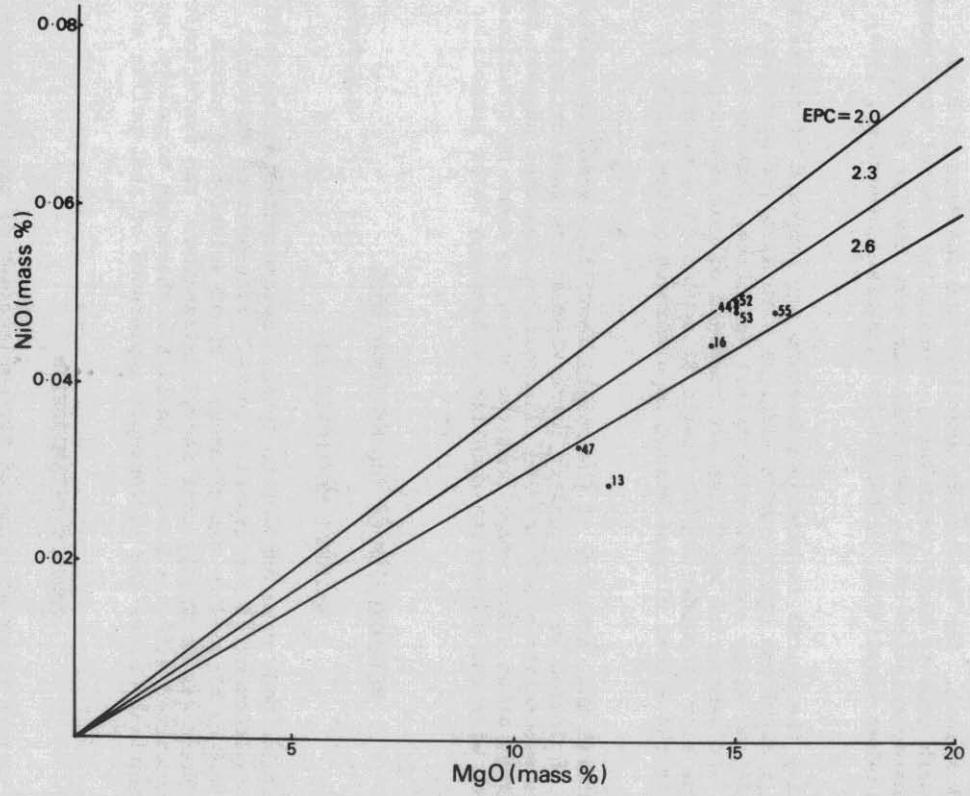

Figure 31. *NiO - MgO diagram with suggested 'primitive' basaltic rocks plotted (after Sato, 1977). Exchange partition coefficients* ($K^{ol\text{-}mag}_{Ni\text{-}Mg}$) *from Häkli and Wright (1967) are also shown.*

5 cm

Xenoliths and megacrysts have been recovered from basaltic rocks at seven localities (appendix 6) within the Ringarooma Quadrangle. Flows of olivine nephelinite contain xenoliths of spinel lherzolite and minor websterite as well as megacrysts of olivine, minor pyroxene and occasional spinel. Remnant areas of an alkali olivine basalt flow containing glomeroporphyritic rosettes of clinopyroxene occur in the region to the northeast of Warrentinna [657509].

The spinel lherzolite xenoliths are mottled green in colour, being dominantly composed of pale yellowish green olivine and dark bottle green orthopyroxene with minor small bright emerald green clinopyroxene and dark brown to black spinel. The websterite xenoliths and rosettes of clinopyroxene are dark grey to black in colour. Overall the mode of occurrence and general characteristics of the xenoliths are very similar to those obtained from other localities, elsewhere in Tasmania (Sutherland, 1974; Varne, 1977).

Chemically the spinel lherzolite xenoliths are composed of forsteritic olivine (Fo_{89}) aluminous othopyroxene ($En_{88.7}$) with exsolved pleonaste, chrome diopside and minor chromian rich spinel (picotite) (tables 1, 2; appendix 6). The websterite xenoliths are composed of bronzite and a chromian poor, aluminous rich diopsidic augite (table 3; appendix 6), whereas the rosettes within the alkali olivine basalt is aluminous salite (table 4, appendix 6).

The textures and chemistry of the spinel lherzolite xenoliths indicate an accidental inclusion in the basaltic magma whereas the same criteria applied to the websterite xenoliths and clinopyroxene rosettes suggest that they were derived at an early stage from the enclosing magma by fractional crystallisation with the websterite xenoliths exhibiting later subsolidus unmixing.

METAMORPHISM OF THE MATHINNA BEDS

N.J.Turner

REGIONAL METAMORPHISM

The Mathinna Beds were subject to dynamic metamorphism during folding prior to the emplacement of the granitic rocks. Fine-grained muscovite crystallised and is aligned in the cleavage. Minor solution of quartz occurred but there was no significant recrystallisation. The syntectonic metamorphism imparted either a slaty or phyllitic character to pelite but did not substantially alter the macroscopic appearance of semi-pelite and psammite.

CONTACT METAMORPHISM

Thermal metamorphism accompanied the emplacement of granitic rocks. Near to granitic contacts, cleaved pelite and semi-pelite were converted to fine-grained, quartz-mica schist, and psammite to fairly massive hornfels. Further from contacts the metamorphism produced spotting in pelite and semi-pelite and partial recrystallisation of psammite. The outermost edges of the aureoles were mapped at the first appearance of spotting in pelite. Outside this boundary no clearly thermal-metamorphic phenomena could be discerned in either hand specimen or thin section. The change from pelite containing no spots to pelite containing spots of 1-2 mm dimension takes place over a few metres. Spots become more numerous and

occur in semi-pelite as well as pure pelite within a short distance of the boundary. The effects of thermal metamorphism become evident in psammite at a substantially greater distance from the boundary.

Dimensions of the aureoles

The surface width of the aureoles ranges from a minimum of 800 m to a maximum of 5.1 km. This variation in width may be interpreted as a result of variation in the magnitude of dip of the contact, that is, the steeper the dip the thinner the aureole. Quantitative dip estimates derived from gravity profiles (Leaman, 1977) are consistent with qualitative estimates based on aureole width for the contact with the Blue Tier Batholith east and north-west of Mt Horror. Positions of profiles are shown in Figure 32. The simple model used for the gravity interpretation is illustrated in Figure 33. The quantitative estimates for the Blue Tier Batholith contact do not apply to the contact of the Scottsdale Batholith on the Kamona profile where a more complex model (fig. 33) of contact relationships is required to accommodate the gravity data.

Graphs A and B (fig. 33) respectively show the variation in the dip of the contact against measured aureole-width and calculated aureole-thickness for the Blue Tier Batholith profiles. An important factor influencing dip determination is that there is a zone in the Mathinna Beds near the contact in which the density has been increased by metamorphism. The width of the zone is unknown. Therefore, values of dip shown in the graphs range from maxima which make no allowance for the zone to minima which assume increased density across the whole aureole. The correlation between increasing dip of the contact and decreasing width of the aureole is quite good.

Thickness of the aureole increases with decreasing dip. This may reflect fundamental aspects of heat transfer from the cooling granite, for example, greater loss of heat across gently-dipping 'roof'sections and more effective heat transfer in the country rocks in the vertical direction. However, since low contact dips are confined to the Mt Horror area the thickened aureole may reflect some peculiarity of that area butthere are no obvious, significant differences between the rocks around Mt Horror and those elsewhere. The Mathinna Beds are similar lithologically to those elsewhere in the tract. Because they are lithologically uniform the Mathinna Beds are assumed to be chemically uniform. Granitic rocks along the contact from Waterhouse to north-east of Mt Horror are of uniform type (porphyritic, coarse-grained biotite granite/adamellite - Dbapc) with the exception of the small body north of Mt Horror (Dbae) which differs only in so far as it contains relatively fewer and smaller phenocrysts. Thus, the heat capacities of the intrusive rocks were probably fairly uniform along the entire contact. There is no widespread evidence that Mt Horror was a 'hot spot' due to the escape of fluid phases up fracture systems. Quartz-wolframite veins are present but known mineralisation is confined to a small locality near 609511. Groves (1977) noted that the locality is more distant from granitic rocks than is the general case for similar mineralisation in north-eastern Tasmania. Anisotropy of thermal conductivity in the Mathinna Beds due to their tectonic fabric may have influenced the form of the aureoles but the scale of the effect was probably insignificant.

Leaman (1977) gives the dip of the Scottsdale Batholith/Mathinna Beds contact on the Kamona profile as about 30° E. Even if the dip was 90° the thickness of the aureole (800 m) would be substantially less than the 1.1 km at 90° extrapolated for the Blue Tier aureole. The model of the contact

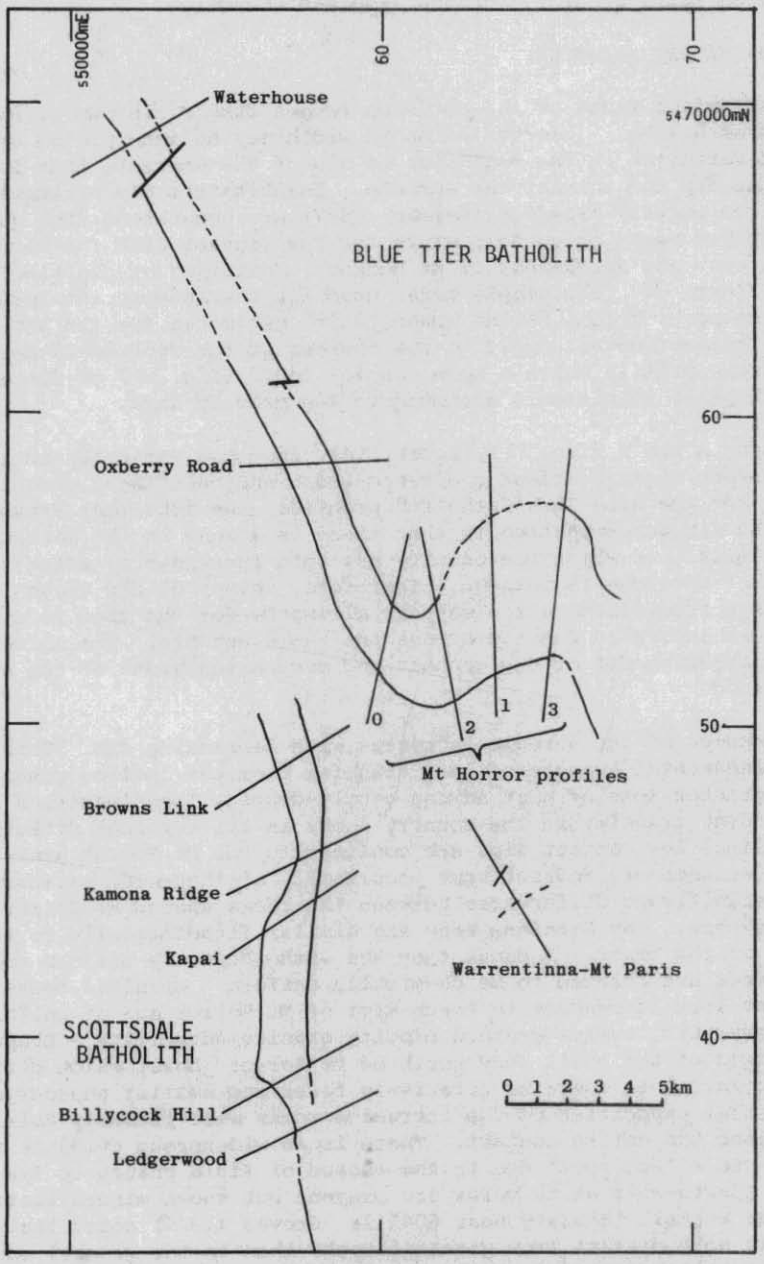

Figure 32. *Locations of gravity profiles across metamorphic aureoles in the Ringarooma-Lyndhurst tract of Mathinna Beds.*

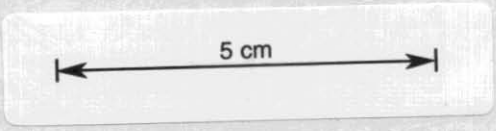

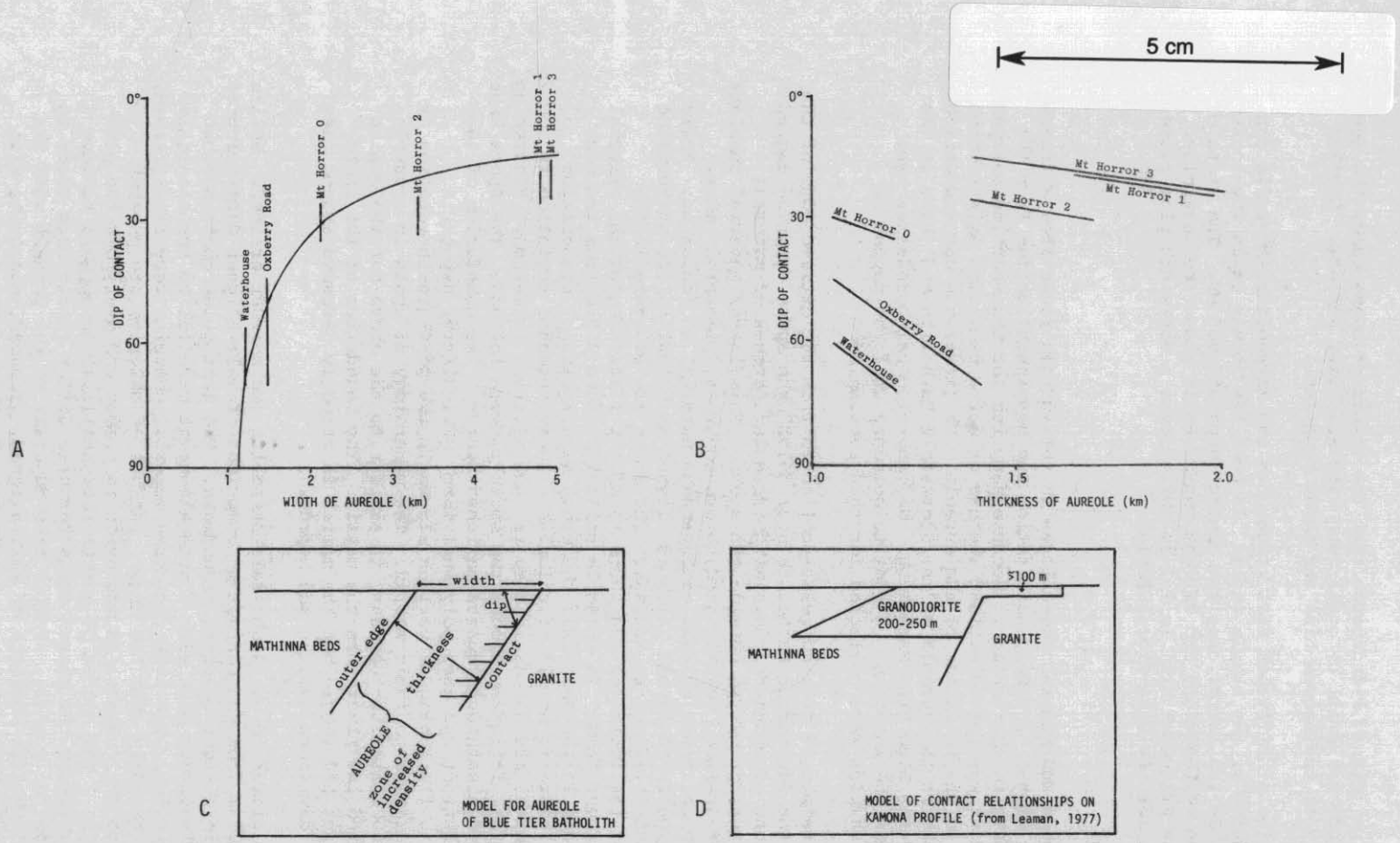

Figure 33. *A: Ranges of possible dip plotted against the width of the aureole for the six profiles east to north-west of Mt Horror. A hypothetical curve for an aureole of constant thickness of 1.1 km is also shown. B: Ranges of possible dip plotted against calculated ranges of possible thickness of the aureole along each profile. C: Model for aureole of Blue Tier Batholith. D: Model of contact relationships on the Kamona profile.*

relationships (fig. 33) indicates that the volume of magma below the level of the contact was small by comparison with Blue Tier contact. Similar models apply to the Browns Link and Kapai profiles.

Profiles at Billycock Hill, Legerwood and Warrentinna-Mt Paris can be accommodated by the simple model. In both the former cases the contacts are steep. In the latter case the contact dips 45°-65° NW. The width of the aureoles at Legerwood and Warrentinna-Mt Paris cannot be determined. The width at Billycock Hill is 1.3 km which gives a dip/width plot close to the data for the Blue Tier aureole.

Petrography

Textures and mineral assemblages in the aureole rocks show a transition in the amount of neocrystallisation and neomineralisation from the outer boundary to the contact. Because sampling for thin-section analysis was limited it was not determined whether or not a variation exists which is related to the thickness of the aureole. No difference was recognised between rocks in the aureole of the Scottsdale Batholith and those in the aureoles of the Blue Tier Batholith. No mineralogical boundaries were mapped within the aureoles. A biotite boundary could be mapped if sufficient samples were collected for thin sectioning.

In a sample of spotted pelite collected from the extreme edge of the aureole of the Scottsdale Batholith near 561527 the spots comprise ragged concentrations of chlorite containing irregular patches of material similar to that occurring outside the spots. This latter material consists of very fine-grained, well-aligned, brown-to-green, pleochroic mica, colourless mica, minor quartz, carbonaceous material and chlorite. There is a foliation in the spots which is aligned with that of the surrounding material, but it is not as intense. The spots are elongate in the direction of the foliation and there is slight flattening of the external foliation around them. In a sample collected about 250 m from the edge of the aureole in the same area the spots have a similar composition except that there is no rim of chlorite. Their internal foliation is continuous with, but not as intense as, the external foliation. Flattening of the external foliation around the spots is more intense. The spots have mica-enriched sheaths and quartz-enriched beards. The boundaries of the spots are distinct and have polygonal form. This latter aspect is attributed to flattening at various stages in the post-growth rotation of the spots relative to their matrix. The mineralogy of spots in a sample collected 500 m from the boundary is similar to the above but the grains are unoriented and finer than the matrix. The boundaries of the spots are indistinct and ragged but the matrix is strongly deformed around them with better developed sheaths and beards.

Rocks closer to the Scottsdale Batholith are coarser grained. Pelite collected 400 m from the contact is comprised of well aligned dark-coloured lenticules in a light-coloured groundmass. The lenticules contain brown to green, pleochroic mica with a good alignment parallel to the elongation of the lenticules. The light coloured material contains very fine-grained, colourless, randomly oriented mica. Patches of chlorite are present. Relatively coarse, colourless muscovite is common and overgrows the pleochroic variety. The amount of quartz recrystallisation appears to have been slight because the quartz grain textures differ little from those in rocks outside the aureole. Pelite from adjacent to the contact with the Scottsdale Batholith consists of well-aligned, greenish, muscovite-rich lenticules in a light coloured groundmass. In thin section the pelite consists of dark patches of chlorite, muscovite and quartz and light

patches of very fine-grained, unoriented, colourless mica and relatively large poikiloblastic plates of muscovite containing small grains of chlorite and quartz. Quartz is a relatively minor constituent. There is a crude overall alignment of mineral grains. Psammite from the same locality consists of granoblastic quartz, muscovite and reddish brown biotite with minor chlorite and accessory tourmaline and opaque minerals. Quartz grains are sutured, fractured and have undulose extinction. There is a good foliation defined by mica alignment. No criterion was established which indicates the relative contributions of mimetic growth and flattening in controlling the foliation in the coarser grained, thermal metamorphic rocks.

Psammite collected from the western part of the foreshore exposure north of Sheoak Hill (fig. 69) is comprised of granoblastic quartz, muscovite and chlorite. Small unaltered biotite grains occur as inclusions in the quartz. Accessory green-brown tourmaline and opaque minerals are present. The pelite is comprised of mainly micaceous material including both relatively coarse-grained, ragged, muscovite grains and fine-grained, colourless or green tinted mica. Minor biotite, chlorite, tourmaline, and opaques may be present. Andalusite is present in pelite in the small zone between Dbapc and the quartz-feldspar porphyry (Dmp). Cordierite is present in mottled pelite in the larger zone of Mathinna Beds between Dmp and the hornblende-biotite granodiorite (Dbg). It occurs as relatively large, poikiloblastic grains in a fine-grained groundmass of biotite and quartz which also comprise the inclusions. The presence of cordiorite- and andalusite-bearing assemblages indicates that the Mathinna Beds in this area reached the amphibolite-hornfels facies of thermal metamorphism.

Cordierite shows alteration to very fine-grained, colourless or green tinted mica. This alteration and the common alteration of biotite to green chlorite are the clearest examples of retrogressive metamorphism observed in the aureoles. The commonly occurring, very fine-grained, randomly oriented, colourless mica is regarded as a retrogressive product. In pelite near Kamona (*SFC*) it is associated with fine-grained quartz in aggregates which have clearly replaced porphyroblasts.

STRUCTURE

MATHINNA BEDS

N.J. Turner

Summary

Structural data were collected in the Ringarooma - Lyndhurst and Gladstone - Boobyalla tracts of Mathinna Beds.

Fold trends range from NNE to NNW in the Ringarooma - Lyndhurst tract and are NNW in the Gladstone - Boobyalla tract. Folds are open to tight, and plunges are shallow northerly or southerly. Some folds have a conical form. Vergence in both tracts is easterly.

Folds and cleavage developed prior to thermal metamorphism. Regional buckling of these early structures around easterly trending axial surfaces and steeply plunging hinges may also have occurred prior to granite emplacement. Flattening occurred after metamorphism and produced crenulation cleavage in areas where the early cleavage was sufficiently oblique to the direction of flattening. The principal trend of crenulation cleavage is north-west. A second, north-east trending crenulation cleavage is developed in at least one locality.

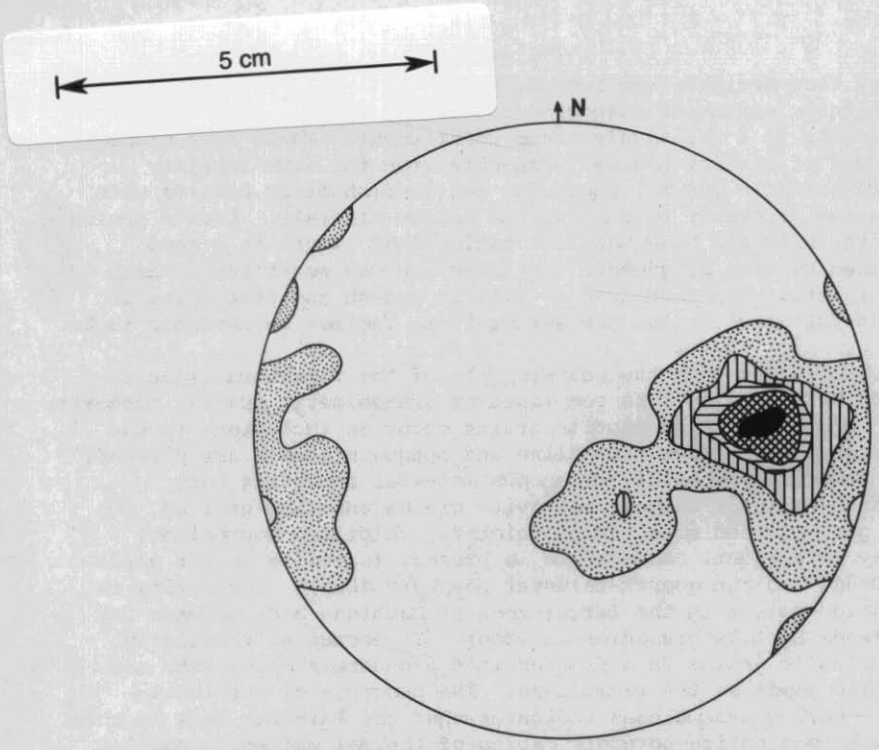

Figure 34. *Mathinna Beds structure. Ringarooma-Lyndhurst tract - structural area 1. Lambert projection of poles to bedding measurements. Source: 27 measurements - AVB; 35 measurements - MPM.*

In most of the Ringarooma - Lyndhurst tract the early cleavage is regionally discordant to fold axial surfaces. This suggests that pre-existing structures oblique to the main flattening direction controlled the direction of fold development during deformation. Cleavage is regionally concordant to axial surfaces in the Gladstone - Boobyalla tract but there is some evidence of local discordance.

RINGAROOMA - LYNDHURST TRACT

The Ringarooma - Lyndhurst tract has been subdivided into three areas on the basis of statistical trends in bedding and early cleavage attitudes. The two small isolated areas west of Ringarooma are probably parts of a fourth area, but insufficient data were collected in them to establish statistical trends.

Area 1

South of Branxholm and across Mt Paris to Rattler Hill, bedding has a strong north-south (0°) strike trend and dips moderately steeply west (fig. 34). No cleavage readings were obtained from the area. The great preponderance of westerly dips implies that vergence is to the east.

Area 2

Extending NNE for about 9 km from Billycock Hill to near 600470 is an area in which bedding has a NNE trend (fig. 35). The bedding diagram is not sufficiently complete to define the regional fold axis, since many beds which dip west also face west and conversely the diagram indicates that the

ADDENDA

BULLETIN 61

Geology of the Ringarooma Boobyalla area.

p. 120, fig. 34:

Contours 0,5,10,15,25%
Number of measurements: 62

p. 121, fig. 35:

Contours 0,5,10,15,20%
Number of measurements: 46

p. 121, fig. 36:

Contours 0,5,15,25,35%
Number of measurements: 44

p. 123, fig. 40:

Contours 0,1,2,3,4%
Number of measurements: 403

p. 124, fig. 41:

Contours 0,1.25,2.5,5,10%
Number of measurements: 256

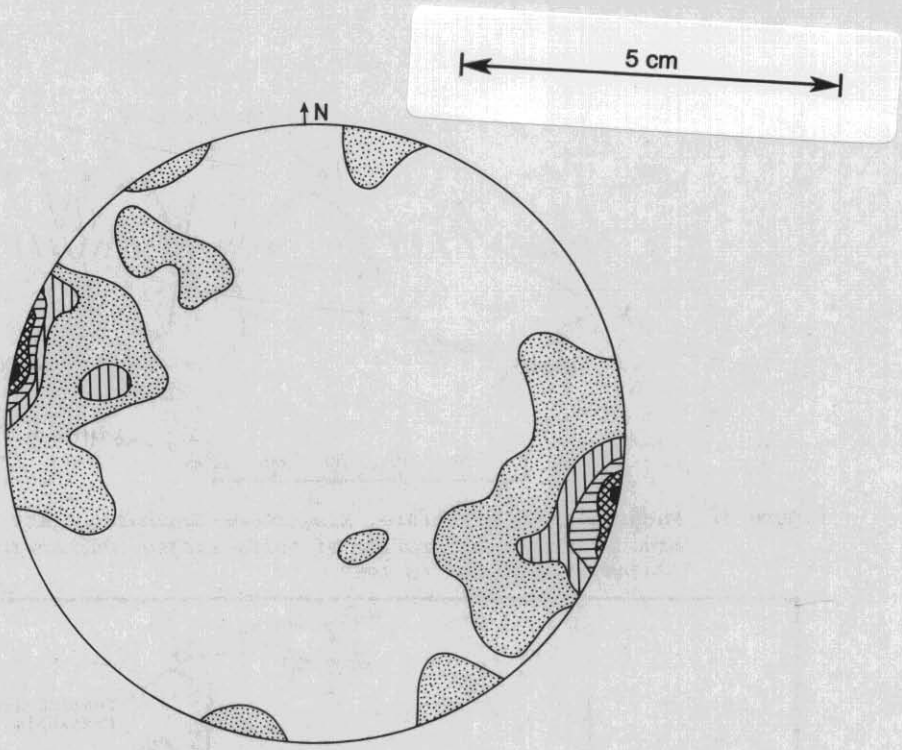

Figure 35. *Mathinna Beds structure. Ringarooma-Lyndhurst tract - structural area 2. Lambert projection of poles to bedding measurements. (NJT).*

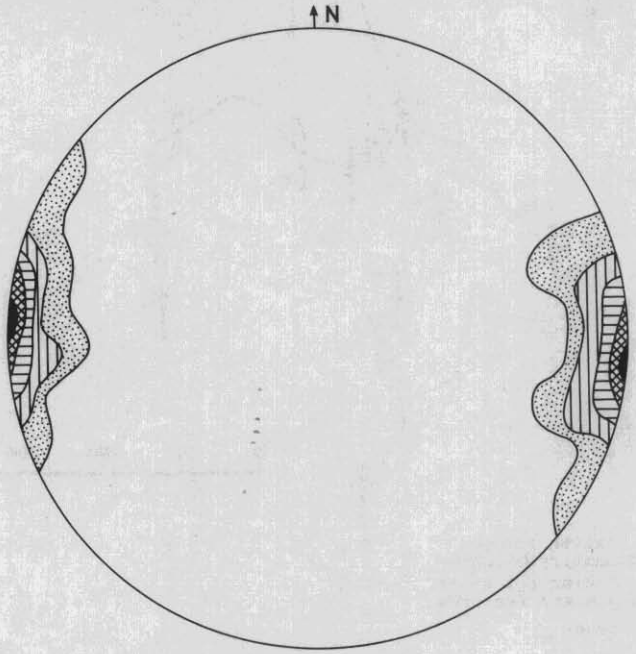

Figure 36. *Mathinna Beds structure. Ringarooma-Lyndhurst tract - structural area 2. Lambert projection of poles to early cleavage measurements.*

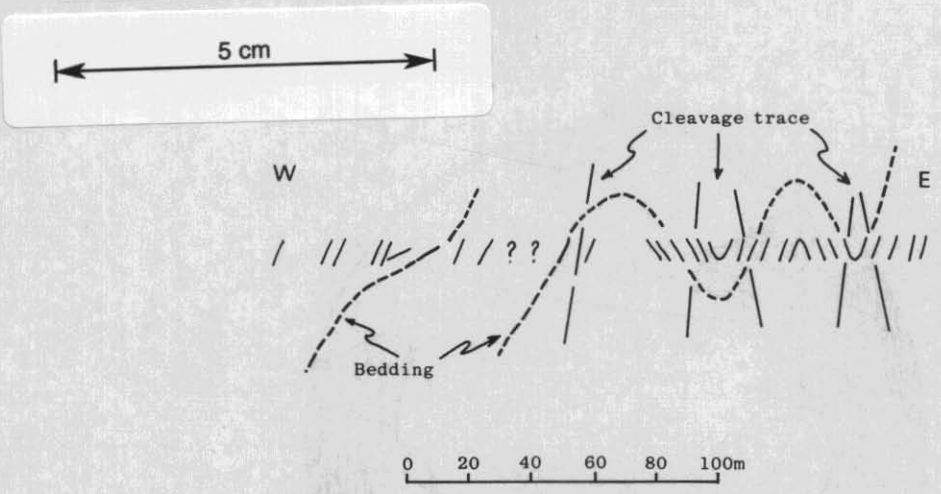

Figure 37. *Mathinna Beds structure. Ringarooma-Lyndhurst tract - structural area 2. Sketch of profile of folds exposed on Fenwick Road near 574544. Plunge 20° to 195°.*

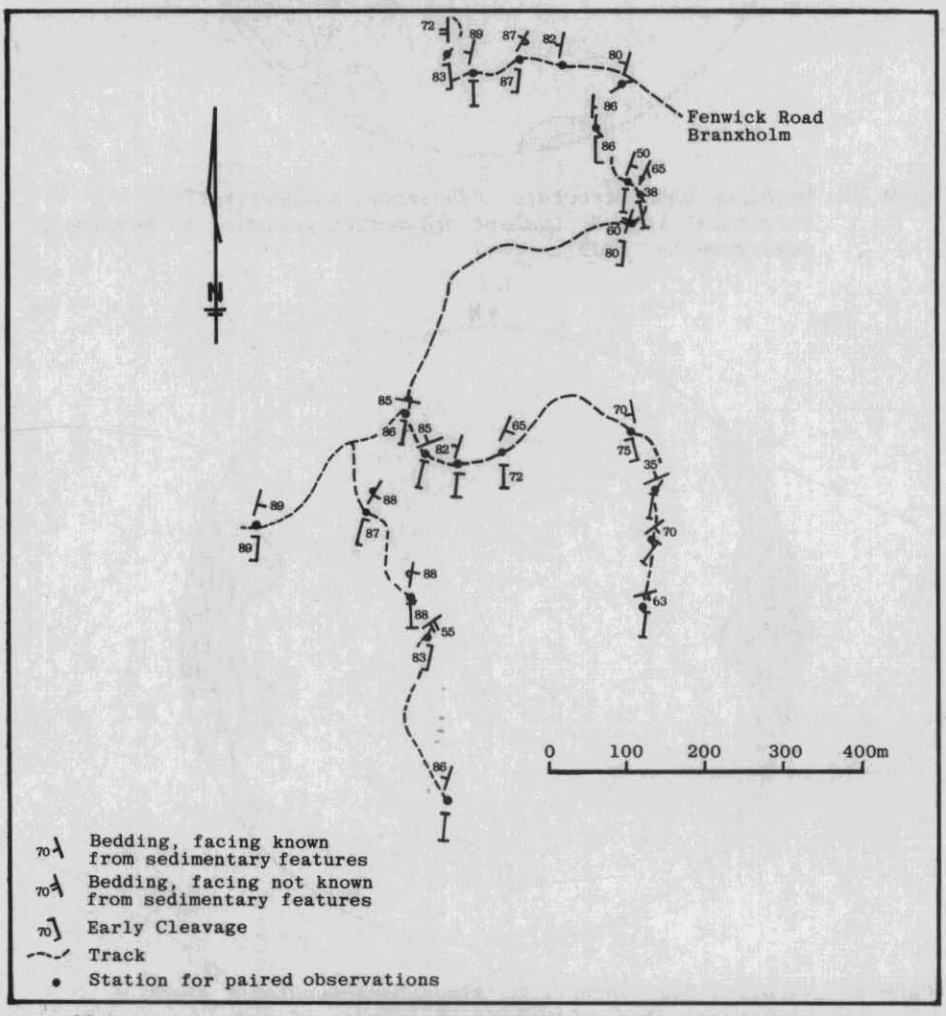

Figure 38. *Mathinna Beds structure. Ringarooma-Lyndhurst tract - structural area 2. Structural observations NE of Kapai Ridge around 580432.*

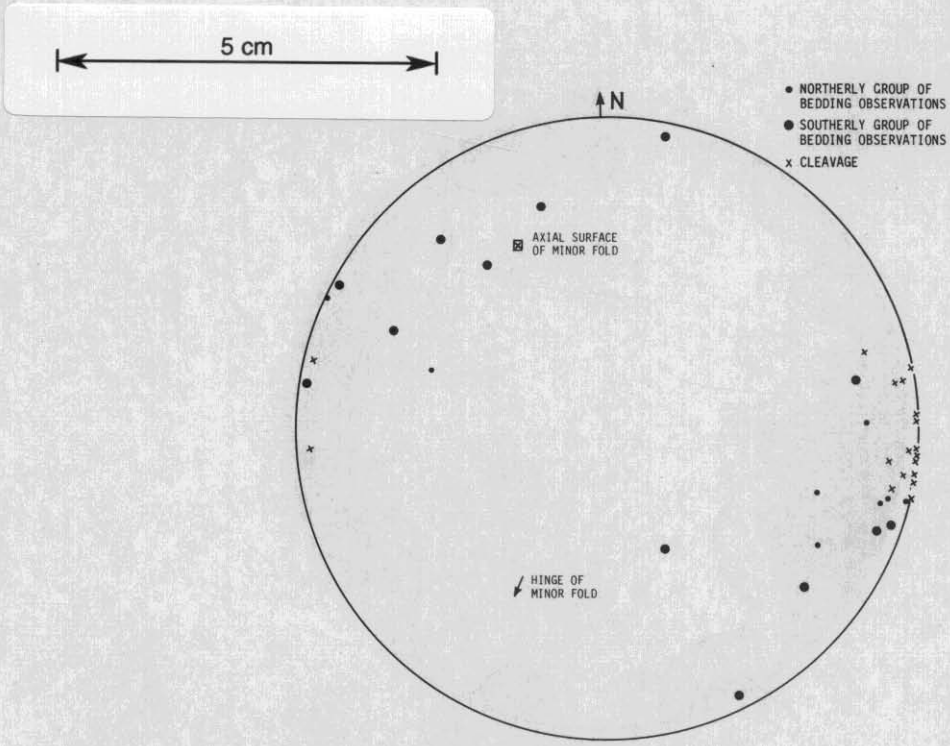

Figure 39. *Mathinna Beds structure. Ringarooma-Lyndhurst tract - structural area 2. Lambert projection of structural observations NE of Kapai Ridge around 580432.*

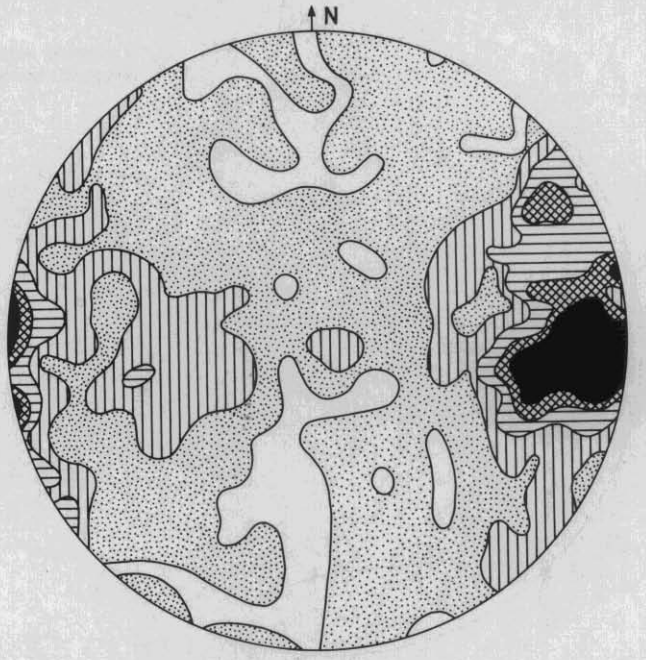

Figure 40. *Mathinna Beds structure. Ringarooma-Lyndhurst tract - structural area 3. Lambert projection of poles to bedding measurements. Source of measurements: 6 - PWB, 105 - AVB, 8 - MPM, 284 - NJT.*

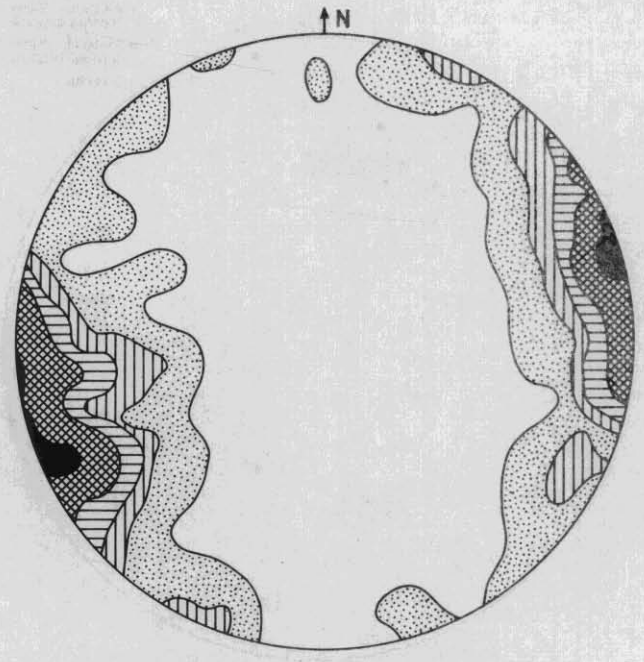

Figure 41. *Mathinna Beds structure. Ringarooma-Lyndhurst tract - structural area 3. Lambert projection of poles to early cleavage measurements. Source of measurements: 8 - PWB, 23 - AVB, 225 - NJT.*

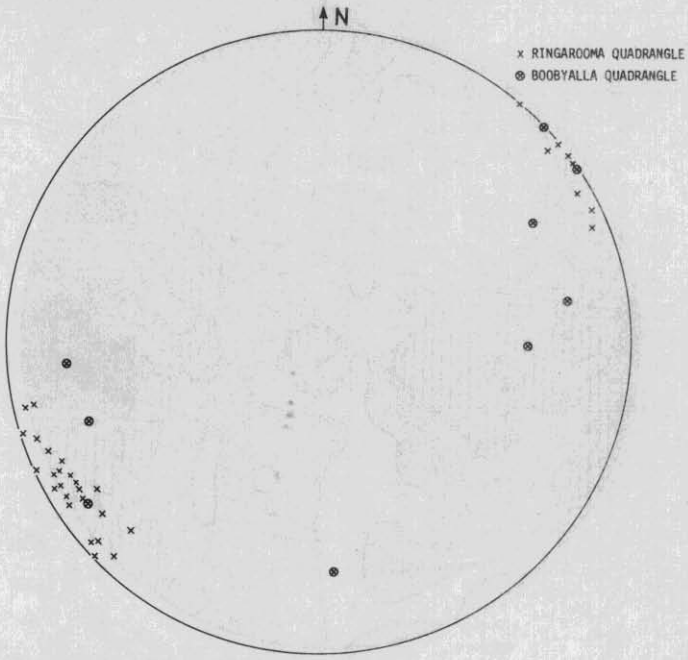

Figure 42. *Mathinna Beds structure. Ringarooma-Lynhurst tract - structural area 3. Lambert projection of poles to crenulation cleavage measurements (42). (NJT).*

5 cm

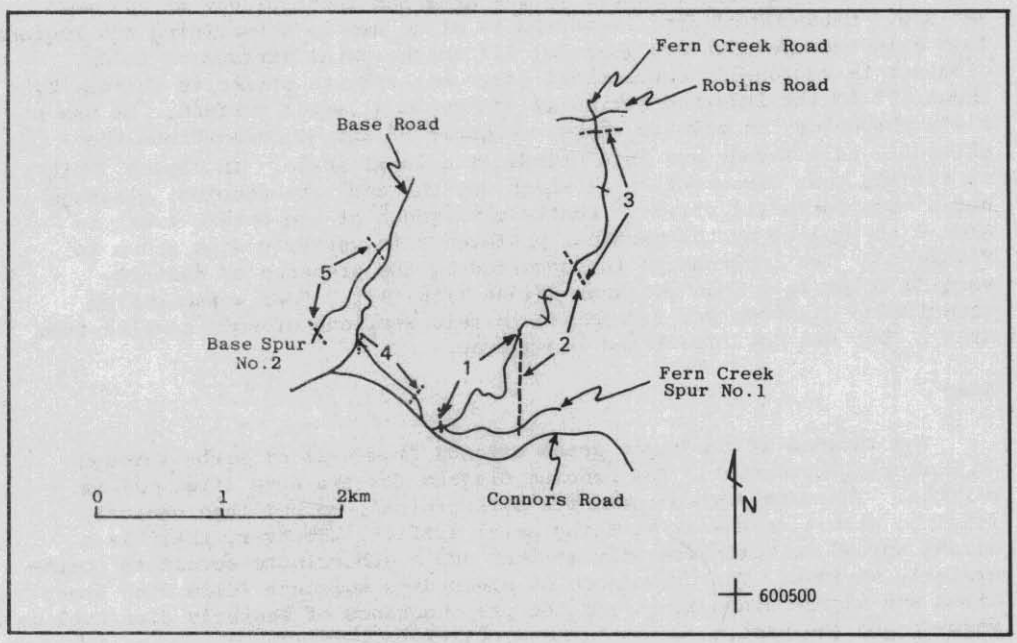

Figure 43. *Mathinna Beds structure. Ringarooma-Lyndhurst tract - structural area 3. Locality map showing location of structural sub-areas east of Forester.*

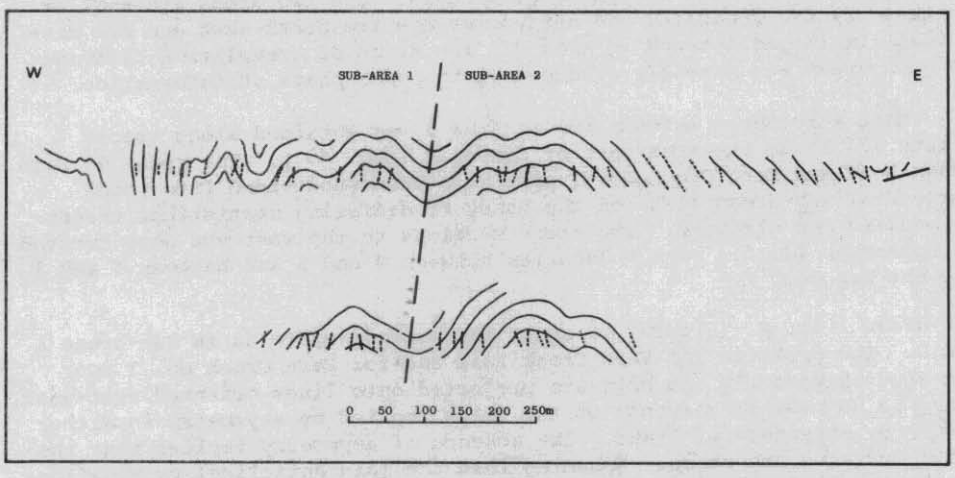

Figure 44. *Mathinna Beds structure. Ringarooma-Lyndhurst tract - structural area 3. Profile of folds in sub-areas 1 and 2, east of Forester showing cleavage traces. Profiles projected onto E-W lines. Upper profile: Fern Creek Road, Lower profile: Fern Creek Spur No. 1.*

folding is cylindroidal rather than conical. The regional axial surface strikes NNE and the folds have steep limbs and narrow hinge zones. Two minor fold hinges were measured in the area and these plunge at 20° and 38° SSW. Cleavage/bedding lineation is of no use in determining the regional fold axis because cleavage does not lie in the axial surface of folds. Cleavage is regionally subvertical (fig. 36) and its strike is oblique by about 10° to the inferred strike of the regional axial surface. It has a slaty morphology in pelitic rocks. Figures 38 and 39 demonstrate the obliquity of cleavage and fold trends at a local scale. In Figure 38 it is evident that irrespective of which way the beds are dipping, cleavage has a more northerly strike. Easterly vergence of the entire tract in Area 2 is implied by the marginal preference to westerly dips shown in Figure 35. The implication is supported by the presence of easterly verging folds in a road cut near 574544 (fig. 37). Post metamorphism crenulation cleavage was recognised in thin sections of some samples from Area 2, but was not identified in outcrop.

Area 3

The largest of the three areas extends from east of Derby through Mt Horror to Lyndhurst. The bedding diagram for the area (fig. 40) is diffuse. The main maximum suggests cylindroidal, rather than conical folding, with a northerly striking axial surface. However, there is a strong spread to north-westerly strikes and a subordinate spread to north-easterly strikes. The prevalence of steep dips suggests folds with steep limbs and narrow hinge zones and the preponderance of westerly dips implies vergence to the east.

The early cleavage is subvertical (fig. 41). It has a wide spread with a main NNW trend which is oblique by about 20° to the inferred trend of the regional axial surface.

Crenulation cleavage measurements are plotted in Figure 42. Measurements were obtained in an area near Forester in the Ringarooma Quadrangle, and in the Boobyalla Quadrangle. The two areas are similar in that trends of bedding and early cleavage are north-east and are discordant to the main trend in Area 3. The trend of crenulation cleavage in both areas was probably produced by the same phase of deformation.

Most structural information in Area 3 was obtained along tracks around 584515 in the area east of Forester (fig. 43). The rocks on Fern Creek Road and Fern Creek No. 1 spur have been subdivided into three structural sub-areas (1-3) on the bases of differing statistical trends in bedding and cleavage. Two track sections to the west are also treated as sub-areas (4, 5). The boundaries between 4 and 5 and between 4 and 1 are not exposed.

Sub-areas 1 and 2. Figure 44 shows the profile of folds in Sub-areas 1 and 2. The profiles for Fern Creek Road and for Fern Creek No. 1 spur are shown separately and both are projected onto lines oriented east-west. There is no overall vergence of the folds implied by asymmetry in either length or steepness of limbs. The absence of asymmetry implies that the axial surfaces are steep. Assuming that the main anticlinal culminations in the two profiles are in the same folds, and that the axial surfaces are subvertical, then the strike of the axial surface is about 0°.

Figures 45 and 46 are projections of cleavage and bedding readings for the two sub-areas. The pattern of bedding attitudes cannot be readily compared with idealised geometrical forms in either case. They are clearly

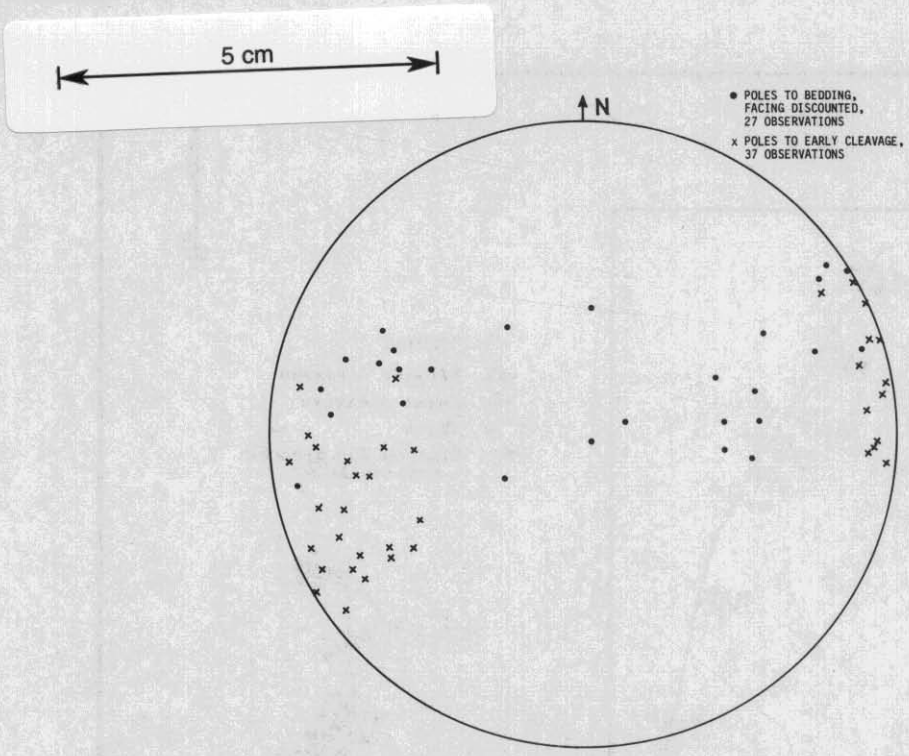

Figure 45. *Mathinna Beds structure. Ringarooma Lyndhurst tract - structural area 3. Lambert projection of structural measurements in sub-area 1, east of Forester.*

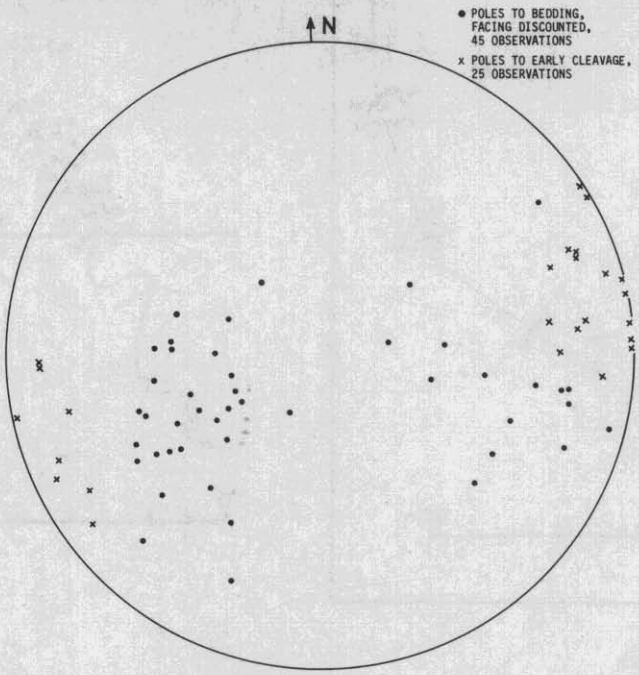

Figure 46. *Mathinna Beds structure. Ringarooma-Lyndhurst tract - structural area 3. Lambert projection of structural measurements in sub-area 2, east of Forester.*

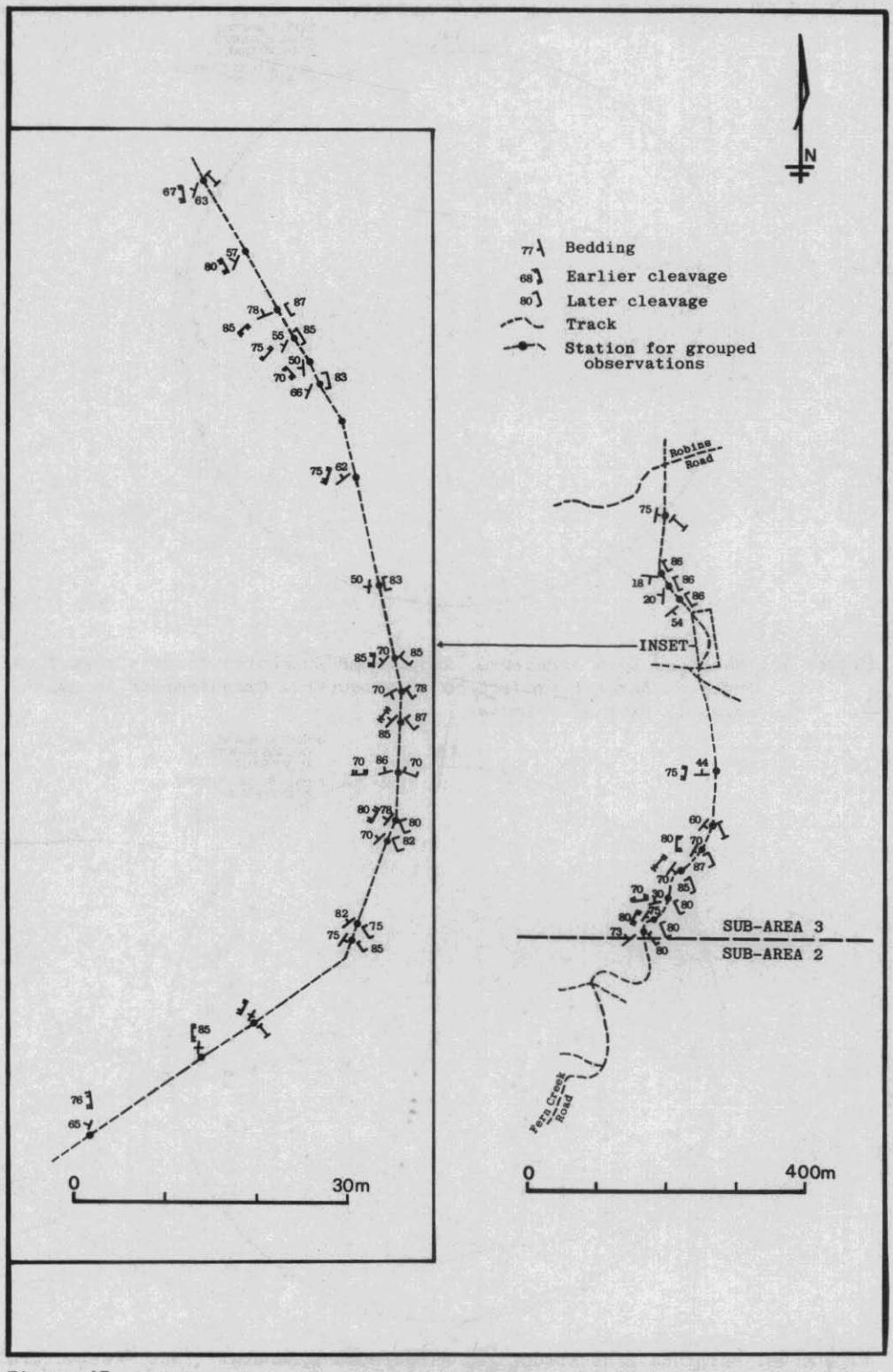

Figure 47. *Mathinna Beds structure. Ringarooma-Lyndhurst tract - structural area 3. Structural observations in sub-area 3, east of Forester.*

5 cm

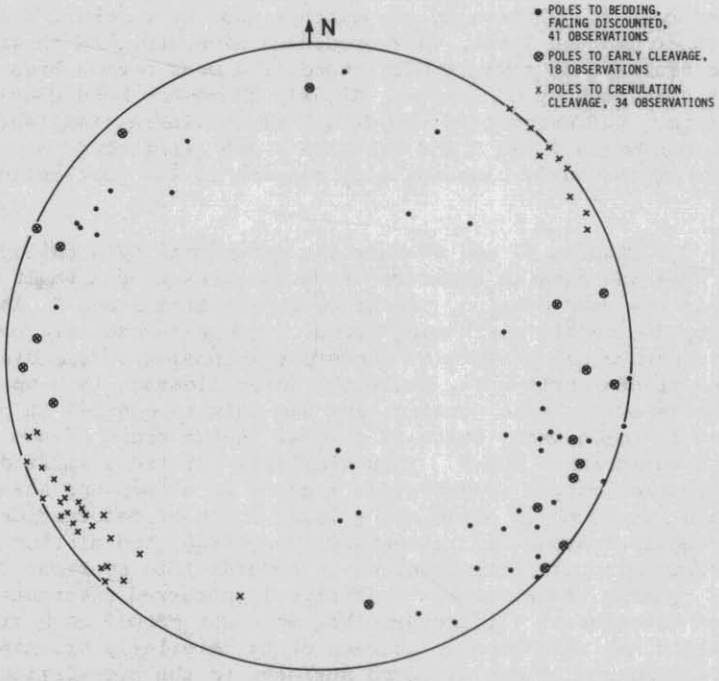

Figure 48. *Mathinna Beds structure. Ringarooma-Lyndhurst tract - structural area 3. Lambert projection of structural measurements in sub-area 3, east of Forester.*

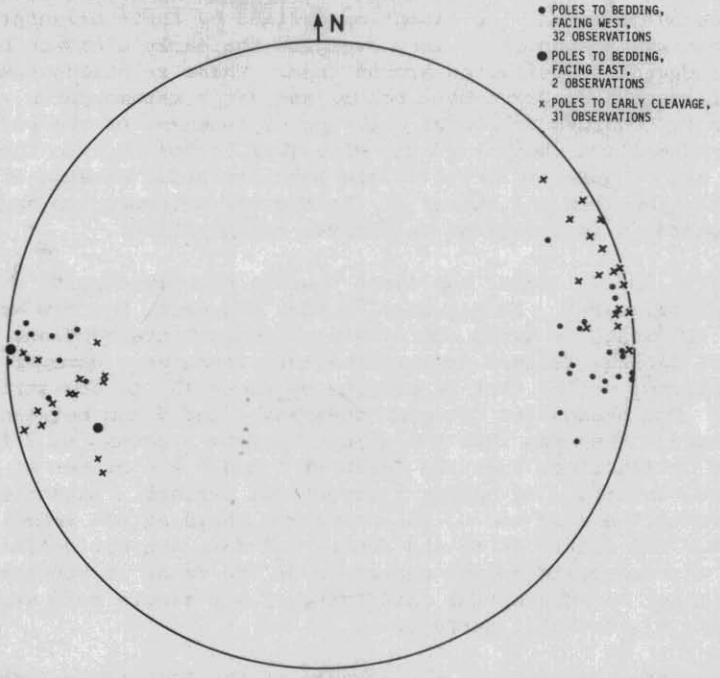

Figure 49. *Mathinna Beds structure. Ringarooma-Lyndhurst tract - structural area 3. Lambert projection of structural measurements in sub-areas 4 and 5, east of Forester.*

5 cm

is continuous with the external foliation. The internal and external foliations are rotated relative to one another and the external foliation is flattened around the spots, thus producing mica enriched sheaths and quartz enriched beards. In some samples there is a weak second mica entrainment which is deflected by the spots. Clearly there has been post-metamorphism deformation. Differences in the detail of strain-related fabric features of rocks in Sub-areas 4 and 5 and Sub-area 3 are attributed to different attitudes of the early cleavage with respect to the post-metamorphic stress.

Sub-area 3. Figures 47 and 48 show the structural data collected in Sub-area 3. The sub-area is separated from Sub-area 2 by a fault which is exposed in the road cutting. Relative to Sub-area 1 and 2, the bedding is rotated to dominantly north-east trends. Two cleavages are present; the earlier cleavage has a slaty or sandstone morphology, depending on lithology, and trends north-east, while the later cleavage is a spaced crenulation with generally weak parting, and was only recognised in pelitic rocks. Its trend is north-west, which is similar to the trend of the cleavage mapped in Sub-areas 1 and 2. This similarity of trend implies that the single cleavage mapped in Sub-areas 1 and 2 is a compound strain containing components from both an early and a later phase of deformation. Although only a single cleavage was recognised in outcrop, two distinct alignments of micaceous minerals were observed in several thin sections from Sub-areas 1 and 2. Quartz grains show a statistical preferred orientation parallel to one of the traces. It appears that what was mapped as a single cleavage in the field may have been an average of two similarly oriented surfaces. The correspondence of one of these surfaces to the crenulation cleavage in Sub-area 3 is possible, but not proven.

The outer boundary of the thermal aureole of the Blue Tier Batholith occurs within Sub-area 3. Elongate metamorphic spots lie within the plane of the early cleavage. No lineation defined by their orientation within that plane was recognised. They overgrow the early cleavage but the crenulation cleavage is deflected around them. These relationships demonstrate that deformation occurred both before and after metamorphism. The metamorphism is regarded as coeval with the emplacement of the porphyritic granite/adamellite (Dbapc) of the Blue Tier Batholith into the position that it now occupies relative to the Mathinna Beds, because of the good correlation between the extent of the thermal metamorphism and the form of the contacts (see section on thermal metamorphism).

Sub-areas 4 and 5. These sub-areas contain steeply dipping strata which face west (fig. 49). In Sub-area 4, they dip east, but dip west in Sub-area 5. Cleavage is steep and cleavage/bedding intersections are consistent with facings derived from sedimentary features. However cleavage has an average strike that is oblique by about 15° to the strike of bedding. The boundaries between Sub-areas 4 and 5 and between 4 and 1 are not exposed. Assuming that the structure from 5 across to 2 is not strongly affected by faulting, then the folds of 1 and 2 are either at the crest of a regional anticline or occupy a structural terrace. Extension of the structure to the east and to the north and south is not immediately apparent. The distribution and density of data are not definitive. In view of the non-cylindroidal character of the folds in Sub-areas 1 and 2, there may not be substantial continuity of any single fold structure along the strike of its axial surface.

The outer boundary of the aureole of the Scottsdale Batholith occurs within Sub-areas 4 and 5. Although only one cleavage was observed in the field, the relationship between it and the metamorphic spots at thin section scale show it to be a compound strain. The spots overgrow a foliation which

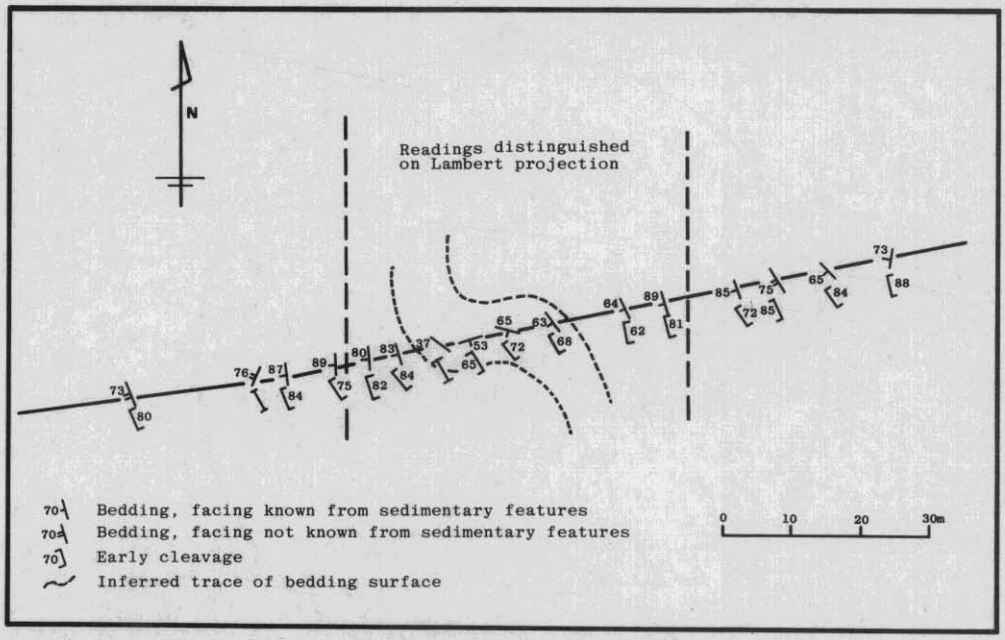

Figure 50. *Mathinna Beds structure. Ringarooma-Lyndhurst tract - structural area 3. Structural observations on Oxberry Road, near Eagle Hill [547580].*

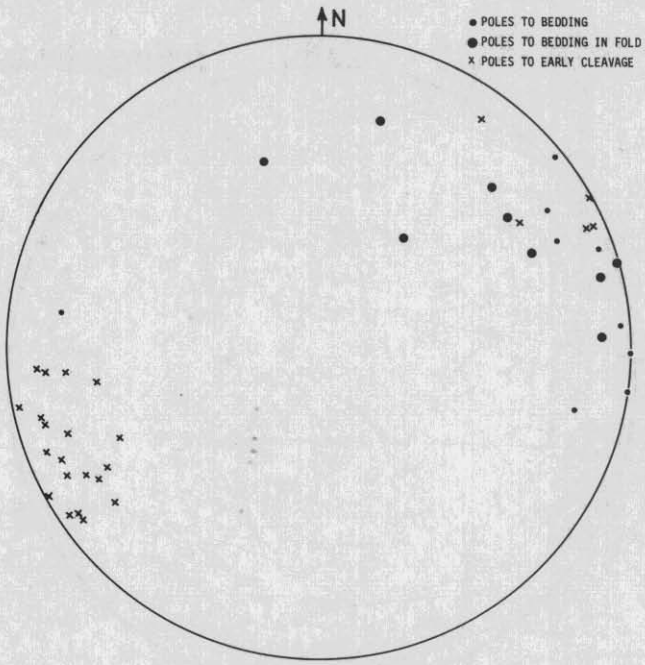

Figure 51. *Mathinna Beds structure. Ringarooma-Lyndhurst tract - structural area 3. Lambert projection of structural measurements on Oxberry Road near Eagle Hill [547580].*

5 cm

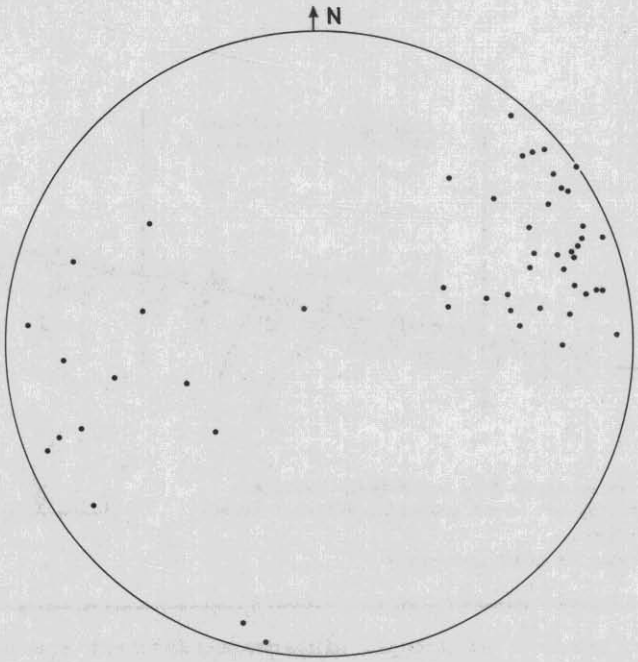

Figure 52. *Mathinna Beds structure. Gladstone-Boobyalla tract. Lambert projection of poles to bedding. Source of measurements: 17 - SFC, 7 - NJT.*

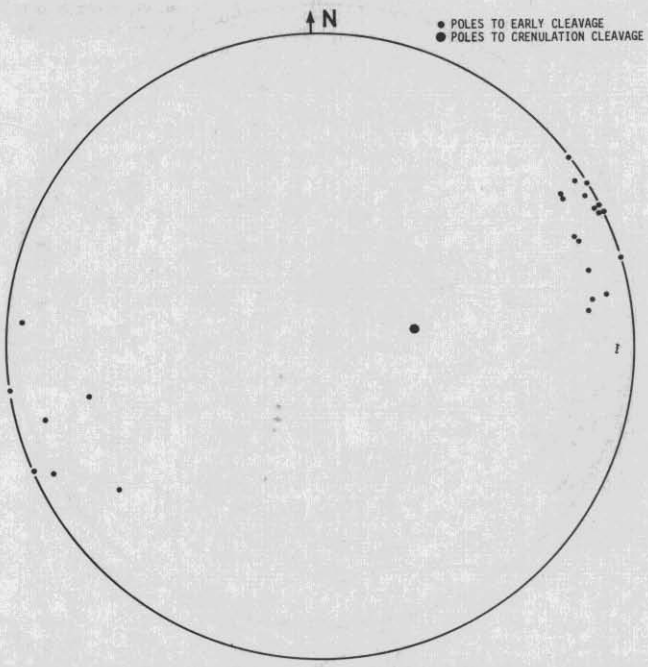

Figure 53. *Mathinna Beds structure. Gladstone-Boobyalla tract. Lambert projection of poles to cleavage. Source of measurements: 17 - SFC, 8 - NJT.*

5 cm

not cylindroidal distributions and are best fitted by cones. In the case of Sub-area 1 the cone has its apex directed south, a half angle of about 10-20° and its axis is sub-horizontal. In the case of Sub-area 2 the cone has its apex directed north, a half angle of about 10° and its axis plunges about 10°S. The strike of the axial surfaces in both cases is about 0°, which is in agreement with the value inferred from the fold profiles. In each sub-area the cleavage is steep and the average strike is oblique by about 20° to the inferred strike of the axial surfaces of the folds.

Oxberry Road

A small fold was delineated on Oxberry Road near Eagle Hill [559583] (figs. 50 and 51). It plunges south-west and verges east. Only one cleavage was recognised in the field and it has a slaty or sandstone morphology. It is oblique to the axial surface of the fold and is not rotated by the fold.

Regional variation in trends

Variations of statistical trends of bedding and early cleavage between Areas 1, 2 and 3 and within Area 3 may be due to regional buckling. The change from NE to N-NNW trends across the boundary from Area 2 to Area 3, and the change from N-NNW to NE trends across the boundary between the two quadrangles suggests that the trend of the axial surface of buckling is E-ESE. A similar axial surface trend is indicated by the change from north to north-east trends across the boundary between Sub-areas 2 and 3 near Forester. Because the early cleavage has steep dips in all areas, the axis of buckling must be steep. Changes of trend are fairly sharp, which indicates that the hinge zones are narrow. Since the fairly linear granite contact between Trig Hill and Lyndhurst does not reflect the change in trend of the structures in the Mathinna Beds, it is inferred that buckling occurred before emplacement of the porphyritic, coarse-grained granite-adamellite (Dbapc).

GLADSTONE - BOOBYALLA TRACT

The Mathinna Beds in the Gladstone - Boobyalla tract have been openly to closely folded about upright, NNW trending axial surfaces. Fold axes plunge gently NNW to SSE. Bedding measurements (fig. 52) show a preponderance of moderate to steep south-west dips. The beds are upright. Dip of cleavage (fig. 53) is predominantly steep south-west to vertical. These common attitudes of cleavage and bedding imply that vergence is easterly.

There is a continuous section over about 1.3 km at the eastern end of the foreshore exposure north of Sheoak Hill in which vergence is easterly. In the small zone of Mathinna Beds near the western end of the foreshore exposure the beds dip and face east.

Regional discordance of cleavage and fold axial surfaces is not implied by Figures 52 and 53. However, bedding-cleavage lineations show a wide scatter, which suggests that the cleavage is not always parallel to the axial surfaces or that locally, there are steeply plunging minor fold hinges (*SFC*).

Crenulation cleavage was recognised in only one outcrop [717722] while a crenulation lineation was found on the early cleavage in one other outcrop (*SFC*). Thermal metamorphism occurred after formation of the early cleavage and before formation of the crenulation cleavage.

GRANITIC ROCKS

SCOTTSDALE BATHOLITH

N.J. Turner

Observations of the fabric of the granitic rocks were made along the eastern margin of the Scottsdale Batholith, while measurements of joint directions were made in some other areas. An area near Tayene (Launceston Quadrangle), at the western edge of the batholith, was investigated in order to establish the regional relationship of the dominant foliation in the granitic rocks with respect to Mathinna Beds contacts.

GRANODIORITE

Macroscopic fabric

One dominant grain lineation (see page 152) was recognised on outcrop surfaces of the biotite-hornblende granodiorite (Dsg). Visual inspection indicates that the dominant lineations on variably oriented surfaces are related to a single dominant foliation. The intensity of this foliation varies considerably; it is well developed in most exposures within a few kilometres of the batholith margin, but near 450610 (about 5km from the margin) it is difficult to discern.

In granodiorite near 555405 are rounded, oblate to triaxial ellipsoidal, melanocratic, quartz-diorite xenoliths (*SFC*). Their shortest axes lie approximately perpendicular to the foliation. The longest axes of triaxial ellipsoidal types show a random distribution in the plane of the foliation. In places where the foliation is not readily visible, rounded ellipsoidal xenoliths have no preferred orientation. The shape of xenoliths does not appear to be related to the intensity of the foliation in the host rock.

An internal foliation concordant with the external foliation is present in rounded, irregularly shaped, porphyroblastic xenoliths near 550430. It is defined by alignment of both groundmass minerals and porphyroblasts. In some examples it is clear that there is no deflection of the external foliation at the xenolith margins.

Microscopic features

Few thin sections of the biotite-hornblende granodiorite (Dsg) were examined. Deformation of grains appears to be less than in strongly foliated granodiorite in the Blue Tier Batholith. A few gently bent biotite flakes were observed, plagioclase grains may be fractured or gently bent and alkali feldspar has undulose extinction. Quartz-quartz boundaries are either straight, gently curved or sutured (*SFC*). Many grains display undulose extinction and, less commonly, deformation bands. In some rocks there are two populations of quartz grains which are distinguished by either, or both, their grain size or strain characteristics. Finer, less undulose grains may be recrystallisation products.

ADAMELLITE

Macroscopic fabric

Outcrop surfaces in the adamellite (Dsaw) trending NNW from 550534 show dominant grain lineations which, by visual inspection, are related to a single dominant foliation. The foliation is generally well developed. No foliations were recorded from other adamellite bodies.

Microscopic features

Few thin sections of the foliated adamellite were examined. Gently bent biotite flakes and fractured plagioclase grains are present. Quartz has undulose extinction and, less commonly, deformation lamellae. Evidence of quartz recrystallisation is inconclusive and similar to that cited for the granodiorite. Fine-grained biotite replaces some coarse grains in one sample. A few gently bent biotite flakes were found in Dsaw around 525376 (*SFC*).

MINOR GRANITIC INTRUSIONS

A thin, steeply inclined dyke of medium- to coarse-grained adamellite occurs at 533353 (*SFC*). It is allotriomorphic granular and contains highly altered plagioclase and potash feldspar, together with about 10% quartz, 5% granular to prismatic clinozoisite and 2% chloritised biotite. Bent and microfaulted plagioclase twin lamellae, kinked biotite plates, highly sutured undulose, and sometimes polygonised quartz, and granulated feldspar indicate considerable deformation. Intense alteration of feldspar, desilication, and growth of clinozoisite may have accompanied deformation. The deformation itself appears to have resulted from movement along dyke walls after emplacement, as the host adamellite is largely undeformed.

REGIONAL RELATIONSHIPS

Foliation in the granodiorite and in the adamellite NNW of 550534 is regionally concordant. Figure 54 is a projection of measurements made in both rock types. Measurements taken south of grid line 5446000 mN have a

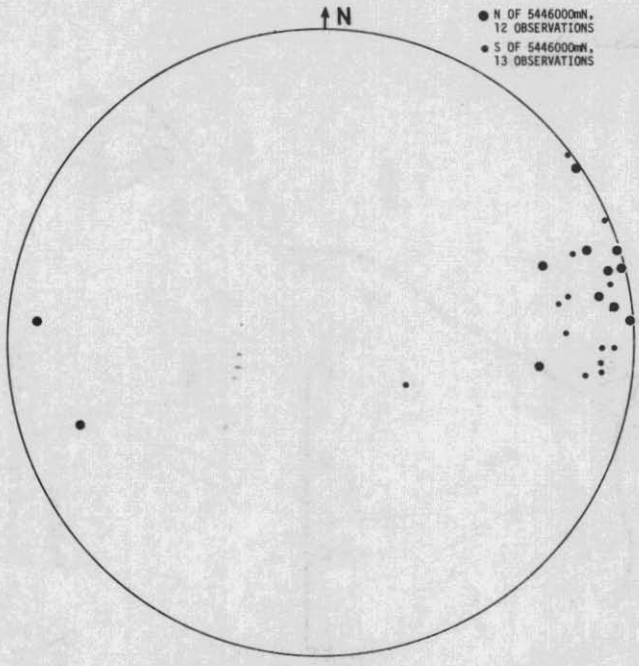

Figure 54. *Dsg and Dsaw structure, Scottsdale Batholith. Lambert projection of poles to foliations near eastern margin of batholith. (NJT)*

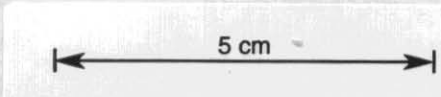

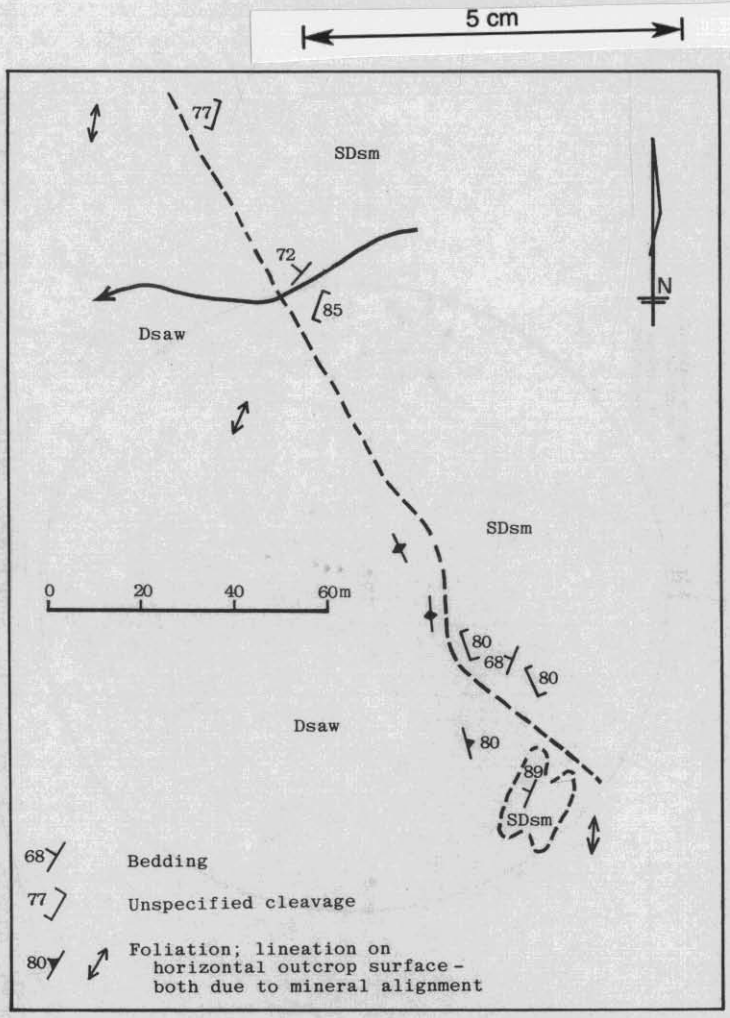

Figure 55. *Dsaw structure, Scottsdale Batholith. observations at contact with Mathinna Beds at Oxberry Creek [525588]. (NJT).*

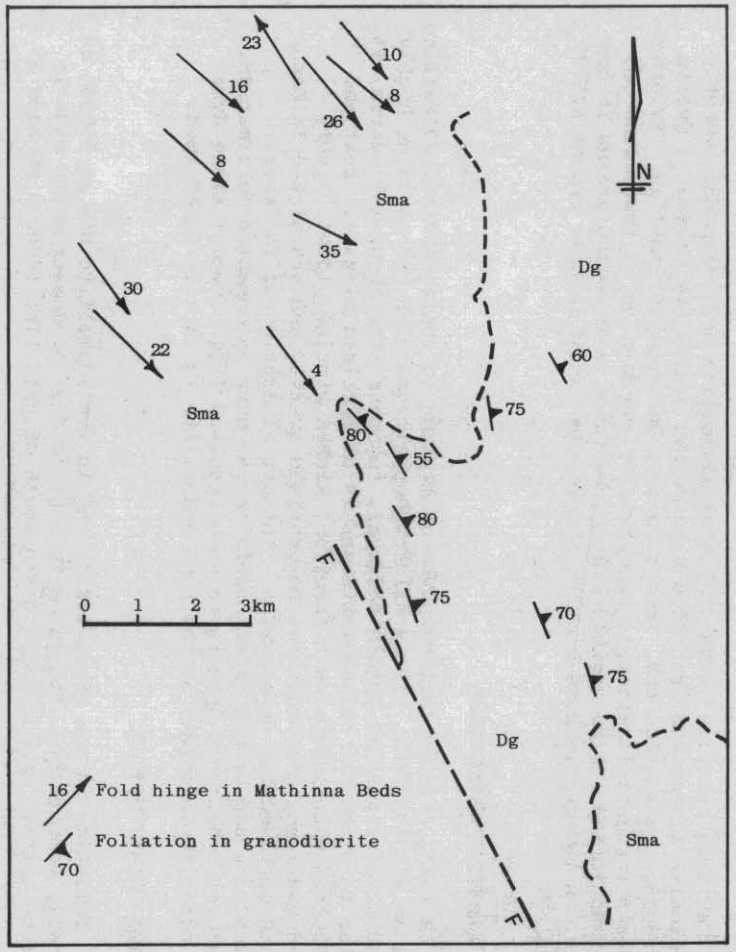

Figure 56. *Dsg structure, Scottsdale Batholith. Structural observations near western margin of batholith at Tayene, Launceston Quadrangle. Source: boundaries and Mathinna Beds structure - Longman et.al. (1964); foliations in granodiorite - NJT.*

different average trend from those to the north. The grid line passes through an area where the trend of the Mathinna Beds contact changes from N-NE to NNW. It also passes through the boundary of structural areas 2 and 3 within the Mathinna Beds. Thus, there is a coincidence in the change of regional trends of bedding and cleavage in the Mathinna Beds, of the contact and of granite foliation.

In the southern area the overall trend of the granite foliation appears to be oblique to the trend of the contact. In the northern area the trends of foliation and contact are subparallel. However, at Oxberry Creek [525588] the foliation appears to be oblique to the contact. Figure 55 is a sketch of structures at Oxberry Creek. The foliation and lineation in the adamellite and cleavage in the contact metamorphosed Mathinna Beds are difficult to discern, therefore the orientations shown in the sketch are tentative. It appears that the foliation in the adamellite is oblique to the contact and approximately concordant with a cleavage in the Mathinna Beds. The relationship of the latter to cleavages elsewhere in the Mathinna Beds is unknown.

A reconnaissance survey was made of foliation in granodiorite at the western edge of the Scottsdale Batholith near Tayene. The dominant foliation in the granodiorite is morphologically similar to the foliation in granodiorite and adamellite at the eastern edge of the batholith. It trends north-west and is oblique to the Mathinna Beds contact and to the regional trend of folds within the Mathinna Beds (fig. 56) - Launceston Quadrangle.

TECTONIC CHARACTER OF FOLIATION

The foliation that has been observed in the Scottsdale Batholith is due to flattening. The important field observations supporting this view are:

(1) Regional concordance in Dsg and Dsaw at the eastern margin.

(2) Apparent discordance of foliation and Mathinna Beds contacts south of 5446000 mN and near Oxberry Creek at the eastern margin, and clear regional discordance at Tayene on the western margin.

(3) Concordant internal foliations in xenoliths.

The nature of the fabric in the central parts of the batholith is poorly known. In one granodiorite locality towards the centre of the batholith [near 450610] the foliation is very weak compared with most areas near the margins. Such a variation in foliation intensity might indicate that the flattening which caused the foliation was due to lateral pressure exerted by forcibly emplaced magma in the central parts of the batholith. This mechanism has been suggested by Gee and Groves (1971) as the cause of foliations in granodiorite at Piccaninny Point (St Marys Quadrangle). The change in foliation trend across grid 5446000 mN might be interpreted as moulding of the foliation around a contact irregularity. However, foliation in the Tayene area shows no response to contact irregularities. Therefore, the foliation is considered to have been caused by tectonic stress.

The change in trend across grid 5446000 mN may also have been caused by the inferred phase of regional buckling about east-west axial surfaces which caused variation in regional structural trends within the Mathinna Beds. Since that phase does not appear to have affected the Mathinna Beds/porphyritic, coarse-grained biotite granite-adamellite (Dbapc) contact between Mt Horror and Waterhouse, it may be that the foliated rocks of the

Scottsdale Batholith are older than that granite. Their foliation morphology is comparable with that of the granodiorite and equigranular, fine- to medium-grained muscovite granite/adamellite (Dbaem) in the Blue Tier Batholith, which also appear to be older than Dbapc. Unfoliated adamellite in the Scottsdale Batholith and Dbapc may be of similar age.

BLUE TIER BATHOLITH

PORPHYRITIC BIOTITE-MINOR MUSCOVITE GRANITE/ADAMELLITE (Dbapc)

P.R. Williams

The internal fabric of granite/adamellite of the Poimena Pluton (Gee and Groves, 1971) has been mentioned by Groves *et al.* (1977) and described by Groves (1968). The internal fabric elements of rocks belonging to this pluton (Dbapc) have been measured over the Ringarooma and Boobyalla Quadrangles. The fabric is defined by an alignment of the *b*-axis of the potash feldspar phenocrysts, which is visible as a planar fabric perpendicular to that direction. In general there is no related fabric present in the rock matrix, although an alignment of groundmass grains was seen at a few localities [*e.g.* 608555] (*NJT*). The phenocrysts are seldom in contact.

Mineral grains in rocks with only a feldspar phenocryst alignment show relatively minor deformation (*NJT*). No kink-banding or microfaulting of biotite or plagioclase is present, although gently bent biotite flakes are present in rocks on Mt Cameron (*SFC*). Large quartz grains contain deformation lamellae and some have developed subgrains [679737]. In other areas large quartz grains are often rimmed by smaller, less undulose quartz. Patches of fine-grained quartz may represent total recrystallisation of larger grains. Potash feldspar crystals usually have strongly undulose extinction.

DETERMINATION OF FABRIC

The fabric of a granite outcrop is determined by the geometric relationship between apparent lineations on different outcrop surfaces. This relationship can be complex (Den Tex, 1954) and many apparent lineations may need to be measured for its determination. In weathered outcrop, however, the three-dimensional form of feldspar phenocrysts can usually be determined, and in such cases a visual impression of the foliation can be obtained. In these cases fewer apparent lineations are necessary to determine the orientation of planar fabrics. The significance of apparent lineation data can be tested by determining the alignment of numerous feldspar crystals on a face and calculating statistical parameters. These three methods are discussed below.

Fifteen faces of an outcrop at 832519 contained an apparent lineation which is plotted in Figure 57. Two planar fabric elements (foliations) can be interpreted from the lineations. The steeply dipping surface is not a good fit, so trace normals (Cruden, 1971) of those lineations which were used to define the great circle were plotted. These lie partly on a great circle, the pole to which could represent a lineation fabric element. However, the definition of points belonging to one trend or another is ambiguous and one trace normal does not fit near the trend. An interpretation of two foliations is preferred. The impression from field observation is of intersecting foliations.

Analysis of a single foliation

Analysis of the significance of apparent lineation data is presented in Figure 58. The pitch of twenty to thirty feldspar phenocrysts from each trace of an outcrop are plotted on a histogram, the peak of which defines the pitch of the lineation. This was found to correspond to visual estimates of the pitch. Groves (1968) also pointed out the correspondence between visual estimates and estimates made from measured faces.

The mean and standard deviation have been determined for all the histograms from three outcrops. With the exception of one face in Fabric 2, the standard deviation of data from each outcrop is consistent. This implies that the lineations, which in each case define a single foliation (fig. 59), accurately represent the intensity of development of the foliation. The best fabric, defined by the lineations, is Fabric 3 followed by Fabrics 2 and 1. The significance of the peaks in Fabric 1 is shown by the fact that the total spread of readings is only 90°.

Examples of measurements on faces which did not give a clear lineation were tested in the same manner and yielded standard deviations of 36° and 50°. For a plot of a single lineation, a standard deviation in excess of 35° indicates a very weak lineation or none at all, and values less than 25° indicate the presence of a well-defined lineation. Plots which have two peaks cannot be analysed in this manner.

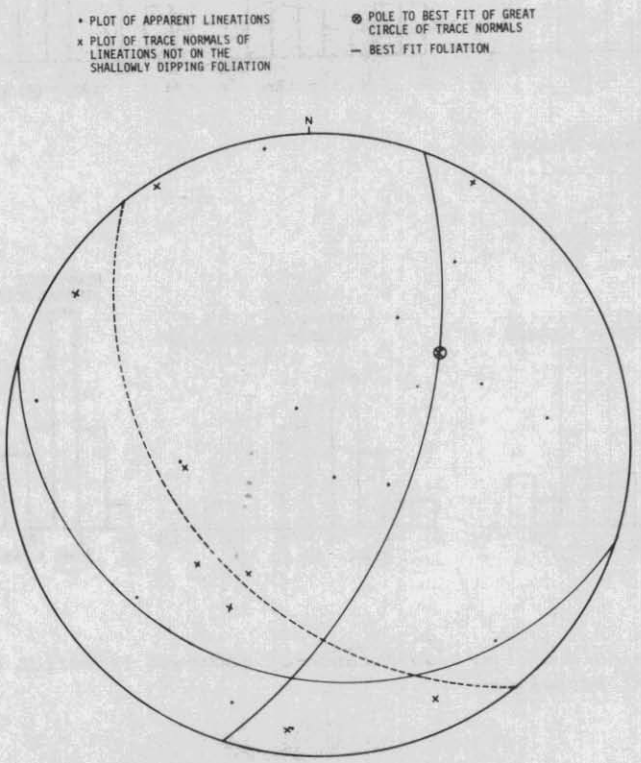

Figure 57. *Plot of apparent lineation measurements of an area of granite/adamellite east of Pioneer [832519].*

5 cm

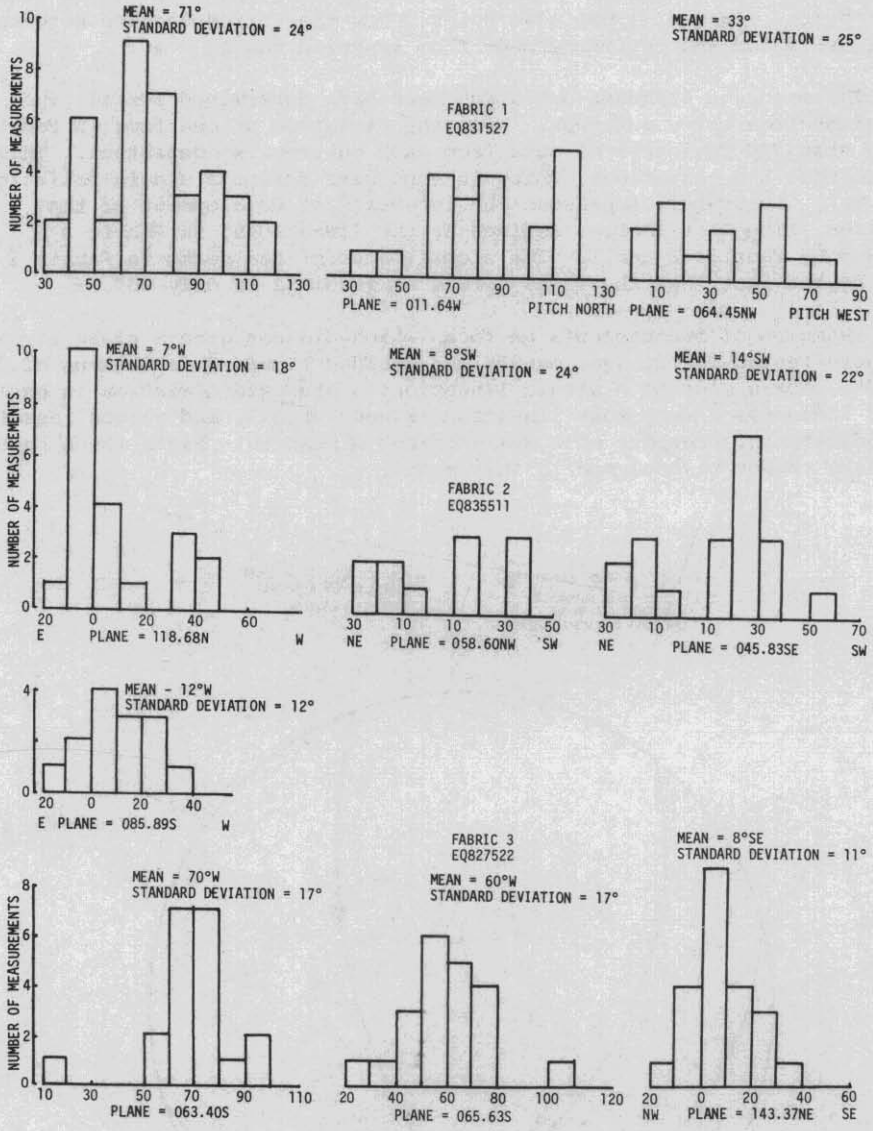

Figure 58. *Analysis of the significance of apparent lineation data, Blue Tier Batholith.*

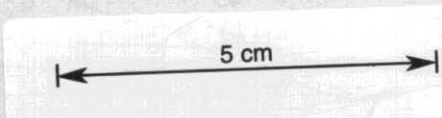

The use of the Gaussian distribution function to test the peaks is not strictly valid, since orientation data are distributed on a circle. Where the scatter is small the arithmetic method can be used, and the standard deviation applied as a criterion of significance. Analysis of the distribution yielding a standard deviation of 50° was tested using von Mise's circular normal function, which gave the same vector mean and a low value for the sum of the cosine deviations. This shows that the arithmetic method is suitable for the statistical analysis, as only data which approximates a Gaussian model in fact indicates a significant lineation.

Analysis of an intersecting foliation

The outcrop analysed in Figure 57 was also analysed by measuring the pitch of a number of feldspar crystals on large faces. The result, shown in Figures 60 and 61 indicates that an interpretation of the fabric as two intersecting foliations is valid. Each histogram is complex, with either two peaks developed or the distribution being skewed. Thus even complex fabrics (at least in this area), such as two intersecting planar surfaces, can be analysed using relatively few (not less than three) suitably orientated outcrop surfaces.

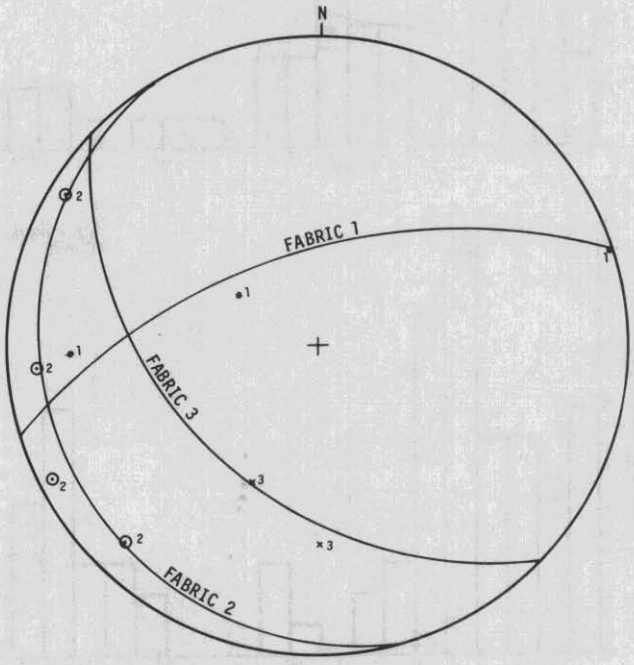

Figure 59. *Interpretation of means (fig. 58) as planar fabrics.*

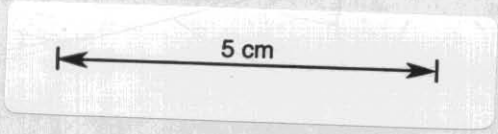

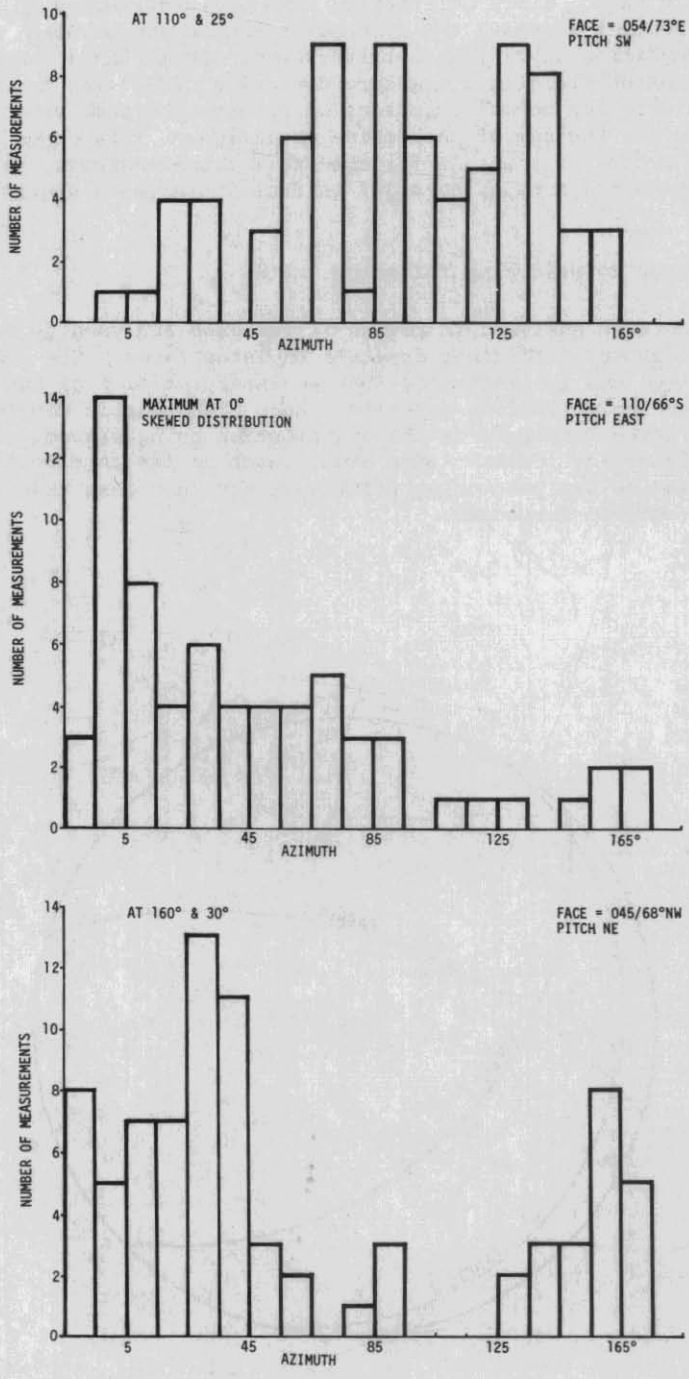

Figure 60. *Analysis of an intersecting foliation, pitch measurements of feldspar crystals on large faces.*

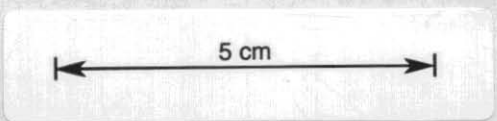

The intersecting nature of two directions of feldspar alignment has been established north of Mt Cameron (*SFC*) and is also a characteristic of the rock fabric in other areas (*NJT*).

Many outcrops of the granite/adamellite are low, gently curved, shallowly dipping surfaces which form just above soil level. It is common in the outcrop to see a good alignment of feldspar phenocrysts but to be unable to establish the planar nature of the fabric. These directions were measured. If a planar fabric is present the value should closely approximate the strike of that fabric.

In surface outcrop of the porphyritic granite belonging to the Poimena Pluton the phenocryst alignment can take the forms shown in Figures 62 and 63. These are accurate field sketches of the alignments. The three dimensional form of these more complex patterns has not been established. Except in Figure 62e, the boundaries between areas of separate feldspar orientation are diffuse and do not represent movement surfaces developed after solidification. There is no evidence to suggest that these are healed fractures.

Analysis of fabric data from a small area

Figure 64 is a map of sixty-one foliation and lineation readings from an area of 600 x 360 m. The strike of the foliations and the lineation data are plotted on a rose diagram (fig. 65) and the foliation readings plotted on an equal area projection net (fig. 66). Three directions are present in the rose diagram which generally coincide with the regions of concentration on the equal area projection. The common directions of 030°-040°, 110°-130° and 170°-180° are rotated with respect to the broad regional pattern of foliation, but are otherwise similar. Figure 64 shows the spatial relationship of these data. Some areas are dominated by one direction or other, but

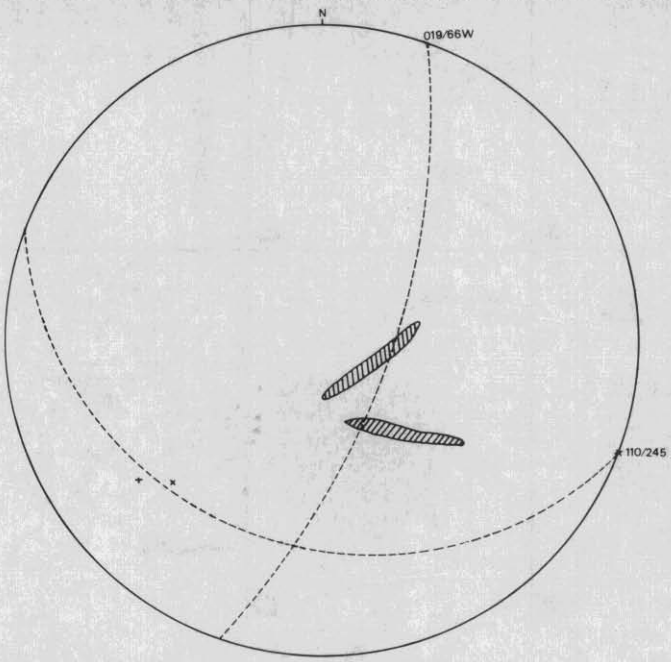

Figure 61. *Stereograms showing lineations from histograms (fig. 60) and their interpretation as two foliations.*

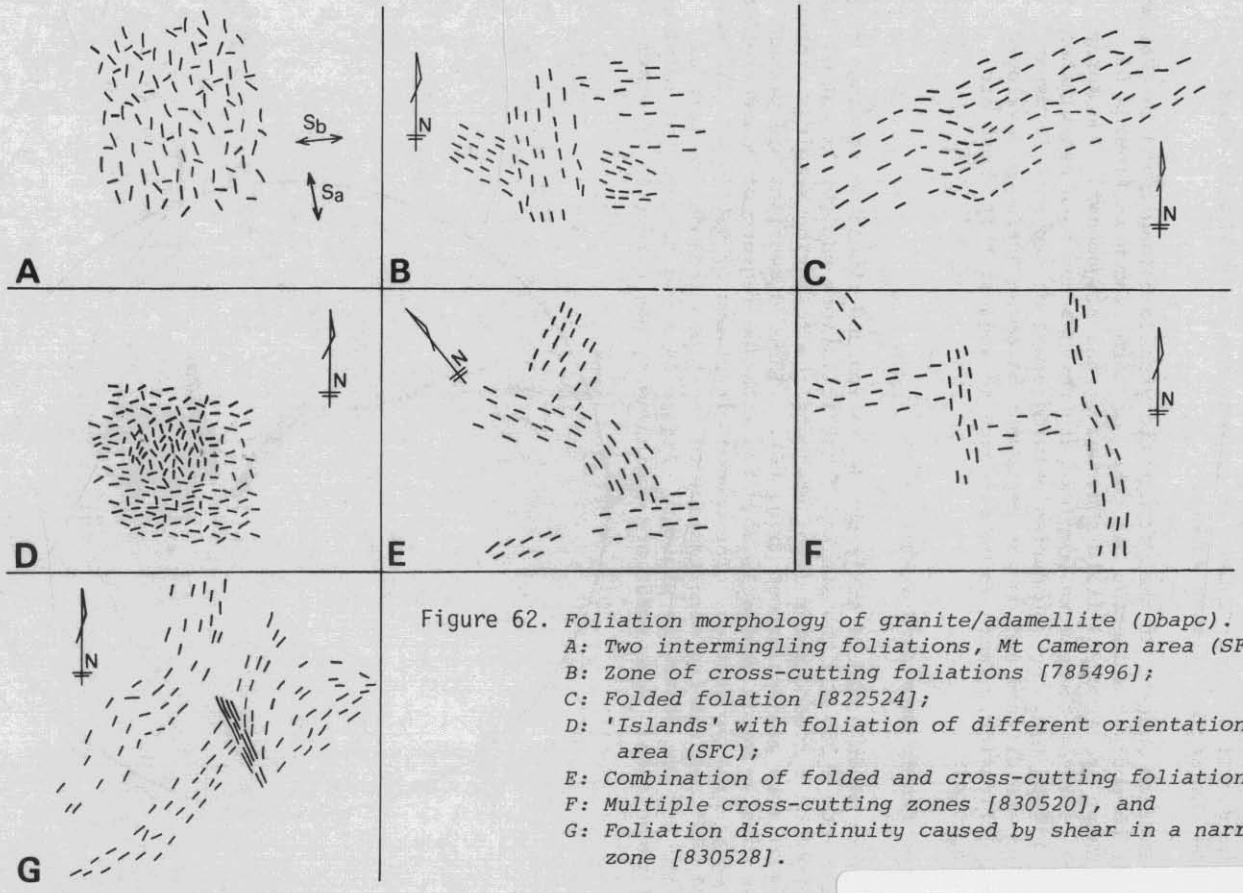

Figure 62. *Foliation morphology of granite/adamellite (Dbapc).*
A: Two intermingling foliations, Mt Cameron area (SFC);
B: Zone of cross-cutting foliations [785496];
C: Folded folation [822524];
D: 'Islands' with foliation of different orientation, Mt Cameron area (SFC);
E: Combination of folded and cross-cutting foliations [818521];
F: Multiple cross-cutting zones [830520], and
G: Foliation discontinuity caused by shear in a narrow discontinuous zone [830528].

5 cm

in each 'domain' fabric directions on one of the other trends is always present. Thus the fabric pattern in this area shows a general north-westerly trend which is intermingled with a well defined north-north-easterly direction.

Regional pattern of fabric orientation

(compiled from data of MPM, PRW, AVB, NJT, PWB, SFC)

The pattern of fabric orientation throughout the Ringarooma and Booby-alla Quadrangles has been established; the results are shown in Figures 67,68. In the area from Weldborough [760390] to Moorina [733460] the dominant direction of the fabric is 340° (fig. 67*a*). East of the road between Herrick [740390] and Mt Cameron [820590] two peaks emerge at 330° and 055°, with a weaker, subsidiary peak at 180° (fig. 67*b*). A number of shallowly dipping foliations are present which fall in a girdle with the north-east trending fabrics. Near Trout Creek [700510] and east of Martins Hill [710590] the dominant fabric trend is 340°, with some shallowly dipping surfaces present (fig. 67*c*).

North of Mt Horror [616536] in the Ringarooma Quadrangle, and in the rocks around Whiterock Tier [600660] and east of the Boobyalla River [700640] in the Boobyalla Quadrangle, the major trend is 325° with a subordinate trend at 035° (fig. 67*d*). A small maximum at about 120°, shown by linea-tions, is derived mainly from a small area north-west of Mt Horror, and the small maximum at about 170° in the lineations diagram is derived mainly from the rocks in the Boobyalla Quadrangle. Shallowly dipping foliations with a north-westerly strike are present in the porphyritic, coarse-grained biotite-minor muscovite granite/adamellite (Dbapc) at 679737. In the few

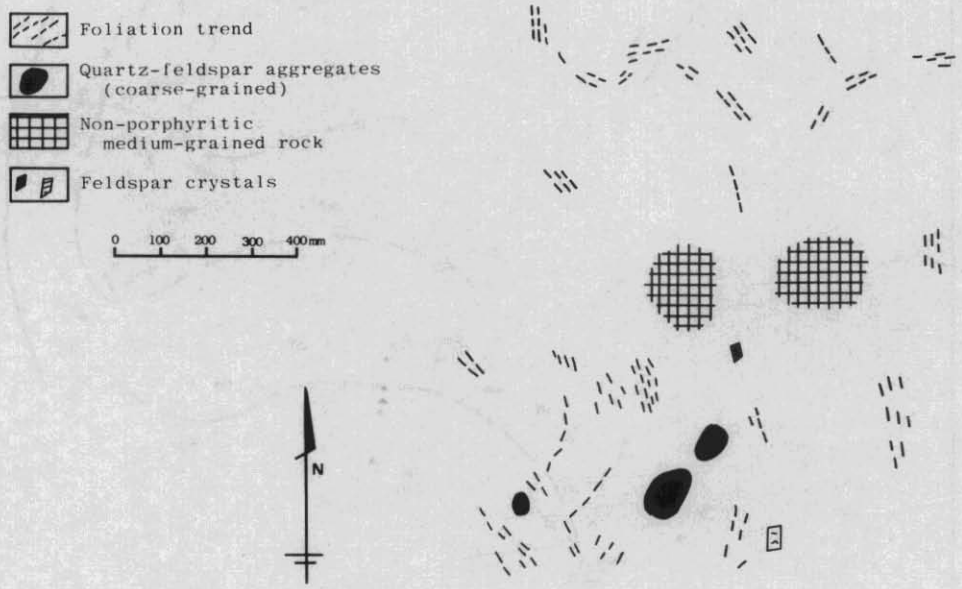

Figure 63. *Variation of phenocryst directions on a single outcrop. Most crystals have their b-axis lying in the plane of the page.*

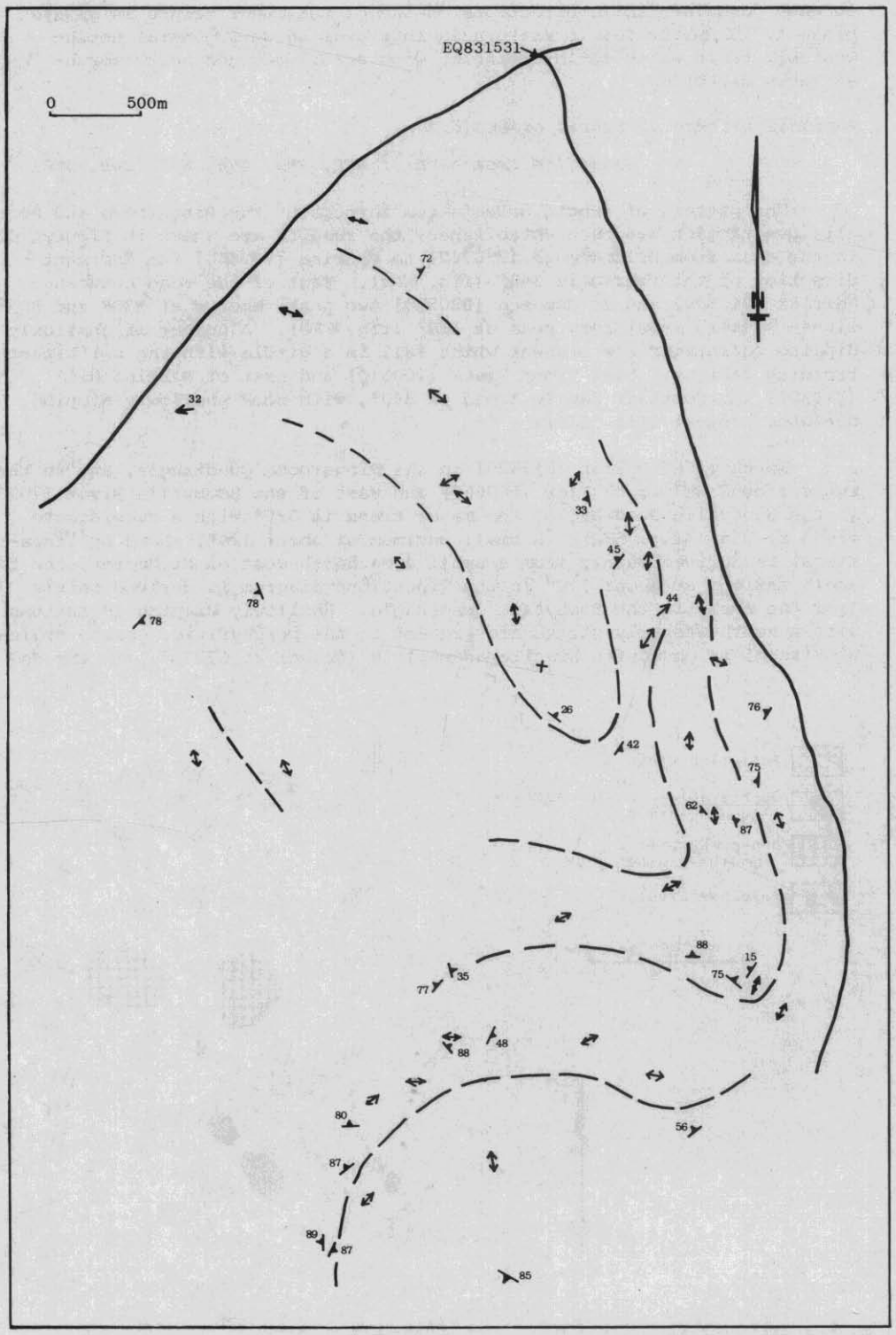

Figure 64. *Foliation and lineation measurements from an area of granite/ adamellite (Dbapc) east of Pioneer.*

5 cm

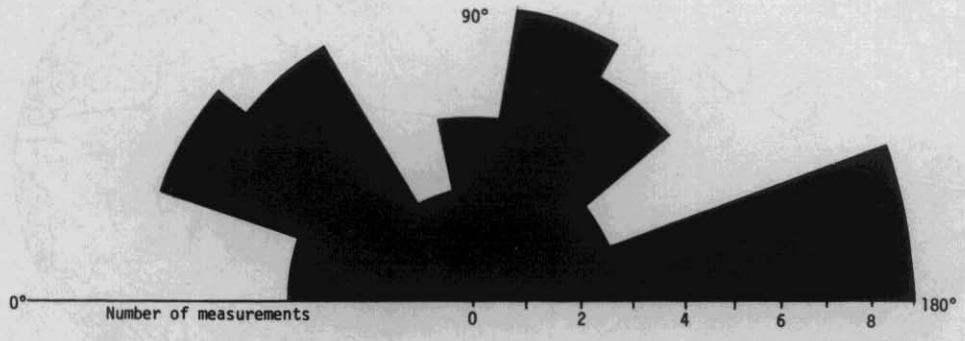

Figure 65. *Rose diagram of strike and lineation measurements from an area of granite/adamellite (Dbapc) east of Pioneer.*

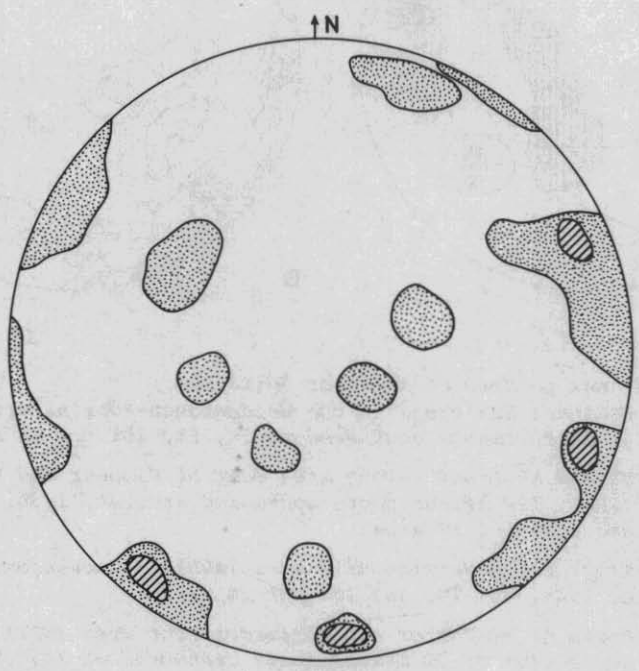

Figure 66. *Equal area projection of foliation measurements from an area of granite/adamellite east of Pioneer.*

5 cm

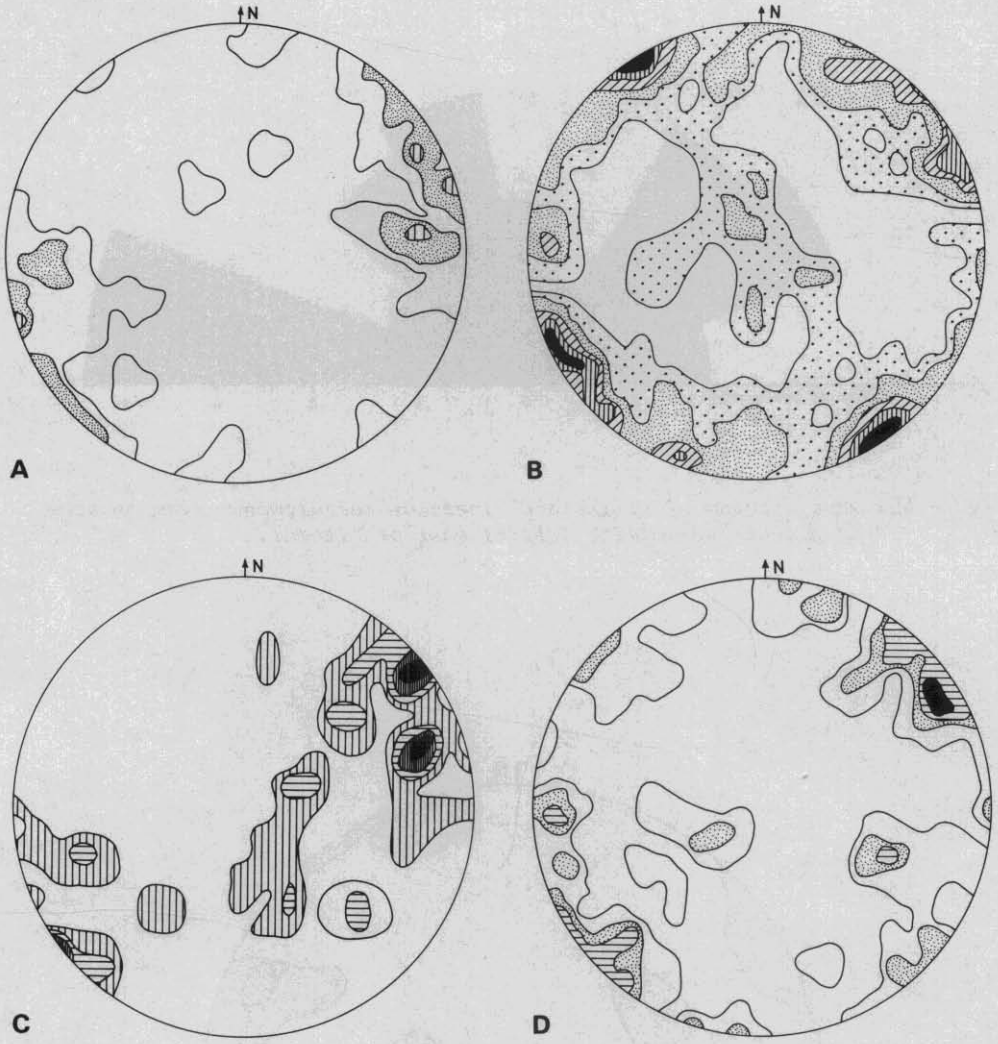

Figure 67. *Regional pattern of feldspar foliation.*

A: Dominant NNW trend in the Weldborough-Moorina area (MPM) 46 measurements contoured at 1%, 5%, 10% per 1% area.

B: NW and NE trend in the area east of Pioneer and Mt Cameron (PRW), 123 measurements contoured at 0.4%, 1.3%, 3.0%, 3.6% and 4.5% per 1% area.

C: Trout Creek-Martins Hill area (AVB), 37 measurements contoured at 1.4%, 4%, 7%, and 10% per 1% area.

D: North of Mt Horror and Whiterock Tier area (NJT). Equal area projection of 52 measurements contoured at 1%, 3%, 5% and 9% per 1% area.

5 cm

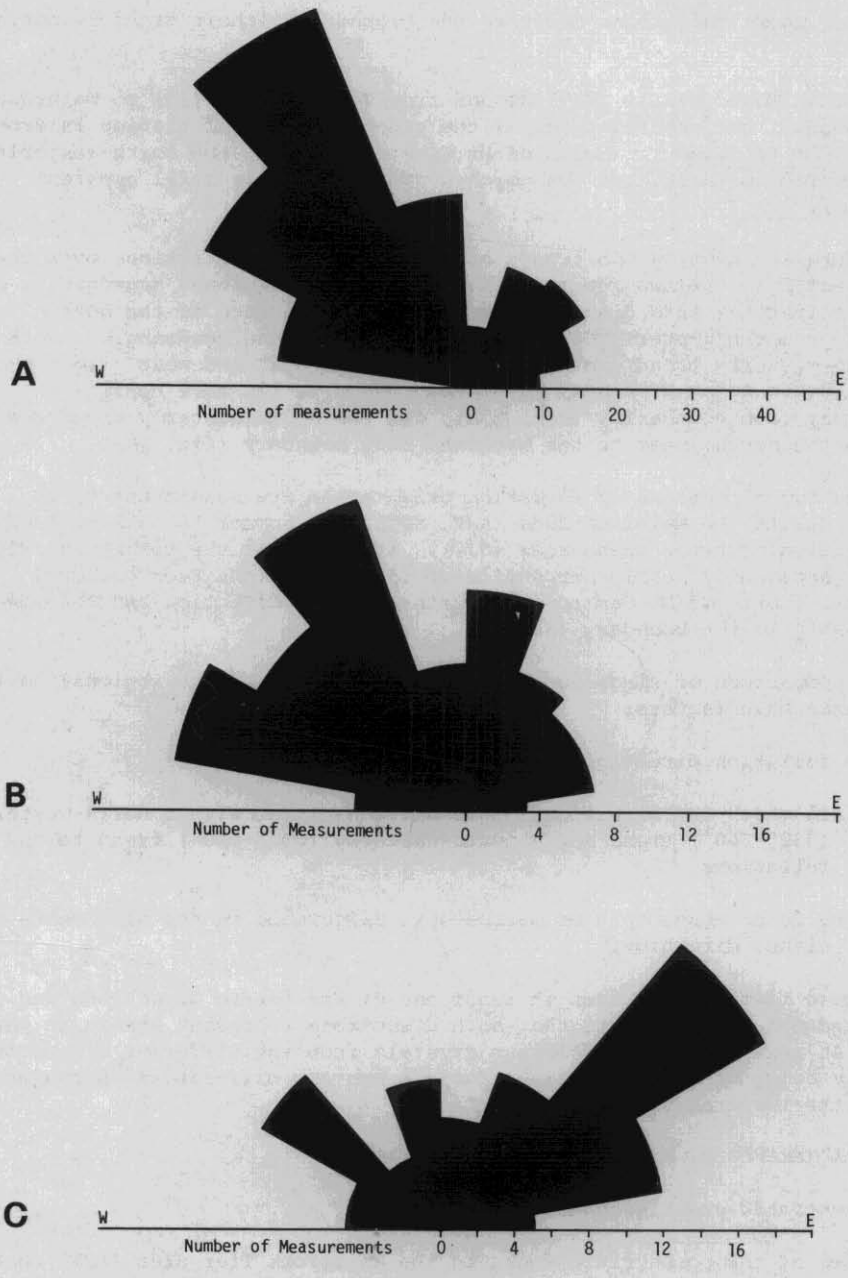

Figure 68. *Regional pattern of feldspar foliation. Rose diagrams.*

A: Lineations on horizontal outcrop surfaces, dominant NW trend. North of Mt Horror and Whiterock Tier area, 217 measurements (NJT).

B: NW and NNE trend of the strike of steeply dipping foliations and horizontal lineations. Tobacco Hill and Tomahawk to Waterhouse, 125 measurements (PWB).

C: NW and strong NE trend of the strike of foliations and horizontal lineations, 80 measurements, N of Mt Cameron (SFC).

5 cm

localities where foliations occur in the groundmass, their trend is north-west (*NJT*).

Around Tobacco Hill [555733] and from Tomahawk [635750] to Waterhouse Point [565805] the general trend of the steeply dipping foliation is from 320° to 340° (fig. 68*b*). North of Mt Cameron [790630] the north-easterly trend becomes dominant, but the north-westerly trend is still apparent (fig. 68*c*).

There are usually two trends of steeply dipping foliations over the area of Dbapc in the two quadrangles. There is no regional segregation of the two foliations into discrete domains. The dominance of the north-easterly or north-westerly directions differs over the quadrangles, with the north-westerly trend dominating in the south-west and west (fig. 68*a*), the two trends being of nearly equal importance in the more central region away from boundaries (fig. 67*b*), and the north-easterly trend dominating in the north, near to the Mathinna Beds boundary (fig. 68*c*).

The two directions of foliation orientation are consistent up to boundaries with the Mathinna Beds (*NJT, SFC*), and appear to take no heed of the direction of these boundaries (*NJT*). At Mt Horror the north-westerly trend is apparently nearly perpendicular to the Mathinna Beds boundary (*NJT*) while north of Mt Cameron the north-easterly direction has the same relationship to the boundary (*SFC*).

A comparison of single outcrops, a small area and the regional pattern shows three main factors:

(a) Two foliation directions are intermingled at all scales.

(b) In all cases the directional data are consistent with a north-westerly (330°-340°) trend and a north-easterly (030°-060°) trend to the foliations.

(c) There is no mesoscopic or macroscopic difference in the alignments in either direction.

These factors show that at least one of the fabric directions was stress induced, and suggests that both directions represent strain in the rocks. An analysis of the feldspar crystals from the different trends is currently being made to establish if there are any differences in character between the two trends.

OTHER PORPHYRITIC ROCKS

Undifferentiated granite/adamellite (Dbau)

Some of the porphyritic rocks in the Whiterock Tier area (*NJT*) contain feldspar phenocryst foliations. The north-westerly and north-easterly trends are present. In thin section only slight bending of muscovite occurs (in an equigranular variety), and in a quartz porphyritic rock the quartz phenocrysts contain strain lamellae and the groundmass quartz has undulose extinction. In equigranular rocks the quartz has undulose extinction. Some potash feldspar grains are undulose.

Fine-grained porphyritic biotite granite/adamellite (Dmgp) and porphyritic garnet-bearing biotite-muscovite granite/adamellite (Dbag)

The north-westerly and north-easterly trend of feldspar foliations was recognised in both these rock units (*NJT*). No evidence of quartz re-

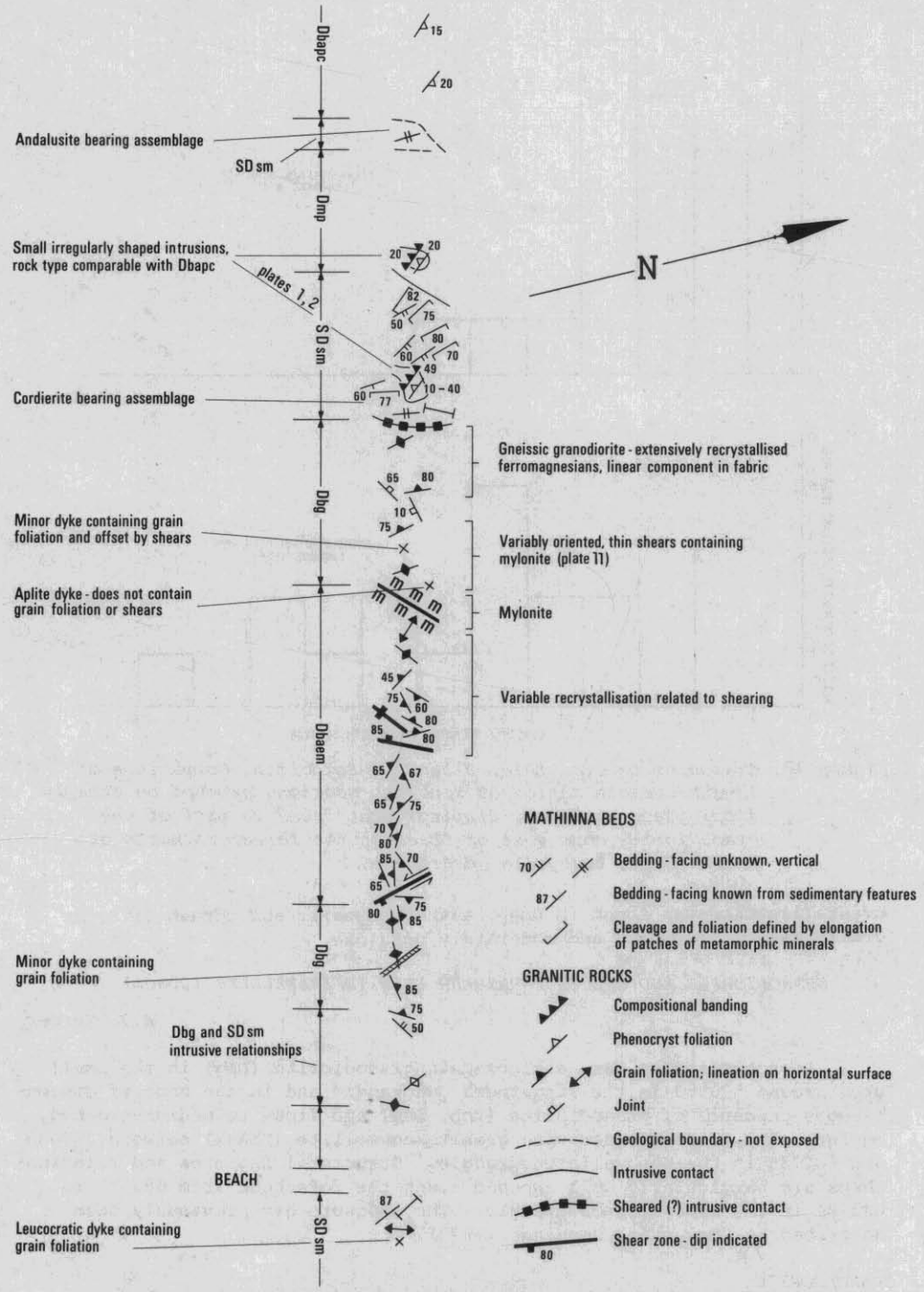

FORESHORE EXPOSURE NORTH OF SHEOAK HILL, BOOBYALLA QUADRANGLE

0 100 200 300 m

Figure 69.

5 cm

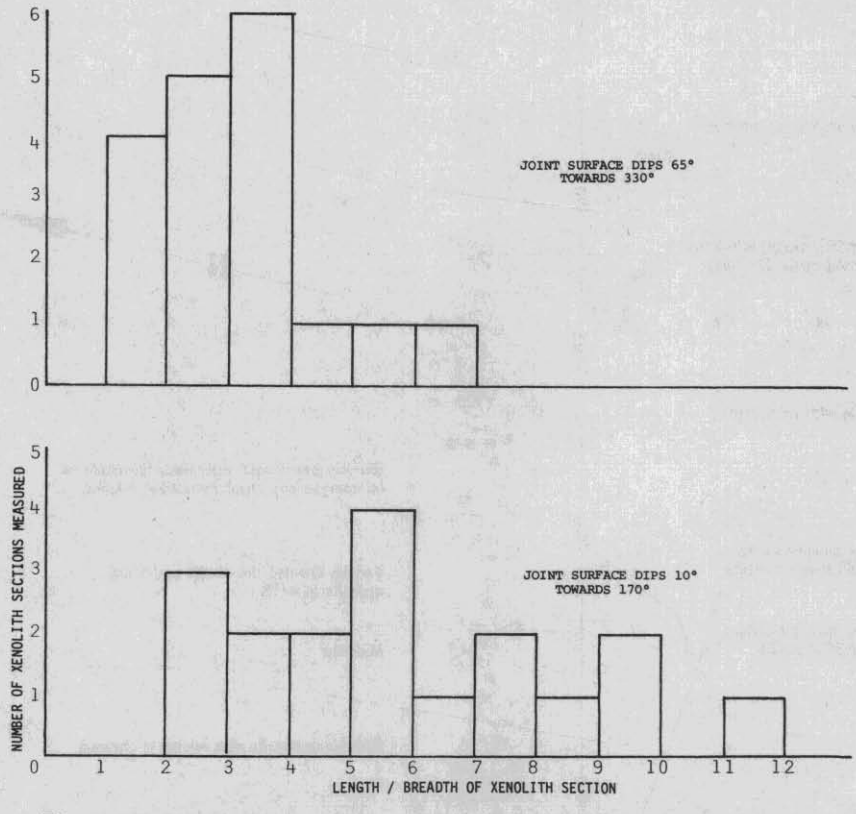

Figure 70. *Granodiorite structure. Blue Tier Batholith. Comparison of length/breadth ratios of xenolith sections exposed on steeply dipping and shallowly dipping joint faces in part of the granodiorite zone west of Dbaem on the foreshore north of Sheoak Hill, Boobyalla Quadrangle.*

crystallisation was found in Dmgp, although quartz and potash feldspar grains may be fractured and moderately undulose.

GRANODIORITE AND THE EQUIGRANULAR GRANITE/ADAMELLITE (Dbaem)

N.J. Turner

Structural data were collected in granodiorite (Dbg) in the small area around 570550 in the Ringarooma Quadrangle and in the zone of discontinuous exposure of granodiorite (Dbb, Dbg) and fine- to medium-grained, equigranular, biotite-muscovite granite/adamellite (Dbaem) between 758638 and 684735 in the Boobyalla Quadrangle. Structural features and relationships are particularly well exposed along the foreshore from 680737 to 693734 in the Boobyalla Quadrangle. The exposure has previously been described by Groves and Jennings (1973).

GRANODIORITE

Macroscopic fabric

Most outcrop surfaces of both Dbb and Dbg show lineations defined by preferred dimensional orientation of grains and patches of grains of all

5 cm

Plate 6. *Grain foliation in granodiorite (Dbb), Lower Boobyalla River area. Fresh outcrop surface. (NJT).*

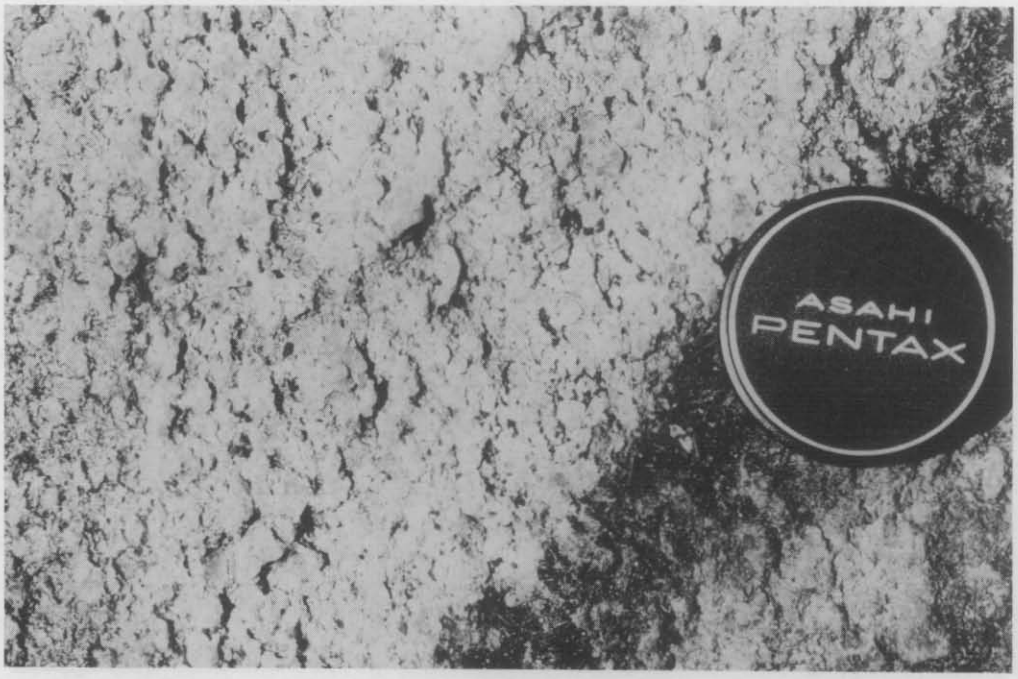

Plate 7. *Grain foliation in granodiorite (Dbb), Lower Boobyalla River area. Outcrop surface etched by weathering. (NJT).*

5 cm

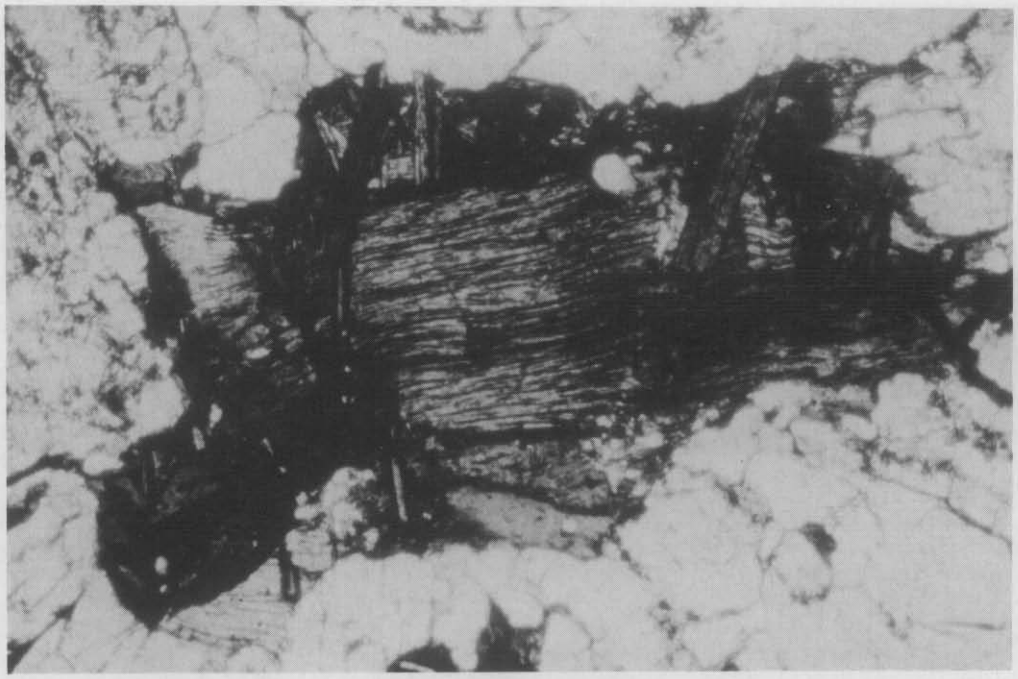

Plate 8. *Coarse, primary grain of biotite which has been deformed and is overgrown by a younger population of finer grains of biotite in biotite-hornblende granodiorite (Dbg) from south of Banca [670555], 73-429. (NJT).*

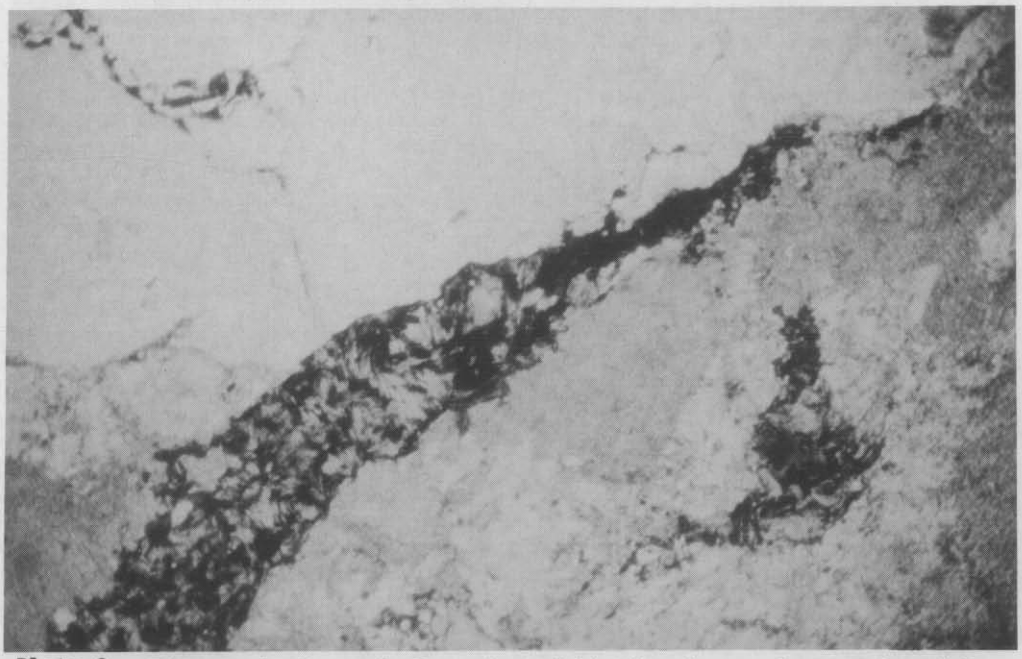

Plate 9. *Fine-grained, randomly-oriented biotite in an elongate lenticle. Lenticles have preferred orientation which partly defines the grain foliation in the rock. Biotite-hornblende granodiorite (Dbg) from the foreshore north of Sheoak Hill [684735], 77-484. (NJT).*

5 cm

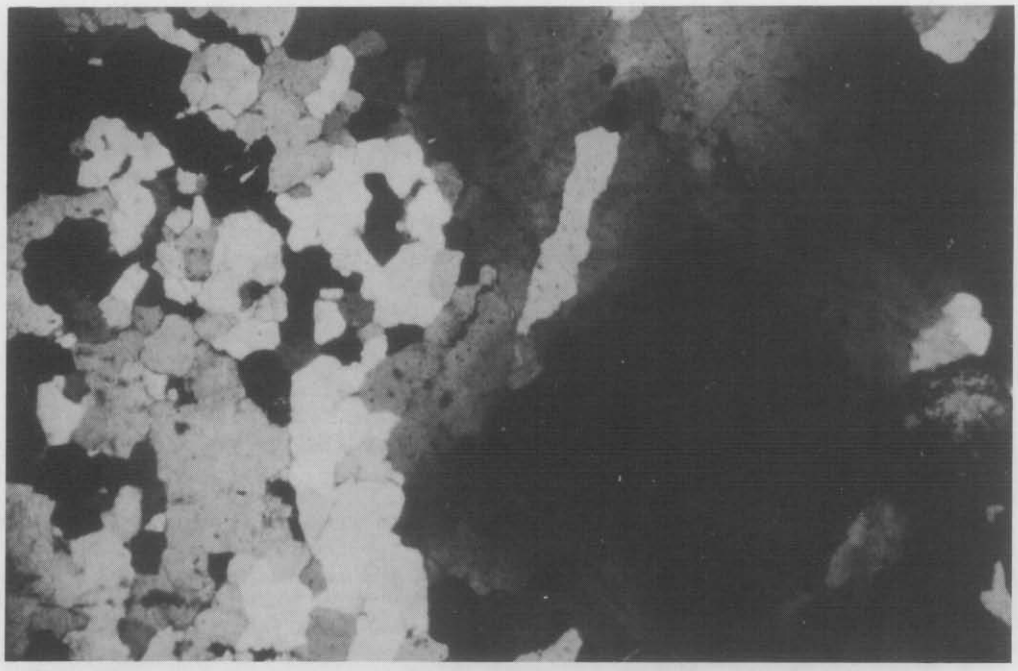

Plate 10. *Coarse, primary grain of quartz in which deformation has caused strongly undulose extinction. The grain is largely replaced by fine-grained, moderately-undulose, recrystallised quartz. Note the sub-grain within the large grain. Biotite-hornblende granodiorite (Dbg) from the foreshore north of Sheoak Hill [691734], 76-659. (NJT).*

Plate 11. *Mylonite-filled shears in foliated biotite-hornblende granodiorite (Dbg) near a contact with granite/adamellite (Bbaem) on the foreshore north of Sheoak Hill. (NJT).*

5 cm

constituent mineral species (plate 6,7). Visual inspection of the outcrops indicates that the lineations reflect the presence of foliations. In some cases several foliations can be discerned, one of which is usually dominant. The intensity of the dominant foliation varies considerably. At 684735 and around 670555 the granodiorite is gneissic. Elsewhere the foliation is generally well developed, but in some exposures it was not discerned.

Additional foliations of different morphology are present in some outcrops and may be parallel or oblique to the dominant grain. At 730694 there is a fabric element defined by parallelism of discrete, elongate stringers of biotite grains. The stringers are a few millimetres wide and up to several centimetres in length. At 691734 there is a foliation defined by preferred dimensional orientation of sparse, alkali-feldspar phenocrysts. It is oblique to the dominant grain, but in exposures to the south-east such phenocryst foliations are parallel to the main grain foliation.

In the Boobyalla River - Little Boobyalla River area rounded, elongate, melanocratic, xenoliths are commonly aligned subparallel to the dominant foliation. At 721700 there are rounded, irregularly shaped, medium-grained, mesocratic, porphyroblastic xenoliths which do not show particularly strong elongation in the direction of the foliation. They contain a foliation which is parallel to, and continuous with, the dominant foliation in the surrounding granodiorite. No deflection of the external foliation around the xenoliths was detected.

At 684735 there are numerous rounded, fine-grained xenoliths of Mathinna Beds hornfels which are oriented within the plane of the single, very strong foliation. The elongation of two-dimensional sections of xenoliths ranges from moderate to extreme. Figure 70 is a comparison of the length/breadth ratios of sections on a shallowly dipping joint surface with sections on a steeply dipping joint surface. The former are generally more elongate than the latter, which indicates that in three dimensions the xenoliths are triaxial ellipsoids with shallowly plunging long axes. A shallowly plunging linear element is also present in the fabric of the granodiorite. It is indicated by the lineation due to the foliation being more intense on subhorizontal than on subvertical surfaces. This locality is the only one where a linear component has been recognised in the fabric of the granodiorite.

Microscopic features

All main mineral species in foliated granodiorite show deformation in thin section, and biotite, hornblende and quartz show variable recrystallisation. No petrofabric analyses have been carried out. McNeil (1965) carried out petrofabric analyses of foliated granodiorite from Piccaninny Point in the St Marys Quadrangle; he found a subhorizontal linear component and steeply dipping planar components in the fabric defined by biotite cleavage planes and two quartz optic axes maxima in the plane perpendicular to the megascopic (biotite) lineation. The structural and intrusive features of the Piccaninny Point area have been discussed by Gee and Groves (1971).

Deformation shown by individual mineral grains is: biotite grains may be bent or kinked; hornblende grains may be bent or fractured; quartz grains may contain strain lamellae and/or have strongly undulose extinction; potash feldspar may have strongly undulose extinction.

Evidence of biotite and hornblende recrystallisation is provided by partial replacement of coarse primary grains by fine grains. In gneissic granodiorite from near 670555 the primary, coarse-grained, kinked biotite grains are overgrown by small, undeformed grains (plate 8). In strongly foliated granodiorite from 684735 (fig. 69) the primary biotite is partially replaced by patches of small grains, and in adjacent gneissic material the biotite consists entirely of small grains which occur in random orientation within thin, short, elongate lenticules (plate 9) that partly define the foliation.

In some granodiorite, particularly that near 691734, there is good textural evidence for substantial recrystallisation of quartz. A primary, coarse-grained population of quartz grains which contain strain lamellae and subgrains, and which may have sutured intergranular margins, are partially replaced by patches of small grains that are generally equidimensional and much less undulose than the parent grains (plate 10). In other granodiorite, the entire quartz content may have the characteristics of the second population, and it is inferred that in such rocks the quartz is entirely a product of recrystallisation.

FINE- TO MEDIUM-GRAINED EQUIGRANULAR BIOTITE-MUSCOVITE GRANITE/ADAMELLITE (Dbaem)

Macroscopic fabric

Like those of the granodiorite, outcrop surfaces of the fine- to medium-grained, equigranular, biotite-muscovite granite/adamellite may show lineations defined by the preferred orientation of grains of all constituent mineral species. Alignment of biotite and chlorite grains is more readily discernible on fresh surfaces than is alignment of quartz and feldspar. The converse is true of surfaces that have been etched by weathering. Intensity of lineation is variable. Nowhere is the intensity comparable with that in the gneissic granodiorite. Lineation is commonly difficult to discern.

Visual inspection of outcrops indicate that in some instances the lineations reflect the presence of foliations. The dominant foliation is steeply dipping and its trend varies from north-west to north-east to east across Dbaem from south to north. In some places only a similarly-trending lineation on subhorizontal outcrop surfaces was recognised. This type of observation was due, in some cases, to the absence of subvertical outcrop surfaces. In other cases such surfaces are present, but no steep lineation was observed; it appears that the dominant foliation is represented by a shallowly plunging lineation in these cases.

A subhorizontal grain foliation was found in some outcrops, and was also found in some of the equigranular phases in Dbau in the Boobyalla Quadrangle. Xenoliths are rare in Dbaem and their relationships to the foliation were not established.

Microscopic features

The major mineral species in the fine- to medium-grained, equigranular, biotite-muscovite granite/adamellite show less deformation than those in the granodiorite. Biotite, plagioclase and muscovite grains may be bent. Quartz and alkali feldspar have undulose extinction. No clear evidence of recrystallisation was found, except in the western part of the foreshore exposure where it is related to post-foliation shearing. Elsewhere quartz generally occurs as elongate patches of moderately undulose, medium sized grains.

This form of occurrence is comparable with the recrystallised quartz in the granodiorite. A small proportion of relatively large grains containing strain lamellae and subgrains were found in one sample, but no relationships were found which clearly indicate that the remainder of the quartz was derived by recrystallisation of them.

FOLIATION RELATIONSHIPS WITH DYKES

In the granodiorite on each side of the fine- to medium-grained, equigranular, biotite-muscovite granite/adamellite (Dbaem) on the foreshore in the Boobyalla Quadrangle (fig. 69) there are thin dykes of medium- to fine-grained equigranular granite or adamellite. The dyke rocks are petrographically similar to Dbaem, and contain clear textural evidence of biotite and quartz recrystallisation. The dominant foliation in the dykes is of the grain type and is concordant with the dominant foliation in the surrounding granodiorite.

Also in the granodiorite on each side of Dbaem on the foreshore are dykes of aplite and aplitic pegmatite. These do not contain foliations. Trending north-east from 678702 is a dyke of quartz-feldspar porphyry (Dmp) which intrudes Dbaem. It does not contain a foliation. A dyke of garnetiferous, quartz-feldspar porphyry (Dmpg) intrudes foliated granodiorite near 733677. It does not contain a grain foliation but phenocryst foliations were observed in places.

POST-FOLIATION SHEARING

Near 684735 on the foreshore (fig. 69) is a gradation from granodiorite to mylonite. Fine-grained mylonite occupies a zone about 15 m wide adjacent to the contact with Dbaem. It is generally dark coloured and contains streaky light coloured bands which are folded. Patches of relict quartz and relict grains of feldspar are present. The quartz occurs as small, equidimensional grains in lenticular patches. Triple junctions are present. The grains are moderately undulose and there is incipient recrystallisation to very fine-grained material along grain margins. Feldspar relicts are partially sericitised and grain margins are pitted and overgrown by groundmass minerals. The grains are undulose, fractured and kinked. The groundmass consists of very fine-grained tremolite/actinolite, quartz and ?feldspar with subordinate, tiny grains of opaques and unaltered biotite. Both the latter are common in lenticular patches, but absent elsewhere.

Further west the mylonite is confined to thin, variably oriented stringers in partially altered granodiorite (plate 11). Despite the presence of unaltered biotite within the fine-grained mylonite, there is strong alteration of biotite to chlorite in granodiorite adjacent to the stringers. Movement along the stringers is demonstrated by relative rotation of the pre-existing grain foliation in blocks of granodiorite, and displacements where the stringers cut through foliated dykes. A small unfoliated dyke of aplitic pegmatite is present in the zone and is not affected by the shearing.

Thin mylonite-filled shears are present throughout the western part of Dbaem on the foreshore. In places there are thin lenses and tabular bodies of mylonite about 100 mm thick. In hand specimen, the mylonite looks like massive grey chert. In thin section, it consists of small, elongate quartz grains and elongate patches of quartz grains in an extremely fine-grained groundmass of equant quartz (? and feldspar) grains. There is about 30% (by volume) of dirty-brown, indeterminate micaceous material in

which there are a few relict feldspar grains. The micaceous material occurs in ragged stringers which have a preferred orientation parallel to the quartz elongation.

Much of Dbaem in the western part is altered. Biotite is absent from some rocks. Where it does occur it is as fine grains in lenticules of purely biotite or intergrown with muscovite or with green, pleochroic mica that has birefringence either near to muscovite or anomalous. The dark mica in many rocks is either the green variety or chlorite. The chlorite is at least partly after biotite. Plagioclase is extremely sericitised. Recrystallisation or granulation of quartz and feldspar to very fine grain size occurs along fractures and in patches. This fine-grained material imparts a silicified appearance to the rocks in hand specimen.

Alteration is strongest in thin zones near the western contact and in pods adjacent to the cherty mylonite bodies. In hand specimen, the highly altered material is very fine-grained and consists of irregularly shaped lenticules of dark green colour about 15 mm long in a fawn or cream groundmass. In thin section, the groundmass consists of very fine-grained, equigranular, equant quartz and feldspar grains, with a small proportion of tiny muscovite flakes. The dark lenticules consist of comparable muscovite, fine-grained chlorite and a substantial proportion of very fine-grained, pale green mica in which there are isolated grains of the other minerals. Texturally, the latter material resembles a retrogressed or altered poikilitic mineral.

Compared to the eastern part, the dominant foliation in the western part of Dbaem has a very variable orientation and is not as uniformly discernible. These features are interpreted as being due to the combined effects of rotation due to shearing and alteration. The grain foliation present in normal Dbaem was not recognised in the highly altered material. However, E. Williams (pers. comm.) considers that a foliation in altered material, defined by thin, spaced fractures coated with dark mineral which is subparallel to the grain foliation in adjacent unaltered Dbaem in at least one locality, is equivalent to the grain foliation. This implies that the alteration predated the foliation. Williams further suggests that the western part of Dbaem is a more leucocratic border facies of the granitic intrusion.

The eastern part of Dbaem is unaffected by shearing except within a few metres of the contact, where there are several zones of cherty mylonite. There is about 60 mm of thinly banded, cherty mylonite at the contact and about 0.5 m of intensely sheared granodiorite. The dominant foliation in both the granodiorite and Dbaem in the immediate vicinity of the contact is rotated in accord with a sinistral horizontal component of shear. Mylonite stringers are present in the granodiorite away from the contact.

The total displacement in the various shear zones on the foreshore is unknown. Near 730690 a similar type of deformation in granodiorite is related to a north-east trending fault which has caused an apparent horizontal, dextral displacement of the granodiorite/Mathinna Beds boundary of about one kilometre (*SFC*). Intense deformation occurs for about 100 m around the fault. There are several sets of thin, anastomosing and discontinuous fractures or stringers containing very fine-grained dark coloured material (mylonite). Many of the fractures are less than 1 mm thick and persist for several tens of centimetres or less. The material in the fractures is an aggregate of light-green mica, chlorite, quartz and carbonate, together with relict feldspars. The layer silicates generally have

little preferred orientation. In the granodiorite there is alteration of feldspars to sericite and alteration of biotite to chlorite. A small zone of very altered and strongly deformed biotite monzonite occurs at 733699. It may have been produced by desilication during deformation.

The shear zones in which mylonite is present only affect Dbaem and granodiorite. The zone near 730690 does not affect the Mathinna Beds/ Dbag (garnetiferous granite/adamellite) boundary and probably developed prior to the intrusion of Dbag. The zone at the western contact of Dbaem on the foreshore formed prior to emplacement of an aplitic pegmatite dyke. It probably also formed prior to emplacement of porphyritic, coarse-grained, biotite-minor muscovite granite/adamellite (Dbapc), since no mylonitic stringers are present, either in the small intrusion near the granodiorite or in the main mass further west. Mineral assemblages in the mylonite in all zones indicate conditions in the greenschist facies of metamorphism, which implies that the granodiorite and Dbaem had cooled substantially prior to shearing. The trend of the zone at 730690 and the western zone on the foreshore is north-east, and the former is dextral. The zone at the eastern contact of Dbaem on the foreshore trends north-west and is sinistral. The zones probably all formed prior to emplacement of the porphyritic coarse-grained granite/adamellite (Dbapc), the dominantly fine- to medium-grained granite/adamellite (Dbau), the garnetiferous granite/ adamellite (Dbag) and late dykes. The north-east, dextral and north-west, and sinistral movements imply conjugation.

REGIONAL STRUCTURAL RELATIONSHIPS

Granodiorite and Dbaem

Across the eastern granodiorite/Dbaem contact on the foreshore (fig. 69) there is approximate concordance of the dominant foliations, albeit with minor rotation due to shearing at the contact. This concordance indicates that the dominant foliations in each rock type are equivalent. This conclusion is supported by the equivalence of the dominant foliation in the granodiorite with that in the Dbaem-type dykes which intrude the granodiorite.

There is also concordance of Dbaem and granodiorite foliations around 701680. The trend of the foliations is NW-NNW, compared with east-west on the foreshore. Assuming that the dominant foliations in both localities and throughout Dbaem are the same foliation, then there is a substantial and roughly continuous change in trend between the localities and from east to west across Dbaem. The variation in trend is not related to regional folding because there is no equivalent change in the trend of structures in the Mathinna Beds. It may be a primary feature of the foliation geometry or it may be due to rotation related to shearing. The trend of the foliation around 670550 in the Ringarooma Quadrangle is NNE.

It has not been proven that the dominant foliations in all areas are the same foliation. However in the Boobyalla Quadrangle, most relationships of the dominant foliations with respect to minor and major intrusions, Mathinna Beds and other structures can be shown to be independent of trend. Therefore, the dominant foliation in all areas of granodiorite and Dbaem in the Boobyalla Quadrangle formed in the same interval relative to other intrusive and structural events.

Granodiorite/Dbaem and Mathinna Beds

The foliation in the small granodiorite body near 670550 in the Ringarooma Quadrangle is discordant to the Mathinna Beds contact. The

contact is not exposed, but is probably intrusive. The relationship of the foliation to structure within the Mathinna Beds is unknown because the latter has not been established in the area adjacent to the contact.

Near 701680 in the Boobyalla Quadrangle the dominant foliation in granodiorite and Dbaem is oblique to intrusive contacts with Mathinna Beds. It is also oblique at the western granodiorite/Mathinna Beds contact on the foreshore. The NW-NNW trend of the foliation throughout much of the area is subparallel to trends of fold axial surfaces and pre-metamorphism cleavage within the Mathinna Beds. The regional trend of the post-metamorphism crenulation cleavage in the Mathinna Beds has not been established in the Boobyalla area.

Granodiorite/Dbaem and Dbapc, Dbau, Dmpg, Dbag

There is a striking morphological contrast between the dominant grain foliation present in the granodiorite and Dbaem and the phenocryst foliations present in Dbapc, in the garnetiferous quartz-feldspar dyke (Dmpg) and the porphyritic parts of the dominantly fine- to medium-grained granite/adamellite (Dbau). There are only a few localities where a grain foliation was recognised in the groundmass of Dbapc. Careful inspection was made of numerous other good exposures and no similar fabric was discerned. Alignment of feldspar phenocrysts does occur in sparsely porphyritic granodiorite, and may either be subparallel or oblique to the dominant grain foliation.

The absence of grain foliation from the aplite and aplitic pegmatite dykes in granodiorite on the foreshore (fig. 69), from the quartz-feldspar dyke (Dmp) in granodiorite near 678702, and from the garnetiferous quartz-feldspar dyke (Dmpg) in granodiorite near 733677 indicates that these minor intrusions occurred after the event which produced the grain foliation. The Dmpg dyke is probably genetically related to the garnetiferous granite/adamellite (Dbag) and therefore Dbag was probably also emplaced after the event.

The small porphyritic, coarse-grained, biotite-minor muscovite granite/adamellite (Dbapc) intrusion in Mathinna Beds near the western end of the foreshore exposure (fig. 69) is within 50 m of an intrusive Mathinna Beds/granodiorite contact. The grain foliation in the granodiorite is oblique to the contact and extremely intense (gneissic). There is no comparable structure in Dbapc, either in the nearby small intrusion or in the main mass further west. It is thought unlikely that the structurally different rocks could have been brought into such close proximity by tectonic transport, since no evidence of substantial faulting was found between them. It is concluded that Dbapc was emplaced after the grain foliation developed in the granodiorite and Dbaem. Since the dominantly fine- to medium-grained granite/adamellite (Dbau) is younger than the Dbapc, it must also be younger than the structures in the granodiorite and Dbaem.

TECTONIC CHARACTER OF FOLIATIONS

The dominant grain foliation in granodiorite was generated by flattening. The field observations supporting this view are:

(1) concordant foliations in minor dykes

(2) discordant relationships with respect to intrusive Mathinna Beds contacts

(3) concordant internal foliations in xenoliths.

The dominant grain foliation in the fine- to medium-grained, equigranular biotite-muscovite granite/adamellite (Dbaem) formed by the same mechanism.

The important observations are:

(1) concordance with foliations in granodiorite

(2) discordant relationships with respect to intrusive Mathinna Beds contacts

(3) concordance of foliations in small patches of coarse-grained adamellite and granodiorite within Dbaem.

Uniformity of foliation trend over large areas and discordance of foliations with respect to intrusive Mathinna Beds contacts indicates that the flattening was tectonic (*c.f.* Gee and Groves, 1971).

SEQUENCE OF INTRUSION AND DEFORMATION IN BOOBYALLA QUADRANGLE

The sequence of some intrusions and the sequence of some deformational events has been inferred from field relationships in the Boobyalla Quadrangle and is summarised below.

(1) Folding and formation of early cleavage in Mathinna Beds.

(2) Intrusion of granodiorite.

(3) Intrusion of Dbaem (equigranular, fine- to medium-grained biotite-muscovite granite/adamellite) and minor dykes of Dbaem-type in granodiorite.

(4) Flattening producing dominant grain foliation in granodiorite and Dbaem with a main NW-NNW trend.

(5) Conjugate shearing with NNW-sinistral and NE-dextral components. Shearing possibly caused rotation of grain foliation in Dbaem and in granodiorite on the foreshore to NE and E-W trends. The granitic rocks were relatively cool when the shearing occurred.

(6) Intrusion of Dmp (quartz-feldspar porphyry) on foreshore.

(7) Intrusion of Dbapc (porphyritic, coarse-grained, biotite-minor muscovite granite/adamellite) and minor layered bodies on foreshore.

(8) Intrusion of Dbau (dominantly fine- to medium-grained granite/adamellite).

(9) Tensional phase(s) producing long north-east trending fractures and shorter north-west and east - west fractures.

Intrusion of Dmp:- quartz-feldspar porphyry (*e.g.* 678702)
Dmpg:- garnetiferous quartz-feldspar porphyry
Dmg:- fine-grained granite/adamellite
Dma:- aplite
Dbag:- porphyritic fine- to coarse-grained garnet-bearing biotite-muscovite granite/adamellite.

(10) Flattening producing phenocryst foliations in Dbapc, Dbau (porphyritic phases), Dmpg and Dbag.

Formation of crenulation cleavages in Mathinna Beds.

No field criteria were recognised that indicate the stress conditions at the time of emplacement of the granodiorite, Dbaem and main mass of Dbapc. The small foliated dykes of Dbaem-type in the granodiorite on the foreshore were emplaced in tensional fractures. The small layered intrusions of Dbapc on the foreshore are discordant to fold structures in the Mathinna Beds and appear to have been permissively emplaced along fractures. Permissive emplacement along fracture controlled directions is suggested by the sub-rectangular outcrop pattern of Dbau in the Whiterock Tier area. The late dykes (Dmp, Dmpg, Dmg, Dma, Dbag) were emplaced along tension fractures. Since Dbag is probably of similar age to Dmpg, its emplacement was also probably permissive.

The dominant strain direction during folding of the Mathinna Beds was N-NNW. This was possibly also the main strain direction after emplacement of granodiorite and Dbaem. With the advent of shearing, the north-east direction became important. Both north-east and north-west directions were important thereafter, with the north-west direction retaining dominance in Dbapc foliations west of the Little Boobyalla River, and the north-east direction being dominant in Dbapc foliations around Mt Cameron. The north-west direction dominated during crenulation cleavage formation in the Ringarooma-Lyndhurst tract of Mathinna Beds. The north-east direction appears to have been the dominant tension direction controlling emplacement of the late dykes.

No significant field relationships were established for the sub-horizontal grain foliations in Dbaem and equigranular phases of Dbau. They may reflect periods when the maximum principal stress was subvertical or alternatively they may have been induced by flow.

REFERENCES

ANONYMOUS. 1930. Results of boring - Echo Lead - New Moorina mine - Moorina, 1930. *Unpubl.Rep.Dep.Mines Tasm.* 1930:150-156.

APPLEBY, W.R.; McEWAN, I.R. 1966. Progress report on the exploration for alluvial tin deposits in N.E. Tasmania and the Furneaux Group. *Unpubl. Rep.Utah Devel.Co.* 139.

AUSTRAL-MALAY TIN LIMITED. 1935. *Pioneer boring.* [Tasmania Department of Mines plan 723].

BAILLIE, P.W. 1973. The structure of the granitic rocks of the Little Mt Horror area. *Tech.Rep.Dep.Mines Tasm.* 15:32-36.

BAILLIE, P.W.; TURNER, N.J.; COX, S.F. 1980. *Geological atlas 1:50 000 series. Sheet 24 (8416S). Boobyalla.* Department of Mines, Tasmania.

BANKS, M.R. 1973. General geology, *in* BANKS, M.R. (ed). *The Lake Country of Tasmania*: 25-34. Royal Society of Tasmania : Hobart.

BANKS, M.R.; SMITH, E.A. 1968. A graptolite from the Mathinna Beds, northeastern Tasmania. *Aust.J.Sci.* 31:118-119.

BOUMA, A.H. 1962. *Sedimentology of some flysch deposits: a graphic approach to facies interpretation.* Elsevier : Amsterdam.

BOWDEN, A.R. 1978. Geomorphic perspective on shallow groundwater potential, coastal north-eastern Tasmania. *Tech.Pap.aust.wat.Resour.Counc.* 36.

BOWLER, J.M. 1971. Pleistocene salinities and climatic change: evidence from lakes and lunettes in south-eastern Australia, *in* MULVANEY, D.J.; GOLSON, J. (ed). *Aboriginal man and environment in Australia*:47-65. ANU Press : Canberra.

BOWLER, J.M. 1976. Aridity in Australia: age, origins and expression in aeolian landforms and sediments. *Earth.Sci.Rev.* 12:170-310.

BRAITHWAITE, J.B. 1977. Great Northern Plains: a possible dredging area. *Tech.Rep.Dep.Mines Tasm.* 20:62-76.

BROWN, A.V. et al. 1977. *Geological atlas 1:50 000 series. Sheet 32 (8415N). Ringarooma.* Department of Mines, Tasmania.

BROWN, B.R. 1976. Bass Basin - some aspects of the petroleum geology. *Monogr.Ser.australas.Inst.Min.Metall.* 7:67-82.

BRYAN, W.B.; FINGER, L.W.; CHAYES, F. 1969. Estimating proportions in petrographic mixing equations by least-squares approximation. *Science* 163:926-927.

CARMICHAEL, I.S.E.; TURNER, F.J.; VERHOOGEN, J. 1974. *Igneous petrology.* McGraw Hill : New York.

CAWTHORN, R.G.; BROWN, P.A. 1976. A model for the formation and crystallisation of corundum-normative calc-alkaline magmas through amphibole fractionation. *J.Geol.* 84:467-476.

CHAPPELL, B.W.; WHITE, A.J.R. 1974. Two contrasting granite types. *Pacific Geol.* 8:173-174.

CHESNUT, W.S. 1965. Report on Ringarooma deep lead tin prospecting. North-east Tasmania, 1964/65. *Unpubl.Rep.Broken Hill Pty Co. Ltd.*

COCKER, J.D. 1977. The geology of the St Helens area: petrology and structure of the granitoid rocks. *Bull.geol.Surv.Tasm.* 55:117-156.

COLHOUN, E.A. 1975. *A Quaternary climatic curve for Tasmania.* Royal Meteorological Society. Australasian Conference on Climate and Climatic Change, Monash University, 7-12 December 1975. (unpubl.)

COLHOUN, E.A. 1978. Late Quaternary environment of Tasmania as a backdrop to man's occupance. *Rec.Qn.Vict.Mus.* 61.

COOKSON, I.C. 1937. The occurrence of fossil plants at Warrentinna, Tasmania. *Pap.Proc.R.Soc.Tasm.* 1936:73-78.

COOMBS, D.S.; WILKINSON, J.F.G. 1969. Lineages and fractionation trends in undersaturated volcanic rocks from the East Otago volcanic province (New Zealand) and related rocks. *J.Petrology* 10:440-501.

CRUDEN, D.M. 1971. Traces of a lineation on random planes. *Bull.geol. Soc.Am.* 82:2303-2305.

DAVIES, J.L. (ed). 1965. *Atlas of Tasmania.* Lands and Surveys Department : Hobart.

DAVIES, J.L. 1967. Tasmanian landforms and Quaternary climates, *in* JENNINGS, J.N.; MABBUTT, J.A. (ed). *Landform studies from Australia and New Guinea*:1-25. Cambridge University Press.

DEN TEX, E. 1954. Sterographic distinction of linear and planar structures from apparent lineations in random exposure planes. *J.geol.Soc.Aust.* 1:55-66.

DETTMANN, M.E. 1963. Upper Mesozoic microfloras from south-eastern Australia. *Proc.R.Soc.Vict.* 77:1-148.

DETTMANN, M.E. 1973. Angiospermous pollen from Albian to Turonian sediments of eastern Australia. *Spec.Publs geol.Soc.Aust.* 4:3-34.

DETTMANN, M.E.; PLAYFORD, G. 1968. Taxonomy of some Cretaceous spores and pollen grains from eastern Australia. *Proc.R.Soc.Vict.* 81:69-94.

DETTMANN, M.E.; PLAYFORD, G. 1969. Palynology of the Australian Cretaceous: a review, *in* CAMPBELL, K.S.W. (ed). *Stratigraphy and palynology: Essays in honour of Dorothy Hill:*174-210. ANU Press : Canberra.

EDWARDS, A.B. 1942. Differentiation of the dolerites of Tasmania. *J.Geol.* 50:451-480, 579-610.

FAURE, G.; POWELL, J.L. 1972. *Strontium isotope geology.* Springer : Berlin.

FREY, F.A.; GREEN, D.H.; ROY, S.D. 1978. Integrated models of basalt petrogenesis: a study of quartz tholeiites to olivine melilites from south eastern Australia utilizing geochemical and experimental petrological data. *J.Petrology* 19:463-513.

GEE, R.D.; GROVES, D.I. 1971. Structural features and mode of emplacement of part of the Blue Tier Batholith in north east Tasmania. *J.geol.Soc.Aust.* 18:41-56.

GEE, R.D.; GROVES, D.I. 1974. Contact structures at a granodiorite intrusion, Piccaninny Point, northeast Tasmania. *Pap.Proc.R.Soc.Tasm.* 107:47-52.

GREEN, T.H. 1978. A model for the formation and crystallisation of corundum-normative calc alkaline magmas through amphibole fractionation: a discussion. *J.Geol.* 86:269-272.

GROVES, D.I. 1968. Preliminary report on the granitic rocks of the Blue Tier tinfield. *Tech.Rep.Dep.Mines Tasm.* 11:38-48.

GROVES, D.I. 1977. The geology, geochemistry and mineralisation of the Blue Tier Batholith. *Bull.geol.Surv.Tasm.* 55:7-116.

GROVES, D.I.; COCKER, J.D.; JENNINGS, D.J. 1977. The Blue Tier Batholith. *Bull.geol.Surv.Tasm.* 55.

GROVES, D.I.; JENNINGS, D.J. 1973. Geology of a coastal section between Tomahawk and Boobyalla. *Tech.Rep.Dep.Mines Tasm.* 16:22-36.

GROVES, D.I.; McCARTHY, T.S. 1978. Fractional crystallisation and the origin of tin deposits in granitoids. *Miner.deposita* 13:11-26.

GROVES, D.I.; TAYLOR, R.G. 1973. Greisenization and mineralization at Anchor tin mine, northeast Tasmania. *Trans.Instn.Min.Metall.* 82B:135-136.

HÄKLI, T.A.; WRIGHT, T.L. 1967. The fractionation of nickel between olivine and augite as a geothermometer. *Geochim.cosmochim.Acta* 31:877-884.

HANSON, G.N. 1978. The application of trace elements to the petrogenesis of igneous rocks of granitic composition. *Earth planet.Sci.Lett.* 38:26-43.

HARRIS, W.K. 1968. Tasmanian Tertiary and Quaternary microfloras. Summary report. *Palaeont.Rep.geol.Surv.S.Aust.* 5/68.

JENNINGS, D.J. 1966. Drilling for tin in the upper Boobyalla area. *Tech.Rep.Dep.Mines Tasm.* 11:28-33.

JENNINGS, D.J. 1967. *Geological atlas 1 mile series. Zone 7 sheet 23 (8316S). Noland Bay.* Department of Mines, Tasmania.

JENNINGS, D.J.; SUTHERLAND, F.L. 1969. Geology of the Cape Portland area, with special reference to the Mesozoic(?) appinitic rocks. *Tech.Rep. Dep.Mines Tasm.* 13:45-82.

KIRKPATRICK, J.B. 1977. *The disappearing heath. A study of the conservation of the coastal heath plant communities of north east and east Tasmania and the Furneaux Group.* Tasmanian Conservation Trust : Hobart.

LEAMAN, D.E. 1973. Summary of geophysical work, Gladstone area. *Tech. Rep.Dep.Mines Tasm.* 16:89-96.

LEAMAN, D.E. 1977. Gravity survey of north-eastern Tasmania. Analysis of pluton margins. *Unpubl.Rep.Dep.Mines Tasm.* 1977/26.

LEAMAN, D.E.; JORDAN, M. 1973. Gravity survey, Great Forester River area, north-eastern Tasmania. *Tech.Rep.Dep.Mines Tasm.* 16:83-85.

LEAMAN, D.E.; MOORE, W.R. 1973. Seismic survey, South Mount Cameron. *Unpubl.Rep.Dep.Mines Tasm.* 1973/72.

LEAMAN, D.E.; SYMONDS, P.A. 1975. Gravity survey of north-eastern Tasmania. *Pap.geol.Surv.Tasm.* 2.

LONGMAN, M.J. 1966. One mile geological map series. K/55-7-39. Launceston. *Explan.Rep.geol.Surv.Tasm.*

LONGMAN, M.J.; MATTHEWS, W.L.; ROWE, S.M. 1964. *Geological atlas 1 mile series. Zone 7 sheet 39 (8315S). Launceston.* Department of Mines, Tasmania.

MANSON, V. 1967. Geochemistry of basaltic rocks: major elements, *in: The Poldervaart treatise on rocks of basaltic composition.* Vol. 1. Wiley : New York.

MARSHALL, B. 1970. Geological atlas 1 mile series. Zone 7 sheet 31 (8315N). Pipers River. *Explan.Rep.Dep.Mines Tasm.*

MARSHALL, B.; BARTON, C.M.; JENNINGS, D.J.; NAQVI, I.H. 1965. *Geological atlas 1 mile series. Zone 7 sheet 31 (8315N). Pipers River.* Department of Mines, Tasmania.

McCARTHY, T.S.; GROVES, D.I. 1979. The Blue Tier Batholith, northeastern Tasmania. *Contrib.Miner.Petrology* 71:193-209.

McDOUGALL, I.; LEGGO, P.J. 1965. Isotopic age determinations on granitic rocks from Tasmania. *J.geol.Soc.Aust.* 12:295-332.

McNEIL, R.D. 1965. The geology of the Mt Elephant - Piccaninny Pass area, Tasmania. *Pap.Proc.R.Soc.Tasm.* 99:27-49.

MOORE, W.R. 1978. Seismic survey and confirmatory drilling in the South Mt Cameron Tertiary basin. *Unpubl.Rep.Dep.Mines Tasm.* 1978/9.

MOORE, W.R. *in prep.* Groundwater investigation and resources of north-eastern Tasmania. *Bull.geol.Surv.Tasm.* 62.

MOORE, W.R.; LEAMAN, D.E. 1974. Further geophysical work, Gladstone. *Tech.Rep.Dep.Mines Tasm.* 17:88-98.

NEUMANN, H.; MEAD, J.; VITALIANO, C.J. 1954. Trace element variations during fractional crystallisation as calculated from the distribution law. *Geochim.cosmochim.Acta* 6:90-99.

NOCKOLDS, S.R. 1954. Average chemical composition of some igneous rocks. *Bull.geol.Soc.Am.* 65:1007-1032.

NYE, P.B. 1925. Teh sub-basaltic tin deposits of the Ringarooma Valley. *Bull.geol.Surv.Tasm.* 35.

PAPIKE, J.J.; CAMERON, K.L.; BALDWIN, A.J. 1974. Amphiboles and pyroxenes: characterization of other than quadrilateral components and estimates of ferric iron from microprobe data. *Abstr.ann.Meet.geol.Soc.Am.* 6:1053-1054.

PARTRIDGE, A.D. 1973. Revision of the spore-pollen zonations in the Bass Basin. *Unpubl.palaeont.Rep.Esso Aust.Ltd* 1973/4.

PARTRIDGE, A.D. 1976. The geological expression of eustacy in the Early Tertiary of the Gippsland Basin. *APEA* 16(1):73-79.

QUILTY, P.G. 1972. The biostratigraphy of the Tasmanian marine Tertiary. *Pap.Proc.R.Soc.Tasm.* 106:25-44.

RINGWOOD, A.E. 1966. The chemical composition and origin of the Earth, *in* HURLEY, P.M. (ed). *Advances in earth science:*287-356. MIT Press : Cambridge, Mass.

RITTMAN, A. 1973. *Stable mineral assemblages of igneous rocks.* Springer : Berlin.

ROBINSON, V.A. 1974. Geological history of the Bass Basin. *APEA J.* 14(1):45-49.

SATO, H. 1977. Nickel content of basaltic magmas and a measure of the degree of olivine fractionation. *Lithos* 10:113-120.

SCOTT, J.B. 1930. Progress report on boring operations, Echo deep lead, New Moorina mine. *Unpubl.Rep.Dep.Mines Tasm.* 1930:81-82.

SEDMIK, E.C.E. 1964. Winnaleah area geophysical surveys, Tasmania 1961-62. *Rec.Bur.miner.Resour.Geol.Geophys.Aust.* 1964/54.

SHAW, D.M. 1970. Trace element fractionation during anatexis. *Geochim. cosmochim.Acta* 34:237-243.

SKRZECZYSKI, R.H. 1971. *The Bridport Granodiorite and its contact aureole.* B.Sc. (Hons) thesis, University of Tasmania : Hobart.

STANDARD, J.C. 1973. Endurance drilling programme, South Mt Cameron, Tasmania. *Unpubl.Rep.BMI Mining Ltd.*

STEIGER, R.H.; JAGER, E. 1977. Subcommission on Geochronology: Convention on the use of decay constants in geo- and cosmochronology. *Earth. planet.Sci.Lett.* 36:359-362.

STORMER, J.C. jr. 1975. A practical two-feldspar geothermometer. *Am.Mineral.* 60:667-674.

STOVER, L.E.; EVANS, P.R. 1973. Upper Cretaceous-Eocene spore-pollen zonation, offshore Gippsland Basin, Australia. *Spec.Publs geol.Soc. Aust.* 4:55-72.

STOVER, L.E.; PARTRIDGE, A.D. 1973. Tertiary and Late Cretaceous spores and pollen from the Gippsland Basin, southeastern Australia. *Proc.R. Soc.Vict.* 85:237-286.

STRECKEISEN, A. 1967. Classification and nomenclature of igneous rocks. *Neues Jb.Mineral.Abh.* 107:144-240.

SUTHERLAND, F.L. 1969. A review of the Tasmanian Cainozoic volcanic province. *Spec.Publ.geol.Soc.Aust.* 2:133-144.

SUTHERLAND, F.L. 1973. The geological development of the southern shores and islands of Bass Strait. *Proc.R.Soc.Vict.* 85:133-144.

SUTHERLAND, F.L. 1974. High pressure inclusions in tholeiitic basalt and the range of lherzolite-bearing magmas in the Tasmanian volcanic province. *Earth planet.Sci.Lett.* 24:317-324.

SUTHERLAND, F.L.; CORBETT, E.B. 1974. The extent of Upper Mesozoic igneous activity in relation to lamprophyric intrusions in Tasmania. *Pap.Proc.R.Soc.Tasm.* 107:175-190.

TWELVETREES, W.H. 1900. *Preliminary report on the deep lead or infra-basaltic stanniferous gravels of the Ringarooma Valley near Derby.* Mines Department, Tasmania.

TWELVETREES, W.H. 1913. [Report on the Clarence Tin Prospecting Association No Liability]. *Rep.Secr.Mines Tasm.* 1912:48-54.

VANDENBERG, A.H.M.; GARRATT, M.J.; SPENCER-JONES, D. 1977. Silurian - Middle Devonian, *in* DOUGLAS, J.G.; FERGUSON, J.A. (ed). *Geology of Victoria. Spec.Publ.geol.Soc.Aust.* 5:45-76.

VARNE, R. 1977. On the origin of spinel lherzolite inclusions in basaltic rocks from Tasmania and elsewhere. *J.Petrology.* 18:1-23.

WARIN, O.N.; APPLEBY, W.R. 1965. Report on the progress investigations for tin in north-east Tasmania. *Unpubl.Rep.Utah Devel.Co.* 135.

WATSON, E.B. 1979. Zinc saturation in felsic liquids. Experimental results and applications to trace element geochemistry. *Contrib. Mineral Petrology* 70:407-419.

WHITE, A.J.R.; CHAPPELL, B.W. 1977. Ultrametamorphic and granitoid genesis. *Tectonophysics* 43:7-22.

WHITNEY, J.A.; STORMER, J.C. jr. 1977. Two-feldspar geothermometry, geobarometry in mesozonal granitic intrusions: three examples from the Piedmont of Georgia. *Contrib.Mineral Petrology* 63:51-64.

WILLIAMS, E. 1959. The sedimentary structures of the Upper Scamander sequence and their significance. *Pap.Proc.R.Soc.Tasm.* 93:29-32.

WINKLER, H.G.F. 1967. *Petrogenesis of metamorphic rocks.* 2 ed. Springer : Berlin.

APPENDIX 1

Tertiary leads and basin in the Winnaleah-Mt Cameron area

A.V. Brown

The remnants of a river system terminating in an internal basin occur north-west of Winnaleah. This system was infilled during the mid-Tertiary with material derived from the surrounding country rock and then covered by basaltic flows during the Middle-Lower Miocene.

RINGAROOMA LEAD

During the mid-Tertiary (Harris, 1968), country rocks of the Ringarooma region acted as source material for the infilling of an active river system, now referred to as the 'Ringarooma Lead'. This lead consists of a main channel with numerous tributaries and ends in an inland basin to the south of Mt Cameron (fig. 71). The basement rock is mainly granitic, but Mathinna Beds occur to the south-west. The main channel of the lead runs roughly due north from west of the present township of Ringarooma, swinging north-easterly under Branxholm, then onto the north-west of Derby, south-east of Winnaleah and north-west of Herrick before spreading out into an inland basin to the south of Mt Cameron. During a time of low sedimentation rate after an erosional phase basaltic magma extruded through basement rocks and capped the lead with more than 100 m of alkali olivine basalt and olivine nephelinite flows.

Field mapping with associated drill hole and seismic data from the Winnaleah area indicates that the downslope direction of the gutter is north-easterly from Derby towards Mt Cameron. The main gutter has a very low gradient, but most of the tributaries, which have been worked for tin, have a fiarly steep initial gradient which then flattens out within approximately 500 m, before reaching the main gutter.

Known tributaries towards the northern end of the lead are the Cascade (Derby) and Main Creek (Mutual) leads (Nye, 1925) from the south-east, Weld Lead (Echo Mine) from the south (Scott, 1930; Anon, 1930); O.K. Lead (Herrick) from the south-east (Nye, 1925); Wyniford Lead (Pioneer) and its tributary, the Gladstone Lead from the south-east (Nye, 1925; Austral-Malay, 1935), Eastern Lead (Warin & Appleby, 1965) from the east and the Endurance (Standard, 1973) - Hasties (Appleby & McEwan, 1966) - Clarence (Twelvetrees, 1913) system from the north-west.

Several previous authors have suggested a possible outlet to Bass Strait, either along the western edge of Mt Cameron, or under the Winnaleah basalt plateau and out under the present Boobyalla River. The present writer considers that the above two suggestions are no longer valid and that the original lead ended in a land locked basin. This conclusion is based on new field mapping, geophysical and drill hole data, as well as the reinterpretation of primary data from previous workers.

Drilling carried out by the Department of Mines during 1972-73 established the depths to the granitic basement along a north-south line from Herrick to the western end of Mt Cameron. Older drilling programmes indicated the shape of the basement around Pioneer (Austral-Malay, 1935), Echo (Scott, 1930) and Clarence (Twelvetrees, 1913) leads. Drilling by the Utah Development Company outlined the shape in the Hasties area and of the Eastern Lead (Appleby & McEwan, 1966), whilst similar work by BMI Mining Pty Ltd on the Endurance Lead (Standard, 1973) gives an idea of the basement topology

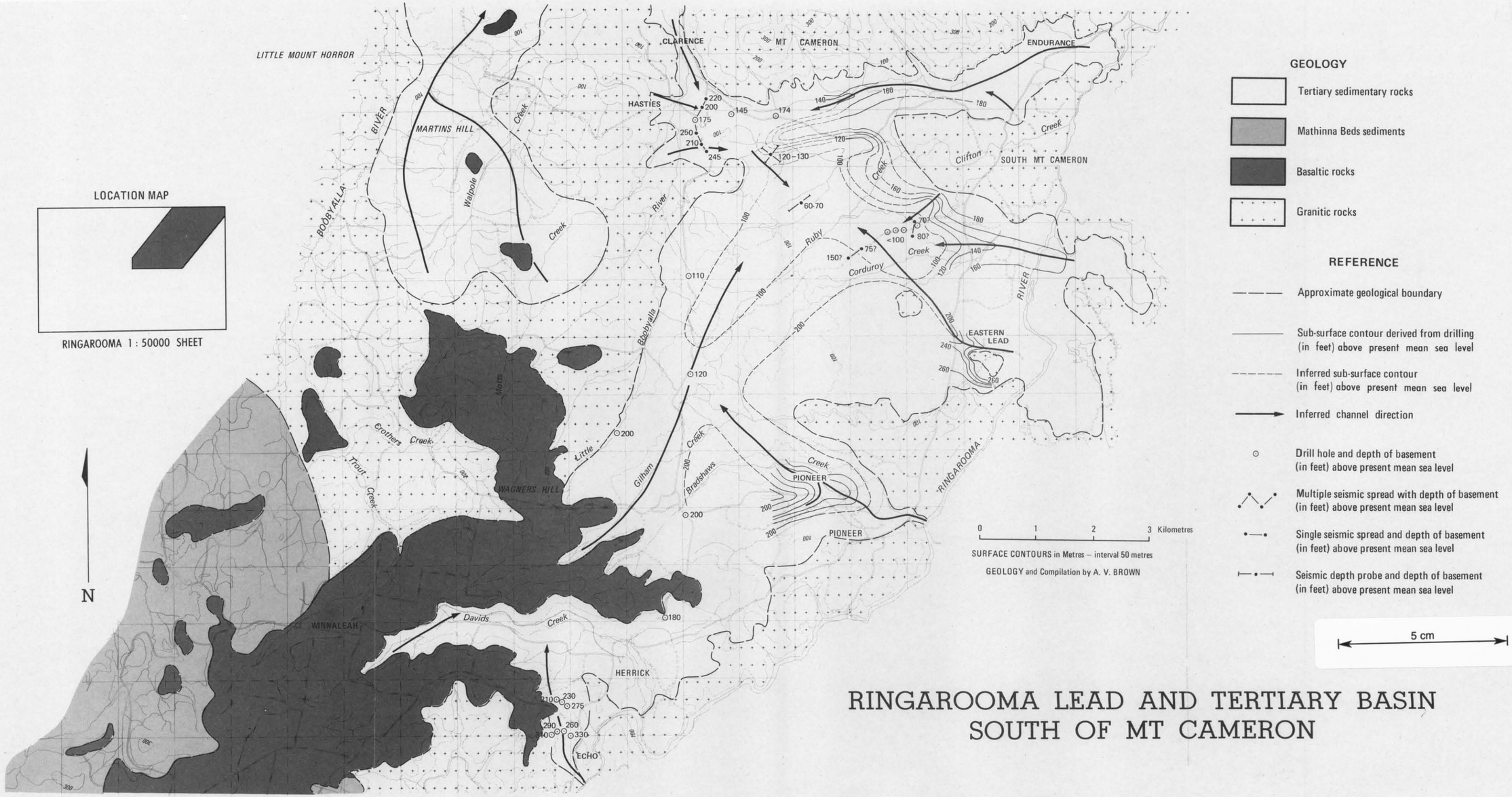

RINGAROOMA LEAD AND TERTIARY BASIN SOUTH OF MT CAMERON

Figure 71

in that area. Recent seismic investigations and drilling by the Department of Mines (Moore, pers.comm.) to the west of the Endurance mine has upgraded the knowledge of the basement shape between Hasties and Endurance.

The deepest point so far encountered in the basin is approximately 800 m south of Mt Cameron. This occurs at a reduced level of 18-21 m above present mean sea level (APMSL) at 762573. This depth was derived from seismic results (Leaman and Moore, 1973), but four drill holes east of this area, on a surface level of 75 m APMSL, all penetrated 45 m of Tertiary sediment without bottoming, thus indicating the depth to solid basement is less than 30 m APMSL (Appleby and McEwan, 1966, D.H 201-204). Approximately 2 km south-west of this point, drill hole data indicates a granitic basement at 36 m APMSL, thus giving a fall of only 13.5 m in approximately 2.25 km. The Wyniford Lead drops from 79 m APMSL under the Pioneer-Gladstone road at Pioneer to 43 m APMSL 800 m to the north-west (in the present Pioneer open cut). From this point, it only drops another 6 m over the next 1.5 km to where it enters the main gutter. Other tributaries have a similar geometry. The deepest proven remaining thickness of sediment occurs in a Department of Mines drill hole (7, Winnaleah area, page 175) on the Herrick-Boobyalla road. The sediment has a thickness of 123 m in this hole.

In the Winnaleah area, ferricrete underlies basaltic rock and overlies the Tertiary sediment. If ferricrete lag overlying Tertiary sediment in other localities can be used as criteria for the basalt-sediment interface, then in the Pioneer-Mt Cameron area the lag would suggest a possible interface at 180 m APMSL. This level corresponds with the interface level over the majority of the area covered by the Winnaleah Sheet. Variations from this level occur in the Herrick area, where the interface occurs at 150 m APMSL and at Derby, where the lowest interface exposed in the Briseis open cut is at approximately 170 m APMSL. This flow is 12 m thick and is overlain by 3 m of sediment. From this level (185 m APMSL), a continuous basalt cover occurs along the open cut to the eastern end where the interface is at about 200 m APMSL. These variations are probably due to a period of erosion, during which small streams cut into the unconsolidated sediment before the extrusion of basalt. Thus in the Pioneer-South Mt Cameron area, at least 75 m of sediment and an unknown thickness of overlying basalt have been eroded and transported to the north of the region. In the Derby-Winnaleah area, most of the sediment and up to 105 m of overlying basalt remains.

Drilling undertaken by BMI Mining Pty Ltd in the Endurance mine area indicates the presence of a gutter along the southern face of Mt Cameron that is separated from the northernmost extent of the Ringarooma Lead by an east-west ridge of granitic rock (Standard, 1973). This ridge is thought to be 21 m under the present day surface, but 30 m higher than the lowest points of the gutter on either side. Drilling and seismic work carried out by the Department of Mines (Moore, pers.comm.) delineated the direction on the westward continuation of this ridge and gutter and confirms that the basement shallows in a southerly direction and that the Hasties-Clarence-Endurance gutters originally emptied in a southerly direction into the inland basin.

Sediments of the lead and basin are very similar in lithology. Basal pebble to coarse cobble conglomerate up to 3 m thick have been exposed overlying granitic basement in the Pioneer open cut. Similar sequences up to 18 m thick have been intersected by five drill holes along the main lead (pp 173-177). The conglomerate is composed of cobbles-pebbles of granitic rock, vein quartz and metamorphosed Mathinna Beds sediment in a matrix of very coarse sand to clay.

Overlying the basal conglomerate are irregularly interbedded and interdigitating beds and lenses, composed of one or more of granule conglomerate, sand and clay. The most common occurrences are beds and lenses of glassy quartz granule conglomerate with a matrix of sand and clay, granule conglomerate lenses, sand and clay lenses and clay lenses. In some places the sand and grit are cemented by iron oxide.

In the Pioneer open cut, the cross-sectional size of a lens can vary from 100 m by 30 m of thick buff coloured clay down to 150 mm by 25 mm of granule conglomerate to coarse sand. In lower parts of the lead and basin, some of the sequences contain carbonaceous material such as tree stems, branches and leaves which are partly altered to coal and in many places replaced by marcasite. Such layers are exposed in the Hasties and Pioneer open cuts and were intersected by two of the five drill holes along the Herrick-Boobyalla road. The overall character of the sediment, as seen in the open cuts and quarries, suggests a deltaic rather than a lacustrine environment.

In general, it appears that after deposition of about 75 m of sediment, the original basement gutters were infilled and the spurs forming the tributary boundaries became covered. This led to a change in the depositional environment from small streams to material from the various sources crossing and intermixing in a deltaic type basin.

Sediment from the area contains microflora that has been correlated with those from marine sediments of Longfordian age (Lower Miocene) by Harris (1968). Harris obtained fifteen samples from five different localities in the Ringarooma area; Branxholm, Wood's property, Endurance, Amber Hill and the New Edina pit. All proved to be of Longfordian age. Potassium-argon age determination of three whole rock basalt samples from flows that overly the Tertiary sediment gave an age range of 15.9± 0.6 Ma (Appendix 2), corresponding to the top of the Lower Miocene.

BOOBYALLA LEAD

Another Tertiary river system, here called the 'Boobyalla Lead', starts in the central north of the Winnaleah Sheet, between the present Boobyalla and Little Boobyalla Rivers. Seismic and gravity work by the Bureau of Mineral Resources in 1961-62 (Sedmik, 1964) outlined this lead which was later confirmed with drilling by BHP (Chesnut, 1965) and the Department of Mines (Jennings, 1966). This northerly trending lead has previously been considered as one of two possible continuations of the Ringarooma Lead, due to an extrapolation joining the two systems by a channel under the basalt plateau. Field mapping and the above mentioned drilling and geophysical work has shown that this is not possible.

The Boobyalla Lead starts as two separate, northerly trending gutters, with a granitic rock basement, to the north of the Winnaleah basalt. About 3 km north of their source, the gutters join into a single channel and continue to deepen to the north. After joining, seismic data suggests that the channel consists of two nearly parallel gutters. Drilling confirms the channel but does not define its shape. In the area of drilling, geophysical data indicates up to 90 m of sediment, whereas drilling has indicated the bottom at between 59 and 61 m.

This system appears to have been infilled at the same time as the Ringarooma Lead, subsequent to which a nearly continuous sedimentary cover extended inland from the sea to the northern face of Mt Cameron, around the

western side of Mt Cameron west to Little Mt Horror, then south-east to between Wagners Hill and the high granite country to the south of Garibaldi. From there, the cover swung to the south-west, between Mathinna Beds sequences to the north-west and granitic hills to the south-east, inland towards the present township of Ringarooma to a level which is currently represented by an altitude of about 180 m APMSL.

LOGS OF DRILL HOLES

During 1972-73, eight cable tool and rotary drill holes were drilled at locations covered by the Winnaleah Sheet of the Ringarooma Quadrangle by the Department of Mines. All these holes were intended to bottom in unweathered basement rock. The placement of the holes was influenced by an attempt to obtain maximum data on the topology of the old Tertiary river valley and the underground water potential of the area. Drill hole No. 2 was not drilled in the area of this report. The following are extracts from drill logs for the holes, as submitted by the drillers, plus summary comments by the writer.

Hole 1 [*676468*]

Depth (m)	*Reduced Level* (m)	*Thickness* (m)	*Remarks*
0	253.0	-	Soil
0.6	252.4	0.6	Chocolate soil
1.5	251.5	0.9	Basaltic clay
3.0	249.9	1.5	Basalt boulder gravel
7.9	245.1	4.9	Basalt boulders
42.7	210.3	34.7	Solid basalt
54.9	198.1	12.2	Softer basalt
62.8	190.2	7.9	Solid basalt
64.0	189.0	1.2	Basaltic clay
67.1	185.9	3.0	Basalt-silt-clay
71.6	181.4	4.6	Clay-gravel
143.2	109.7	71.6	Sand-clay
161.5	91.4	18.3	Ironstone-gravel
178.3	74.7	16.8	Gravel-clay
205.7+	47.2		Sandstone - (Mathinna Beds)

Surface 253.0 m
Basalt 67.1 m thick
Tertiary 111.3 m thick

Basement Mathinna Beds at R.L. 74.7 m
Basalt-Tertiary interface at R.L. 185.9 m

Hole 3 [*685478*]

Depth (m)	*Reduced Level* (m)	*Thickness* (m)	*Remarks*
0	292.6	-	Soil
0.6	292.0	0.6	Chocolate soil
3.0	289.6	2.4	Soil and boulders (basalt)
19.8	272.8	16.8	Basaltic clay and stones (?)
24.4	268.2	4.6	Basalt
25.9	266.7	1.5	Basaltic clay and pebbles
27.7	264.9	1.8	Hard basalt

Hole 3 (continued)

Depth (m)	*Reduced Level* (m)	*Thickness* (m)	*Remarks*
33.2	259.4	5.5	Honeycomb basalt with clay seams
61.9	230.7	28.7	Hard basalt

Hole abandoned.

Hole 4 [698504]

Depth (m)	*Reduced Level* (m)	*Thickness* (m)	*Remarks*
0	213.4	-	Soil
1.2	212.2	1.2	Chocolate soil
3.7	209.7	2.4	Basaltic clay
7.6	205.7	4.0	Weathered basalt
8.8	204.5	1.2	Basalt
11.0	202.4	2.1	Clay and pebbles
25.9	187.5	14.9	Hard basalt
29.9	183.5	4.0	Clay and sand
39.9	173.4	10.1	Hard basalt
42.1	171.3	2.1	Hard sand
45.1	168.2	3.0	Basalt (?)
96.0	117.3	50.9	Clay and sand
101.5	111.9	5.5	Clay
109.7	103.6	2.1	Clay and sand
112.2	101.2		Clay
120.7	92.7		
132.6	80.8	11.9	Clay and gravel
145.1	68.3	12.5	Coarse stone and clay
163.1	50.3	18.0	Boulders and clay (coarse gravel and clay)
168.9	44.5	5.8	Soft sandstone (?) (Fine sand, A.V.B.)
176.5	38.4	6.1	Sandstone (?) (Fine sand, A.V.B.)

Hole abandoned at 175 m.

Hole 5 [747502]

Depth (m)	*Reduced Level* (m)	*Thickness* (m)	*Remarks*
0	134.1	-	Tertiary sediments in quarry 6 m under basalt
12.2	121.9	12.2	Gravel and clay
33.5	100.6	21.3	Rotten wood - pyrite - clay - gravel
42.7	91.4	9.1	Gravel
54.9	79.2	12.2	Clay-gravel-pyrite
56.4	77.7	1.5	Rounded pebbles-gravel-pyrite

Hole 5 (continued)

Depth (m)	*Reduced Level* (m)	*Thickness* (m)	*Remarks*
59.4	74.7	3.0	Fine gravel
73.2	61.0	13.7	Rounded pebbles-gravel
100.6	33.5	27.4	Decomposed granite
100.6+	-	?	Hard granite

Surface 134.1 m

Soft granite-hard granite interface R.L. 33.5 m

Basalt-Tertiary sediment interface 140.2 m

Tertiary sediment thickness 79.2 m

Tertiary sediment-decomposed granite interface R.L. 61 m

Decomposed granite thickness 27.4 m

Hole 6 [*751519*]

Depth (m)	*Reduced Level* (m)	*Thickness* (m)	*Remarks*
0	118.9	-	Black-grey soil and gravel
0.3	118.6	0.3	Soil
1.5	117.3	1.2	Hard gravel
4.9	114.0	3.4	Gravel, clay and clay seams
10.1	108.8	5.2	Gravel
17.1	101.8	7.0	Clay
24.4	94.5	7.3	Clay and gravel
36.6	82.3	12.2	Gravel
54.9	64.0	18.3	Rounded pebbles-clay-gravel
61.0	57.9	6.1	Decomposed granite
61.0+	-	?	Hard granite

Surface 118.9 m in Tertiary sediments

Decomposed granite-hard granite interface R.L. 57.9 m

Tertiary sediments-decomposed granite interface R.L. 64 m

Decomposed granite thickness - 6.1 m

Hole 7 [*742543*]

Depth (m)	*Reduced Level* (m)	*Thickness* (m)	*Remarks*
0	167.6	-	Black-grey soil and gravel
0.3	167.3	0.3	Surface soil
2.1	165.5	1.8	Clay
22.3	145.4	20.1	Gravel and clay
30.2	137.5	7.9	Gravel
40.2	127.4	10.1	Clay and gravel
44.2	123.4	4.0	Gravel
50.3	117.3	6.1	Clay and gravel
53.3	114.3	3.0	Coarse gravel
59.1	108.5	5.8	Clay

Hole 7 (continued)

Depth (m)	*Reduced Level* (m)	*Thickness* (m)	*Remarks*
72.5	95.1	13.4	Coarse gravel
82.3	85.3	9.8	Clay
94.5	73.2	12.2	Clay and gravel
74.7	62.5	10.7	Clay-rotten wood-pyrite
108.5	59.1	3.4	Gravel
123.4	44.2	14.9	Rounded pebbles and clay and gravel
132.6+	35.1	9.1+	Soft granite
-?	?	?	Hard granite

Surface 176.8 m
Tertiary sediment-soft granite interface R.L. 44.2 m

Tertiary sediment thickness 123.4 m
Weathered granite 9.1 m+ thick

Hole 8 [751560]

Depth (m)	*Reduced Level* (m)	*Thickness* (m)	*Remarks*
0	134.1	-	Black-grey soil and gravel
0.3	133.8	0.3	Soil
1.8	132.3	1.5	Hard gravel
5.2	128.9	3.4	Gravel
13.1	121.3	7.9	Hard gravel
22.3	112.2	9.0	Gravel
27.1	107.3	4.9	Clay
30.2	104.2	3.0	Clay, rotten wood, pyrite
32.3	102.1	2.1	Gravel, pyrite
48.2	86.3	15.8	Clay, gravel, rotten wood, pyrite
63.4	71.0	15.2	Gravel and clay seams
65.8	68.6	2.4	Clay with small amounts of gravel
105.6	26.9	41.8	Gravel, clay
108.5	25.9	0.9	Harder granite
111.3	23.2	2.7	Soft granite
111.6	22.9	0.3	Harder granite
115.2	19.2	3.7	Soft granite
117.7	16.8	2.4	Harder granite
118.3+	-	?	Hard solid granite

Surface 134.1 m
Soft granite-Tertiary sediment interface R.L. 25.9 m

Hard granite - soft granite interface R.L. 16.8 m
Tertiary sediment thickness 107.3 m
Weathered granite thickness 10.1 m

Hole 9 [753589]

Depth (m)	*Reduced Level* (m)	*Thickness* (m)	*Remarks*
0	83.8	-	Black-grey soil with gravel
0.3	83.5	0.3	Soil
0.9	82.9	0.6	Hard cemented gravel
6.7	77.1	5.8	Gravel, clay
16.5	67.4	9.8	Clay, gravel
29.0	54.9	12.5	Gravel and clay
32.9	50.9	4.0	Soft decomposed granite
34.1	49.7	1.2	Hard decomposed granite
35.1	48.8	0.9	Soft decomposed granite
44.5	39.3	9.4	Hard decomposed granite
46.6	37.2	2.1	Gravel, clay (?)
48.8	35.1	2.1	Granite gravel (?)
49.4+	-	?	Hard granite

Surface 83.8 m
Decomposed granite-hard granite interface R.L. 35.1 m

Tertiary sediment-decomposed granite interface R.L. 50.9 m
Decomposed granite thickness - 15.8 m
Tertiary sediment thickness - 32.9 m

APPENDIX 2

Whole rock K/Ar Ages of basalts

A.V. Brown

Table 1. WHOLE ROCK K-Ar AGES OF BASALTS

Sample No.	% K	$^{*}Ar^{40}/K^{40}$ ($x10^{-4}$)	$\%Ar^{40}$ atmos	Age ($x10^{6}$ yrs.)
72-316	0.931 0.928	9.337	63.8	15.9 ± 0.6
W1-4	1.284 1.275	9.3962	26.2	16.0 ± 0.3
W3-1	1.000 1.001	9.1556	39.8	15.6 ± 0.3

Decay constants $\lambda e = 0.584 \times 10^{-10}/yr$, $\lambda\beta = 4.72 \times 10^{-10}/yr$.

Atomic abundance $K^{40} = 0.0119$ atom %

Sample No. : 72-316 - Olivine nephelinite
Grid refs. : EQ720492 (59/707374)
Amdel ref. : Basalt 3 - BMR - 2/1/10 - AN 1003/76

Sample No. : W1-4 - Porphyritic alkali olivine basalt
Grid refs. : EQ661538 (59/643409)
Amdel ref. : W1-4 - BMR - 2/1/10 - 1600/77

Sample No. : W3-1 - Alkali olivine basalt
Grid refs. : EQ724526 (59/712395)
Amdel ref. : W3-1 - BMR - 2/1/10 - 1600/77

APPENDIX 3

Cretaceous K/Ar ages from north-eastern Tasmania

I. McDougall
D.C. Green

HORNBLENDES

Cape Portland and East Stony Head (I. McDougall, 1979)†

	% K	$^{40}Ar^{*} \times 10^{-5}$ std cc/gm	$\%^{40}Ar^{*}$	Age ± 2 s.d. (Ma)
Augite-hornblende porphyrite Loc 9 (Vinegar Hill) Tech.Rep.Dep.Mines 13 Museum TS 633 EQ829874	1.214) 1.206)	0.49493	84.9	102.3 ± 2.6
Dyke, Cape Portland, collected D. Jennings EQ806872 ≡ Loc 21, Tech.Rep.13.	1.235) 1.232)	0.49945	93.4	101.3 ± 2.6
Beach Boulders East Stony Head TS 78/549 EQ046625	1.031) 1.031)	0.41880	90.0	101.6 ± 2.6

Decay constants $\lambda_{\beta} = 4.962 \times 10^{-10}$/yr, $\lambda_{e} + \lambda'_{e} = 0.5811 \times 10^{-10}$/yr.

Atomic abundance mol $^{40}K/K = 0.1167 \times 10^{-3}$ (Steiger and Jäger, 1977)

BIOTITES

Cape Portland (C. Brooks, 1971)†

	Rb/Sr age (Ma)	K/Ar age (Ma)
Porphyrite 680916	103 ± 23	91 ± 1 (93)*
Dyke 680917	94 ± 20	-
Dyke 680918	98 ± 23	-

* K-Ar ages recalculated using decay constants and atomic abundance figures recommended by Steiger and Jäger, 1977.

† *In litt.*

These new K-Ar dates on hornblendes prepared in 1978 and now dated by Dr I. McDougall at the Australian National University give a more secure basis to the age of the Cretaceous intrusive rocks at Cape Portland. Hitherto the dates provided by Dr C. Brooks in a letter to the Director of Mines dated 14 June 1971 have been referred to as unpublished data; *e.g.* in Sutherland and Corbett (1974) where the Rb/Sr and K/Ar ages on sample 680916 are quoted with reference to a Department of Mines report that was anticipated but never published.

The unpublished biotite dates by Brooks quoted above are unsatisfactory in that no analytical data are included or comments made on the decay constants used at the time. One would guess that if the normal K-Ar decay constants used at that time apply, the K-Ar age quoted would be increased by $\sim$ 2 m.y. if the modifications recommended by Steiger and Jäger (1977) are applied. The Rb-Sr ages may require a downward revision of some 3 m.y. if a ^{87}Rb half life of 5×10^{10} years was used.

The new dates confirm the middle Cretaceous (Albian) age of the Cape Portland complex and reinforce comments in correspondence (23 July 1971 to Dr Brooks and reply 16 September 1971) that the Rb/Sr date represents the age of crystallisation of the rock. The high error limits (±20 to 23 Ma) placed on the Rb-Sr ages do not suggest great confidence in the results but the reason is not specified.

Hornblende is generally considered to be more retentive of radiogenic argon than biotite, for this reason the new hornblende K-Ar ages of around 102 Ma are the best estimate for the age of emplacement of the Cape Portland dykes and porphyrite complex.

The coarsely crystalline hornblende gabbro boulders (TS 78/549) from East Stony Head beach about 20 km north-east of George Town were collected by D.J. Jennings from a wave-cut platform beneath basalt cliffs. The size of the boulders precludes any appreciable longshore drift. One boulder contains a large included fragment of dolerite - a feature common at Cape Portland. It is likely that these boulders are from a nearby Mesozoic plug or dyke and similar to some of the other hornblendic rocks in north-east Tasmania described by Sutherland and Corbett (1974).

In his current study of the Cretaceous Otway Group volcanogenic sediments, Mr Ian Duddy of the Department of Geology at the University of Melbourne has investigated the Cretaceous intrusives of north-eastern Tasmania as a possible source. Electron microprobe compositional data on the dated hornblendes (including the East Stony Head sample) are essentially identical. The similarity in composition of these hornblendes and those of hornblendes from 'andesitic' fragments in the Otway Group of the Bass Basin support the observation of F.L. Sutherland in Sutherland and Corbett (1974) that the mid-Cretaceous igneous episode provided much of the volcanogenic material for the stratigraphically equivalent Strzelecki Group in the offshore Gippsland Basin.

The dates listed here confirm that at least part of these sedimentary Groups may be as young as Albian - *cf.* Dettmann and Playford, 1969. Sediments of a similar type and age occur in the Bass Basin (Durroon 1 well).

Acknowledgement is made of the considerable assistance given by Richard Rudowzki in the final stages of mineral preparation at the Australian National University.

Initial mineral separations were made with the assistance of the staff

at the Launceston Department of Mines laboratories and R. Woolley in Hobart using magnetic separation facilities provided by the University of Tasmania.

APPENDIX 4

Physiography and geomorphology of the Scottsdale Trough

W.R. Moore

The Scottsdale Trough forms a distinct physiographic unit which is a reflection of the geology. The area covered by the trough is included in four quadrangles; Pipers River (Marshall *et al.*, 1965), Noland Bay (Jennings, 1967), Ringarooma (Brown *et al.*, 1977) and Boobyalla (Baillie *et al.*, 1980). Over two-thirds of the trough is covered by the Boobyalla-Ringarooma Quadrangles.

BOUNDARY SCARPS AND RIDGES OF THE SCOTTSDALE TROUGH

The Scottsdale Trough occupies a tract of low country up to 22 km wide, and is bounded on three sides by conspicuous scarps of the neighbouring highland areas, with the coast forming the fourth side. The trough extends from the coast south for 20-25 km to the high plateau area of the Scottsdale Batholith.

The eastern and western borders of the trough are two continuous NNE-SSW trending scarps; these form the Sideling-Blumont Range in the west and Billycock Hill, Kapai Ridge and Kamona Ridge in the east. Both of these scarps fall rapidly in height northwards, but continue as boundary ridges to the coast. On the western side of the basin the ridge forms Duncraggen Hill and Ockerby Hill to the coast at Bridport, while on the eastern side the boundary ridge forms Williams Hill, Bulger Hills and Toddy Plains ridge at Waterhouse Road.

Both of the boundary ridges follow the granodiorite/Mathinna Beds contact and are formed by the presence of the erosion resistant band of rocks of the contact metamorphic aureole. The more easily eroded granodiorite forms the strip of low relief country bordering this contact on both sides of the Scottsdale Trough.

In the south-western corner of the trough the granodiorite forms the low hill country around Springfield, the upper Brid River and West Scottsdale, and to the north the low undulating country of the Nabowla and Duncraggen embayments (Marshall *et al.*, 1965; Marshall, 1970). Near the coast, granodiorite crops out as isolated low rounded hills, as at Granite Point, or as flat outcrops as in the Brewers Creek-Hurst Creek and Bridport-Barnbougle areas on the coastal plain.

In the south-eastern corner, the granodiorite crops out in the low lying hills and valleys of Tulendeena and Kamona, then north to the Great Forester River-Pearly Brook valley and the Great Forester River at Wonder Valley. Granodiorite forms rare isolated low rounded hills, as at Red Quarry [450583], but generally occurs as flat slab outcrops exposed through the Quaternary sediments on the coastal plain along the eastern margin of the trough at Toddys Plain and Marengo.

The southern border of the Scottsdale Trough lacks the distinctive continuity of the eastern and western borders, but is still a recognisable and major physiographic feature. This border is an irregular but high and steep NE-SW trending scarp which forms the edge of the high plateau (800 m level) of the Scottsdale Batholith, known as the Maurice High Plains. At the south-west corner of the trough, this scarp forms Bonners Hill, and becomes offset to the south at Springfield by the Springfield Tertiary

basin of the upper Great Forester River to form the dissected but continuous NE-SW trending scarp from Mount Helen to Trewalla Hill and Rocky Gully. Here the scarp is again offset to the south by the Tulendeena valley to Billycock Hill, the south-eastern corner of the trough.

Within the southern part of the Scottsdale Trough are two areas of high relief, one the isolated large granite cupola of Mt Stronach (497 m) and the second the razorback ridge of Walduck Hill, formed by the narrow belt of metamorphosed Mathinna Beds sediments that separate the adamellite and granodiorite along the western side of the Scottsdale Batholith.

These two high relief areas separate the main Tertiary sedimentary Scottsdale basin from the peripheral and shallower Tertiary sedimentary basins at Springfield and Tonganah, and an area of thin residual Tertiary sediment in the MacKenzie Rivulet valley. These peripheral Tertiary sedimentary areas, and Mt Stronach and Walduck Hill, form the southern section of the Scottsdale Trough and cover approximately one-third of its total area.

The remaining two-thirds of the trough is subdivided into three physiographic units. These units, from south to north, are:

(a) The red soil plateau

(b) The central dissected plateau

(c) The coastal plain

THE RED SOIL PLATEAU

This area, centred around the town of Scottsdale, is a low undulating plateau with a fertile deep red soil cover derived from the weathering of basalt. It extends from West Scottsdale north-east to North Scottsdale, and from Springfield north to Jetsonville. The plateau is a remnant of a more extensive basalt plateau that extended northwards towards the coast; the greater portion of this basalt has been removed by erosion.

The high red soil covered plateau landscape in the Ringarooma-Winnaleah area to the east, with its deeply incised valleys with cliffed outcrops of thick basalt flows, is not present at Scottsdale. At Scottsdale the original flows were thin and have subsequently been so deeply weathered that the landscape is rounded and subdued with a low relief.

The flat, narrow red-soil ridges at Jetsonville and North Scottsdale indicate the position of the Tertiary valleys, down which the original basalts flowed towards the coast before combining and spreading to cover the Tertiary sediments of the Scottsdale basin.

THE CENTRAL DISSECTED PLATEAU

In this area, the covering basalt sheet has been removed by erosion, the former presence being indicated by a 1.0-1.5 m thick ferricrete horizon that caps the highest hills and ridges. This iron-cemented horizon is the top of a locally thick sedimentary sequence of unconsolidated clay, sand and granules (grit) of the Scottsdale Tertiary basin.

Where this ferricrete protecting layer has been removed, the erosion of the soft underlying sediments is rapid. Its presence produces a mesa

type of landscape of flat-topped ridges, hills and small irregular shaped plateaus. The valley heads and sides are steep, while the valleys are shallow, wide and swampy, with no permanent flowing streams. All the through flowing rivers in the Scottsdale Trough are located on the marginal granodiorite areas or flowing on now exposed granodiorite, which formed dividing ridges in the Tertiary basin (*e.g.* Tuckers Creek, Hurst Creek and Coxs Rivulet). All streams originating in the trough are non permanent, because of the high permeability and porosity of the underlying thick Tertiary sedimentary sequence.

The accordance of summit level between the red soil basalt plateau and the ferricrete horizons of the old dissected Tertiary plateau is readily appreciated by looking north from North Scottsdale towards the coast.

THE COASTAL PLAIN

The third physiographic unit is the flat coastal plain, which in the Scottsdale Trough is an old marine embayment 4-8 km wide situated between the granodiorite/Mathinna Beds contact ridge at Bridport in the west, and the Toddys Plain ridge near Waterhouse in the east. The southern boundary is the Tertiary hill country to the south.

Two marine terraces are present on this coastal plain, the lower terrace sloping to 7.6 m and the upper terrace to 30-36 m height. The two terraces are separated by a low line of seven metre high cliffs in the west towards Bridport (Marshall, 1970), and elsewhere by a steep break in slope. The inland boundary of the upper terrace is less distinctive but is marked by a line of hills, some of which show spur trimming.

The Great Forester River reaches the coastal plain at Wonder Valley and swings to the west in a wide 15 km arc, originally flowing out through the coastal sand dunes at Bridport. The Great Forester flood plain is wide and extensive and has been incised in the two marine terraces. The other major streams, such as Hurst Creek, Tuckers Creek and Coxs Rivulet all formerly joined the Great Forester River on the coastal plain, before the latter was diverted through Adams Cut, and show well developed river terraces.

Along the coast is a wide belt of actively migrating sand dunes, with an older series of stabilised parabolic and longitudinal dunes inland. Isolated old longitudinal dunes are also present on both the marine terraces. The geomorphology of the dunes and their stratigraphic relationship has been studied in detail by Bowden (1978) and Baillie (this volume).

Small isolated deposits of windblown sand are common, and are frequently draped where any difference of relief occurs on the coastal plain. The low angle of these unconsolidated sands has flattened the slopes of the previous topography. These deposits occur along the valley sides of flood plains, on marine terrace slopes, around isolated granodiorite and silcrete hills, and along hills and in the valleys bordering the coastal plain.

APPENDIX 5

Additional trace element analyses of granitic rocks.

M.P. McClenaghan

Table 1. ADDITIONAL TRACE ELEMENTS FROM THE GRANITIC ROCKS LISTED IN TABLE 5.

Plot No.	1	2	3	4	5	6	7	8	9	10	11	12
Analysis No.	735120	735121	735126	735127	735128	735129	735130	735131	735132	735133	735134	735135
Cu	11	36	5	<5	<5	8	<5	40	19	<5	16	9
Ag	<10	<10	<10	<10	<10	<10	<10	<10	<10	<10	<10	<10
Zn	73	58	54	62	37	70	51	44	62	54	61	84
Pb	23	20	39	27	26	22	23	27	25	29	25	29
As	15	14	18	21	30	27	20	16	<15	25	19	29

Plot No.	13	14	15	16	17	18	19	20	21	22	23	24
Analysis No.	735136	735137	735138	735139	735140	735141	735142	735143	735144	735145	735146	735147
Cu	12	<5	15	30	15	9	<5	<5	40	27	25	10
Ag	<10	<10	<10	<10	<10	<10	<10	<10	<10	<10	<10	<10
Zn	31	77	119	48	48	64	15	68	128	73	60	87
Pb	33	26	18	24	26	24	28	30	16	26	19	25
As	15	28	23	20	<15	26	18	33	23	28	15	28

Plot No.	25	26	39	40	41	42	43	44	45	46	47	48
Analysis No.	735148	735149	741645	741646	742515	742516	742517	742518	742519	742520	742521	742522
Cu	<5	<5	21	5	<5	<5	<5	<5	<5	6	<5	<5
Ag	<10	<10	<3	<3	<3	<3	<3	<3	<3	<3	<3	<3
Zn	104	66	62	78	46	53	50	51	50	36	42	56
Pb	29	26	23	21	29	20	16	15	12	34	13	26
As	30	20	<11	<11	<10	11	<10	<10	16	<10	<10	<10
Co					<6	<6	<6	<6	<6	<6	<6	<6

Table 1. (continued)

Plot No.	49	50	51	52	53	54	55	56	57	58	59	60
Analysis No.	742523	742524	742525	742526	742527	742528	742529	742530	742536	742596	742596	742598
Cu	6	6	10	<5	<5	<5	<5	6	16	<5	<5	<5
Ag	<3	<3	<3	<3	<3	<3	<3	<3	<3	<3	<3	<3
Zn	39	58	46	36	44	57	51	54	62	58	56	26
Pb	33	26	23	36	33	18	15	12	34	15	15	18
As	16	<10	<10	<10	<10	<10	<10	<10	<10	<10	<10	12
Co	<6	<6	<6	<6	7	<6	<6	<6	<6	<6	<6	<6

Plot No.	61	62	63	64	65	66	67	68	69	70
Analysis No.	742599	742600	742601	742602	742603	742604	742605	742606	742607	742608
Cu	7	<5	5	<5	<5	<5	<5	<5	6	<5
Ag	<3	<3	<3	<3	<3	<3	<3	<3	<3	<3
Zn	32	83	41	56	47	51	55	22	22	52
Pb	14	17	11	12	16	18	23	10	41	8
As	<10	<10	<10	32	<10	13	19	<10	13	<10
Co	<6	6	<6	<6	<6	<6	<6	<6	<6	<6

APPENDIX 6

Electron microprobe analyses of spinel and websterite xenoliths from olivine - nepheline flows at Wagners Hill and Telita.

A.V. Brown

Table 1. ELECTRON MICROPROBE ANALYSES OF MINERALS FROM SPINEL LHERZOLITE: 72-381A/761159[1]

Mineral	1:Ol*	2:Ol+	3:Opx*	4:Opx	5:Cpx+	6:Cpx*	7:Sp*	8:Sp*	9:Sp*	10:Sp*
SiO_2	40.15	40.80	54.16	54.29	52.92	52.75	-	-	-	-
TiO_2	-	-	0.22	0.17	0.22	0.40	0.10	0.13	0.27	0.23
Al_2O_3	-	-	4.59	4.65	5.01	5.37	58.75	57.33	47.09	47.31
FeO	11.19	10.91	7.76	7.10	2.75	2.61	10.52	10.92	12.09	12.29
MnO	-	0.12	-	-	-	-	-	-	-	-
MgO	48.55	48.17	32.23	32.53	15.75	15.39	20.93	19.91	18.49	18.39
CaO	-	n.d	0.57	0.67	21.34	21.07	-	-	-	-
Na_2O	-	n.d	-	-	1.11	1.54	-	-	-	-
K_2O	-	n.d	-	-	0.18	-	-	-	-	-
Cr_2O_3	0.10	-	0.45	0.60	0.72	0.86	9.7	11.71	22.05	21.78
TOTAL[2]	(98.65)	(102.73)	(100.84)	(100.32)	(99.88)	(99.18)	(100.19)	(99.87)	(100.56)	(101.45)
Structural Formula										
Na	-	-	-	-	0.0776	0.1078	-	-	-	-
Mg	1.7853	1.7629	1.6715	1.6831	0.8501	0.8300	0.8023	0.7690	0.7474	0.7433
Al	0.9905	1.0036	0.1883	0.1901	0.2137	0.2289	1.7810	1.7512	1.5052	1.5122
Si			1.8841	1.8842	1.9160	1.9088	-	-	-	-
K	-	-	-	-	0.0083	-	-	-	-	-
Ca	-	-	0.0214	0.0250	0.8277	0.8170	-	-	-	-
Ti	-	-	0.0057	0.0044	0.0059	0.0109	0.0019	0.0025	0.0054	0.0048
Cr	0.0020	-	0.0125	0.0164	0.0205	0.0247	0.1974	0.2400	0.4729	0.4669
Mn	-	-	-	-	-		-	-	-	-
Cr	0.2309	0.2243	0.2257	0.2061	0.0834	0.0790	0.2264	0.2369	0.2743	0.2786
TOTAL	3.0089	2.9964	4.0092	4.0093	4.0032	4.0071	3.0090	2.9996	3.0052	3.0058
							Recalculated Structural Formula[3]			
Mg	88.5	88.7	87.1	87.9	48.3	48.1	Al	1.7759	1.7512	1.5028	1.5094
Ca	-	-	1.1	1.3	47.0	47.3	Cr	0.1966	0.2400	0.4719	0.4659
Fe	11.5	11.3	11.8	10.8	4.7	4.6	Fe^{3+}	0.0237	0.0032	0.0155	0.0143
							Ti	0.0020	0.0025	0.0047	0.0057
$\frac{100\ Mg}{Mg + Fe}$							Mg	0.7998	0.7690	0.7417	0.7460
							Fe^{2+}	0.2019	0.2335	0.2627	0.2597
(mol%)	88.5	88.7	88.1	89.1	91.1	91.3					
$\frac{100\ Cr}{Cr + Al}$											
(mol%)	-	-	6.2	8.0	8.8	9.7		10.0	12.0	23.9	23.6

Table 2. ELECTRON MICROPROBE ANALYSES OF MINERALS FROM SPINEL LHERZOLITE: 72-311 AND 74-648/761162[1]

Specimen No.	72-311			74-648/761162		
Mineral	1:Ol+	2:Opx+	3:Cpx+	4:Ol+	5:Opx+	6:Cpx+
SiO_2	40.34	55.23	52.84	40.68	55.93	53.10
TiO_2	-	-	0.32	-	-	0.40
Al_2O_3	-	4.51	5.53	-	3.09	4.20
FeO	10.91	6.66	2.72	10.46	6.78	2.35
MnO	n.d	n.d	n.d	n.d	n.d	n.d
MgO	48.74	31.73	15.64	48.87	33.07	16.07
CaO	n.d	1.56	21.00	-	0.63	22.07
Na_2O	n.d	n.d	1.18	-	-	0.80
K_2O	n.d	n.d	n.d	n.d	n.d	n.d
Cr_2O_3	-	0.31	0.73	-	0.50	1.01
TOTAL[2]	(98.95)	(102.88)	(99.64)	(97.52)	(103.94)	(95.31)
Structural Formula[3]						
Na	-	-	0.0829	-	-	0.056
Mg	1.7888	1.6372	0.8422	1.7882	1.7042	0.8668
Al	-	0.1839	0.2357	-	0.1259	0.1790
Si	0.9932	1.9118	1.9091	0.9986	1.9336	1.9220
K	-	-	-	-	-	-
Ca	-	0.0579	0.8130	-	-	-
Ti	-	-	0.0087	-	-	0.0110
Cr	-	0.0085	0.0210	-	0.0137	0.0289
Mn	-	-	-	-	-	-
Fe	0.2247	0.1927	0.0827	0.2146	0.1960	0.0710
TOTAL	3.0067	3.9920	3.9953	3.0014	3.9966	3.9911
Mg	88.8	86.7	48.4	89.3	88.6	48.3
Ca	-	3.1	46.8	-	1.2	47.7
Fe	11.2	10.2	4.8	10.7	10.2	4.0
$\frac{100\ Mg}{Mg + Fe}$ (mol%)	88.8	89.5	91.0	89.3	89.7	90.8
$\frac{100\ Cr}{Cr + Al}$ (mol%)	-	4.4	8.1	-	9.8	13.9

Table 3. ELECTRON MICROPROBE ANALYSES OF MINERALS FROM WEBSTERITE NODULES: 72-384/761160 AND 72-386/761161[1]

Specimen No.	72-384/761160						72-386/761161			
Mineral	1:Opx+	2:Opx+	3:Cpx+	4:Cpx+	5:Opx inter-growth in Cpx+	6:Cpx inter-growth in Opx+	7:Opx+	8:Opx+	9:Cpx+	10:Cpx*
SiO_2	53.51	53.47	51.42	51.19	53.84	51.17	53.60	52.26	51.12	49.74
TiO_2	0.18	0.27	0.76	0.86	0.14	0.96	0.17	0.32	0.91	1.37
Al_2O_3	3.72	4.04	5.72	5.83	4.11	6.06	3.46	5.69	5.82	7.84
FeO	13.28	12.15	6.06	6.12	12.99	6.10	13.10	14.33	6.06	6.74
MnO	0.12	0.18	n.d	n.d	0.15	n.d	0.18	-	n.d	
MgO	28.26	16.27	14.24	14.27	27.26	14.30	27.99	26.32	14.25	13.35
CaO	0.76	3.52	20.23	20.14	1.23	19.87	1.36	0.92	20.31	19.45
Na_2O	n.d	n.d	1.15	1.16	n.d	1.05	n.d	-	1.13	1.28
K_2O	n.d	n.d	n.d	n.d	0.28	n.d	n.d	-	0.07	
Cr_2O_3	0.16	0.10	0.42	0.42	n.d	0.49	0.13	0.18	0.34	0.23
TOTAL[2]	(98.43)	(100.77)	(99.92)	(101.50)	(98.09)	(99.02)	(98.62)	(101.53)	(98.33)	(101.70)
Structural Formula[3]										
Na	-	-	0.0814	0.0827	-	0.0747	-	-	0.0803	0.0912
Mg	1.5023	1.3999	0.7783	0.7802	1.4489	0.7807	1.4897	1.4056	0.7792	0.7312
Al	0.1562	0.1702	0.2473	0.2520	1.1728	0.2614	0.1458	0.2402	0.2519	0.3396
Si	1.9087	1.9113	1.8849	1.8776	1.9197	1.8744	1.9140	1.8725	1.8759	1.8276
K	-	-	-	-	0.0128	-	-	-	0.0031	-
Ca	0.0292	0.1347	0.7944	0.7916	0.0471	0.7799	0.0521	0.0355	0.7984	0.7657
Ti	0.0049	0.0073	0.0210	0.0237	0.0036	0.0265	0.0045	0.0085	0.0250	0.0378
Cr	0.0045	0.0029	0.0122	0.0123	-	0.0142	0.0038	0.0050	0.0100	0.0068
Mn	0.0038	0.0053	-	-	0.0045	-	0.0056	-	-	-
Fe	0.3963	0.3631	0.1856	0.1878	0.3872	0.1869	0.3912	0.4295	0.1859	0.2072
TOTAL	4.0060	3.9948	4.0051	4.0079	3.9967	3.9986	4.0067	3.9968	4.0098	4.0071
Mg	77.9	73.8	44.3	44.3	76.9	44.7	77.1	75.1	44.2	42.9
Ca	1.5	7.1	45.2	45.0	2.5	44.6	2.7	1.9	45.3	44.9
Fe	20.6	19.1	10.6	10.7	20.6	10.7	20.2	23.0	10.5	12.2
100 Mg / Mg + Fe (mol%)	79.1	70.5	80.7	80.5	78.9	80.7	79.2	76.6	80.8	77.9
100 Cr / Cr + Al (mol%)	2.8	1.6	4.7	4.6	-	5.1	2.5	2.1	3.8	1.9

ADDENDA

p. 188-190, tables 1-3:

Footnotes to tables:

Ol = olivine, Opx = orthopyroxene,
Cpx = clinopyroxene, Sp = spinel.
n.d. indicates not determined, a dash that the element was not detected.

(1) 72-XXX = Department of Mines sample registration number, 7611XX = laboratory registration no.
(2) Total = machine total before normalisation. Total iron is reported as FeO.
(3) Structural formula recalculated on the basis of $RO/R_2O_3 = 1:1$ for Fe_2O_3.

* Electron microprobe analysis by A.V.Brown using the JEOL JXA-50 with Edax Si (Li) detector, Central Science Laboratories, University of Tasmania.
+ Electron microprobe analysis by F.L.Sutherland using the TPD microprobe, Research School of Earth Sciences, Australian National University. Facilities provided by N.G.Ware.

p. 190a

Table 4. ANALYSIS OF SPINEL LHERZOLITE AND WEBSTERITE XENOLITHS FROM OLIVINE NEPHELINE FLOWS AT WAGNERS HILL AND TELITA

Analysis No.	761159	761160	761161	761162
SiO_2	44.10	51.20	50.20	45.10
TiO_2	0.13	0.49	0.55	0.16
Al_2O_3	3.10	4.70	4.90	2.10
Fe_2O_3	1.10	1.60	1.40	0.61
FeO	8.50	9.80	9.80	8.30
MnO	0.16	0.21	0.19	0.16
MgO	39.00	23.50	23.80	40.10
CaO	2.80	7.10	6.60	1.20
Na_2O	0.21	0.60	0.55	0.11
K_2O	0.04	0.05	0.08	0.08
P_2O_5	0.02	0.03	0.04	0.02
H_2O^+	0.58	0.77	1.30	1.20
H_2O^-	0.14	0.12	0.22	0.27
CO_2	0.17	0.24	0.20	0.83
Total	100.05	100.41	99.83	100.24
Mg value	89.1	81.1	81.3	89.6
Ni (ppm)	1900	630	570	2000
Cr (ppm)	2800	1900	1600	4100

Analysis No.	*Xenolith*	*Departmental No.*	*Parent rock*
761159	Spinel lherzolite	72-381A	761163,72-381B
761160	Websterite	72-384A	761164,72-384B
761161	Websterite	72-386A	761165,72-386B
761162	Spinel lherzolite	74-648A	761166,72-648B

APPENDIX 7

Preliminary palynological investigation of Boobyalla DDH1, 1977-1979.

S.M. Forsyth

SUMMARY

In the conglomeratic sequence penetrated by Boobyalla DDH1 a latest Cretaceous (late Senonian) microflora belonging to either the *Tricolpites longus* zone or the *Tricolporites lilliei* zone occurs at 65 m depth. In four samples from 65 m to 245.1 m an early Mesozoic component occurs consistently in the microfloras. This component consists chiefly of palynomorphs occurring in Triassic coal measures and supports the lithological identification of clasts in the conglomerate as being derived from coal measure rocks. From 225 m and lower samples, apart from the Early Mesozoic palynomorphs, only meagre Late Mesozoic microfloras were obtained and some samples were barren. Excepting *Tricolpites* sp. cf. *T.gillii* Cookson, *T.* sp. aff *T.gillii* from 225 m, and a possible contaminant *Gambierina* sp. from 365.6 m, the few species found are more typical of earlier Cretaceous microfloras. *Cicatricosisporites* sp. cf. *C.australiensis* (Cookson) Potonié indicates that 347.5 m depth is not older than the Cretaceous. It is not known whether the Late Mesozoic palynomorphs below 65 m are reworked.

INTRODUCTION

Boobyalla DDH1 drilled a sequence of sedimentary rocks occupying a graben-like feature south of Boobyalla in far north-eastern Tasmania. Drilling terminated at 417.2 m before reaching basement. For the major part the drilled sequence consists of conglomerate with an impure muddy matrix that contains variable amounts of sand, silt, and granule grade detritus. The conglomerate clasts range from pebbles to boulders several metres thick, but slightly rounded cobbles predominate. The cobble framework ranges from closed to open and certain portions of the core consist of matrix only with no clast intersections. The larger clasts consist of dolerite, granitic rocks, quartzite and slate probably derived from the Mathinna Beds, quartz arenite, lithic arenite and grey siltstone probably derived from Triassic rocks. The dolerite is similar to that found as Middle Jurassic intrusions and provides a maximum age constraint on the inferred graben development. Matrix colour ranges from brick red through chocolate to almost black.

A series of core samples were selected by W.R. Moore, P.W. Baillie and the author for preliminary palynological analysis.

PALYNOLOGY

A list of sample data is given in Table 1. Samples were processed by standard hot HF, HCl treatment and oxidised from 5 to 10 minutes using Schultz solution. This was followed by treatment with dilute alkali and heavy liquid separation where warranted.

The residues are discussed below under depth headings.

Samples from 388.4 to 302.3 m

The more oxidised samples, with red-brown matrix from 302.3 m and medium brown-chocolate matrix from 328.1 m, contained no palynomorphs, although woody tissue may be present at 328.1 m. The matrix from 365.6 m

Table 1. LIST OF SAMPLES, BOOBYALLA DDH1.

Sample depth (m)	Lithology	Sample number	Preparation number	Palynological slides
63.8	Coalified wood	SB10	P32	
65	Light grey coarse siltstone	SB9	P31	1127, 1128, 1135, 1136, 1138, 1139, 1140, 1141, 1142
225	Lithic sandstone and siltstone	SB7	P29	1123, 1124, 1131, 1132
231.9	Grey mudstone clasts	SB6	P28	1112, 1113, 1121, 1122
245.1	Grey muddy sandy matrix and sandstone clasts	SB8	P30	1125, 1126, 1133, 1134
302.3	Red-brown slightly sandy mudstone matrix of conglomerate	SB5	P27	1120
328.1	Medium brown-chocolate siltstone matrix of conglomerate	SB4	P26	1119
347.5	Chocolate coloured sandy mudstone matrix of conglomerate	SB2	P24	1129, 1130
365.6	Olive brown sandy granule mudstone matrix of conglomerate	SB3	P25	1116, 1117
388.4	Chocolate coloured slightly sandy mudstone matrix of conglomerate	SB1	P23	Temporary slide

contained fine organic matter but no palynomorphs, excepting a well preserved but cleanly broken *Gambierina* sp. which may be a contaminant introduced during drilling. The matrix from 388.4 and 347.5 m contained cellular cuticle, xylem fragments and *Circulisporites* sp. *Cicatricosisporites* sp. cf. *C.australiensis* (Cookson) Potonié and palynomorphs probably referrable to *Ceratosporites equalis* Cookson and Dettmann are also present at 347.5 m. *Lycopodiumsporites* sp. occurs at 388.4 m.

C.australiensis has been recorded from rocks as young as the *Nothofagidites senectus* zone (Stover and Partridge, 1973) but is more typical of the Neocomanian through Turonian (Dettmann and Playford, 1969). Should the broken specimen of *Gambierina* sp. not be a contaminant, then 365.6 m could be as young or younger than the *N.senectus* zone.

Samples from 225 to 245.1 m

The samples contain a mixture of Early and Late Mesozoic palynomorphs.

Sample depth (m)	*Early Mesozoic*	*Early-Late Mesozoic*	*Late Mesozoic*
245.1	*Aratrisporites* sp. cf. *A.banksi* Playford	*Leptolepidites* sp. *Osmundacidites* sp.	*?Cicatricosisporites* sp.
234.9	*Semiretisporis denmeadi* (de Jersey) de Jersey *Aratrisporites parvispinosus* Leschik *emend.* Playford *Clavatriletes* sp. cf. *C.hammenii* Herbst		*?Foraminisporis* sp.
225	*Falcisporites* spp. *Polypodiisporites ipsviciensis* (de Jersey) Playford & Dettmann *Semiretisporis denmeadi* (de Jersey) de Jersey *A. banksi* *Craterisporites rotundus* de Jersey *Neoraistrickia* sp. *Uvaesporites verrucosus* (de Jersey) Helby *Densoisporites playfordi* (Balme) Dettmann	*Leptolepidites* sp. *Cycadopites nitidus* (Balme) de Jersey Yellow cuticle and fungal remains	*?Cicatricosisporites* sp. *Klukisporites* sp. cf. *K.scaberis* (Cookson & Dettmann) Dettmann aff. *Reticulatisporites pudens* Balme *Tricolpites* sp. cf. *T.gillii* Cookson *T.* sp. aff. *T.gillii*

A brown specimen of *D.playfordi* is probably derived from Early Triassic rocks whilst the remaining yellow Early Mesozoic forms are typical of those occurring in Tasmanian Middle-Late Triassic coal measures. This supports the initial recognition based on lithology of clasts of Triassic coal measure rocks.

Many of the Cretaceous palynomorphs are poorly orientated due to buckling. This may indicate reworking or movement of matrix and precludes positive identifications. However *Klukisporites scaberis* is probably present together with specimens of *Cicatricosisporites*. Simple triangular tricolpate pollen are present at 225 m including a form close to *T.gillii*.

Sample from 65 m

The residue consists of cellular cuticle, xylem fragments, a large range of fungal remains, plus a well preserved and fairly diverse microflora with *Tricolpites sabulosus* Dettmann and Playford (dispersed and tetrads common). *T.gillii* (common), *Proteacidites* spp. and *Nothofagidites senectus* Dettmann and Playford. *Uvaesporites verrucosus*, *Neoraistrickia taylorii* Playford and Dettmann, *Krauselisporites* sp. cf. *K.verrucifer*

(de Jersey) and *Protohaploxypinus* indicate the presence of a Triassic component.

Palynomorphs tentatively identified are:

Leptolepidites sp.
C.equalis
Neoraistrickia sp. cf. *N.truncatus* (Cookson) Potonié
Stereisporites regium (Drozhastichich) Drugg
Tricolpites confessus Stover
T. sp. cf. *T.gillii*
T.longus Stover and Evans
Nyssapollenites sp.
Phimopollenites pannosus (Dettmann & Playford) Dettmann
Triorites sp. B
T. sp. C
Gambierina rudata
Dilwynites granulatus Harris
Proteacidites sp. cf. *P. angulatus* Stover
P. sp. cf. *P.palisadus* Couper
P. sp. A
Phyllocladidites reticulosaccatus Harris
Tsugapollenites sp. cf. *T. segmentatus* (Balme)

Palynomorphs positively identified are:

Laevigatosporites ovatus Wilson & Webster
Baculatisporites disconformis Stover
Tricolpites gillii
T.renmarkensis Harris M.S. Partridge
T.sabulosus
Triorites sp. A
N.senectus
Araucariacites australis Cookson
Microcachyridites antarticus Cookson
Trisaccites microsaccatus (Couper) Couper
Phyllocladidites mawsonii Cookson and Couper

The microflora indicates assignment to either the *Tricolporites lilliei* zone or the *Tricolpites longus* zone (see fig. 72, 73) of the latest Cretaceous (Stover and Partridge, 1973; Partridge, 1976). Only a single tentatively identified *Dilwynites granulatus* was observed, therefore choice of zone assignment to the *Tricolpites longus* zone is not assured, although the low proportion of *Nothofagidites* (<2%) is consistent with such an age.

DISCUSSION

Subsequent to undertaking this study further samples of carbonaceous mudstone have become available from shallow drilling a few kilometres east of Boobyalla DDH1. This mudstone contains microfloras with common *Nothofagidites senectus, Gambierina rudata, Tricolpites sabulosus, T.gillii* with *Proteacidites* spp. including *P.palisadus, Triorites* sp. A and possibly *Aequitriradites spinulosus*. *Classopollis* sp. is very common in some samples.

Although there is always a degree of uncertainty regarding the origin of microfloras in conglomerates, the bedded nature of the rocks at 65 m and the lack of such diverse Late Cretaceous microfloras at greater depths suggests that the microflora at 65 m was not derived by reworking from the other Late Cretaceous sediments nearby, but is approximately coeval with them.

Early Mesozoic microfloras have been recycled into the conglomerate, but it is by no means clear whether the meagre Cretaceous microfloras below 65 m are recycled or deposited directly into the conglomerate.

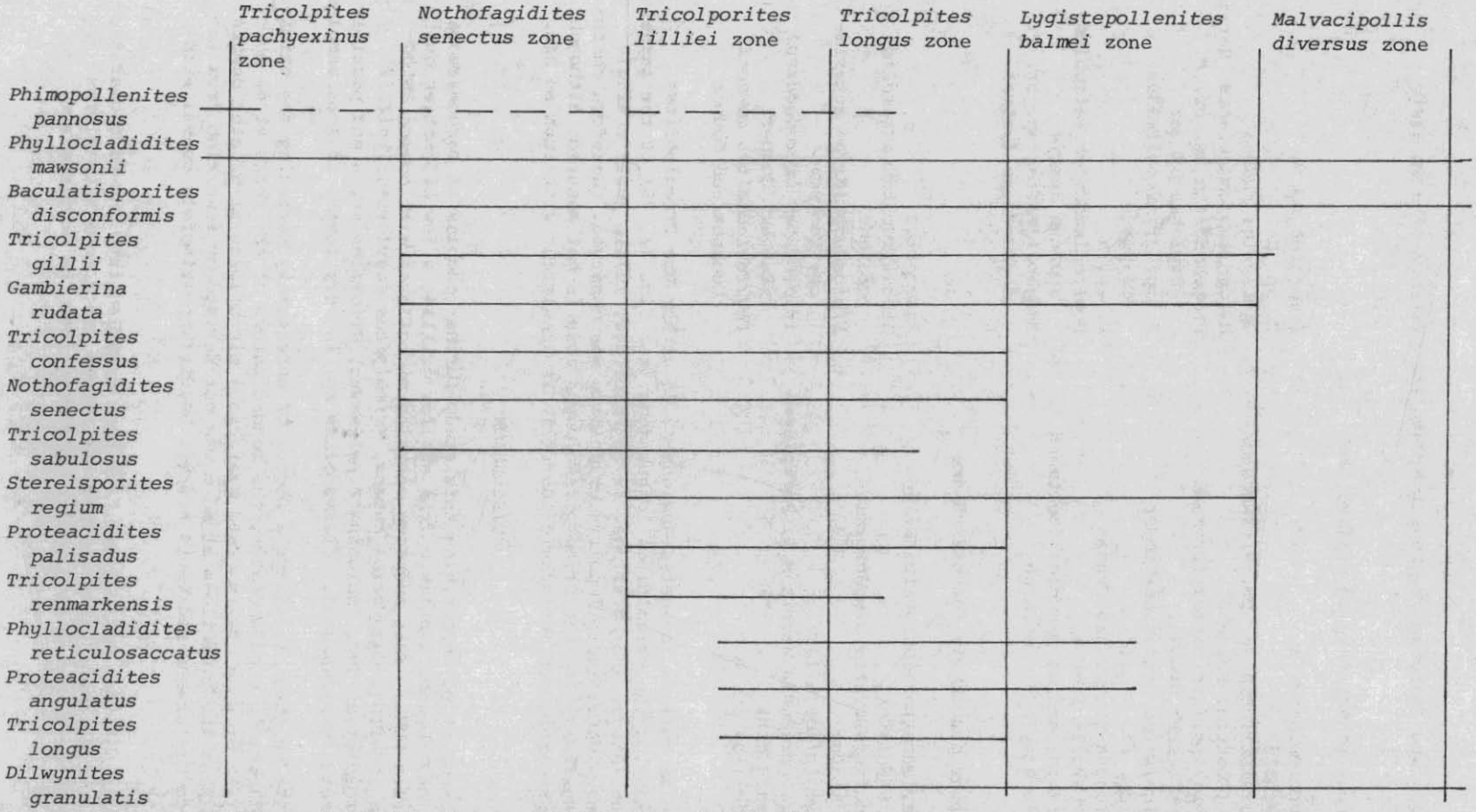

After Dettmann and Playford (1969), Stover and Partridge (1973), Stover and Evans (1973), and Partridge (1973).

Figure 72. *Ranges of selected palynomorph species.*

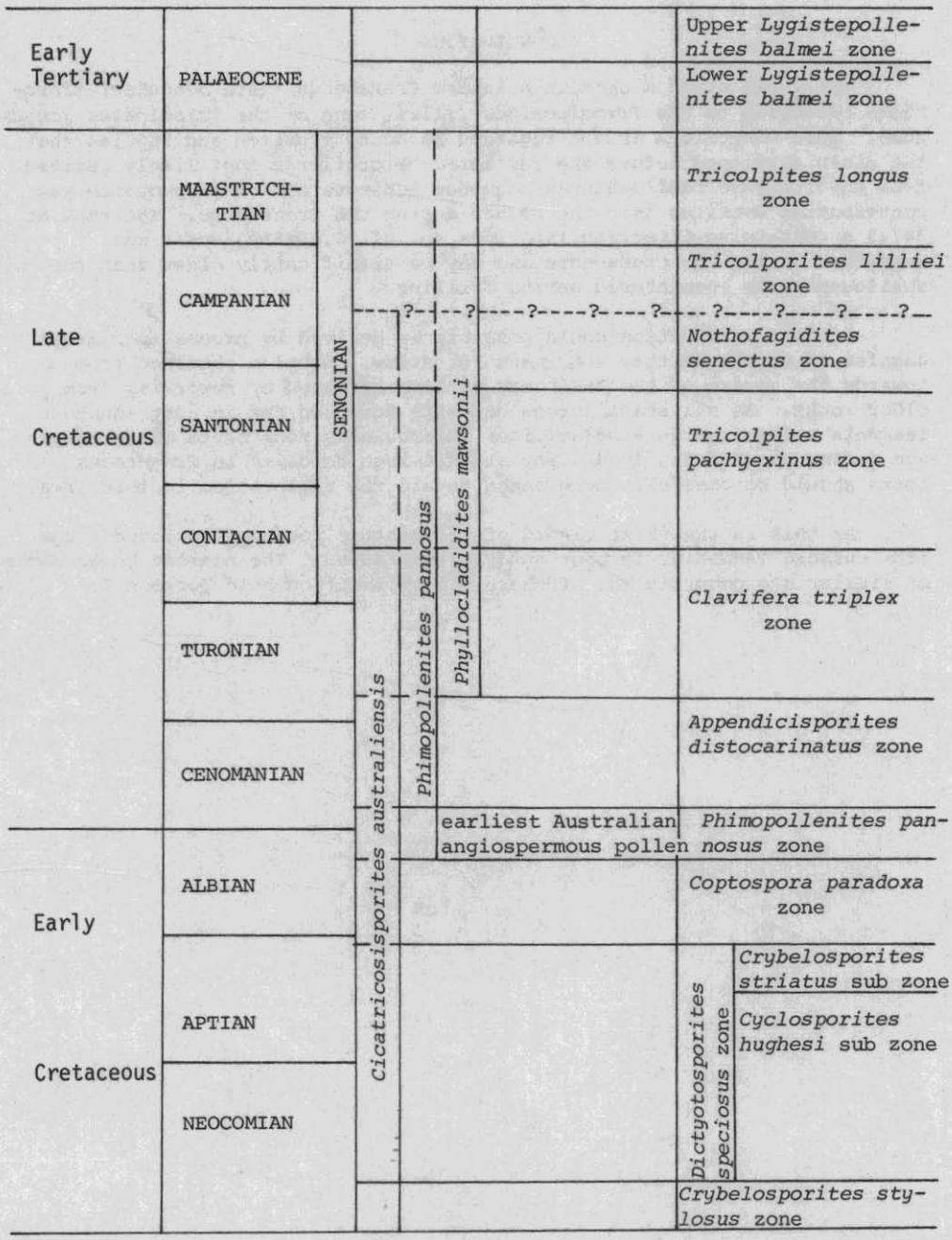

Figure 73. *Cretaceous microflora zones (after Dettmann and Playford, 1969; Stover and Partridge, 1973; Partridge, 1976).*

CONCLUSIONS

The rocks at 65 m contain a latest Cretaceous (late Senonian) microflora belonging to the *Tricolporites lilliei* zone or the *Tricolpites longus* zone. This microflora is not regarded as being recycled and implies that the basin developed before the Tertiary. Microfloras most likely derived from the Triassic coal measures sequence indicate that this sequence was contributing detritus into the graben during the Cretaceous. The rock at 347.5 m containing *Cicatricosisporites* sp. cf. *C.australiensis* was deposited during the Cretaceous and may be significantly older than the shallower rocks encountered during drilling.

Further information could possibly be derived by processing larger samples to obtain further specimens for study. Samples obtained from towards the centre of the basin may be less affected by reworking from older rocks. As all stanniferous deposits dated so far in north-eastern Tasmania belong to the *Proteacidites tuberculatus* zone or to Quaternary age sediments (Harris, 1968), any stanniferous deposits in Cretaceous rocks should be carefully documented to aid tin exploration in this area.

As this is the first record of sedimentary rocks of Cretaceous age from onshore Tasmania, further study is warranted. The nearest known rocks of similar age occur in the offshore oil exploration hole Durroon I.